



**Structural Modelling and Earthquake Analysis
of a Hospital Building located within The
Tjörnes Fracture Zone in Iceland**

Höskuldur Goði Þorbjargarson

Thesis of 30 ECTS credits

**Master of Science in Civil Engineering with
specialization in Structural Design**

June 2016



Structural Modelling and Earthquake Analysis of a Hospital Building located within the Tjörnes Fracture Zone in Iceland

Höskuldur Goði Þorbjargarson

Thesis of 30 ECTS credits submitted to the School of Science and Engineering
at Reykjavík University in partial fulfillment
of the requirements for the degree of
**Master of Science in Civil Engineering with
specialization in Structural Design**

June 2016

Supervisors:

Jónas Þór Snæbjörnsson
Professor, Reykjavík University, Iceland

Benedikt Halldórsson
Director of Research, Earthquake Engineering Research Centre

Examiner:

Torfi G. Sigurðsson, MSc.
General Manager at Mannvit Ltd.

Abstract

The Tjörnes fracture zone (TFZ) is one of the two most active seismic regions in Iceland. It is of vital importance for civil protection and security of the local residents living in that area to have a fully functioning hospital close by, when a major earthquake event occurs within the TFZ. The main focus of this study is to examine the structural characteristics, dynamic behaviour and structural integrity of the hospital in the town of Húsavík in North Iceland.

A structural monitoring system was installed in the building in May 2015. The structural monitoring system is a part of the multidisciplinary strong motion array, ICEAR-RAY II, which is in operation in North Iceland. The measurements have been ongoing for one year and three notable events have occurred that provide useful full-scale records of the building excitation and response and which have been used to determine key dynamic properties and response characteristics as well as for validation of the structural model. A finite element model was constructed using the structural design software Sap2000 (www.csiberkeley.com). The first natural frequency of the building is 7.4 Hz, and the damping ratio at low intensity excitation was found to be of the order, 2 - 3% of critical.

Building codes and standard civil engineering practises have evolved considerably since the construction of the hospital in 1964. Especially with regard to seismic design requirements. Individual building components and structural design details will be examined with this in mind. The earthquake excitation used for the analysis is the EN-1998-1 Response spectra and records of strong ground motion from earthquake events that occurred in the South Iceland seismic zone in June 2000 and May 2008.

The building has many load carrying walls, in a structural system that provides a lot of redundancy. The building deformations are found to be small, or 1 cm or less for a design response spectral analysis. The same can be said about the story drift which is found to be well within the limits prescribed by EN1998-1.

Structural verification of selected cross sections was performed using M-N interaction diagram and shear capacity calculations according to EN 1992-1. The cross sections resist the interaction between axial force and bending moment but the shear capacity is not satisfactory for earthquake excitation. Concrete stresses are generally found to be low. The density ratio of walls compared to the floor area was calculated to be 7 % total and experiments have shown that this is a indicator of a good seismic performance.

Ágrip

Húsavík er staðsett á einu virkasta jarðskjálfta svæði á Íslandi, (Tjörnes fracture zone). Þess vegna er mikilvægt öryggisatriði þegar stórir jarðskjálftar ganga yfir að fólk geti leitað til heilbrigðisstofnunar í nágrenninu. Megin áhersla þessa verkefnis er að meta eiginleika burðarvirkja hreyfifræðilega svörun og áreiðanleika burðarvirkis Heilbrigðisstofnunar þingeyinga á Húsavík.

Hröðunarmælum var komið fyrir í spítalanum í maí 2015. Hröðunarmælarnir eru hluti af mælakerfinu ICEARRAY II sem rekið er af rannsóknarmiðstöð Háskóla Íslands í jarðskjálftaverkfræði. Þrír nothæfir atburðir hafa verið mældir á því eina ári sem mælakerfið hefur verið í spítalanum. Atburðirnir gefa raunverulegar mælingar á viðbrögðum byggingarinnar þegar jarðskjálfti ríður yfir. Mælingarnar voru notaðar til að ákvarða nokkra lykil eiginleika og einnig til þess að fínstilla viðbragð FEM líkans sem var byggt upp í FEM forritinu SAP2000 (www.csiberkeley.com). Fyrsta eigintíðni byggingarinnar er 7,4 Hz og dempunarhlutfall við upphaf jarðhreyfinga var á bilinu 2 - 3%.

Reglugerðir og hefðir í byggingariðnaði hafa þróast og breyst síðan húsið var byggt árið 1964. Það á þá sérstaklega við þegar litið er til burðarvirkjahönnunar mannvirkja sem gangast undir jarðskjálftaálag. Sérstakir byggingarhlutar verða skoðaðir með þetta í huga. Við styrkathugun byggingarhluta er notast við svörunarróf sem skilgreint er í EN 1998-1 ásamt því að notast er við hröðunarmælingar frá atburðum sem mældir voru í júní 2000 og maí 2008 á suðurlandi.

Byggingin sem um ræðir hefur mikið af steypum veggjum sem ná alveg á milli hæða og gefa verulega stífni og taka upp stóra krafta. Færslur byggingarhluta eru mjög litlar eða um 1 cm eða minna fyrir svörunarrófsgreininguna. Mismunafærslur á milli hæða eru sömuleiðis vel innan marka sem staðallinn EN 1998-1 setur. Það eru þó undir sérstökum álagstílfellum að ástæða getur verið til að yfirfara ákveðna byggingarhluta.

Styrkathugun sérstakra byggingarhluta var athuguð með tilliti til samverkunar normalkrafta of beygjuvægis ásamt athugun á skerþoli byggingarhlutanna með tilliti til EN 1992-1. Styrkur þversniðana er nægur ef samverkun normalkrafta og beygjuvægis er skoðuð en skerþol þversniðana er ekki nægjanlegt fyrir áraun vegna jarðskjálfta. Spennudreifing í steinsteypu er almennt lág. Þverskurðarflatarmál berandi veggja var reiknað sem hlutfall af grunnflatarmáli byggingarinnar, Berandi veggir eru 7% af grunn-flatarmáli byggingarinnar og hefur reynsla tilrauna sýnt að byggingar með svo hátt hlutfall veggja reynist vel undir jarðskjálftaálagi.

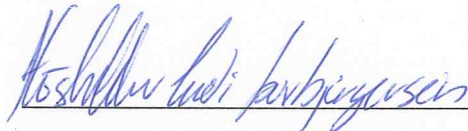
Structural Modelling and Earthquake Analysis of a Hospital Building located within the Tjörnes Fracture Zone in Iceland

Höskuldur Goði Þorbjargarson

30 ECTS thesis submitted to the School of Science and Engineering
at Reykjavík University in partial fulfillment
of the requirements for the degree of
**Master of Science in Civil Engineering with
specialization in Structural Design**

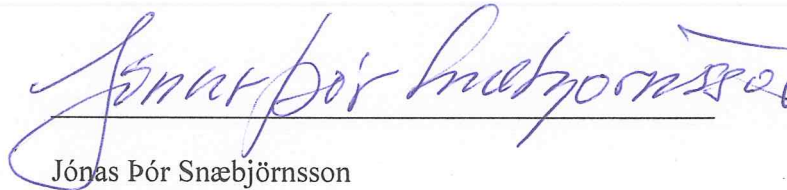
June 2016

Student:



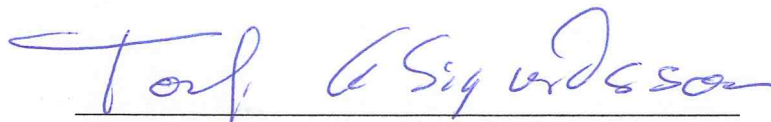
Höskuldur Goði Þorbjargarson

Supervisor:



Jónas Þór Snæbjörnsson

Examiner:



Torfi G. Sigurðsson

Aknowledgements

This project has been very interesting and challenging and my sincere gratitude is expressed to my supervisors Jónas Þór Snæbjörnsson and Benedikt Halldórsson for their great amount of time, knowledge and guidance in order to improve this work.

Also I want to express my gratitude to Eyþór R. Þórhallsson and Guðbrandur Steinþórsson for valuable recommendations during the work of this project.

I want to thank the Earthquake Engineering Research Centre of the University of Iceland for the cooperation, the access to the monitoring system and the data. Also I want to thank the EERC for inviting me to the workshop on earthquakes in north Iceland on Húsavík 31 May – 3 June, 2016.

Contents

Abstract	I
Ágrip	III
Aknowledgements	VII
List of figures	XVI
List of tables	XVII
1 Introduction	1
1.1 Background	1
1.2 Problem statement	1
1.3 Aim and objectives	2
1.4 Research methodology	2
1.5 Scope of work	3
2 Earthquake action and structural response	5
2.1 Earthquake	5
2.2 Seismic information	7
2.2.1 Methods of analysis	9
2.2.2 Response spectra according to Eurocode 8	10
2.2.3 Icelandic and local seismicity	11
2.3 Structural dynamics	14
2.3.1 Single degree of freedom systems	14
2.3.2 Multi degree of freedom systems	18
2.3.3 Time domain analysis	20
2.3.4 Frequency domain analysis	21
2.4 System identification	22
3 The case studied	23
3.1 The building	23
3.2 Material properties of concrete	25
3.3 The monitoring-system	26
4 Earthquake induced Acceleration data	31
4.1 Introduction	31
4.2 Data recorded on site	32
4.3 Earthquake data in the hospital	33

4.3.1	Event 3	34
4.3.2	Event 4	39
4.4	Strong motion data and seismic information	45
4.4.1	Earthquakes June 2000	45
4.4.2	Earthquake May 2008	46
4.4.3	Selection criteria and selected data	46
5	Finite element modelling and system identification	49
5.1	The modelling process	50
5.1.1	Total mass	51
5.1.2	Elastic modulus	53
5.2	Modal analysis and model validation	53
5.2.1	Response measured vs. computed	55
6	Analysis and results	61
6.1	Response spectra analysis	61
6.1.1	Shear forces	61
6.1.2	Displacements	63
6.1.3	Damage limitations	64
6.2	Time history analysis	66
6.2.1	Flagbjarnarholt	66
6.3	Structural integrity	68
6.3.1	Axial force and bending moments	75
6.3.2	Shear forces	79
6.3.3	Walls	80
7	Conclusion	83
	Appendix	87
A	Earthquakes on southern Iceland	89
A.1	Flagbjarnarholt	90
A.2	Kaldarholt	92
A.3	Selfoss EERC	94
A.4	Sólheimar	96
A.5	Þjórsártún	98
A.6	Selfoss city hall	100
A.7	Hveragerði Retirement house	102
A.8	Ljósafoss-hydroelectric power station	104
B	Time history response	107
B.1	Flagbjarnarholt	108
B.2	Kaldarholt	112
B.3	Sólheimar	116
B.4	Þjorsartun	120
B.5	Selfoss city hall	124
B.6	Retirement home	128
B.7	Earthquake engineering research centre	132

B.8	Borgarhraun	136
B.9	Ljosafoss power station	140
C	Earthquake induced forces	145
C.1	Retirement house	146
C.2	Sólheimar	148
D	Design of building components	151
E	Shear calculations	157

List of Figures

2.1	Tectonic plates on top and worldwide earthquake distribution	6
2.2	Travel path mechanisms of body waves	7
2.3	Travel path mechanisms of surface waves	7
2.4	Attenuation relationship	8
2.5	Hazard map for Iceland	8
2.6	Elastic horizontal spectra for ground types A to E	11
2.7	The tectonic setting of iceland	12
2.8	Distribution of earthquakes in north Iceland	13
2.9	The seismic source zones and lineaments near Húsavík	14
2.10	Single degree of freedom system	15
2.11	Data showing motions decay in a freely vibrating SDOF system	15
2.12	Multi degree of freedom systems	18
2.13	Mode shapes for different times in vibration cycle	19
2.14	Schematic of system identification problem	22
2.15	Ground motion input gives simultaneous displacement output	22
3.1	The Húsavík hospital	23
3.2	The Húsavík hospital	24
3.3	Design drawing of the hospital	24
3.4	A ultrasonic pulse velocity measurement	25
3.5	Plan view of location of the sensors	27
3.6	Vertical cross section of the building	28
3.7	Location of main station	29
3.8	Location of sensor 2	29
3.9	Location of sensor 3	30
4.1	The distribution of accelerographs on Húsavík	32
4.2	Húsavík hospital time history acceleration, ground floor	34
4.3	Húsavík hospital fourier spectra, ground floor	35
4.4	Húsavík hospital horizontal elastic response spectra	35
4.5	Húsavík hospital vertical elastic response spectra	36
4.6	Húsavík hospital time history acceleration, roof	36
4.7	Húsavík hospital time history relative acceleration, roof	37
4.8	Húsavík hospital time history acceleration, 4th floor	37
4.9	Húsavík hospital time history relative acceleration, 4th floor	38
4.10	Húsavík hospital Power spectral density x-component	38
4.11	Húsavík hospital Power spectral density y-component	39
4.12	Húsavík hospital Power spectral density z-component	39
4.13	Húsavík hospital time history acceleration, ground floor	40

4.14	Húsavík hospital fourier spectra, ground floor	40
4.15	Húsavík hospital horizontal elastic response spectra	41
4.16	Húsavík hospital vertical elastic response spectra	41
4.17	Húsavík hospital time history acceleration, roof	42
4.18	Húsavík hospital time history relative acceleration, roof	42
4.19	Húsavík hospital time history acceleration, 4th floor	43
4.20	Húsavík hospital time history relative acceleration, 4th floor	43
4.21	Húsavík hospital Power spectral density x-component	44
4.22	Húsavík hospital Power spectral density y-component	44
4.23	Húsavík hospital Power spectral density z-component	45
4.24	Horizontal response spectra from measured data on Húsavík	47
4.25	Vertical response spectra from measured data on Húsavík	47
4.26	Horizontal response spectra from measured data on south Iceland	48
4.27	Vertical response spectra from measured data on south Iceland	48
5.1	3D model of the building	49
5.2	Modelled part of the hospital	51
5.3	The distribution of mass in the building	52
5.4	The first mode of the building	54
5.5	The second mode of the building	54
5.6	The third mode of the building	55
5.7	Response, 4th floor sensor recorded vs. computed	56
5.8	Fourier spectra, 4th floor sensor recorded vs. computed	57
5.9	Response, 4th floor sensor recorded vs. computed	57
5.10	Fourier spectra, 4th floor sensor recorded vs. computed	58
5.11	Response, roof sensor recorded vs. computed	58
5.12	Fourier spectra, roof sensor recorded vs. computed	59
5.13	Response, roof sensor recorded vs. computed	59
5.14	Fourier spectra, roof sensor recorded vs. computed	60
6.1	Storey shear for each earthquake action both directions	62
6.2	Displacement for each earthquake action	63
6.3	Storey drifts control for each earthquake action in both directions	65
6.4	Storey shear for Flagbjarnarholt earthquake action	66
6.5	Displacement for Flagbjarnarholt earthquake action	67
6.6	Storey drifts for Flagbjarnarholt earthquake action	68
6.7	Wall facing S-W, critical cross sections used for further inspection	69
6.8	Wall facing N-E, critical cross sections used for further inspection	69
6.9	Wall facing S-E, critical cross sections used for further inspection	70
6.10	Wall facing N-W, critical cross sections used for further inspection	70
6.11	The reinforcement of column A	71
6.12	The reinforcement of column B, C and D	71
6.13	The earthquake induced forces against time for column A1	73
6.14	The earthquake induced forces against time for column B1	73
6.15	The earthquake induced forces against time for column A1	74
6.16	The earthquake induced forces against time for column B4	74
6.17	The natural periods for first three modes vs. the response spectra	75
6.18	M - N diagram	76
6.19	M - N diagram for column A	77

6.20	M - N diagram for column B	77
6.21	The beam cross sections	78
6.22	N-M diagram for beam 1	78
6.23	N-M diagram for beam 2	79
6.24	The counting order of walls	81
A.1	Acceleration Flagbjarnarholt	90
A.2	Fourier spectra Flagbjarnarholt	90
A.3	Horizontal response spectra Flagbjarnarholt	91
A.4	Vertical response spectra Flagbjarnarholt	91
A.5	Acceleration Kaldarholt	92
A.6	Fourier spectra Kaldarholt	92
A.7	Horizontal response spectra Kaldarholt	93
A.8	Horizontal response spectra Kaldarholt	93
A.9	Acceleration Selfoss EERC	94
A.10	Fourier spectra Selfoss EERC	94
A.11	Horizontal response spectra Selfoss EERC	95
A.12	Vertical response spectra Selfoss EERC	95
A.13	Acceleration Sólheimar	96
A.14	Fourier spectra Sólheimar	96
A.15	Horizontal response spectra Sólheimar	97
A.16	Vertical response spectra Sólheimar	97
A.17	Acceleration Þjórsártún	98
A.18	Fourier spectra Þjórsártún	98
A.19	Horizontal response spectra Þjórsártún	99
A.20	Vertical response spectra Þjórsártún	99
A.21	Acceleration Selfoss city hall	100
A.22	Fourier spectra Selfoss city hall	100
A.23	Horizontal response spectra Selfoss city hall	101
A.24	Vertical response spectra Selfoss city hall	101
A.25	Acceleration Hveragerði retirement house	102
A.26	Fourier spectra Hveragerði retirement house	102
A.27	Horizontal response spectra Hveragerði retirement house	103
A.28	Vertical response spectra Hveragerði retirement house	103
A.29	Acceleration Ljósafoss hydro elctric power station	104
A.30	Fourier spectra Ljósafoss hydro elctric power station	104
A.31	Horizontal response spectra Ljósafoss hydro elctric power station	105
A.32	Vertical response spectra Ljósafoss hydro elctric power station	105
B.1	Storey shear for Flagbjarnarholt earthquake action	108
B.2	Displacement for Flagbjarnarholt earthquake action	109
B.3	Storey drifts for Flagbjarnarholt earthquake action	110
B.4	Storey shear for Kaldarholt earthquake action	112
B.5	Displacement for Kaldarholt earthquake action	113
B.6	Storey drifts for Kaldarholt earthquake action	114
B.7	Storey shear for Sólheimar earthquake action	116
B.8	Displacement for Sólheimar earthquake action	117
B.9	Storey drifts for Sólheimar earthquake action	118
B.10	Storey shear for Þjórsártún earthquake action	120

B.11	Displacement for Þjórsártún earthquake action	121
B.12	Storey drifts for Þjórsártún earthquake action	122
B.13	Storey shear for Selfoss city hall earthquake action	124
B.14	Displacement for Selfoss city hall earthquake action	125
B.15	Storey drifts for Selfoss city hall earthquake action	126
B.16	Storey shear for Retirement home earthquake action	128
B.17	Displacement for Retirement home earthquake action	129
B.18	Storey drifts for Retirement home earthquake action	130
B.19	Storey shear for EERC earthquake action	132
B.20	Displacement for EERC earthquake action	133
B.21	Storey drifts for EERC earthquake action	134
B.22	Storey shear for Borgarhraun earthquake action	136
B.23	Displacement for Borgarhraun earthquake action	137
B.24	Storey drifts for Borgarhraun earthquake action	138
B.25	Storey shear for Ljósafoss power station earthquake action	140
B.26	Displacement for Ljósafoss power station earthquake action	141
B.27	Storey drifts for Ljósafoss power station earthquake action	142
C.1	The earthquake induced forces against time for column A1	146
C.2	The earthquake induced forces against time for column B1	146
C.3	The earthquake induced forces against time for column A4	147
C.4	The earthquake induced forces against time for column B4	147
C.5	The earthquake induced forces against time for column A1	148
C.6	The earthquake induced forces against time for column B1	148
C.7	The earthquake induced forces against time for column A4	149
C.8	The earthquake induced forces against time for column B4	149
D.1	The reinforcement of columns	151

List of Tables

2.1	Recommended type 1 elastic response spectra values	10
3.1	E modulus measurements	26
3.2	Location of the sensors of strong motion station IS-706D within the building	27
4.1	Earthquake data recorded at Húsavík	33
4.2	Comparison of data measured in the hospital	33
4.3	Earthquake data collected from The European Strong-motion database .	46
5.1	Total mass of the building per floor	53
5.2	The 12 first modes of the building	54
6.1	Summary of earthquake induced forces	72
6.2	The shear capacity of cross sections	79
6.3	The density ratio of walls in x direction	81
6.4	The density ratio of walls in y direction	82
B.1	Section cut earthquake induced forces Flagbjarnarholt	111
B.2	Section cut earthquake induced forces Kaldarholt	115
B.3	Section cut earthquake induced forces Sólheimar	119
B.4	Section cut earthquake induced forces Þjórsártún	123
B.5	Section cut earthquake induced forces Selfoss city hall	127
B.6	Section cut earthquake induced forces Retirement home	131
B.7	Section cut earthquake induced forces EERC	135
B.8	Section cut earthquake induced forces Borgarhraun	139
B.9	Section cut earthquake induced forces Ljósafoss power station	143

1. Introduction

1.1 Background

This thesis is in the field of earthquake engineering and focuses on dynamic behaviour of a multi-story reinforced concrete building in northern Iceland. The main aspects of the study include structural modelling, system identification and analysis of the response to earthquake strong ground motion.

The case study examined is a hospital built in the late sixties in the town Húsavík on northern Iceland. The town is within the Tjörnes fracture zone and severe earthquake hazard persists on the area. The building's integrity during earthquakes is of vital importance for civil protection and security of local residency.

The main emphasis of the thesis is to develop reliable structural model of the building to support structural monitoring and analysis and furthermore to undertake initial check of structural integrity of the building during induced earthquake excitation. The building will be examined in accordance with the Eurocode standards and critical building components will be examined and compared to modern structural design requirements.

1.2 Problem statement

The hospital is of vital importance for the residents located in and around the area. The Seismic hazard is known and there have been speculations regarding the location and structural integrity of the building. The main focus of this thesis is to examine the structural c

haracteristics and dynamic behaviour of the building to evaluate whether the building can resist strong earthquake excitation. Building codes and standard practises have evolved considerably over the past decades in the field of civil engineering. The building and specific details of the structure will be examined with this in mind.

The earthquake excitation used, is the EN-1998-1 response spectra and strong ground motion measured in southern Iceland in 2000 and 2008. The dynamic properties and response characteristics are obtained with the aid of a monitoring system installed in the building that has provided few examples of full scale records for the building

1.3 Aim and objectives

The aim of this thesis is to develop a structural model to confirm the structural integrity of the Hospital on Húsavík. The focus on the study will be on evaluating the building performance under earthquake excitation.

The main objectives of the study are as followed.

- To set up a monitoring system in the building and monitor the structural response of the 4 story reinforced concrete building
- To construct and calibrate a FE model of the structure.
- To use recorded strong ground motion to estimate structural characteristics of the building.
- To choose suitable excitation for response evaluation.
- To evaluate the response of the building.
- To review the structural integrity of critical building components.

1.4 Research methodology

This research is a case study based on full scale experimental data, dynamic analysis, finite element modelling and design detailing of critical building components. The Earthquake engineering Centre of the University of Iceland (EERC-UI) have array of accelerometers located in the town of Húsavík called ICEARRAY II. The project have been ongoing since 2012. The projects main emphasis is to monitor strong motions from earthquakes in the Tjörnes fracture zone and the Northern Volcanic zone of Iceland and mapping the incoherence of strong motion across the town of Húsavík. The town is located on top of the Húsavík-Flatey Fault system (HFF) which is the largest transform fault in Iceland. In case of strong earthquake event on the HFF the project aims to capture the intense near-fault motion and the associated permanent displacements [1].

This thesis is part of the ICEARRAY II project and is somewhat a consequence of speculations due to earthquake hazard on the area. The accelerometers are provided by The EERC-UI and the recordings have been ongoing for one year now and few notable events have occurred.

1.5 Scope of work

The preparations started in May 2015 with three weeks introduction of the monitoring system at the Earthquake Engineering Research Center at the town of Selfoss. The introduction was followed by an on site visit and installation of the monitoring system and measurements of the concrete E-modulus. After the visit the FE modelling started.

The main work of this thesis started January 2016 The thesis is divided into seven main chapters along with references and appendixes. The following list explains the subject covered in each chapter.

- Chapter one introduces the project and its aim and it also discusses the objectives and expectations.
- Chapter two contains general and local information about local seismicity and the methodology used for processing of data.
- Chapter three gives description of the building and the installed monitoring system.
- Chapter four contains processing of the earthquake induced acceleration data, both the data measured in the hospital and also the ground motion data gathered from the European strong motion database.
- Chapter five introduces the finite element modelling and system identification of the building.
- Chapter six contains the analysis performed and the main results of calculations along with inspection of reinforced detailing.
- Chapter seven contains the main findings and the conclusions deducted from the results.

2. Earthquake action and structural response

2.1 Earthquake

An earthquake is described as a sudden ground motion caused by instantaneous release of strain that has accumulated over long time in the earth's crust. The most destructive earthquakes are caused by dislocation of the crust [2].

Understanding of the earth's composition is important for further details. The earth has four major layers, the inner core, outer core, mantle and crust. The top of the mantle and the crust make up a thin skin on the surface of the earth, this skin is however not all in one piece but in many pieces like a puzzle and those puzzles move slowly around and slide past one another and bump into each other. These puzzles are called tectonic plates (lithosphere), and the edges of the plates are called the plate boundaries. Most of the earthquakes around the world occur on the plate boundaries since the edges of the plates are rough they get stuck while rest of the plate keeps moving. An earthquake will happen when the plate has moved far enough and the edges unstuck on one of the faults, this phenomena is explained by the theory of large scale tectonic processes, referred to as plate tectonics. The plate tectonics theory derives from the theory of continental drift and seafloor spreading [2] [3].

The theory of continental drift assumes that the lithosphere is divided into 15 rigid plates including continental and oceanic crusts. Earthquakes frequently occur at the plate boundaries and the plate boundaries are also called seismic belts. The two most seismically active belts are the Circum-Pacific and Eurasian belts. Figure 2.1 gives graphical vision on how the earthquakes worldwide follow the plate boundaries and the distribution of earthquakes around the world

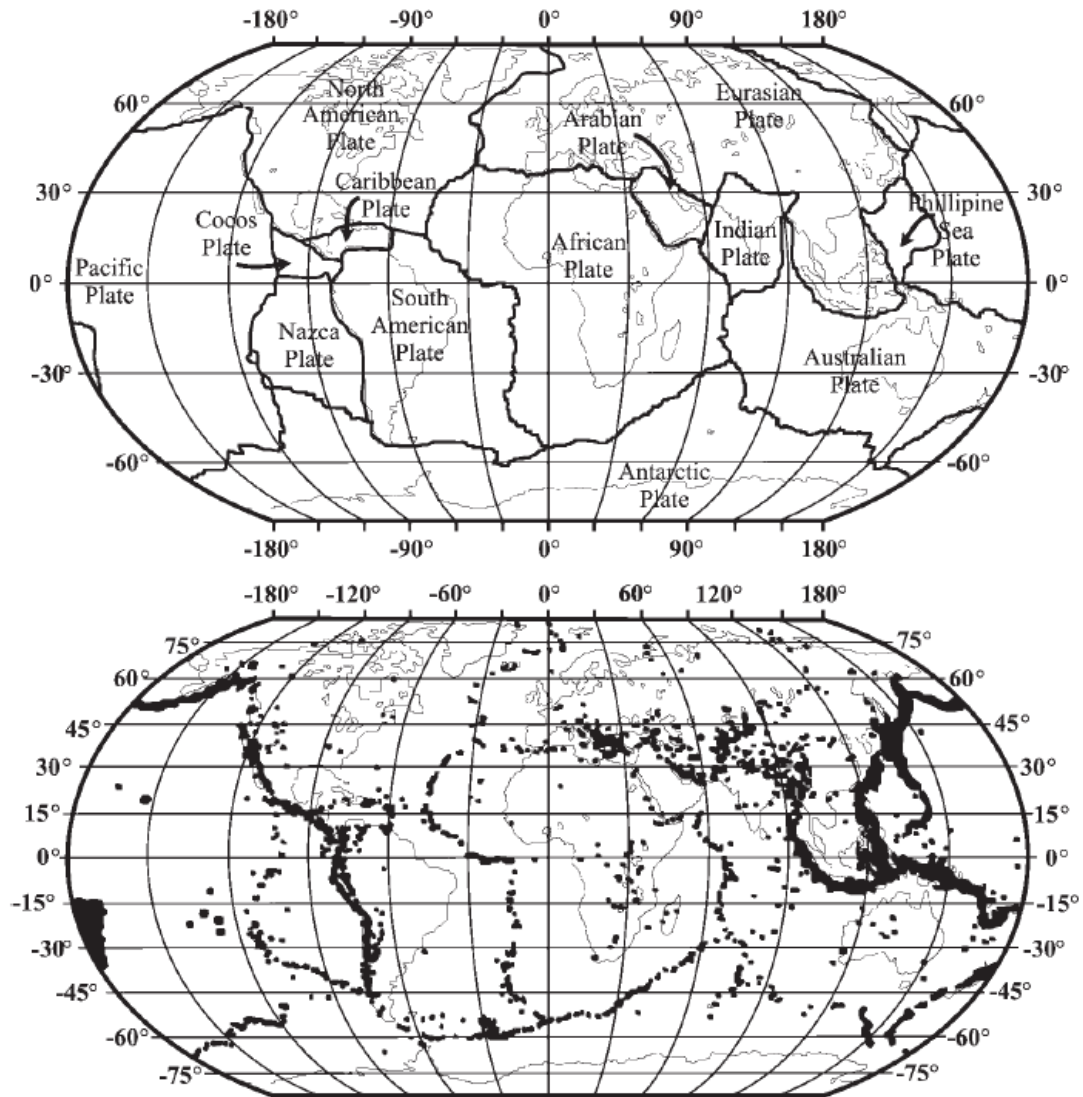


Figure 2.1: Tectonic plates on top and worldwide earthquake distribution [3]

Seismic waves are a result of fault ruptures caused by brittle fractures of the earth's crust that dissipate up to 10 % of the the total plate tectonic energy. The elastic seismic waves can be classified as two types, body waves and surface waves. The ground motion is generally a combination of these waves, especially near field. Body waves also known as P and S waves are often called preliminary tremors because they are felt first in most earthquakes. P-waves have little damage capability. S-waves cause vertical and horizontal side to side motion and can cause significant damage. The arrival time and speed of body waves depends upon the density and elastic properties of the rock and soil that they will pass on their way. P-waves travel faster at 1.5 to 8 km/s while S-waves usually travel at 50 - 60 % of the speed of P-waves [3].

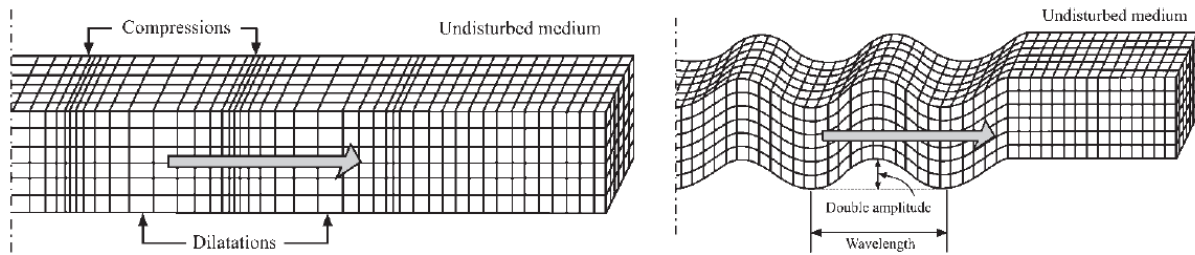


Figure 2.2: Travel path mechanisms of body waves: P-waves to left and S-waves to right [3]

Surface waves include Love waves (LQ-waves) and Rayleigh waves (LR-waves). These waves generally induce large displacements and hence are also called principal motion. Surface waves are most noticeable in shallow earthquakes. Surface waves are likely to cause severe damage to structural systems during earthquakes because of their long duration [3].

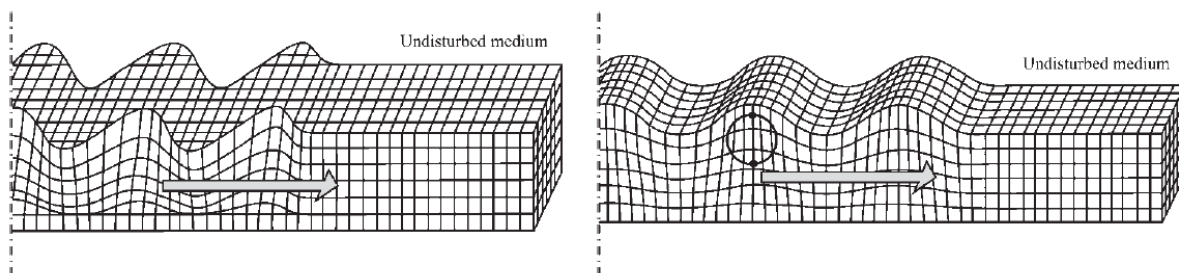


Figure 2.3: Travel path mechanisms of surface waves: Love-waves to left and Rayleigh-waves to right [3]

2.2 Seismic information

Estimation of ground motion expected at each location in the future should be based on hazard assessment according to Eurocode 8. The seismic action to be considered for design purposes is normally represented by hazard curves that show the exceedance probability of a certain seismologic parameter, this parameter can be the peak ground acceleration, velocity or displacement for a given period of exposure, at a certain location [4].

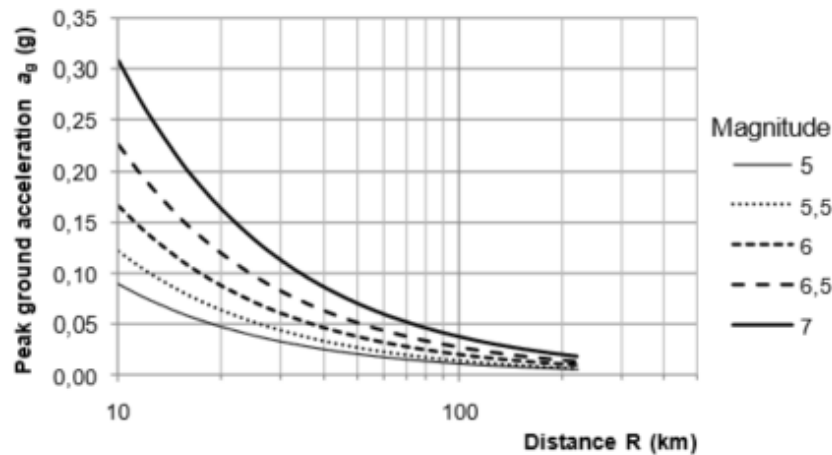


Figure 2.4: Attenuation relationship for peak ground acceleration proposed by Ambraseys [4]

Peak values of ground motion parameters are however not a good measure of local intensity and possible damage without the epicentral distance see figure 2.4. Seismic hazard is therefore often described by the values of the spectral ordinates. Still Eurocode 8 describes earthquake hazard only by the value of reference peak ground acceleration on ground type A. For each country, the seismic hazard is described by a zonation map defined by the national authorities. This map divides national territories into seismic zones and the hazard within each zone is assumed to be constant. Figure 2.5 is a hazard map for Iceland [4] [5].

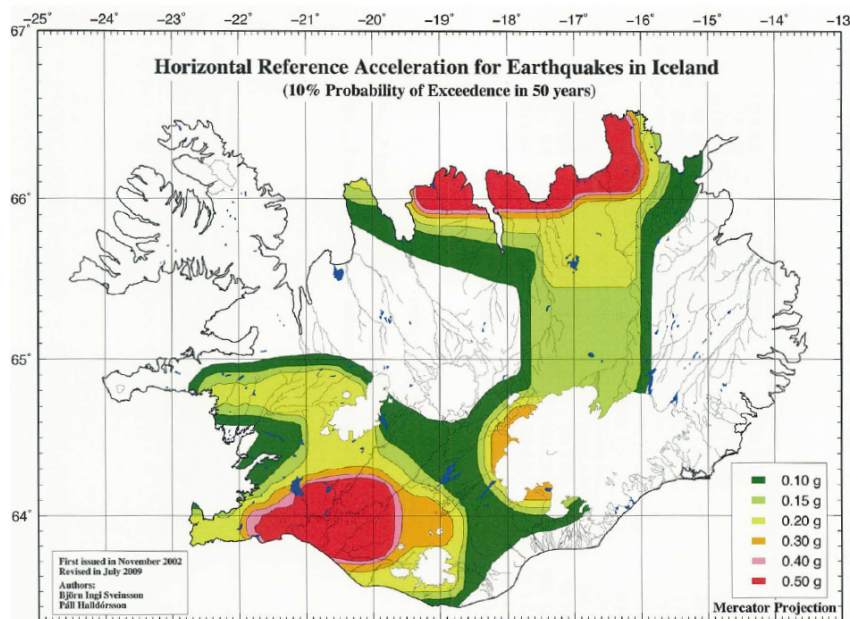


Figure 2.5: Hazard map for Iceland. Horizontal reference acceleration type A ground with a mean return period of 475 years [5].

2.2.1 Methods of analysis

To evaluation of deformations and internal forces induced by applied loads or ground excitations is an necessary part of designing structures to resist earthquakes. The procedure of structural analysis requires the following [6]

- Representation of earthquake ground motions.
- Model of the structure.
- Method of analysis.

For the representation of earthquake ground motions there are essentially three methods available. The response spectrum, lateral load distribution and representation of time-history. The response spectrum is a plot of the peak of steady state response of series of oscillations with varying natural frequency or period, which are forced into motion by the same base vibration. The lateral load distribution is a function of ground and structure natural periods, based on the assumptions that the structure response is controlled by the vibration modes. Representation of time-history acceleration in function of site-recorded ground motions or artificial accelerogram compatible with the design response spectrum [6].

A set of structural analysis methods are used in practice and their complexity varies from very simple to the most complex ones. The simplified analyses call for engineering judgement. The difference of the methods is the way that they contain seismic input and the idealization of the structural response. Design philosophy according to current codes requires that a structure must not collapse and should retain its structural integrity under rare strong earthquakes and can not be damaged by frequent moderate earthquakes. Five distinct analytical procedures methods of structural analysis can be used [6].

- Linear equivalent static analysis
- Linear response spectrum analysis
- Linear dynamic analysis
- Non-linear static (Push-over) analysis
- Non-linear dynamic (Time-history) analysis

2.2.2 Response spectra according to Eurocode 8

The elastic design response spectra is well known in civil and earthquake engineering it represents earthquakes in the form of an equivalent force applied to structure. The forces are determined from the maximum acceleration response of the structure under expected induced ground shaking [7].

The horizontal elastic response spectra is defined by the following expressions:

$$0 \leq T \leq T_B : S_e(T) = a_g \cdot S \left[1 + \frac{T}{T_B} \cdot (\eta \cdot 2.5 - 1) \right] \quad (2.1)$$

$$T_B \leq T \leq T_C : S_e(T) = a_g \cdot S \cdot \eta \cdot 2.5 \quad (2.2)$$

$$T_C \leq T \leq T_D : S_e(T) = a_g \cdot S \cdot \eta \cdot 2.5 \cdot \left[\frac{T_C}{T} \right] \quad (2.3)$$

$$T_D \leq T \leq 4s : S_e(T) = a_g \cdot S \cdot \eta \cdot 2.5 \cdot \left[\frac{T_C T_D}{T^2} \right] \quad (2.4)$$

The values of the periods T_B , T_C and T_D and the soil factor S describing the shape of the elastic response spectrum depend upon the ground type. Horizontal spectra of type 1 is showed in figure 2.6 for ground types A to E. If deep geology is not accounted for it is recommended to use both types 1 and 2 [5].

Table 2.1: The values of parameters describing the recommended type 1 elastic response spectra according to Eurocode 8 [5]

Ground type	Description of stratigraphic profile	$V_{s,30}$	N_{SPT}	C_u	S	$T_B(B)$	$T_C(B)$	$T_D(B)$
[-]	[-]	m/s	blows/30cm	kPa	[-]	[-]	[-]	[-]
A	Rock or rock like geological formation	> 800	[-]	[-]	1.0	0.15	0.4	2.0
B	Very dense sand, gravel or very stiff clay	360 - 800	> 50	> 250	1.2	0.15	0.5	2.0
C	Deep deposits of dense sand, gravel or stiff clay	180 - 360	15 - 50	70 - 250	1.15	0.2	0.6	2.0
D	Deposits of loose to medium cohesionless soil	< 180	< 15	< 70	1.35	0.2	0.8	2.0
E	A soil of a surface alluvium layer	[-]	[-]	[-]	1.4	0.15	0.5	2.0

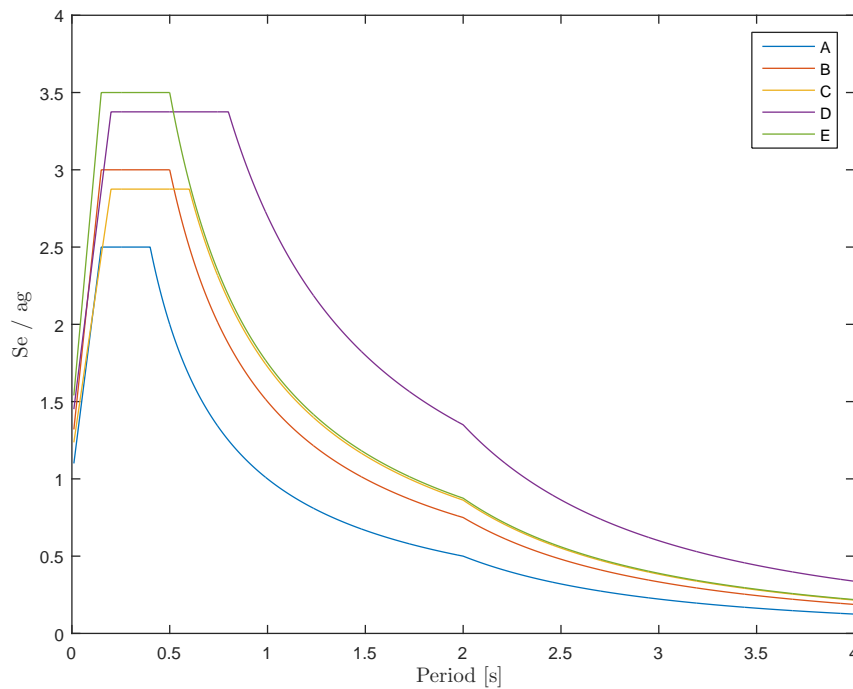


Figure 2.6: Elastic horizontal type 1 spectra for ground types A to E

Figure 2.6 shows the recommended horizontal response spectra according to different ground types. The effects due to ground conditions are clear and the peak acceleration is very dependant of ground parameters as is the duration of the maximum acceleration due to certain period.

2.2.3 Icelandic and local seismicity

Icelandic seismicity is very dependent on the geological setting of the country. Iceland is located at the intersection of the Mid-Atlantic ridge and the Greenland-Iceland-Faeroe ridge. The Mid-Atlantic ridge lies on the diverging plate boundary of the American and the Eurasian plates as figure 2.7 shows. According to repeated regional GPS measurements it is believed that the spreading rate is near 1 cm/y [8].

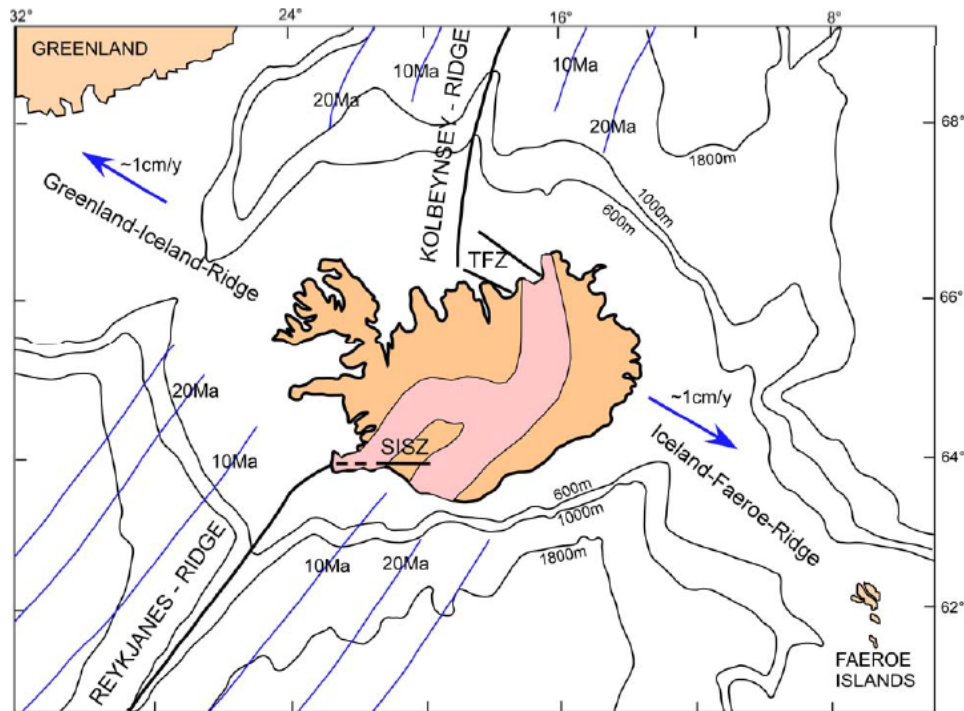


Figure 2.7: The tectonic setting of iceland [8]

The largest earthquakes in Iceland have occurred within the fracture zones i.e. the South Iceland seismic zone and the Tjörnes fracture zone. These earthquakes are mostly associated with a strike-slip motion at shallow depth of 5 to 10 km. In the South Iceland seismic zone earthquakes tend to occur every 100 years as sequences. A known sequence started 1896 and finished after six earthquakes with $M_{Max} = 7$ in 1912. After 100 years there was another sequence which started in June 2000 and finished on May 2008 with $M_{Max} = 6,3$ [9].

Seismicity in Northeast Iceland can mainly be attributed to the Tjörnes fracture zone. Seismicity in this region has been monitored since 1994 and earthquakes cluster on two northwest trending lineaments named Grímsey-Kópasker lineament and the Húsavík-Flatey fault (HFF). Figure 2.9 shows the Tjörnes fracture zone and relevant lineaments. Figure 2.8 shows distribution of large earthquakes in northern Iceland on HFF and Grímsey-Kópasker lineament [8].

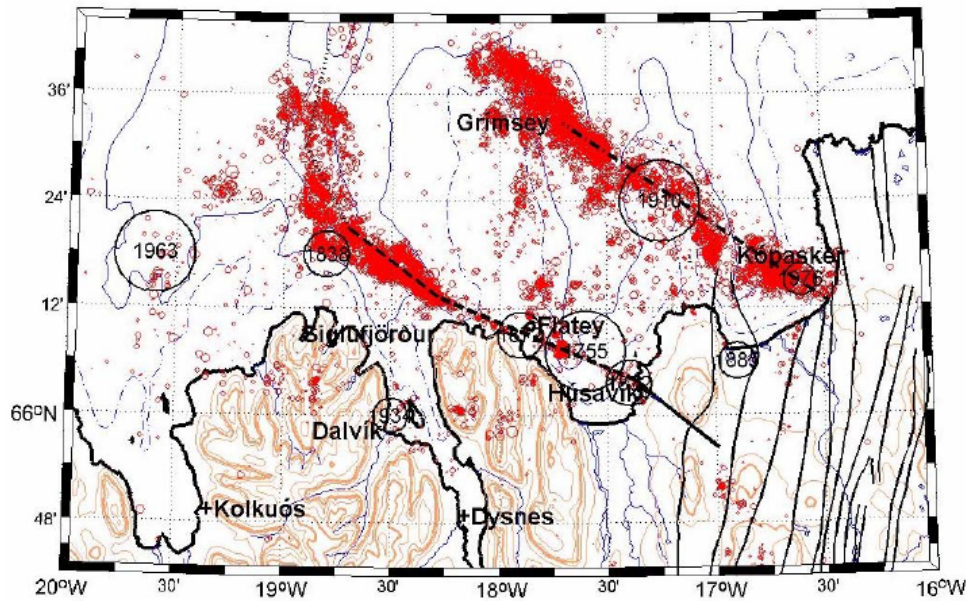


Figure 2.8: Distribution of earthquakes ($M \leq 6$) in north Iceland [8]

The main emphasis in this thesis is the seismic activity in the Húsavík area and the related hazards. The main activity in the region are due to large earthquakes on the Húsavík Flatey fault. The only damaging earthquake on the HFF known before 1755 occurred in 1260, and is described in medieval annals from the region as the great earthquake in Flatey. Though the HFF is known for earthquakes estimated to be of magnitude 7 no major earthquake has occurred since 1872. Notable earthquake sequences within the zone occurred in 1940 to 1944 and the largest earthquake was of magnitude 5.6. No earthquakes have exceeded magnitude 4 on the fault since 1973 [8].

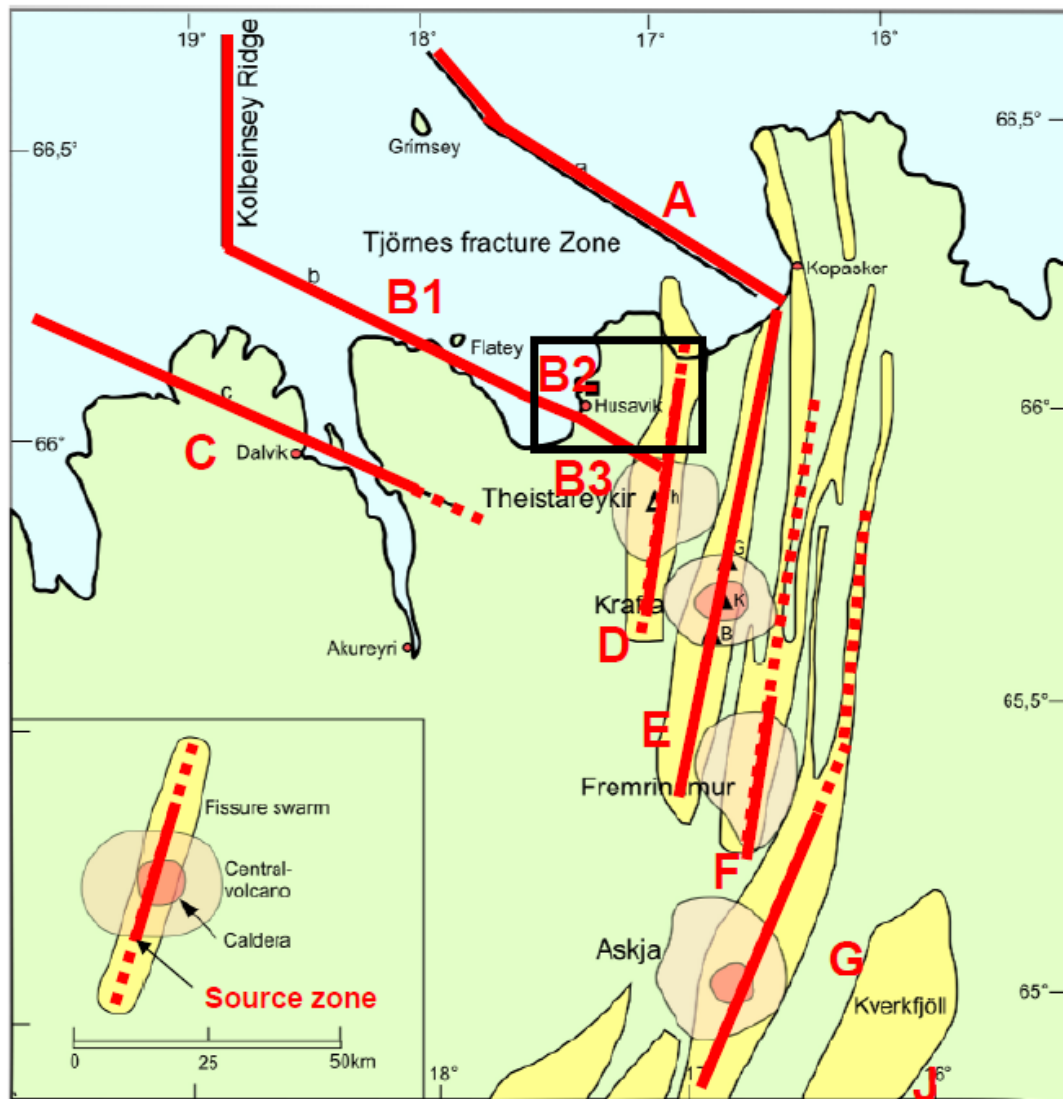


Figure 2.9: The seismic source zones and lineaments near Húsavík. The solid red lines indicate seismic source zones producing earthquakes with magnitude greater than or equal to 4 and the dotted lines refer to source zones where event magnitude does not exceed 4. [8]

2.3 Structural dynamics

2.3.1 Single degree of freedom systems

Earthquakes induce dynamic excitations on structures. The load causes structures to vibrate in response to the dynamic excitation. For simple structures this behaviour can be described through a single degree of freedom system (SDOF). Single degree of freedom system can be idealized as lumped mass m , supported by a massless structure with stiffness k in the lateral direction. As the vibration amplitude of the structure

decays as the excitation terminates, the system is considered to have certain amount of damping, c [10].

Figure 2.10 shows a simple SDOF model as a lumped mass system. The mass is assumed to be fixed, the spring and the damper assumed to have no mass and the mass is only considered to be able to move in one direction, along the length of the spring.

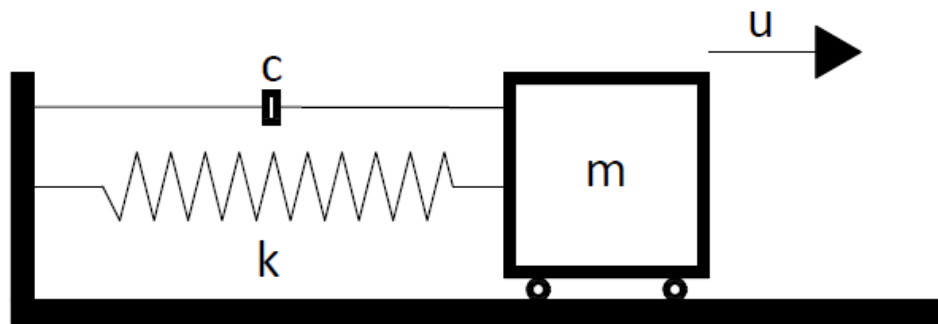


Figure 2.10: Lumped mass SDOF system commonly known as mass spring damper system

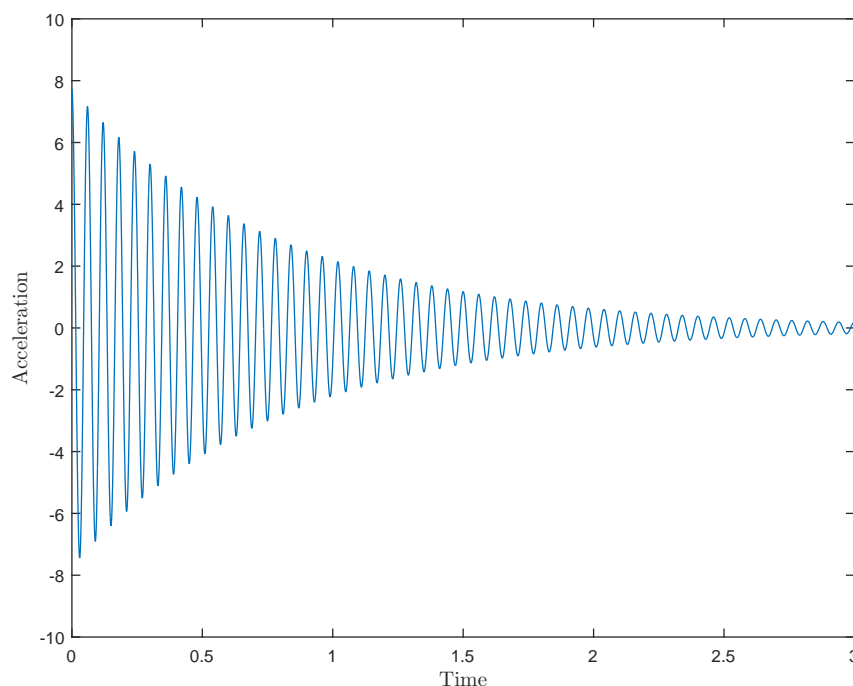


Figure 2.11: Experimental data showing the motions decay in a freely vibrating SDOF system.

It is called free vibration when a structure is disturbed from its static equilibrium state and is allowed to vibrate without any external dynamic excitation. The rate of the motion decay in free vibration is controlled by the damping see figure 2.11. There-

fore the natural frequency and critical damping ratio of structure can be decided from experimental data [10].

Free vibration of a structure is when a structure has been disrupted from its static state and is vibrating freely without external load. The equation of motion for a free vibration of SDOF system is expressed as:

$$m\ddot{u} + c\dot{u} + ku = 0 \quad (2.5)$$

Where u is the displacement of the system, \dot{u} is the first derivative velocity and \ddot{u} is the second derivative acceleration.

The natural frequency of system describes the number of vibration cycles over time unit. The natural frequency has the time unit of radians per second and can be evaluated by:

$$\omega_n = \sqrt{\frac{k}{m}} \quad (2.6)$$

The time it takes undamped system of free vibration to go one cycle is called the natural period of vibration of the system and is evaluated by:

$$T_n = \frac{2\pi}{\omega_n} \quad (2.7)$$

A system completes $1/T_n$ cycles in 1 second. This is called the natural cyclic frequency of vibration and has the unit Hz, that expression is denoted by:

$$f_n = \frac{1}{T_n} \quad (2.8)$$

The natural vibration properties mentioned in equations 2.6, 2.7 and 2.8 depend only on the mass and stiffness of the structure. For example we consider two SDOF systems with same mass. The stiffer system will have higher natural frequency and shorter natural period. Likewise, the heavier structure of two having same stiffness will have lower natural frequency and the longer period [10].

The damping coefficient is a measure of the energy degenerated in a cycle of free vibration or in a cycle of forced harmonic vibration. The critical damping ratio(ζ) is a function of the mass, damping and the natural frequency of the system [10].

$$\zeta = \frac{c}{2m\omega_n} \quad (2.9)$$

To find the damping ratio of underdamped system in the time domain the logarithmic decrement is used. The logarithmic decrement is the natural log of the amplitudes of any two consecutive peaks separated by period T_D . The logarithmic decrement is denoted by δ and is expressed as:

$$\delta = \ln \frac{u_i}{u_{i+1}} = \frac{2\pi\zeta}{\sqrt{1-\zeta^2}} \quad (2.10)$$

The logarithmic decrement can be approximated if the critical damping ratio is small and the following expression applies.

$$\sqrt{1-\zeta^2} \simeq 1 \quad (2.11)$$

The approximated value for the logarithmic decrement is then

$$\delta \simeq 2\pi\zeta \quad (2.12)$$

Underdamped ($\zeta < 1$) systems are of special interest for structural engineers. Underdamped systems oscillate about its equilibrium position with a progressively decreasing amplitude. Civil engineering structures of all types typically fall into this category and generally have damping ratio less than 10 %. [10]. Damping of structures has major impact on the response and accurate estimation of the critical damping ratio is important [11].

A structure that experiences earthquake excitation is assumed to move along with the ground. The motion of a SDOF system excited by ground motion is expressed by equation

$$m\ddot{u} + c\dot{u} + ku = -m\ddot{u}_g(t) \quad (2.13)$$

The earthquake excitation produces external force equal to $-m\ddot{u}_g(t)$ acting on top of the structure in opposite direction. Added mass will lead to increase in dynamic force acting on the structure. The response of a system that undergoes earthquake excitation is only dependent on the natural frequency and critical damping ratio. This can be shown by dividing equation 2.13 with the mass. This will result in the following [10].

$$\ddot{u} + 2\zeta\omega_n\dot{u} + \omega_n^2 u = -\ddot{u}_g(t) \quad (2.14)$$

2.3.2 Multi degree of freedom systems

All structures are multi degree of freedom systems. Similar to the SDOF system a MDOF system can be thought of as many lumped masses, m_i , supported by mass-less columns each with certain stiffness, k_i and damping, c_i . The MDOF system can also be demonstrated as serial connected mass-spring-damper SDOF systems, where the masses move independently in the direction of the springs.

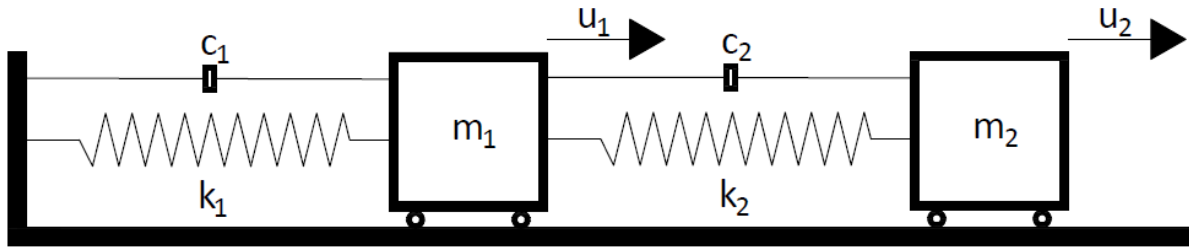


Figure 2.12: MDOF lumped mass spring damper system

The equation of motion for a forced vibration of a MDOF system can be expressed as:

$$[M]\ddot{\vec{u}} + [C]\dot{\vec{u}} + [K]\vec{u} = \vec{P} \quad (2.15)$$

Where \vec{P} is the external load vector acting on the structure e.g. earthquake excitation. Acceleration, velocity and displacement vectors are represented with overline arrow. [10]. Similarly the equation of motion for free vibration of MDOF system can be expressed as

$$[M]\ddot{\vec{u}} + [C]\dot{\vec{u}} + [K]\vec{u} = 0 \quad (2.16)$$

Where $[M]$ equals mass matrix, $[C]$ equals damping matrix and $[K]$ equals stiffness matrix.

Buildings vibrate in different dynamic parameters for each mode shape. The mode shapes with the lowest frequencies generally provide the greatest response. For MDOF system the natural frequencies and mode shapes can be computed for each mode of vibration by the eigenvalue problem.

$$[k - \omega_n^2 m]\Phi_n = 0 \quad (2.17)$$

The natural vibration properties for MDOF system are evaluated as previously described for SDOF systems. Different mode shapes are demonstrated on figure 2.13

according to the lumped mass system. The figure shows mode shape one and two for different times in one vibration cycle [10].

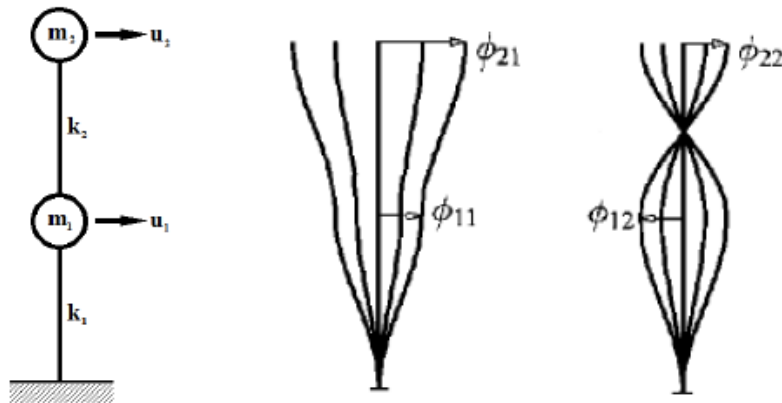


Figure 2.13: Mode shapes for different times in vibration cycle [10].

Modal analysis of linear damped MDOF system is preferable when we have systems with many degrees of freedom. The transformation to modal coordinates is an efficient way to define the dynamic response of a system. The equation of motion is as before:

$$[M]\ddot{\vec{u}} + [C]\dot{\vec{u}} + [K]\vec{u} = \vec{P}(t) \quad (2.18)$$

The vector $\vec{P}(t)$ is the load vector at any given time. The modal matrix is defined as Φ where the n-th column of the matrix is the n-th mode shape of the system. This means that

$$\vec{u} = [\Phi]\vec{q} \quad (2.19)$$

$$\dot{\vec{u}} = [\Phi]\dot{\vec{q}} \quad (2.20)$$

$$\ddot{\vec{u}} = [\Phi]\ddot{\vec{q}} \quad (2.21)$$

By performing a modal decoupling of equation 2.18 by replacing and pre multiplying by the transpose of Φ we get the equation

$$[\Phi]^T[M][\Phi]\ddot{\vec{q}} + [\Phi]^T[C][\Phi]\dot{\vec{q}} + [\Phi]^T[K][\Phi]\vec{q} = [\Phi]^T\vec{P}(t) \quad (2.22)$$

This relation can be described as followed due to the orthogonality properties of the

mode shapes.

$$[M^*]\ddot{\vec{q}} + [C^*]\dot{\vec{q}} + [K^*]\vec{q} = \vec{P}(t) \quad (2.23)$$

The diagonal modal matrices in equation 2.23 are marked with the symbol "*" and means that number of coupled equations have been replaced by number of single degree of freedom systems. This will give equation of motion on the following form for every mode [10].

$$m_n^*\ddot{q}_n + c_n^*\dot{q}_n + k_n^*q_n = p_n^*(t) \quad (2.24)$$

2.3.3 Time domain analysis

The analytical solution of the equation of motion for a single or multi degree of freedom is usually not possible if the excitation $p(t)$ or the ground acceleration $\ddot{u}_g(t)$ varies arbitrarily with time or if the system is nonlinear. To calculate the dynamic response of such problems numerical time stepping methods for integration of differential equations can be used [10].

For an inelastic system the equation of motion to be solved numerically is

$$[M]\ddot{\vec{u}} + [C]\dot{\vec{u}} + [K]\vec{u} = \vec{P} \quad (2.25)$$

Although the time stepping method is capable of calculating problems regardless of the damping type including nonlinear damping we assume the system to have linear viscous damping in this example. The time interval is usually taken as a constant and the response is determined at the discrete time instants t_i . The acceleration, velocity and displacement is assumed to be known. The numerical calculations will enable us to compute the response quantities u_{i+1} , \dot{u}_{i+1} and \ddot{u}_{i+1} at time $i + 1$.

$$\Delta t_i = t_{i+1} - t_i \quad (2.26)$$

$$m\ddot{u}_i + c\dot{u}_i + ku_i = p_i \quad (2.27)$$

$$m\ddot{u}_{i+1} + c\dot{u}_{i+1} + ku_{i+1} = p_{i+1} \quad (2.28)$$

In the field of earthquake engineering it is common to use Newmark's beta method to calculate dynamic response quantities of structures. The integration process of new-

mark's beta method can be described as followed.

$$\dot{u}_{i+1} + [(1 - \gamma)\Delta t]\ddot{u}_i + (\gamma\Delta t)\ddot{u}_{i+1} \quad (2.29)$$

$$u_{i+1} = u_i + (\Delta t)\dot{u}_i + \left[\left(\frac{1}{2} - \beta\right)(\Delta t)^2\right]\ddot{u}_i + [\beta(\Delta t)^2]\ddot{u}_{i+1} \quad (2.30)$$

The variation of acceleration over a time step is defined by the parameters β and γ that determines the stability and accuracy characteristics of the method. The typical selection for γ is $\frac{1}{2}$ and the β parameter is either set as $\frac{1}{4}$ and then the constant average acceleration method is used or the parameter is set to $\frac{1}{6}$ and then the linear acceleration method is used.

2.3.4 Frequency domain analysis

Frequency domain spectral analysis can be performed in order to obtain the response of linear systems subjected to random excitations [12]. The Fourier transform is a powerful method to derive the solution of linear differential equations especially for SDOF systems and therefore the frequency domain analysis is commonly used [10].

The Fourier transform $P(\omega)$ with excitation function $p(t)$ is evaluated as:

$$P(\omega) = F[p(t)] = \int_{-\infty}^{\infty} p(t)e^{-i\omega t} dt \quad (2.31)$$

The Fourier transform $U(\omega)$ of the solution $u(t)$ of the differential equation is then given by:

$$U(\omega) = H(\omega)P(\omega) \quad (2.32)$$

The complex frequency response function $H(\omega)$ describes the response of the system to harmonic excitation. The desired solution is then given by the inverse Fourier transform of $U(\omega)$

$$u(t) = \frac{1}{2\pi} \int_{-\infty}^{\infty} H(\omega)P(\omega)e^{i\omega t} d\omega \quad (2.33)$$

For dynamic analysis of linear systems The frequency response method can be used under any type of excitation [10].

2.4 System identification

The main goal of any system identification analysis is to evaluate the properties of an unknown system according to known input and output from the system. Figure 2.14 shows the process of system identification [13].

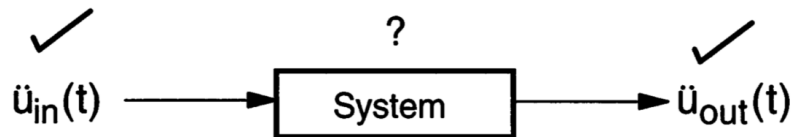


Figure 2.14: Schematic of system identification problem [13]

System identification in structural dynamics refers to an estimation of the dynamic characteristics of a structure based on recordings of its dynamic motion. Considering structural dynamics the characteristics of a structure that can be estimated with system identification are damping ratios, mode shapes, frequencies and participation factors. To obtain these parameters it is in most cases sufficient to use a pair of input and output recordings [14].

Such as earthquake input excitation and output response. The ground acceleration is recorded as input parameter and the output is the response at higher level in the building recorded at exact same time. Figure 2.15 shows the principle.

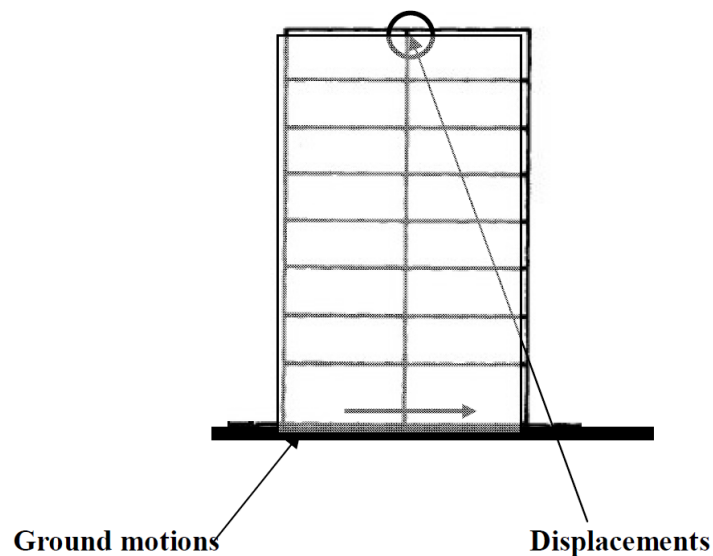


Figure 2.15: Ground motion input gives simultaneous displacement output [6]

3. The case studied

3.1 The building

The study building is a multi-story reinforced concrete structure built 1964. The building has 4 stories total, above ground level there are 3 storeys and a small tower for technical utilities e.g. ventilation. The basement is partially buried as can be seen on figures 3.1 and 3.2.

The total height of the building is 15,2 meters. The size of the ground level is 633 square meters with length of 28,5 m and width of 22,2 m. The structural system consists of concrete walls, columns, beams and slabs, the thickness of the slabs varies from 120 - 240 mm.



Figure 3.1: The Húsavík hospital seen from south west direction



Figure 3.2: The Húsavík hospital seen from north west direction

The plan view of the hospital is showed in figure 3.3. The figure is a plan view for 1st floor of the hospital and shows the connection to the retirement home Hvammur to the left and connection to the health care to the right. As can be seen on figure 3.3 the building has many load carrying walls in both directions and the structural system provides a lot of redundancy.

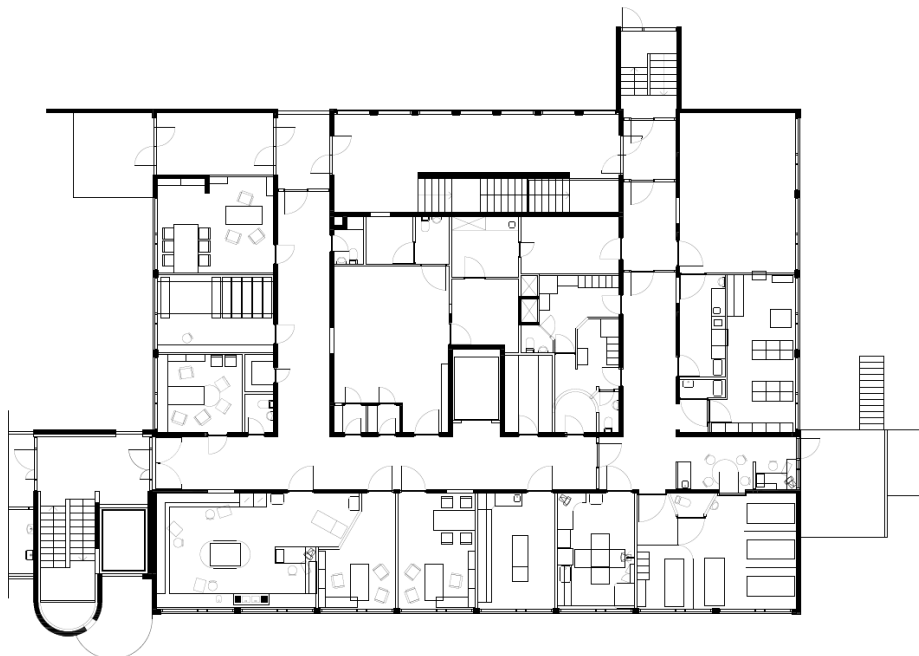


Figure 3.3: Design drawing of the hospital 1st floor [15]

The concepts of structural design in seismic areas have evolved fast since the first methods that were developed due to experience of catastrophic events in early 1900 such

as the Messina earthquake in 1909. Seismic design can be split into three generations of methods. The first methods used was to design structures to withstand uniform horizontal accelerations of the order of 0.1g. Experimental data gathered after the Long beach earthquake in 1933 showed that the ground accelerations could be much higher or near 0.5g [7].

Since then the seismic codes have evolved and to day the Eurocode represents the current 3rd generation. This generation makes it possible to specify a way to take the energy dissipation into account according to the type of lateral resistance and the type of structural material used along with geotechnical aspects.

3.2 Material properties of concrete

According to the building documentation the concrete used is equivalent to the strength class C25/30 in the Eurocodes. The corresponding modulus of elasticity is $E_{CM} = 31$ GPa [16]. To assess the accuracy of the modulus of elasticity in the concrete used in the building ultrasonic pulse velocity measurements were undertaken. To perform the measurements an instrument manufactured by CNS Instruments Ltd. was used.

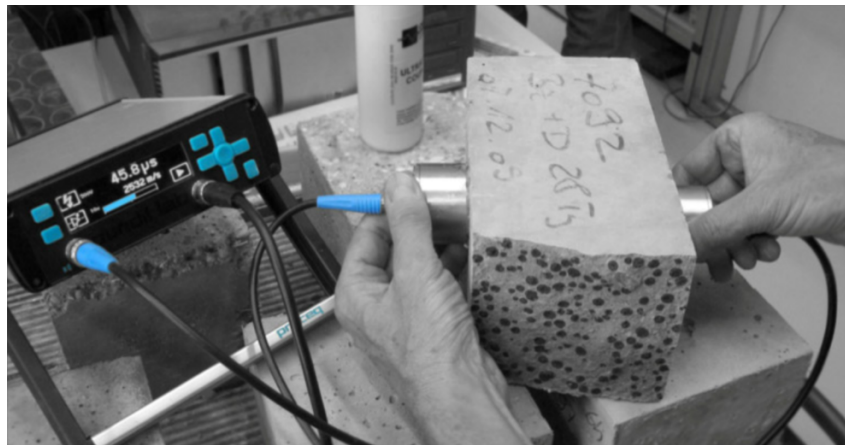


Figure 3.4: A ultrasonic pulse velocity measurement

The instrument shoots pulses of sound waves between the receivers and the relationship between the velocity and time of the sound passing through the wall determines the modulus of elasticity of the wall, equation 3.1 is used to calculate the modulus.

$$E = \frac{V_L^2 \rho (1 + \nu)(1 - 2\nu)}{1 - \nu} \quad (3.1)$$

Table 3.1: E modulus measurements in the hospital

Floor	Location	Time	Distance	Velocity	Poisson's ratio	Density	E
		μs	mm	m/s	-	kg/m^3	GPa
Basement	Workshop	64	230	3594	0.2	2400	27.9
Basement	Laundry	55.5	218	3928	0.2	2400	33.3
Basement	Stairway	65	240	3692	0.2	2400	29.4
1. floor	Stairway	64	226	3531	0.2	2400	26.9
1. floor	WC	56.6	224	3958	0.2	2400	33.8
1. floor	WC	57	231	4053	0.2	2400	35.5
2. floor	Living room	67	226	3373	0.2	2400	24.6
2. floor	Living room	62	235	3790	0.2	2400	31.0
2. floor	Column room 212	101	360	3564	0.2	2400	27.4
3. floor	Corner over 212	46.7	170	3640	0.2	2400	28.6
3. floor	vaktstofa	61.7	241	3906	0.2	2400	33.0
3. floor	Living room	54.5	222	4073	0.2	2400	35.8
Average				3759		Average	30.6

The E-modulus measurements were performed on three different places for each floor as can be seen in table 3.1 and because of relatively low value for the laundry room on 3rd floor the 4th measurement was taken in the living room. That is important to measure only through concrete when performing the measurements to approximate the E modulus, any flaw, reinforcement or plumbing will distort the measurement.

The test results are very close to the expected modulus. The elastic modulus according to EN 1992-1 for C25/30 concrete is 31 GPa and according to the Icelandic national annex this value should be decreased by 0,9 to consider Icelandic aggregates. The E modulus is then near 28 GPa. The measured value is 30,6 GPa, the nominal density of normal weight concrete is taken as 2400 kg/m³ in accordance with Table A.1 in EN1991-1-1:2002 Further calculations in this study are therefore depending on the reduced value according to EN 1991-1-1.

3.3 The monitoring-system

The monitoring system was installed in the building in middle of may 2015 and consists of 3 triaxial accelerometers located at three levels in the building. The accelerometers record any response and the sampling rate is 200 Hz. The ground motion is recorded through sensor on the ground floor and the response is recorded with the

other two sensors located on the floor in the utility room on 5th floor and at the top corner of the fourth floor. Figure 3.6 shows the height level of the sensors.

The sensor's location and their components are explained in figures 3.5 and 3.6. Figure 3.5 shows a plan view of the building at no particular height. The components of all the sensors has the same degree from north. Table 3.2 shows the coordinates of the sensors. The top right corner of the figure shows the orientation of the building relative to north direction and it can be seen that the long side has direction of 318° from north and the short side is 90° less to north or 228° . The components pointing 318° and 228° from north is positive on the sensors recordings.

Table 3.2: Location of the sensors of strong motion station IS-706D within the building

Name	Nr	Location	X	Y	Z
[-]	[-]	[-]	[m]	[m]	[m]
IS 706D1	Sensor 1	Roof	16.2	16	12.4
IS 706D2	Sensor 2	4th floor	28.1	0.4	12.1
IS 706D3	Sensor 3	Ground	15	10.5	-0.6

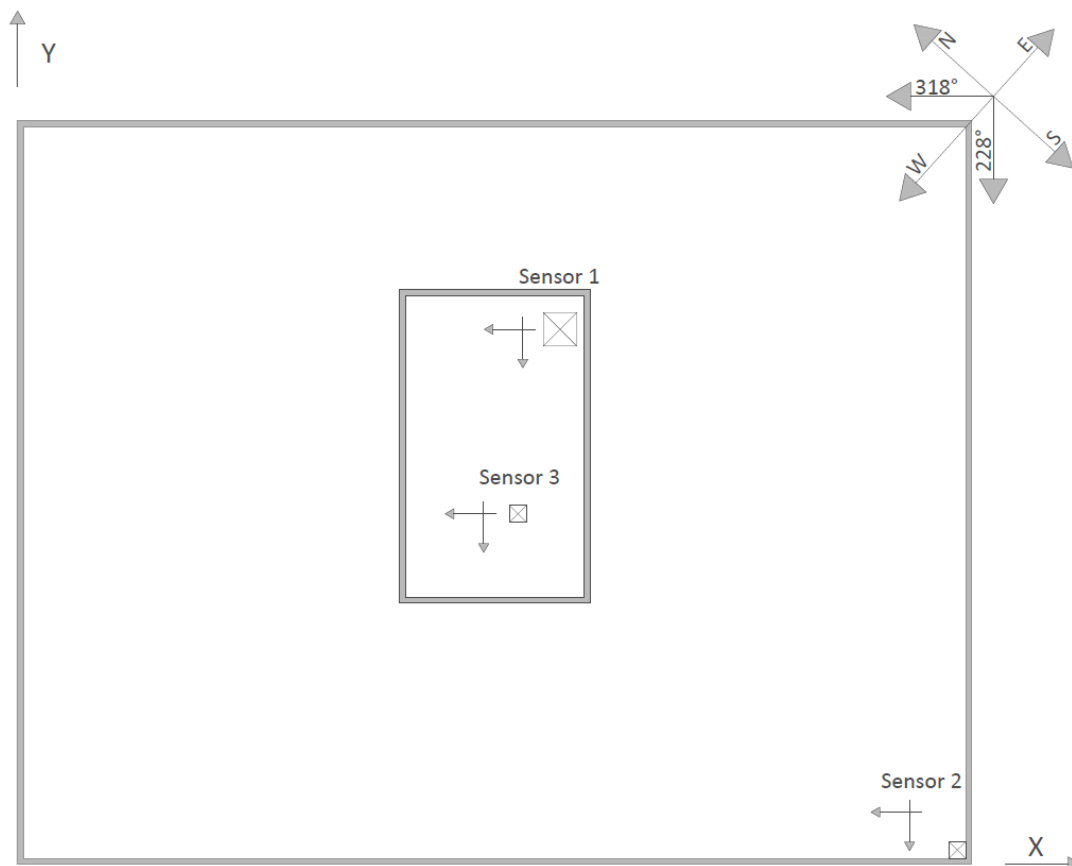


Figure 3.5: Plan view of location of the sensors, The long side is parallel to the 318° from north and positive direction of the grid in SAP2000 model

Figure 3.6 shows the location of the sensors according to floor levels. The positive

components of the global grid used in the SAP2000 model are marked on the figure. The figure also shows the positive components of the sensors.

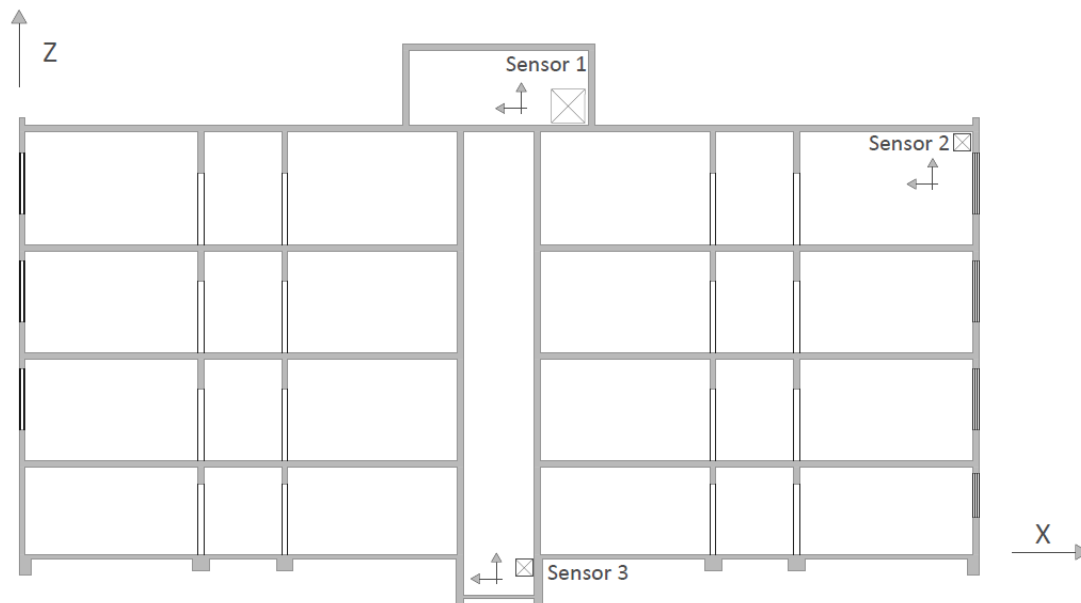


Figure 3.6: Vertical cross section of the building showing location of the monitor system according to floor levels

The monitoring system is produced and manufactured by Canterbury Seismic Instruments in New Zealand. The monitoring system is of the type CUSP-3. The CUSP - 3 range is specifically aimed at three target applications; free-field strong motion arrays, structural health monitoring and vibration monitoring. Further information on their homepage www.csi.net.nz [17].

The instrument settings offer many different filters and triggering options. This gives us the opportunity to reject unwanted data, for instance the vibration from the ventilation. The reliability of the data depends heavily on the type of configuration of the triggering system. The CUSP-3 instrument records data from the sensors if conditions defined before have been fulfilled and if there is sufficient data storage space. The timing of the events are derived from three sources, GPS based timing, NTP internet timing or from the internal clock [18].

Figure 3.7 shows the main station sensor 1 located at the roof. This station is the power supplier for the other two accelerometers and they are connected through Ethernet cable. Inside the box is a backup battery in case of power failure during earthquake. This sensor provides the response of the building at the top.

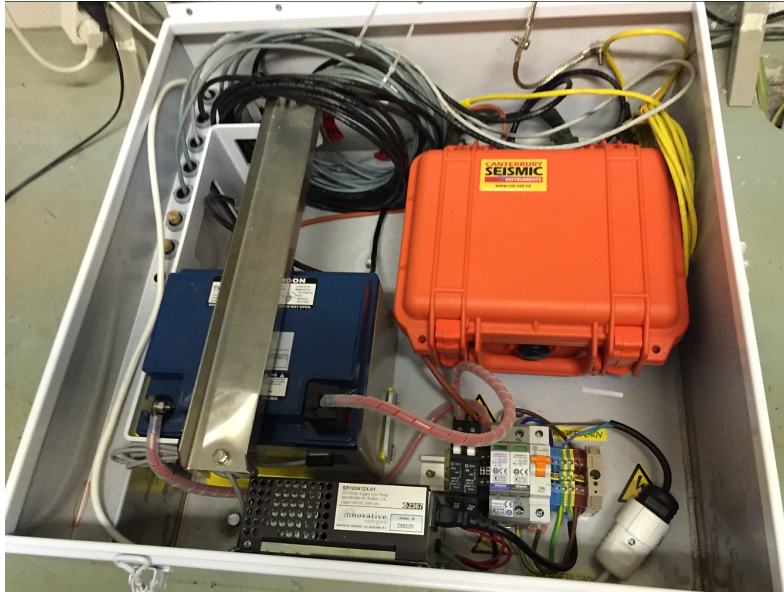


Figure 3.7: The main station sensor 1 located at the utility room on the roof

Figure 3.8 shows sensor 2 located at 4th floor top corner. This sensor is connected through Ethernet cable to the main station and provides the response of the building in the top corner of 4th floor.



Figure 3.8: Sensor 2 located at 4th floor top corner

Figure 3.9 shows sensor 3 located at the ground floor in the hoist way. This sensor like the other is connected through Ethernet cable to the main station and provides recordings for the ground motion.

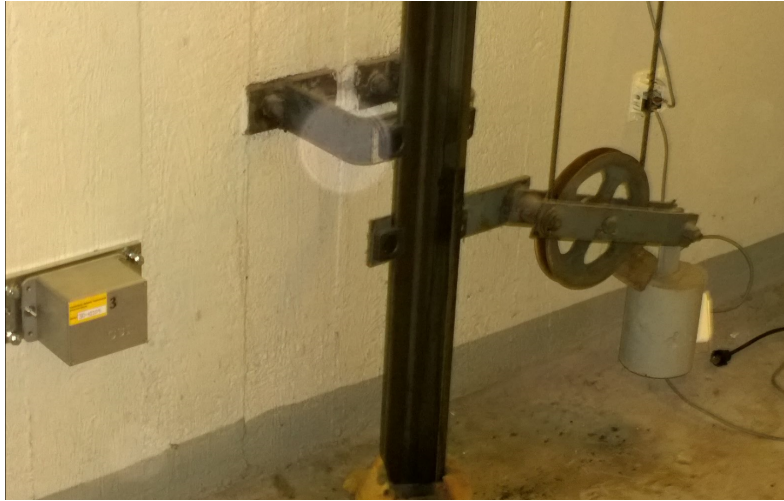


Figure 3.9: Sensor 3 located at the ground floor in the hoist way

The setup of the sensors provides ground motion and appropriate response in the building during induced acceleration. The relative acceleration from the ground motion and the response on the top is useful to analyse the system. The off centre location of accelerometers at the top floor allows to evaluate torsional motion.

To synchronize the recordings in the Hospital with recordings at other stations in the Icearray II network, it is necessary to correct the internal clock in the CUSP-3 data acquisition unit regularly. This correction can be archived through a GPS connection or through NTP Internet timing. As the station is connected to the fixed line high speed Internet in the building, the NTP option was chosen for the case at hand.

4. Earthquake induced Acceleration data

4.1 Introduction

The acceleration data used in this thesis is gathered from transfer zones in north and south Iceland. These locations are known to have the highest earthquake hazard in Iceland as can be seen on figure 2.5. The data recorded in the building originates from small earthquakes in the vicinity of Húsavík whereas the data comes from the European strong motion database from the south Iceland seismic zone [1].

The earthquake data used from Húsavík is recorded with free field accelerometers located widely across the town of Húsavík as figure 4.1 shows and is known as Icearray II. The ground motion and structural response of the hospital is recorded with three accelerometers as described in chapter 3.3 and the data used for further calculations in this thesis regarding Húsavík hospital is shown in table 4.1 [1].

The structural response monitoring of the hospital gives us information to estimate the structural characteristics of the building. By using the ground acceleration as input and the response on upper floors as output we can validate the building FEM with certain accuracy.

The data used from the south Iceland is from the destructive earthquakes in June 2000 and May 2008. The earthquakes June 17th and 21st caused considerable damage of structures and inventories of dislocations and ground subsidence were significant in the near-fault zone [19]. The Ölfus earthquake from May 2008 was the third most destructive earthquake to take place in the south Icelandic seismic zone. The earthquake epicenter in recent years was at the westernmost part of the seismic zone between the towns of Hveragerði and Selfoss. Despite the high intensity ground motion the earthquake resulted in no loss of life and limited structural damage [20].

The earthquake data used from south Iceland is used to estimate the response of the hospital to strong ground motion and for structural integrity checks.

4.2 Data recorded on site

The monitoring system installed in Húsavík hospital has the identification IS706C and is part of the Icearray II system showed on figure 4.1. The main emphasis in this thesis is the structural monitoring of the hospital but for the data recorded around the town is also relevant for the overall view of the local seismicity. The instruments have recorded a few notable events in the last 12 months. Table 4.1 contains an overview on the events of interest recorded by Icearray II, for selected stations. Station IS706D3 is the sensor located in the basement of the hospital.

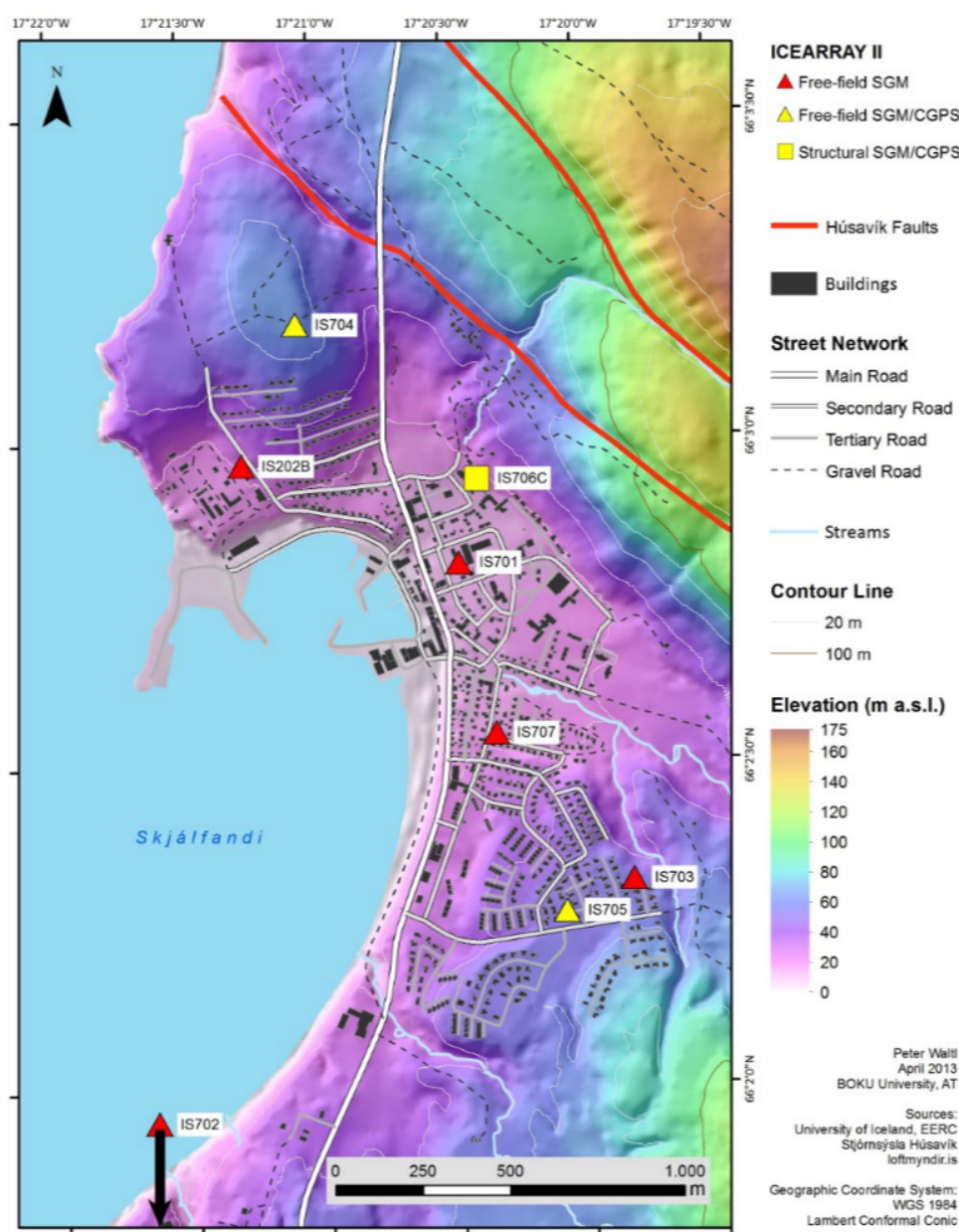


Figure 4.1: The distribution of accelerographs on Húsavík

Table 4.1: Earthquake data recorded at Húsavík

Event	Nr	Date	Time	Station Name	Magnitude	Latitude	Longitude
		[-]	[-]	[-]	[Mw]	[degree]	[degree]
1	IS 702	29/05/2015	00:41:33	Kaldbakur		66.04	17.36
	IS 706D3	29/05/2015	00:41:33	Húsavík hospital		66.05	17.34
	IS 707	29/05/2015	00:41:33	Garðarsbraut		66.04	17.34
2	IS 706D3	23/09/2015	16:01:33	Húsavík hospital		66.05	17.34
3	IS 702	21/01/2016	04:01:38	Kaldbakur		66.04	17.36
	IS 706D3	21/01/2016	04:01:38	Húsavík hospital	3.7	66.05	17.34
	IS707	21/01/2016	04:01:38	Garðarsbraut		66.04	17.34
4	IS 702	21/01/2016	04:03:22	Kaldbakur		66.04	17.36
	IS 706D3	21/01/2016	04:03:22	Húsavík hospital		66.05	17.34
	IS707	21/01/2016	04:03:22	Garðarsbraut	2.97	66.04	17.34

4.3 Earthquake data in the hospital

The instruments in the hospital have recorded 4 notable earthquake events, although all of them were small with PGA at the building of less than 1% of g . In this chapter the data is inspected. The events are numbered in order of date and time see table 4.1. Events 3 and 4 are of most interest to us and used for further calculations.

For the ground motion the acceleration is plotted against time, Fourier spectra is plotted and elastic response spectra is computed for both vertical and horizontal components. For the response the absolute and relative acceleration is plotted for every component along with the power spectral density for each component for both of the response sensors. Table 4.2 gives comparison of the events 3 and 4 for sensors 1 and 2. The peak ground acceleration is compared to the absolute response in the response sensors.

Table 4.2: Comparison of data measured in the hospital, events 3 and 4.

Event	Sensor	Peak ground acceleration			Peak absolute response			PA/PGA		
		x	y	z	x	y	z	x	y	z
		[cm/s ²]	[cm/s ²]	[cm/s ²]	[cm/s ²]	[cm/s ²]	[cm/s ²]	[-]	[-]	[-]
3	Sensor 1	0.61	0.62	0.66	2.32	3.4	1.08	3.8	5.5	1.6
3	Sensor 2	0.61	0.62	0.66	3.00	2.96	1.20	4.9	4.8	1.8
4	Sensor 1	0.63	0.48	0.44	3.26	2.88	0.64	5.2	6.0	1.5
4	Sensor 2	0.63	0.48	0.44	3.40	2.68	1.33	5.4	5.6	3.0

4.3.1 Event 3

The event 21.01.2016 04:01:38 is measured at station 706D3 in the basement of the hospital. The event had magnitude of 3,7 Mw and epicentral distance of 4,74 km. The peak vertical acceleration was 0,68 cm/s^2 and peak horizontal acceleration was 3,4 cm/s^2 .

Figure 4.2 shows the time history response for sensor 3 on the ground floor for components x,y,z. The figure shows the acceleration for the first 18 seconds. Figure 4.3 shows the amplitude spectrum for every component of sensor 3 on ground floor. Figures 4.4 and 4.5 show the elastic response spectra for components x,y,z normalized and compared to the Eurocode response spectra. The response spectra is calculated for damping ratio of 5 % and ground type A. As can be seen on figure 4.4 the event gives primarily energy at low periods, and has a high seismic coefficient, which is typical for small near-field events. Figure 4.4 shows the normalized Eurocode response spectra, type I, for comparison, which gives a peak response at different period range and has lower seismic coefficient, which is more representative of large events. Figure 4.4 shows the same comparison for the vertical component. Section 4.4.3 shows a summary for the response spectra including comparison to type2 spectra for horizontal data measured on Húsavík.

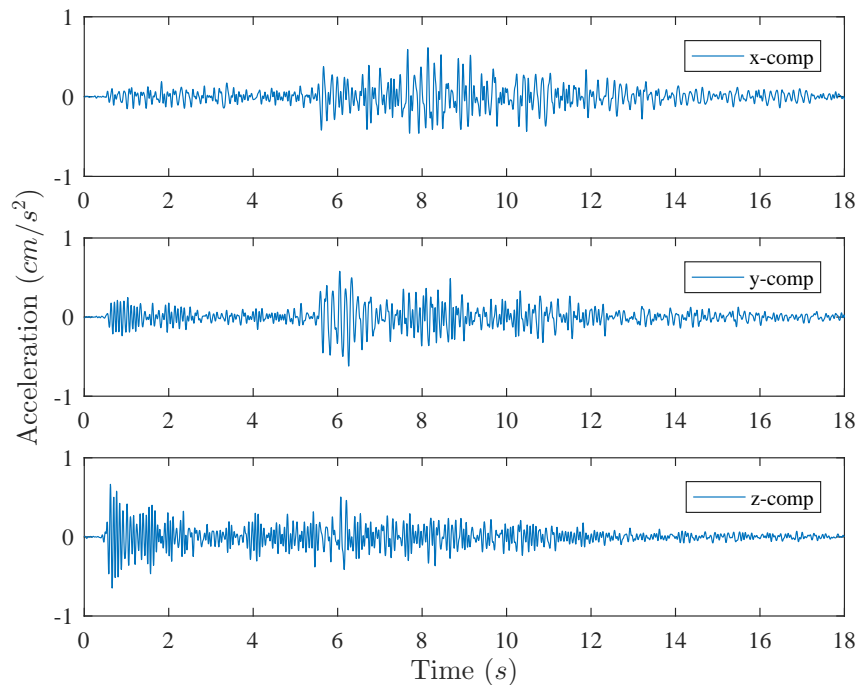


Figure 4.2: Acceleration ground floor sensor

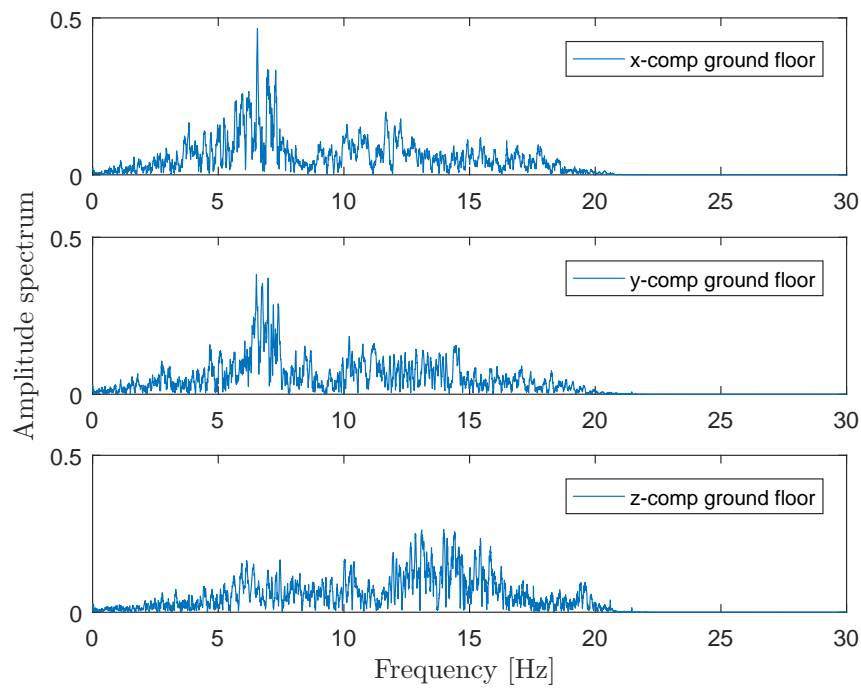


Figure 4.3: Fourier spectra for ground floor sensor

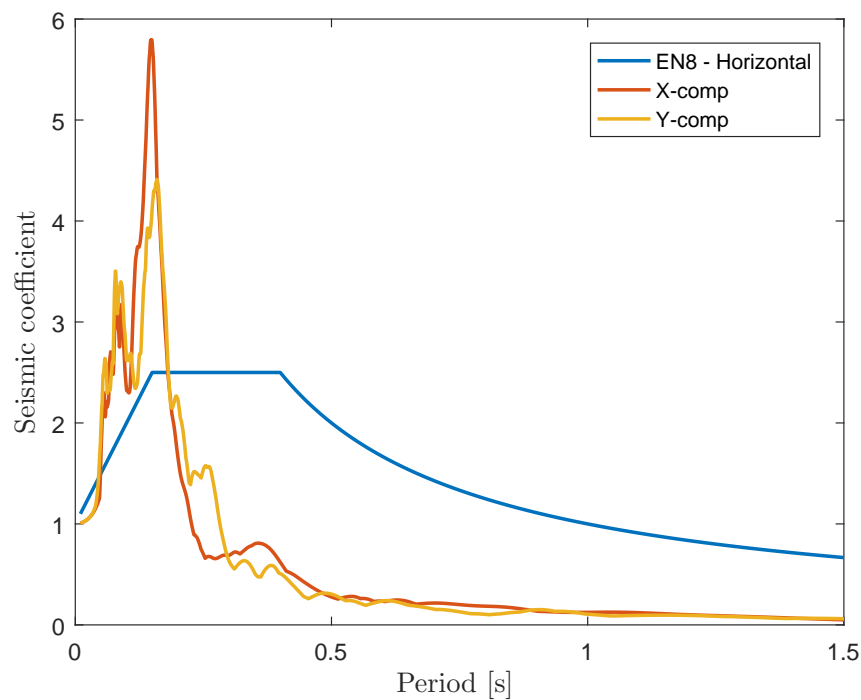


Figure 4.4: Normalized horizontal elastic response spectra of ground acceleration with 5% damping

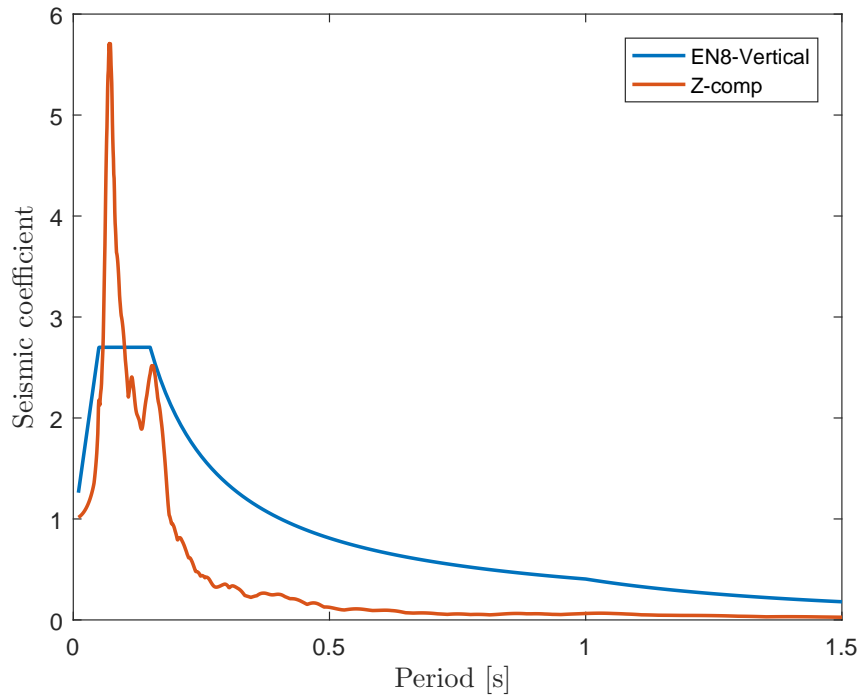


Figure 4.5: Normalized Vertical elastic response spectra of ground acceleration with 5% damping

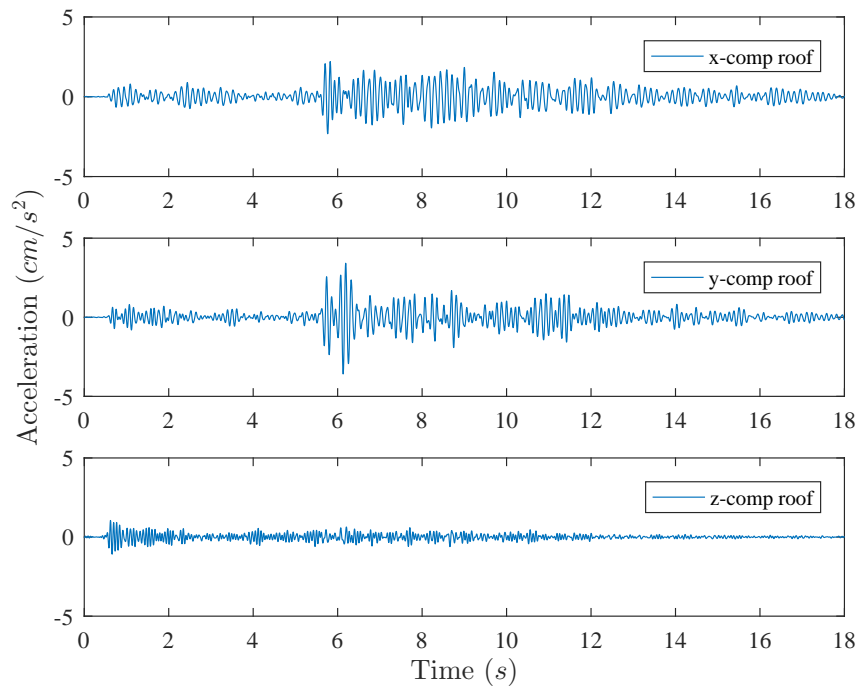


Figure 4.6: Total acceleration from the roof sensor

Figure 4.6 shows the time history response for sensor 1 on the roof for components x, y, z . The figure shows the acceleration for the first 18 seconds.

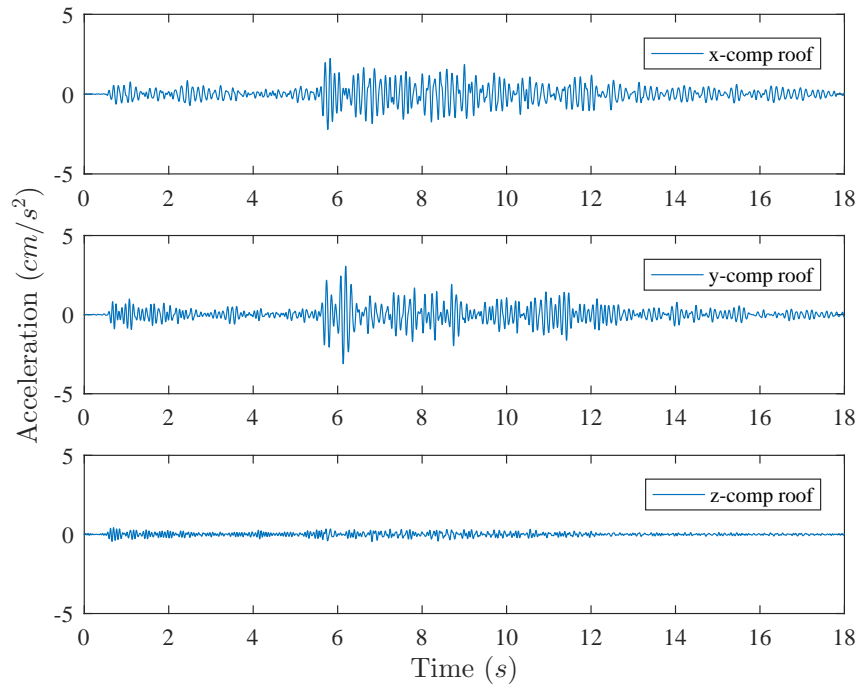


Figure 4.7: Relative acceleration at the roof sensor location

Figure 4.7 shows the relative response for sensor 1 on the roof where the acceleration from the ground sensor has been deducted.

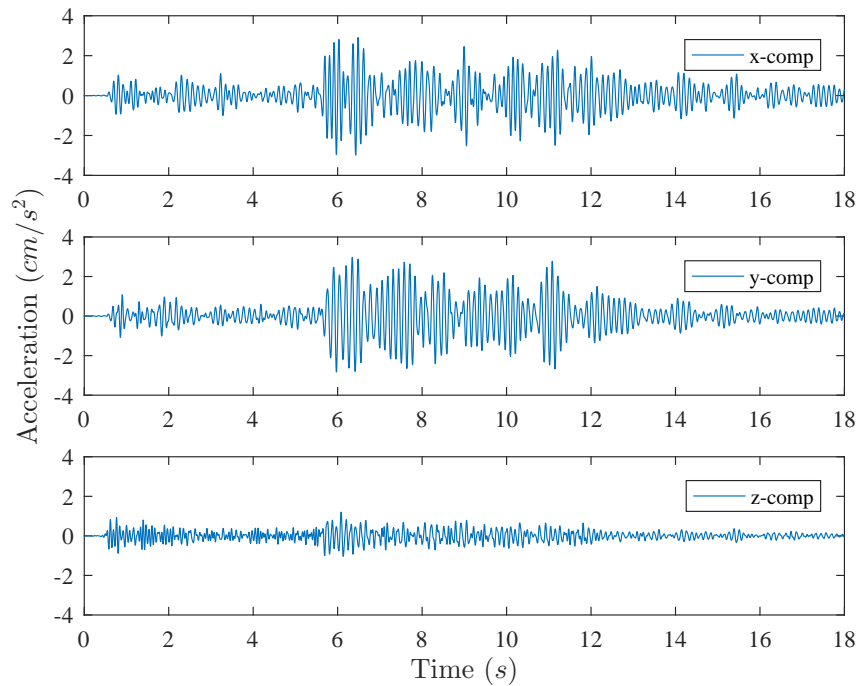


Figure 4.8: Total acceleration from the 4th floor sensor

Figure 4.8 shows the time history response for sensor 2 on the 4th floor for components x,y,z. The figure shows the acceleration for the first 18 seconds.

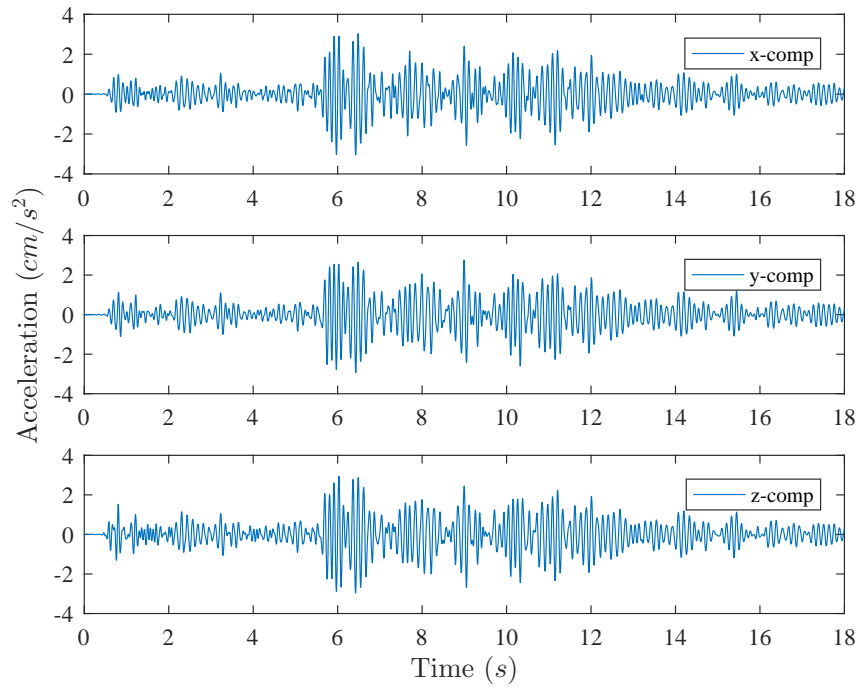


Figure 4.9: Relative acceleration at the 4th floor sensor location.

Figure 4.9 shows relative acceleration for sensor on 4th floor where the acceleration from the ground sensor has been deducted.

Figures 4.10, 4.11 and 4.12 shows the power spectral density for response on sensors on roof and 4th floor. The figures are plotted for each component for both response sensors, the roof and 4th floor.

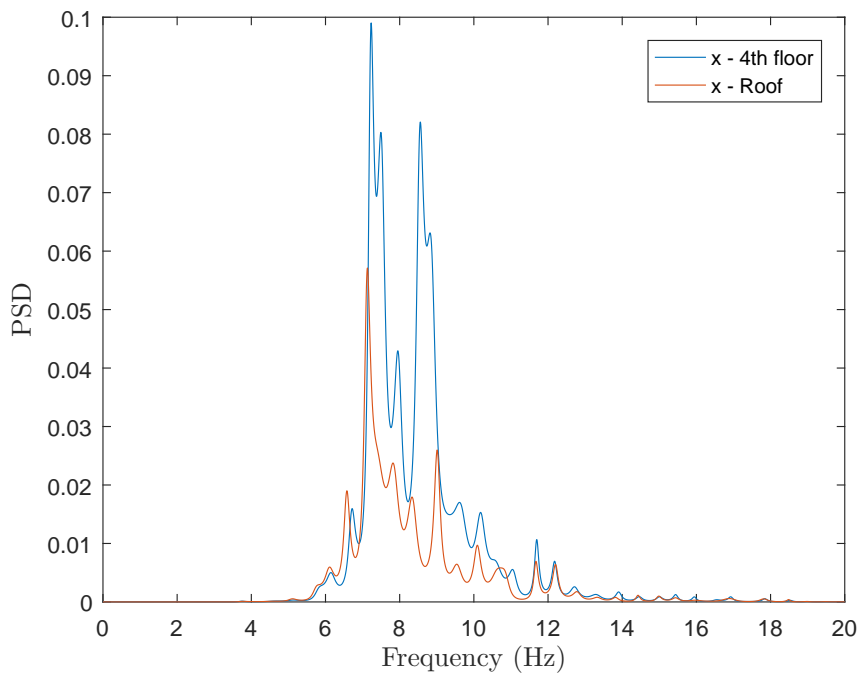


Figure 4.10: Power spectral density for x - components

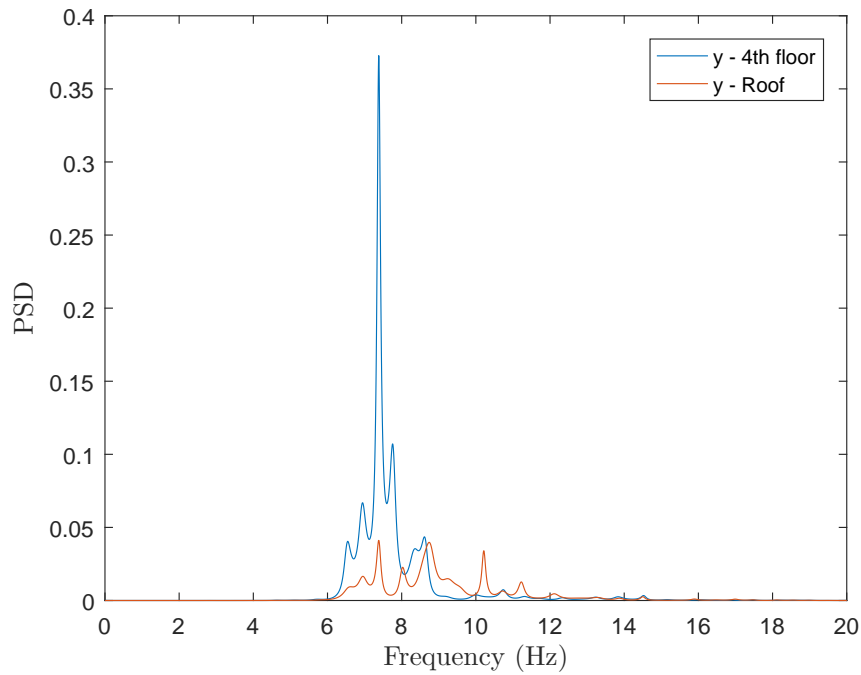


Figure 4.11: Power spectral density for y - components

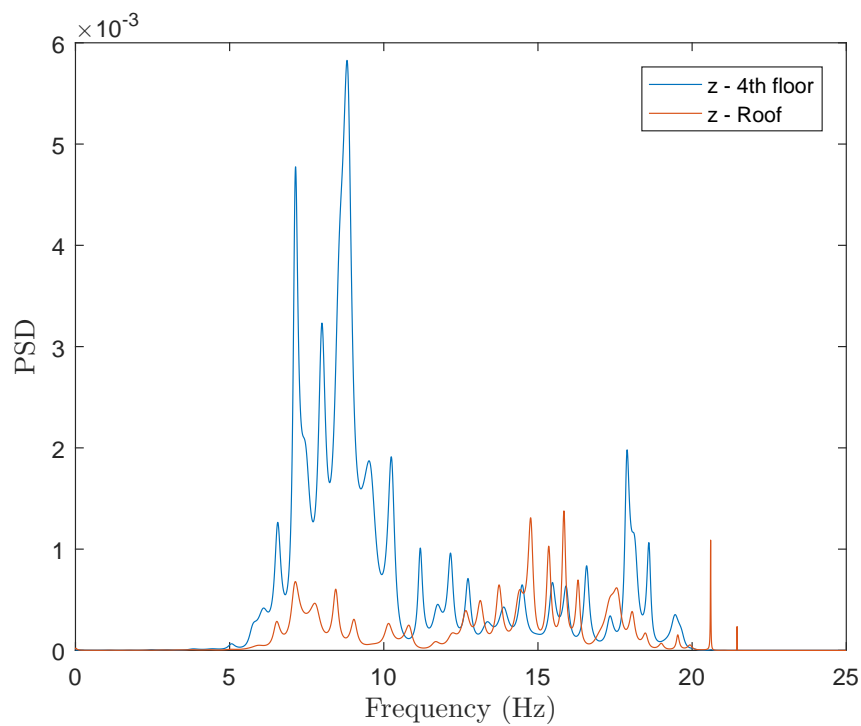


Figure 4.12: Power spectral density for z - components

4.3.2 Event 4

The event 21.01.016 04:03:22 is measured at station 706D3 in the hospital. The event had magnitude of approximately 3 Mw and epicentral distance of 6,55 km. The peak

vertical acceleration was $0,62 \text{ cm/s}^2$ and peak horizontal acceleration was $0,66 \text{ cm/s}^2$ as can be seen in table 4.1.

Figure 4.13 shows the time history response for sensor 2 on the ground floor for each component. The figure shows the acceleration for the first 18 seconds. Figure 4.14 shows the amplitude spectrum for each component of sensor 3 on ground floor.

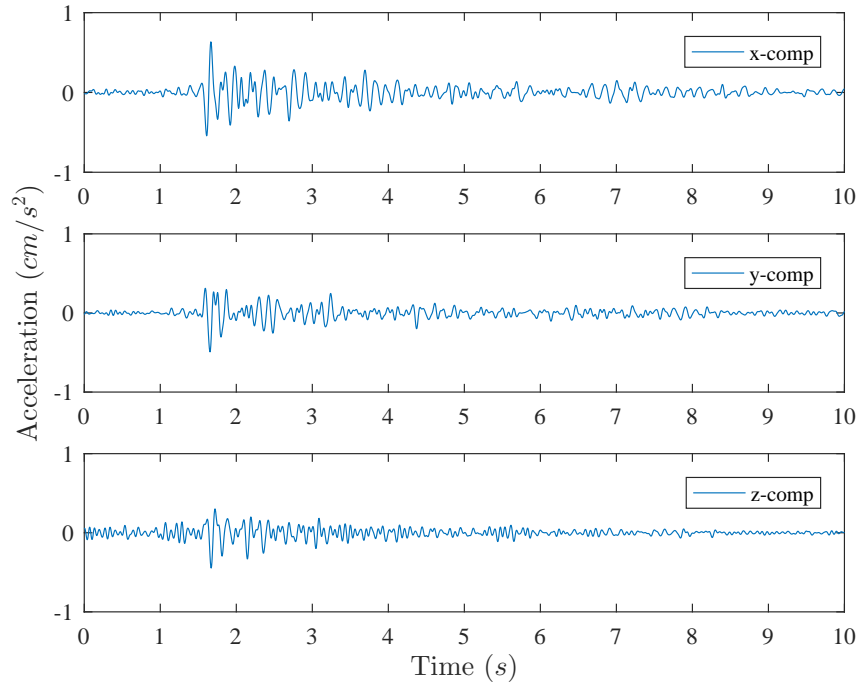


Figure 4.13: Acceleration ground floor sensor

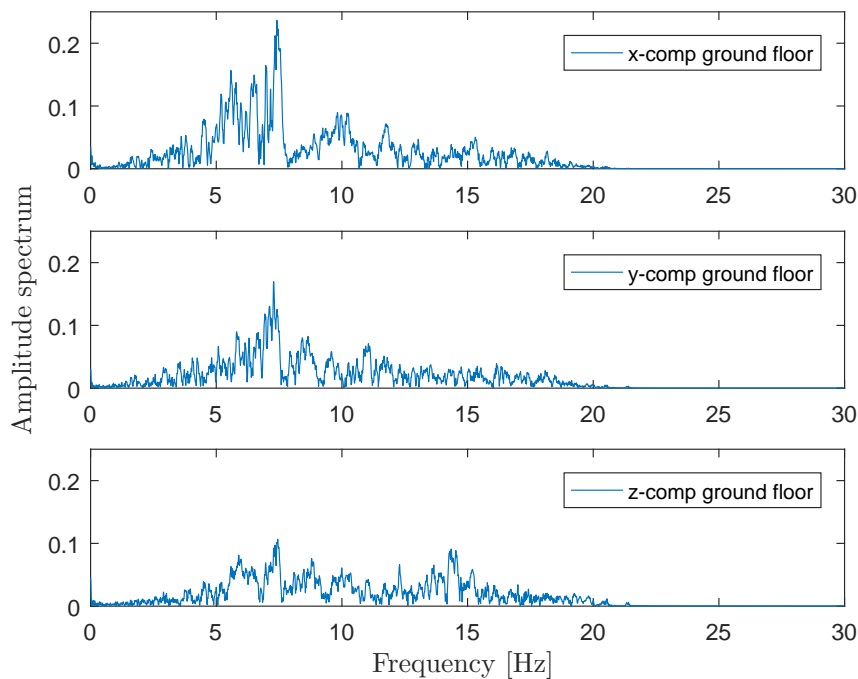


Figure 4.14: Fourier spectra for ground floor sensor

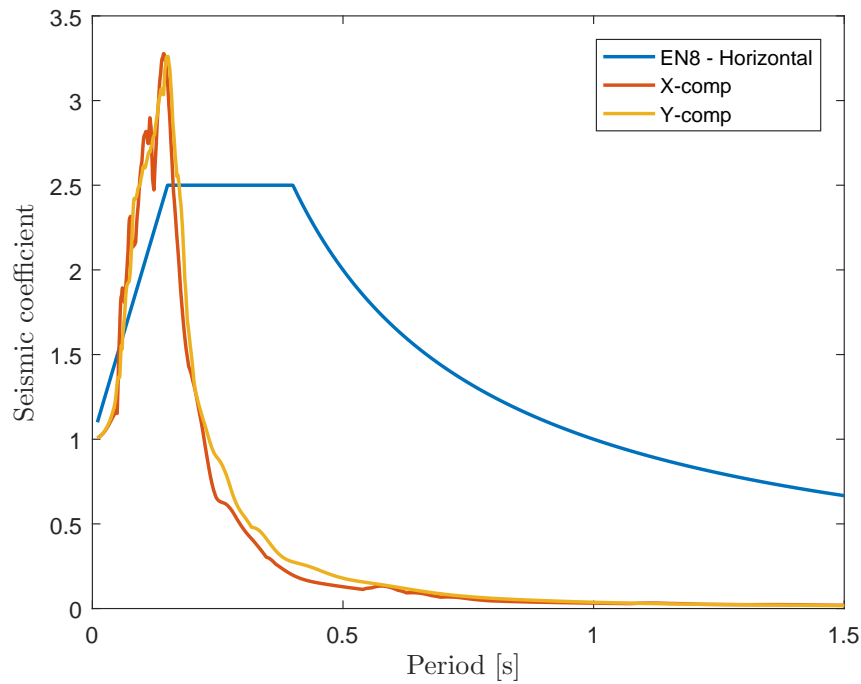


Figure 4.15: Normalized horizontal elastic response spectra of ground acceleration with 5% damping

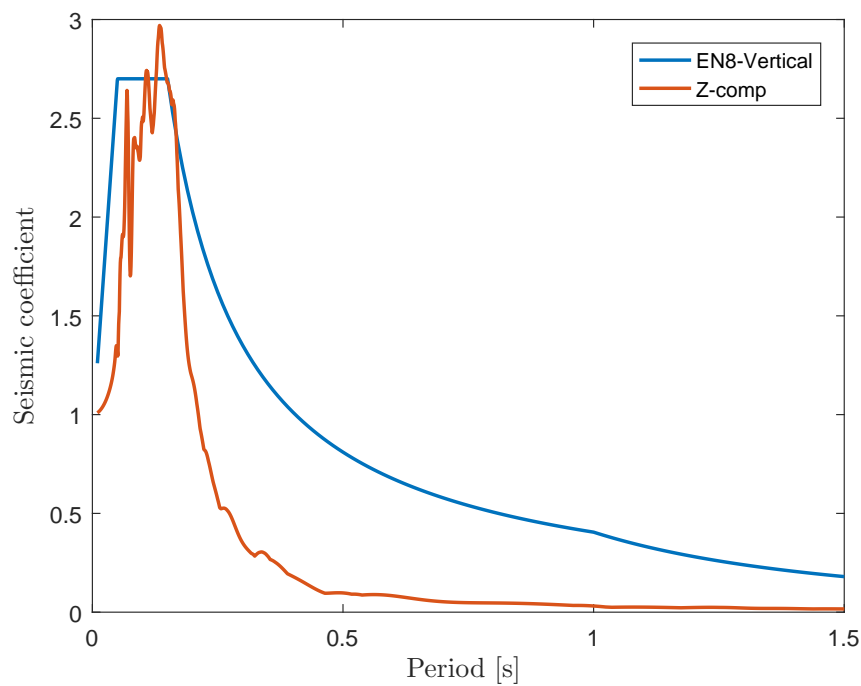


Figure 4.16: Normalized Vertical elastic response spectra of ground acceleration with 5% damping

Figures 4.15 and 4.5 show the elastic response spectra for each component normalized and compared to Eurocode response spectra. The response spectra is calculated for damping ratio of 5 % and type A ground.

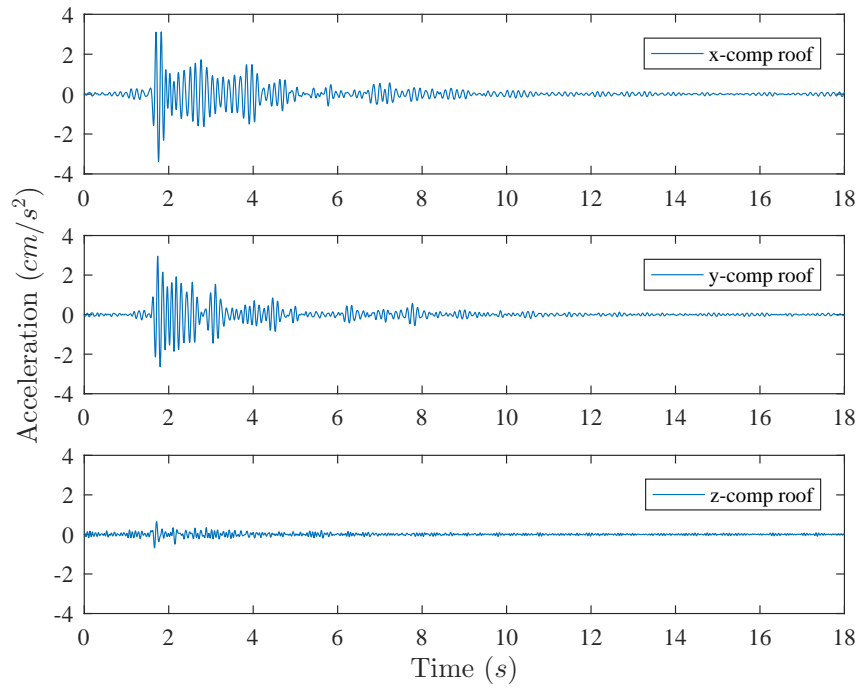


Figure 4.17: Acceleration Roof sensor

Figure 4.17 shows the time history response for sensor 1 on the roof for each component. The figure shows the acceleration for the first 18 seconds.

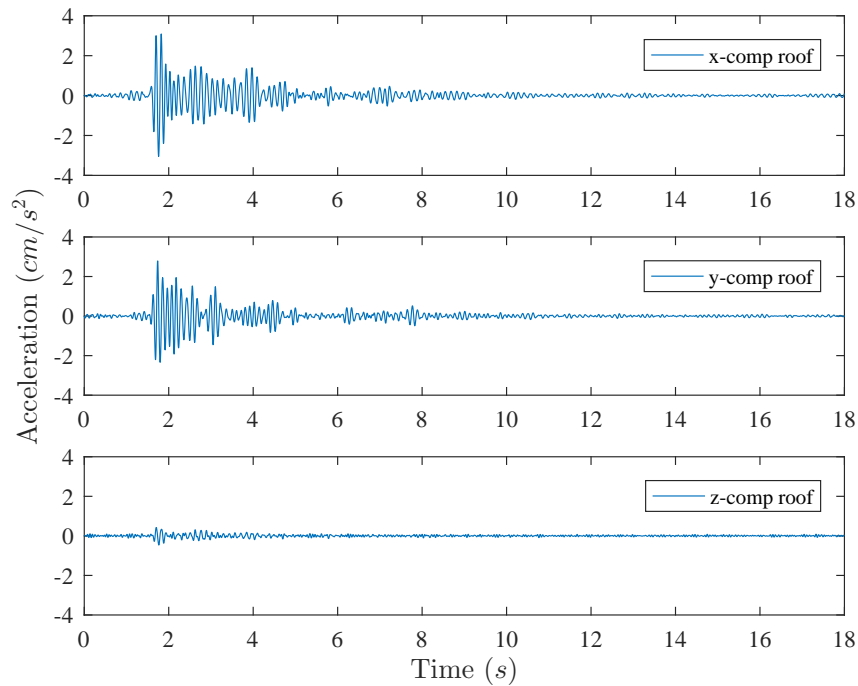


Figure 4.18: Relative acceleration Roof sensor

Figure 4.18 shows the relative response for sensor 1 on the roof where the acceleration from the ground sensor has been deducted.

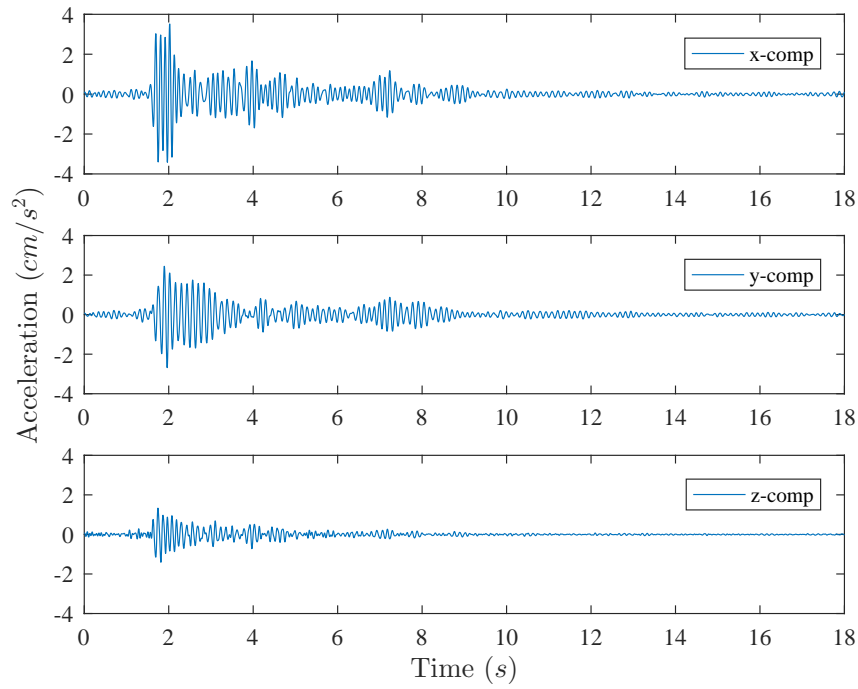


Figure 4.19: Acceleration 4th floor sensor

Figure 4.19 shows the time history response for sensor 2 on the 4th floor for each component. The figure shows the acceleration for the first 18 seconds.

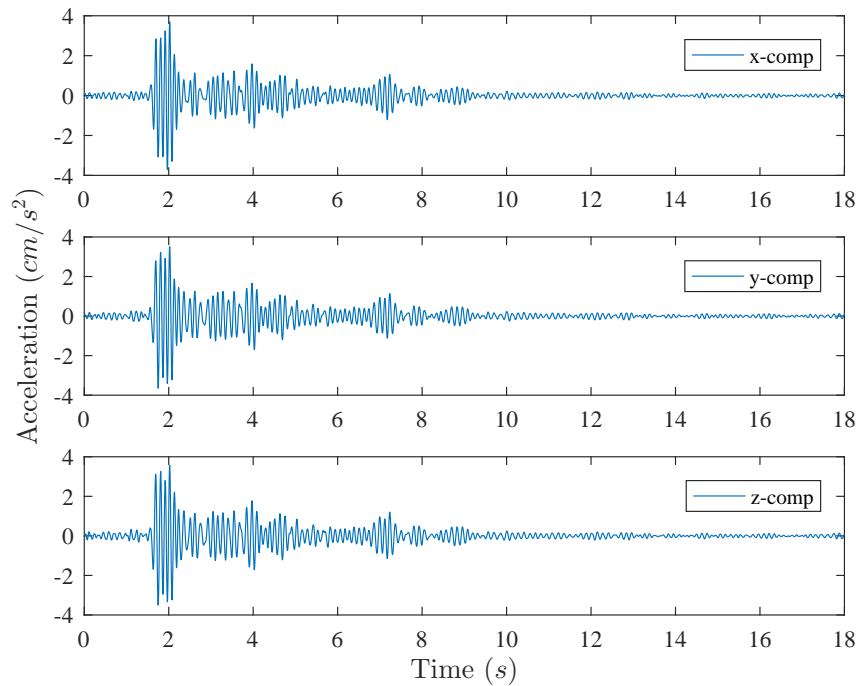


Figure 4.20: Relative acceleration 4th floor sensor

Figure 4.20 shows relative acceleration for sensor in 4th floor where the acceleration from the ground sensor has been deducted.

Figures 4.21, 4.22 and 4.23 shows the power spectral density for response on sensors on roof and 4th floor. The figures are plotted for same component on different sensor.

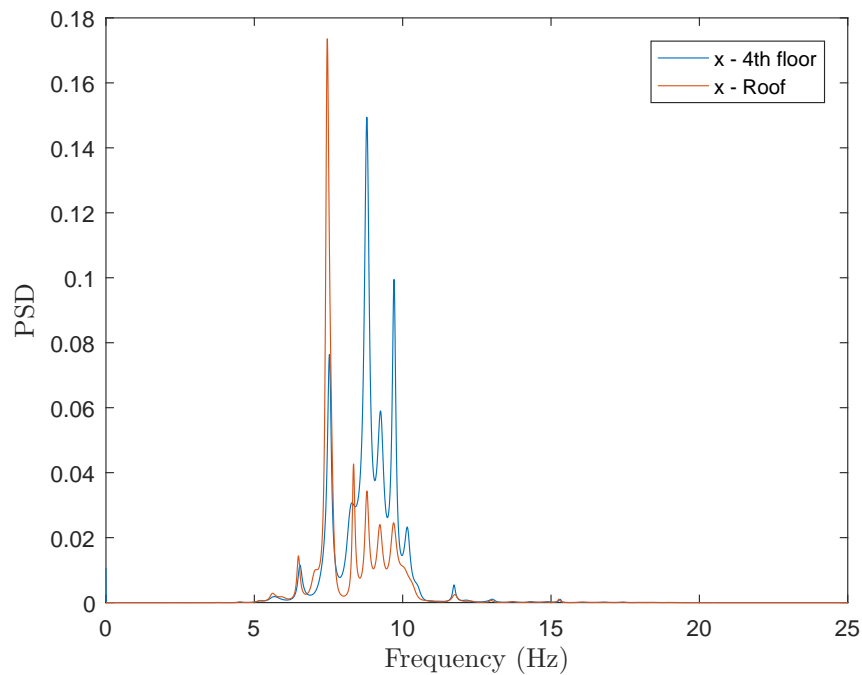


Figure 4.21: Power spectral density for x - components

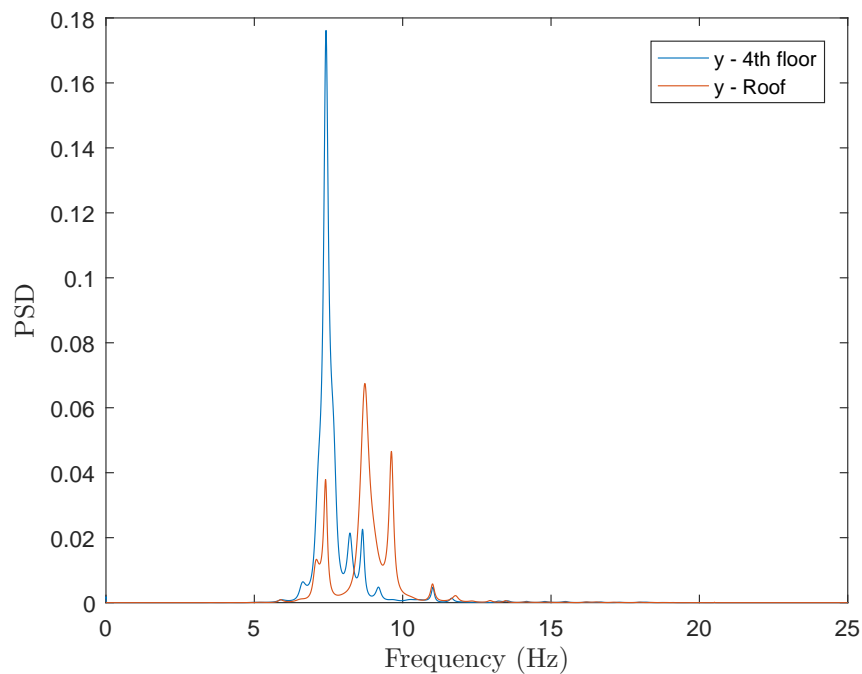


Figure 4.22: Power spectral density for y - components

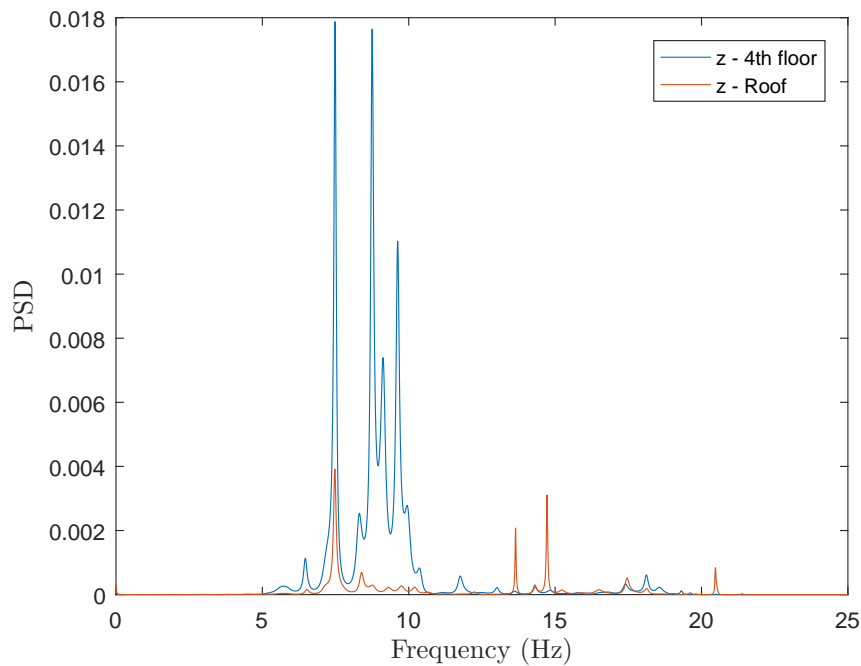


Figure 4.23: Power spectral density for z - components

4.4 Strong motion data and seismic information

The earthquake data used in this thesis is collected from the website www.isesd.hi.is. The European Strong-motion database includes collection of Icelandic earthquakes and for this thesis selected time series from 2000 and 2008 are used. The events picked are showed in table 4.3 along with general information.

4.4.1 Earthquakes June 2000

Two major earthquakes struck south Iceland in June 2000. The first earthquake $M_w 6,5$ was a right lateral strike slip earthquake, with fault striking in the north-south direction and approximate focal depth of 6,3 km struck on June 17 2000, 15:41, (GMT). The second earthquake $M_w 6,5$ struck June 21 2000, at 00:52; (GMT). This earthquake was also a right-lateral strike slip earthquake, with fault striking in the north-south direction and with approximate focal depth of 5,3 km. There were several after-shocks in the area but they were of magnitude less than $M_w 5$ [9].

4.4.2 Earthquake May 2008

Strong earthquake took place in western part of south Iceland at 15:45 UTC on May 29 2008. The earthquake consisted of a slip on two separate faults. This earthquake was a right lateral strike-slip earthquake with fault striking in the north-south direction. The magnitude of the combined events was estimated as $M_w 6,3$ [20] [9].

4.4.3 Selection criteria and selected data

The selection criteria for earthquakes used to examine the response of the building mainly depends on the PGA value. The PGA value depends mainly on magnitude and epicentral distance. High magnitude and short epicentral distance produces high PGA value. The desired earthquake is therefore high magnitude near field event. The local geology includes both rock and stiff soil sites [3].

The stations of interest are listed in table 4.3 and figures in appendix A. As can be seen in table 4.3 the magnitude is 6,3 - 6,5 M_w . Local geology is either rock or stiff soil and is selected to simulate the local geology of the site. The epicentral distance varies from 5 - 22 km. The peak vertical acceleration ranges from 0,71 - 6,54 m/s^2 and peak horizontal acceleration ranges from 1,28 - 7,1 m/s^2 . The most powerful earthquake of those in the table is Kaldarholt with 6,5 magnitude, PHA 6,136 and PVA 6,541.

Table 4.3: Earthquake data collected from The European Strong-motion database

Date	Time	Station name	Magnitude	Latitude	Longitude	Distance	PHA	PVA
[-]	[-]	[-]	[M_w]	[degree]	[degree]	[km]	[m/s^2]	[m/s^2]
17/06/2000	15:40:41	Flagbjarnarholt	6.5	64.01	20.18	5	3.3	2.7
17/06/2000	15:40:41	Kaldarholt	6.5	64.02	20.34	7	6.1	6.5
21/06/2000	00:51:48	Sólheimar	6.4	64.06	20.64	11	7.1	4.1
21/06/2000	00:51:48	Þjórsártún	6.4	63.93	20.56	6	5.6	3.2
29/05/2008	15:45:59	Selfoss - city hall	6.3	63.94	21.00	8	5.3	2.5
29/05/2008	15:45:59	Retirement house	6.3	64.00	21.19	9	6.5	4.3
29/05/2008	15:45:59	EERC	6.3	63.94	21.00	8	5.3	3.7
29/05/2008	15:45:59	Borgarhraun	6.3	64.00	21.19	9	6.6	5.3
29/05/2008	15:45:59	Ljósafoss power station	6.3	64.10	21.01	9	1.3	0.7

The recorded data from Húsavík and the data from south Iceland earthquakes can be compared to standardized response spectra from Eurocode 8. Following figures are comparative plots for the time histories used. Horizontal and vertical components are plotted on a separate figure for each case and compared to response spectra according to EN 1998-1. The mean and the mean + one standard deviation was calculated and

plotted on the figures. Figure 4.24 and 4.25 represent measured data from Húsavík. Figure 4.26 and 4.27 represent data from south Iceland. The figures show the sensitivity at lower periods for both Húsavík and south Iceland measurements. For south Iceland measurements there are two peaks within the 0.5 second period this can be seen on figure 4.26.

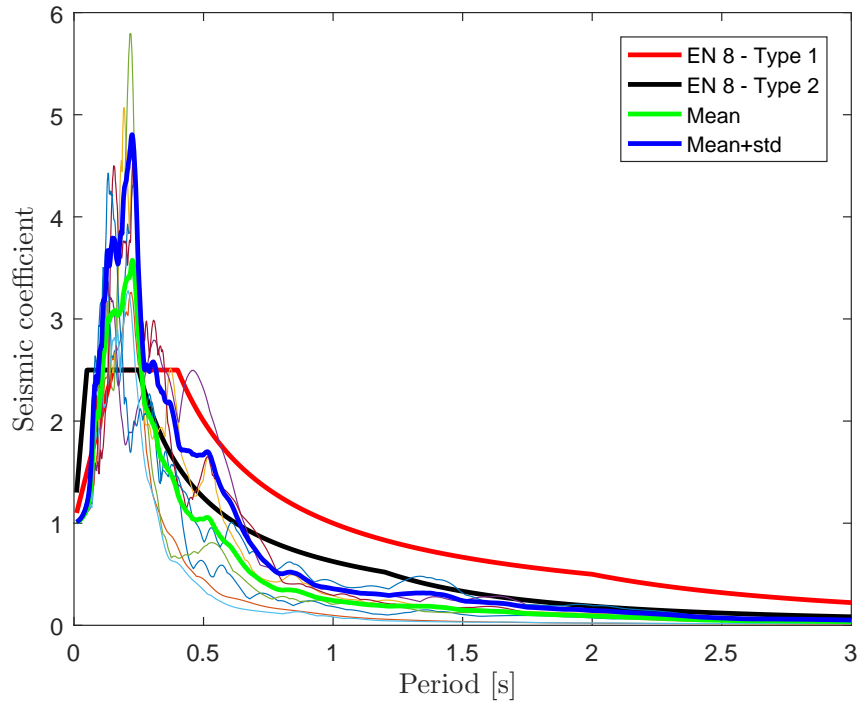


Figure 4.24: Horizontal response spectra from measured data on Húsavík

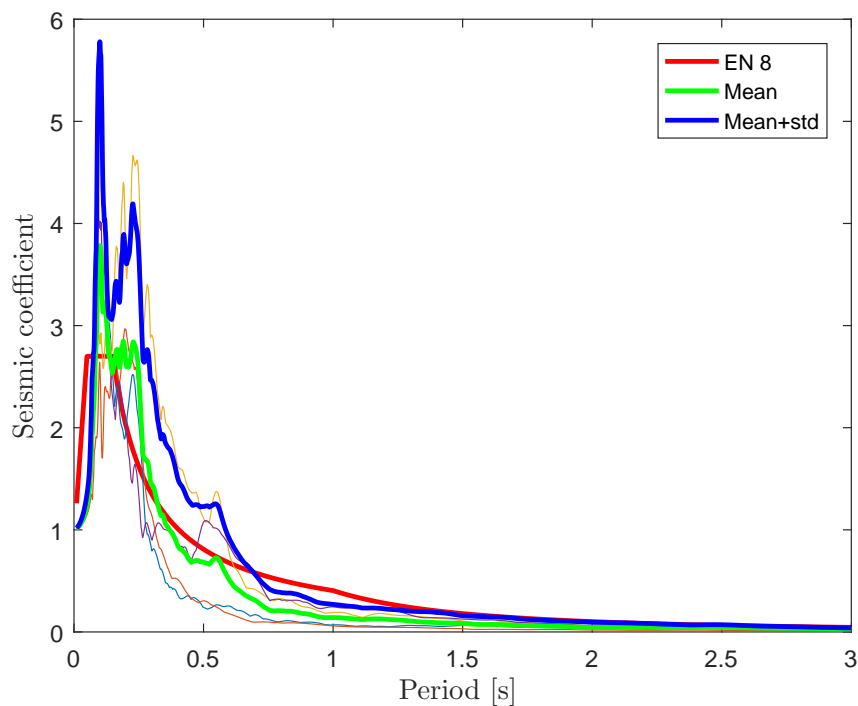


Figure 4.25: Vertical response spectra from measured data on Húsavík

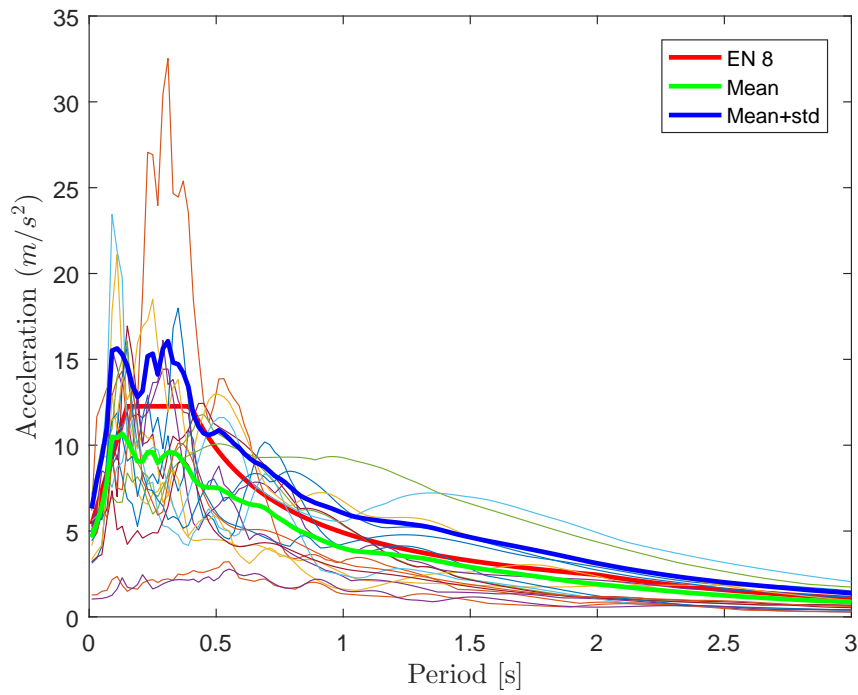


Figure 4.26: Horizontal response spectra from measured data on south Iceland

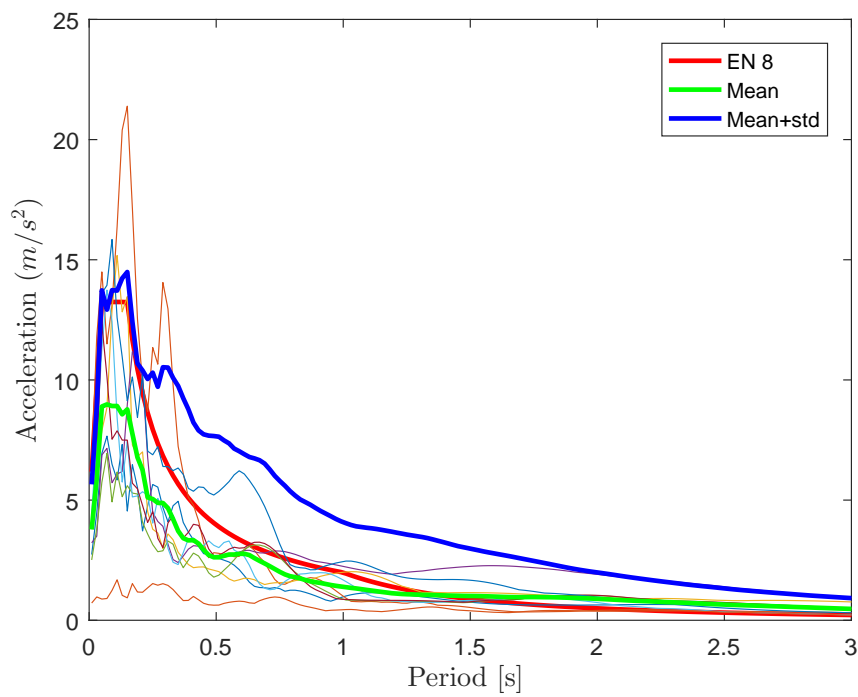


Figure 4.27: Vertical response spectra from measured data on south Iceland

5. Finite element modelling and system identification

The finite element modelling is carried out using the software SAP2000, version 15. The software is a structural analysis program that can handle various analysis from simple static 2D frame analysis to a complicated 3D non-linear dynamic analysis. In this chapter 3D model of the building is prepared to extend and interpret the information provided by the full scale recordings of the building response to the environmental excitations. The modelling process is carried out along with the modal analysis and calibration of the model.

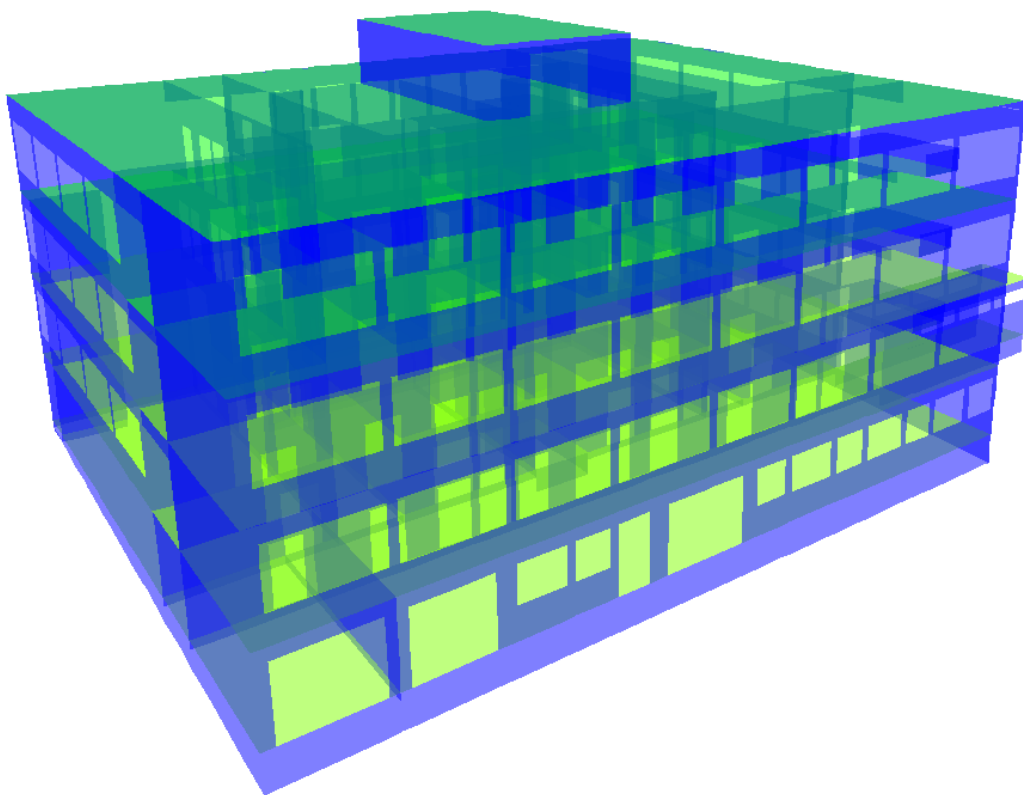


Figure 5.1: 3D model of the building in SAP2000

5.1 The modelling process

The model is based on available structural drawings made by the engineering firm Sigurður Thoroddsen (VST) and architectural drawings made by ATH vinnustofa. The construction of the model is also dependent on a site inspection where dimensions, structural elements and elastic modulus of concrete were verified as described in chapter 3.2.

The model consists of all the elements that contribute to the stiffness of the building including reinforced concrete walls, beams, columns and slabs. The building stands on an inclined bedrock and the foundation base walls imitate the formation of the site. The initial Boundary conditions of the model allow rotations but not translation.

The construction of the model consists of shell elements. The location of windows doors and other constrains controlled the modelling approach. The sizes of the shell elements dependant on the location of openings and constraints in the model but the goal is to have each shell element as square as possible. The smallest size shell element in the model is 300x300mm.

Figure 5.2 gives a plan view of the first floor without the stairway on the left. The FE model is constructed identical. The stairway core on the NW side of the building is not included in the model directly, as there is a tension joint between the main building and the newer stairway core that will minimize the transfer of forces between the two. However, during the calibration of the model, it was decided to include some stiffness from the shear core through spring supports at the points where the shear core connects to the building. The added stiffness from the stairway is estimated to be 455 MN=m for 22 joints and total of 10 GN=m.



Figure 5.2: Modelled part of the hospital 1st floor

As mentioned in chapter 3.2 the concrete used in the building is equivalent to the C25/30 in current Eurocodes. The modulus of elasticity is $E_{CM} = 28$ GPa. The density of reinforced concrete is assumed to be $\rho = 2500$ kg/m³ and the poisons's ratio $\nu = 0,2$. [16].

The analysis of the model allows for imposed load on floor slab about 30% of the live load for the building, this should reflect a realistic load at normal condition. According to table 6.2 in Eurocode EN 1991-1-1 the recommended imposed load on floors for category 3C is 3-5 kN/m². It is a convenient way to assign the load as a area load on the slab [21].

5.1.1 Total mass

The total mass of the building depends on the self weight of the structure and the added mass due to building materials that do not contribute to strength of the structure such as glass, doors, insulation, cement mortar and other technical equipment. The structure is modelled thoroughly in SAP2000 and the mass is calculated according to density of concrete 2400 kg/m³. The mass of the structure is 2946 tons and added mass is 1513 tons.

The added mass is estimated according to available drawings of structural walls in the hospital of as well a site visit. The added mass on outer walls is estimated 80

kg/m^2 . The walls contain doors, glass windows, insulation on the inside and mortar layer on either side of the wall. Inner walls are estimated 70 kg/m^2 . The inner walls contain openings (doors) and cement mortar layer on both sides. The slabs are estimated to be 220 kg/m^2 the mass is composite of cement mortar on floor and imposed load. The roof is 100 kg/m^2 . To account for loose mass in the building as well as light non-bearing walls and partitions, 30% of the user imposed load defined according to EN1991-1-1:2002 was used i.e. 30% of $3 \text{ to } 5 \text{ kN/m}^2$ for Category 3C, which includes Hospitals.

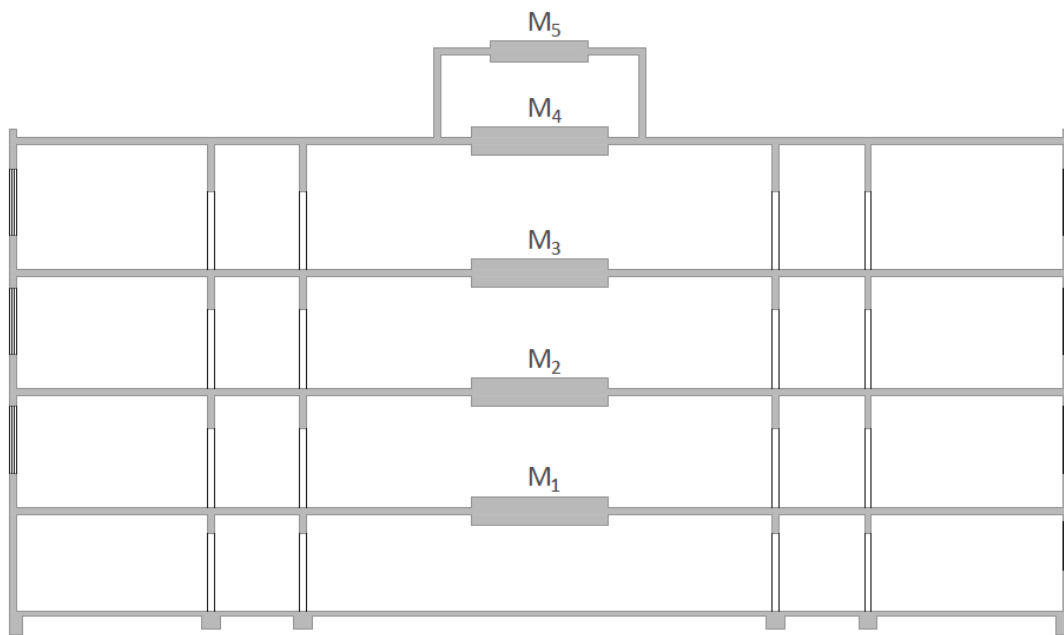


Figure 5.3: The distribution of mass in the building

The mass is estimated for each floor of the building [22]. The building is 4 floors plus utility tower. Figure 5.3 shows schematic figure of the mass distribution as lumped mass system. The mass of the cellar includes both the cellar and 1st floor slab, other levels include the walls and slabs over each floor. The walls on 1st floor correspond to the slab on second floor. The mass for each floor is estimated in table 5.1 according to total mass of the model and area of walls and slabs at given floor.

Table 5.1: Total mass of the building per floor

Total mass of building per floor	Area walls	Area slab	Wall/area	Mass per floor
	m ²	m ²	ratio	Tons
celler and foundation	1662	1335	0.29	1309
1st floor	1502	646	0.21	938
2nd floor	1454	641	0.21	915
3rd floor	1528	633	0.21	943
Roof and Utility room	759	54	0.08	355
Sum	6904	3309	1.00	4459

5.1.2 Elastic modulus

The initial model of the hospital showed somewhat higher stiffness than the recordings imply. The elastic modulus of concrete was measured in the concrete wall core in the building. The measurements give estimation of the elasticity on local basis. The mean of our measurement is 30,5 GPa according to table 3.1. The on site recordings in the hospital imply however that the elastic modulus is lower than the measurement of the dynamic modulus indicated. Cracks in the concrete cross sections can confirm the behaviour of some extent. The elastic modulus is decreased in the SAP model to 26 GPa.

5.2 Modal analysis and model validation

The modal analysis uses the overall mass and stiffness of a structure to find the various periods at which it will naturally resonate. The analysis was carried out in the finite element software. Table 5.2 shows the 12 first modes after modification of mass and stiffness of the model according to measured strong ground motion in the hospital.

Table 5.2: The 12 first modes of the building

Mode	Period	Frequency
[-]	[s]	[Hz]
1	0.1364	7.33
2	0.1163	8.60
3	0.1097	9.11
4	0.0758	13.19
5	0.0701	14.26
6	0.0654	15.30
7	0.0505	19.81
8	0.0483	20.69
9	0.0440	22.75
10	0.0322	31.10
11	0.0267	37.44
12	0.0253	39.55

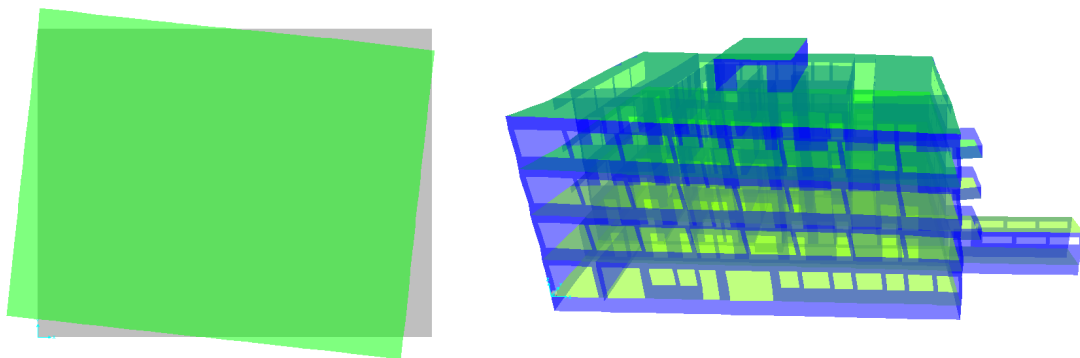


Figure 5.4: The first mode of the building, the natural period is 0.1364 seconds and natural frequency is 7,33 Hz

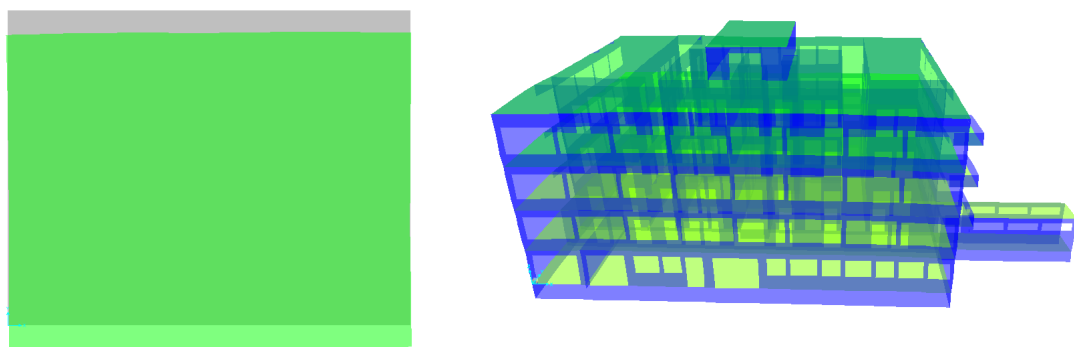


Figure 5.5: The second mode of the building, the natural period is 0.1163 seconds and natural frequency is 8,60 Hz

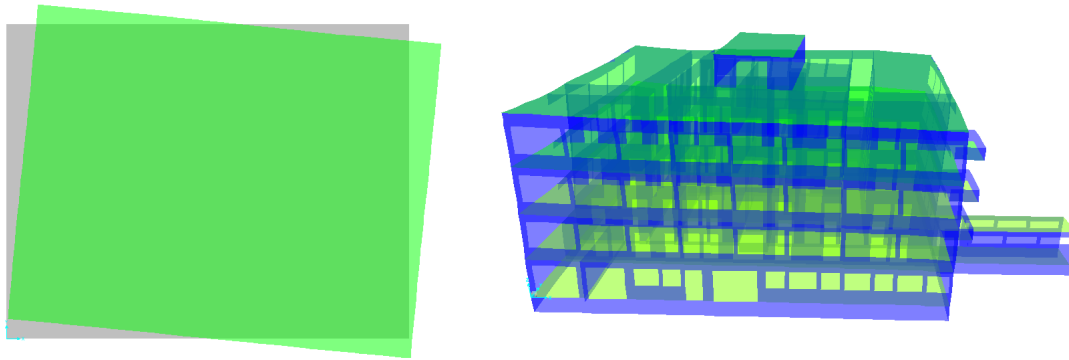


Figure 5.6: The third mode of the building, the natural period is 0.1097 seconds and natural frequency is 9,11 Hz

Calibration of the model is necessary to adjust the computer model to the reality as it appears to us from the measurements performed in the hospital. According to the measured data on site the fundamental frequency of the house is near 7,4 Hz as can be seen in section 5.2.1 and in the power spectral density plots in section 4.3 which show clearly the first three natural frequencies of the building. Modification of the model is mainly to adjust the structures response to the reality reflected by the measurements. The adjustments involve estimation of the total mass of the building and the elastic modulus of concrete . The total mass is the mass of the structure plus the added mass and 30% of the imposed load. The elastic modulus of the building was estimated on site with ultrasonic pulse velocity measurement. The measurements give good local estimation on the elastic modulus but in reality the modulus is lower because of cracks in the concrete.

5.2.1 Response measured vs. computed

The recorded data gathered at Húsavík hospital is used to adjust the FE model to reality. The earthquake response of a structure is calculated based on an acceleration at its base. The calculations are based on modal parameters from The FE model such as modal participation factors, frequencies, damping and joint displacements. Earthquake excitation at structures base is compared to the known response in sensor 1 on roof and sensor 2 on 4th floor. Frequency analysis is efficient way to calibrate the FE model.

The calculations for the FE model and the response recorded at Húsavík hospital is compared in following figures. The ground acceleration used is event 3 according to table 4.1. The comparative plots are published first for the sensor on 4th floor and then for the sensor on the roof. The analysis is subjected to constant 5% damping for

all modes except first three modes that have controlled damping of 3 %, 1,5% and 2% respectively.

Figures 5.7 and 5.8 show that the computed values give good approximation of the measured values. The acceleration plot has a PSA of $3,8 \text{ cm/s}^2$ at approximately 6.4 seconds for computed values. The measured values give a lower value of PSA or $2,9 \text{ cm/s}^2$ at 6,3 seconds. The Fourier spectrum shows computed frequency of 7.39 Hz and the measured values give exact same frequency for mode 1.

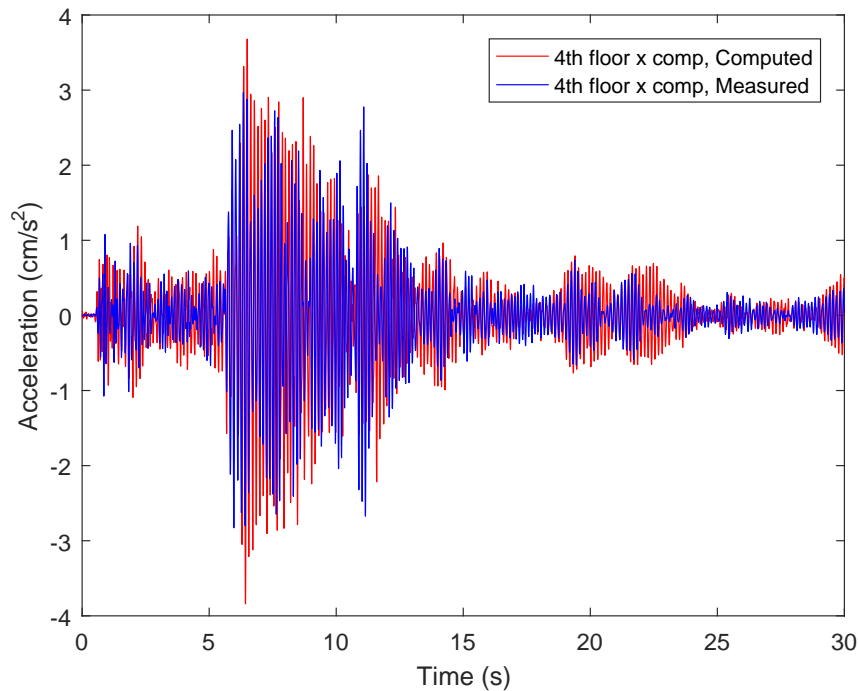


Figure 5.7: Response, 4th floor sensor recorded vs. computed

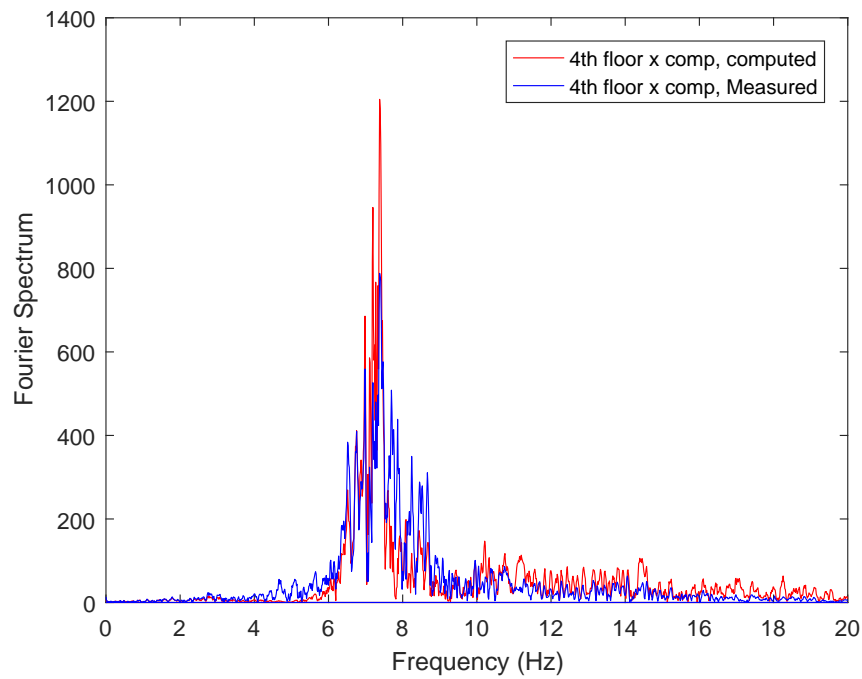


Figure 5.8: Fourier spectra, 4th floor sensor recorded vs. computed

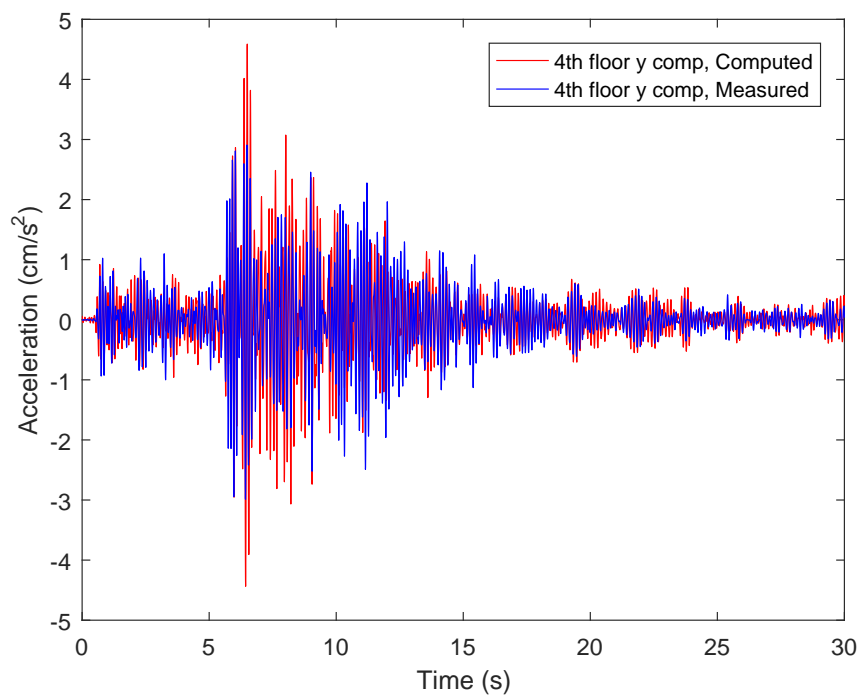


Figure 5.9: Response, 4th floor sensor recorded vs. computed

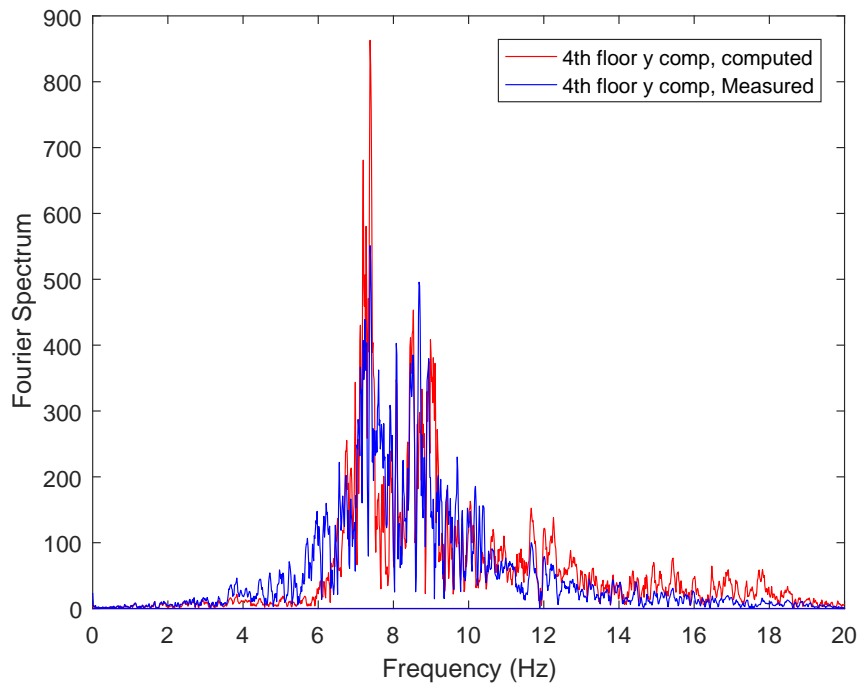


Figure 5.10: Fourier spectra, 4th floor sensor recorded vs. computed

Figures 5.9 and 5.8 show that the computed values give good approximation of the measured values. The acceleration plot has a PSA of $4,6 \text{ cm/s}^2$ at approximately 6.5 seconds for computed values. The measured values give higher value of PSA or $2,9 \text{ cm/s}^2$ at 6,4 seconds. The Fourier spectrum shows computed frequency of 7.37 Hz and the measured values give exact same frequency for mode 1.

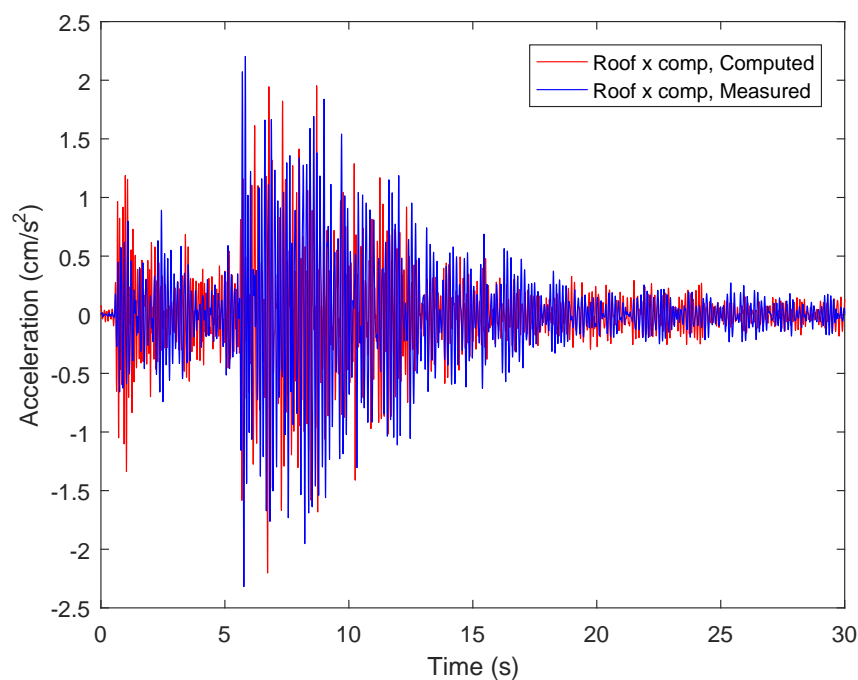


Figure 5.11: Response, roof sensor recorded vs. computed

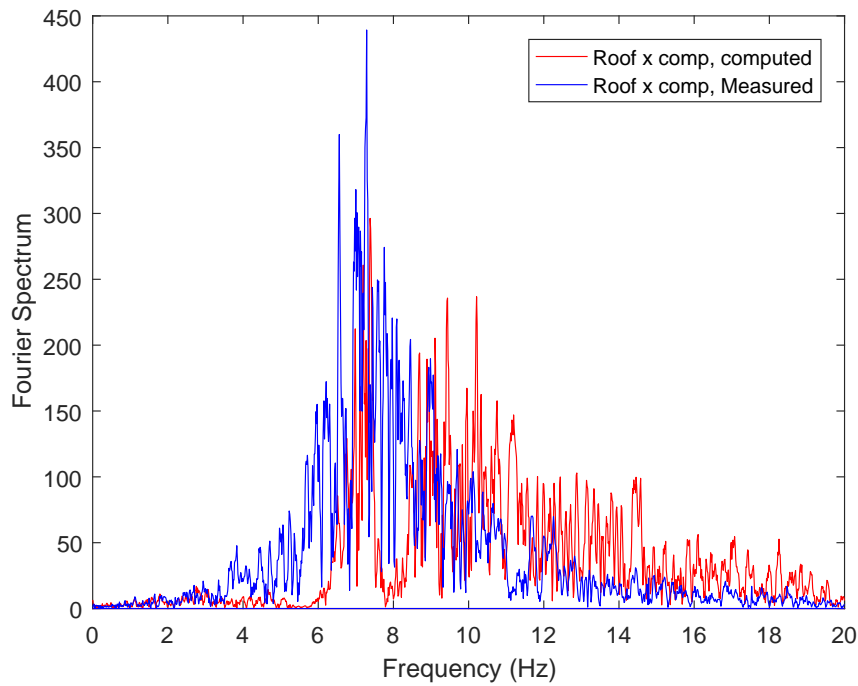


Figure 5.12: Fourier spectra, roof sensor recorded vs. computed

Figures 5.11 and 5.12 show that the computed values give good approximation of the measured values. The acceleration plot has a PSA of $2,2 \text{ cm/s}^2$ at approximately 6.7 seconds for computed values. The measured values give higher value of PSA or $2,3 \text{ cm/s}^2$ at 5,7 seconds. The Fourier spectrum shows computed frequency of 7.38 Hz and the measured values give frequency of 7,29 Hz for mode 1.

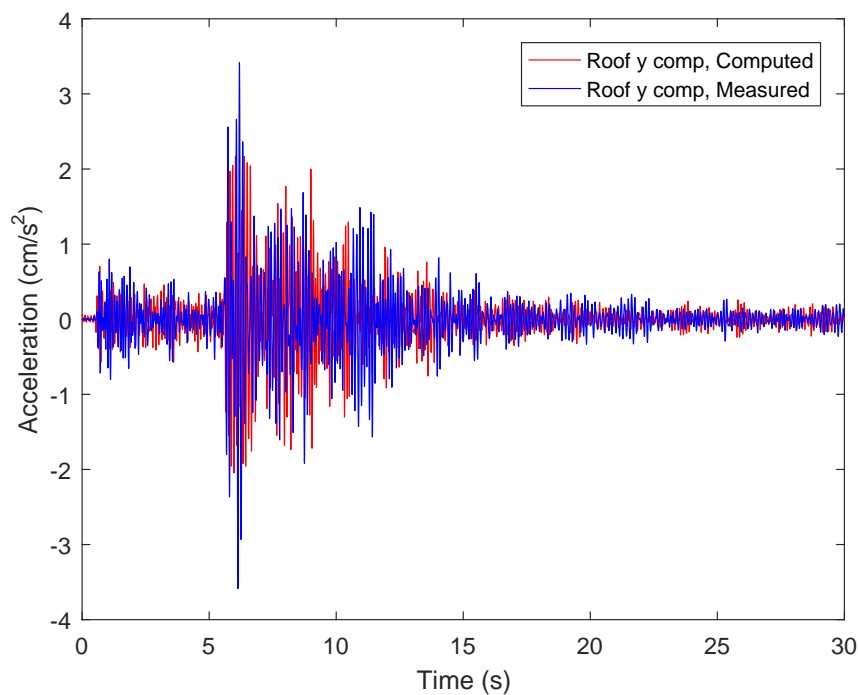


Figure 5.13: Response, roof sensor recorded vs. computed

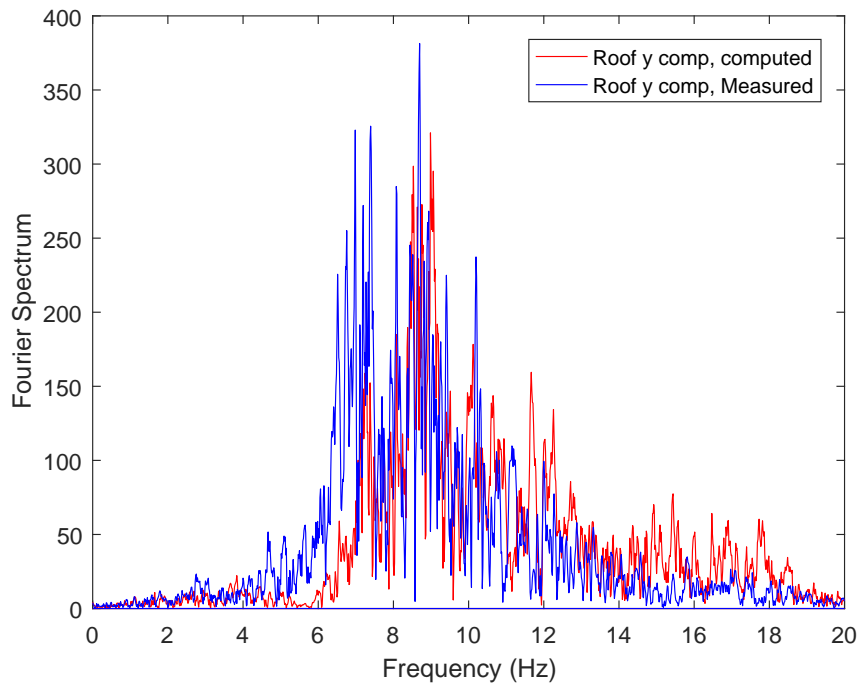


Figure 5.14: Fourier spectra, roof sensor recorded vs. computed

Figures 5.13 and 5.14 show that the computed values give good approximation of the measured values. The acceleration plot has a PSA of $2,16 \text{ cm/s}^2$ at approximately 6,3 seconds for computed values. The measured values give higher value of PSA or $3,42 \text{ cm/s}^2$ at 6,2 seconds. The Fourier spectrum shows computed frequency of 8,7 Hz and the measured values give frequency of 8,53 Hz for mode 1.

The comparison of computed and measured response of the structure gives good idea of the functionality of the FE model. The sensors gives a good estimation on the response. The Fourier spectrum for sensor on roof does not suit the computed values as expected for the x direction. This could by some extent be explained by assumptions made in the construction of the FE model. The stair between floors are not modelled and neither are the openings in the floor slabs modelled. Figure 5.12 show that the calculated mode shapes underestimate the torsion at the location of the roof sensor.

6. Analysis and results

This chapter will show the main results from the response analyses performed. The response of the building will be calculated with the use of the SAP2000 software. Computed values and figures will be published in the text for clarification. The earthquake response of the building will be checked for a seismic hazard represented by the Eurocode spectrum and time histories based on earthquake strong ground motion measurements gathered from South Iceland.

6.1 Response spectra analysis

The Eurocode response spectrum is used to represent the seismic action. The spectrum is defined as horizontal spectrum of type 1 for soil A and reference peak ground acceleration of $a_{gR} = 0.5g$ and damping is assumed to be 5%. The corresponding values for the definition of the spectra can be found in table 2.1 and in chapter 3 in EN 1998-1 [5]. The lower bound factor beta is defined by the Icelandic national annex. The recommended beta factor is 0.2. The behaviour factor is set to the minimum recommended value 1,5 according to table 5.1 in EN 1998-1. The calculated load is increased by the importance factor 1,4 for importance class IV [5].

The response spectra is defined for three directions. The spectra is defined for full acceleration in x (RS 0°) and y (RS 90°) directions and equally distributed acceleration in xy (RS 45°) direction.

6.1.1 Shear forces

The base and story shear forces are obtained according to the response spectrum analysis. The forces are picked out of the model with the section cut tool. The section cut tool calculates forces by summing the joint forces within objects which are entirely within the cutting plane and included in the section cut group. The story shears are picked out and plotted along the elevation for all directions. Figure 6.1 shows the storey shear

for each earthquake action and both directions x and y. The x values are above and y values beneath for each earthquake action.

The maximum base shear of 15650 kN is obtained for the RS° earthquake action. The base share is calculated to be near 40% of the total weight of the building. Compared to total mass of 4459 ton.

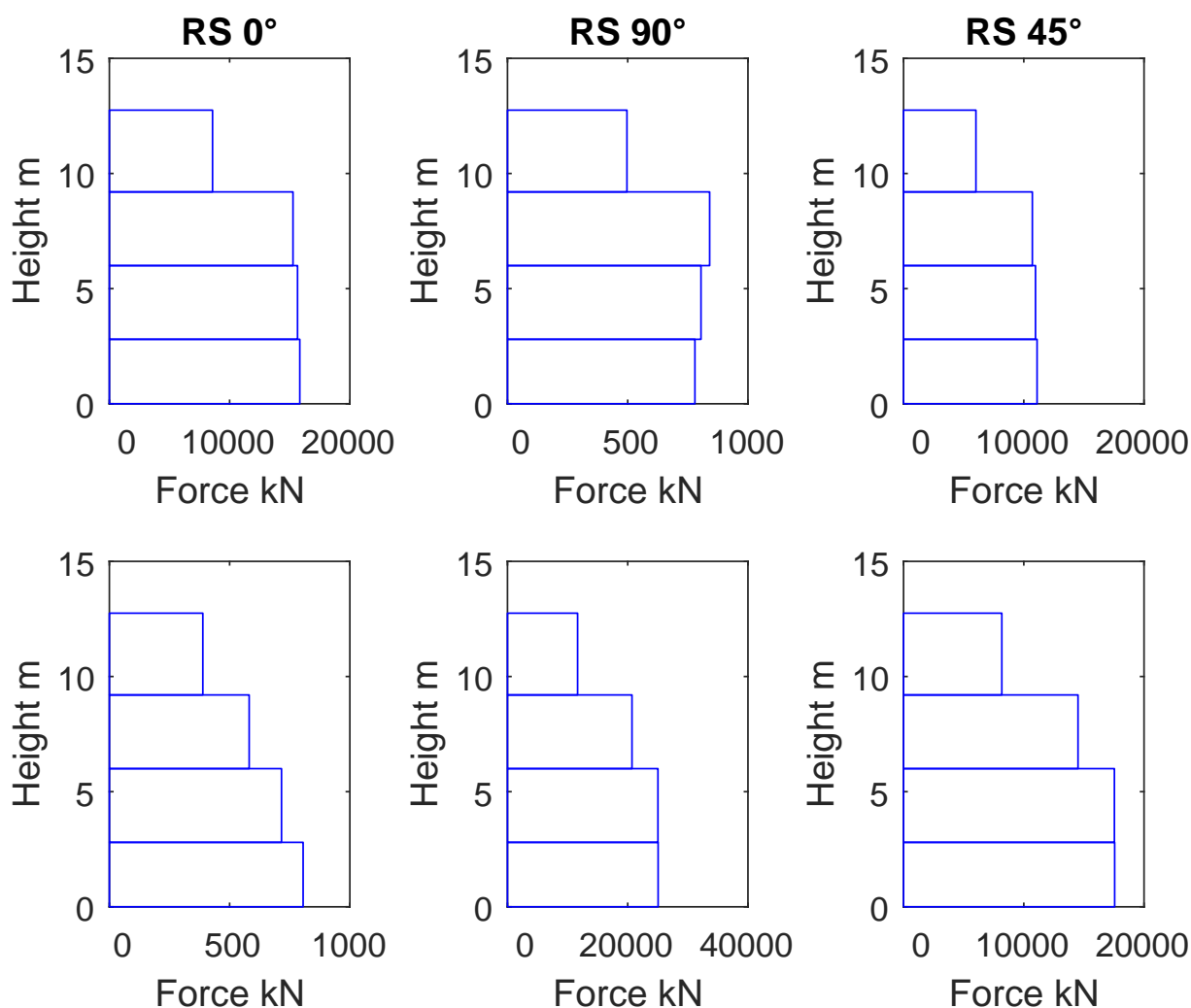


Figure 6.1: Storey shear for each earthquake action both directions. Earthquake action is represented as column and directions as line with x above and y below.

6.1.2 Displacements

The maximum displacements due to response spectrum analysis are obtained on the south west corner. The displacement is measured on each floor level for each earthquake action. According to EN 1998-1 the actual displacements of a structure shall be calculated as the product of the behaviour factor q and the calculated displacement. This is to cancel the behaviour factor out for the service limit state. The measured displacement in the model is therefore multiplied by the behaviour factor q as equation 6.1 shows.

$$d_s = d_e \cdot q \quad (6.1)$$

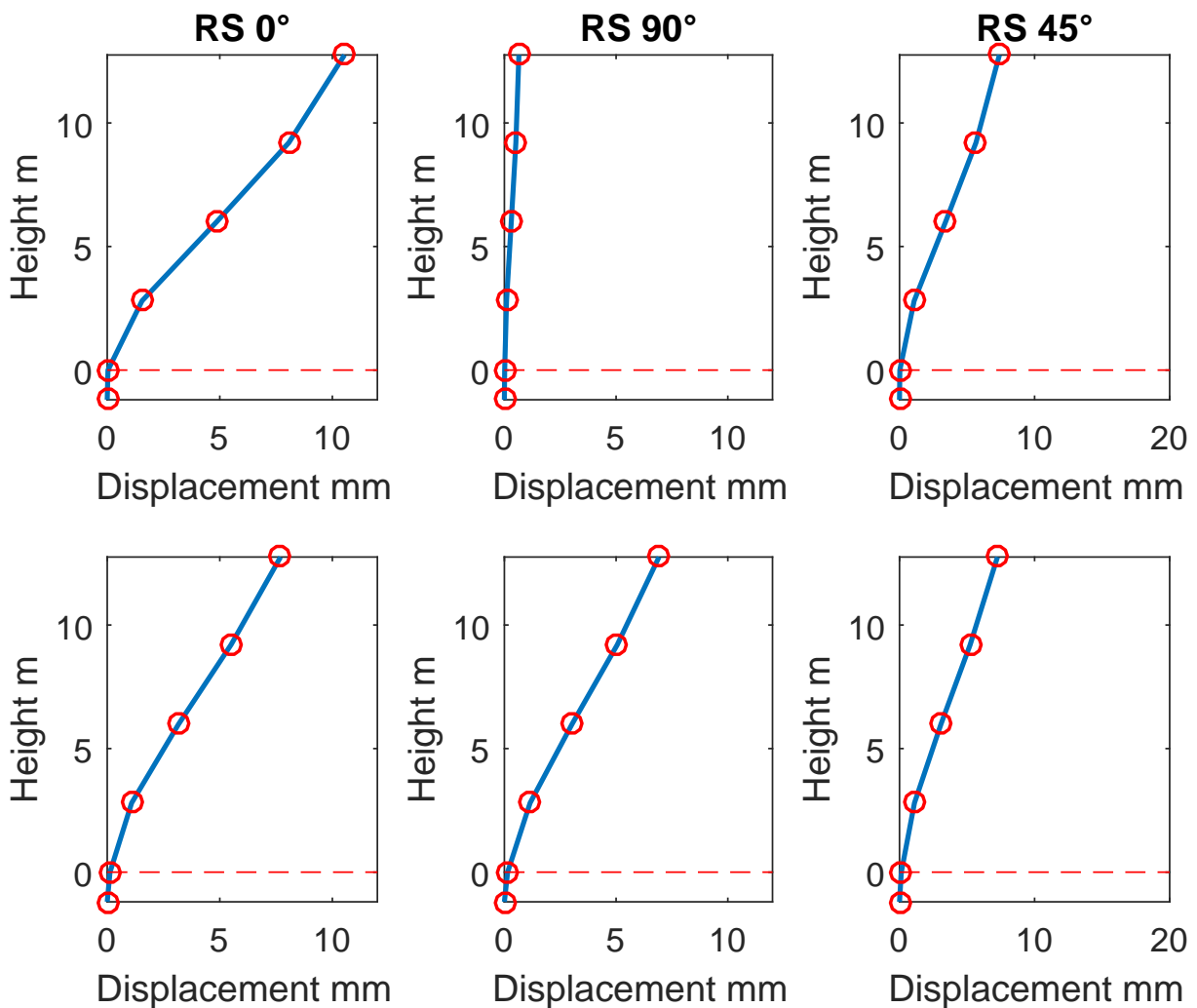


Figure 6.2: Displacement for each earthquake action in both directions. The earthquake action is represented as column and directions as line with x above and y below.

6.1.3 Damage limitations

Damage limitations according to EN-1998-1 are calculated for the building. The damage limitation is verified in terms of interstorey drift using equation 6.2. The interstorey drift is the difference of the lateral displacements evaluated in section 6.1.2 and is denoted as d_r . The reduction factor v , takes into account the lower return period of the seismic action associated with the damage limitation requirement. The reduction factor depends on the importance class of the building. The hospital is classified as a building whose integrity during earthquakes is of vital importance for civil protection and the importance class is IV, and v is reduction factor which takes into account the lower return period of the seismic action associated with the damage limitation requirement and amounts to 0.4. According to EN 1998-1 the damage limitations criteria is given by three categories for α . The factor α takes into account the type of non structural elements and their arrangement into the structure and amounts to 0.005, 0.0075, and 0.01 [5] [4].

$$d_r \cdot v \leq \alpha \cdot h \quad \rightarrow \quad \frac{d_r}{h} \leq \frac{\alpha}{v} \quad (6.2)$$

Figure 6.3 shows that drifts of the building examined are below the strict criteria for a building having non-structural elements of brittle materials attached to the structure. The criteria is fulfilled for any storey, any earthquake action and in any direction. The damage criteria is fulfilled if the storey drift will not exceed the conditions on figure 6.3 represented as green, red and blue lines.

- Green - Structural elements of brittle materials attached to the structure
- Red - Ductile non-structural elements
- Blue - Non-structural elements fixed in a way so as not to interfere with structural deformations or without non-structural elements

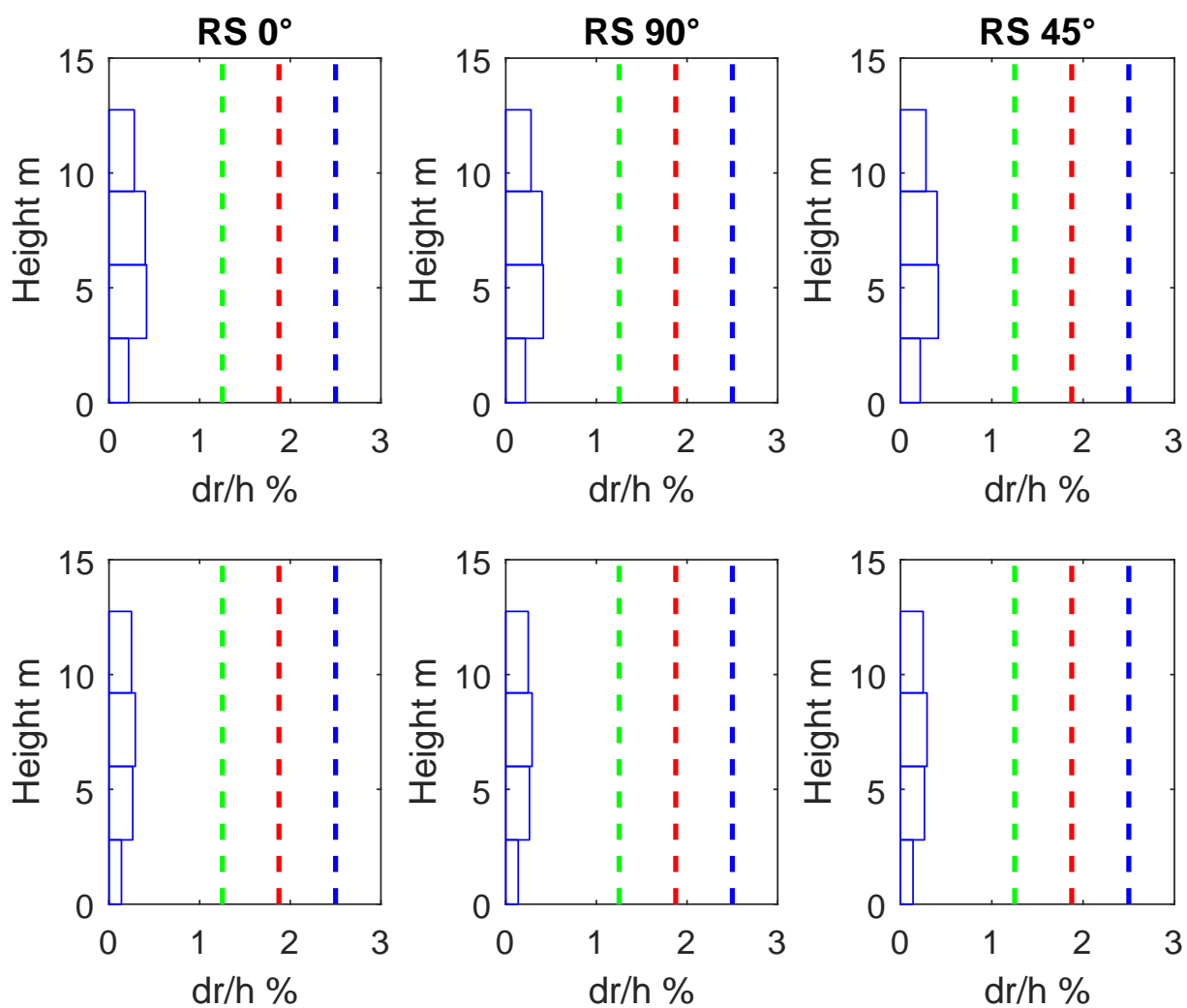


Figure 6.3: Storey drifts control for each earthquake action in both directions. Earthquake action is represented as column and directions as line with x above and y below.

6.2 Time history analysis

Time history analysis are based on data gathered from the IESD. The data is from southern Iceland as described in chapter 4.4.

6.2.1 Flagbjarnarholt

The maximum base shear of 11150 kN is obtained for the Flagbjarnarholt max earthquake action in x direction. The base share is calculated to be near 28 % of the total weight of the building. Compared to total mass of 4459 ton.

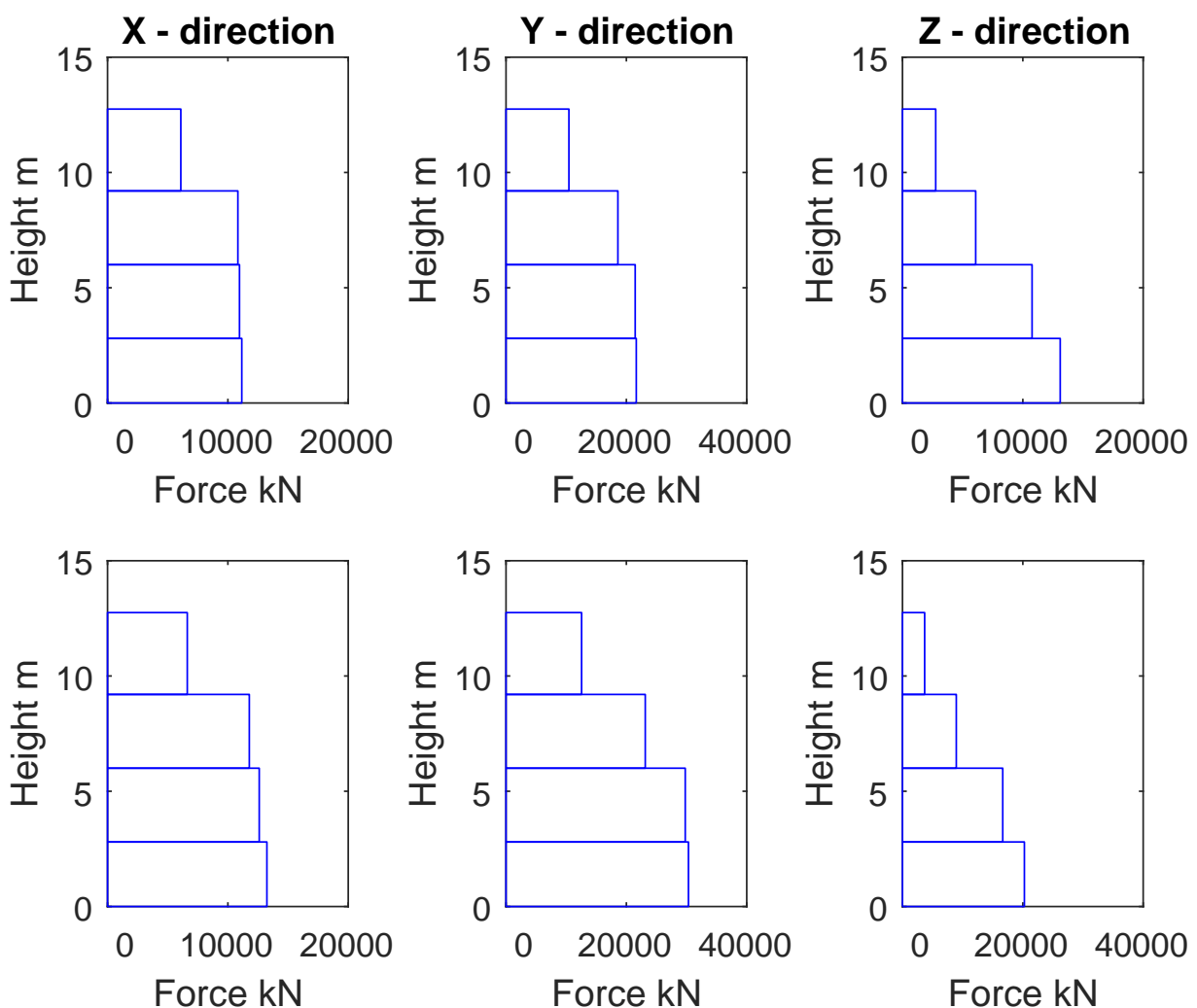


Figure 6.4: Storey shear for Flagbjarnarholt earthquake action. the columns represent direction and lines represent max and min values with max values above.

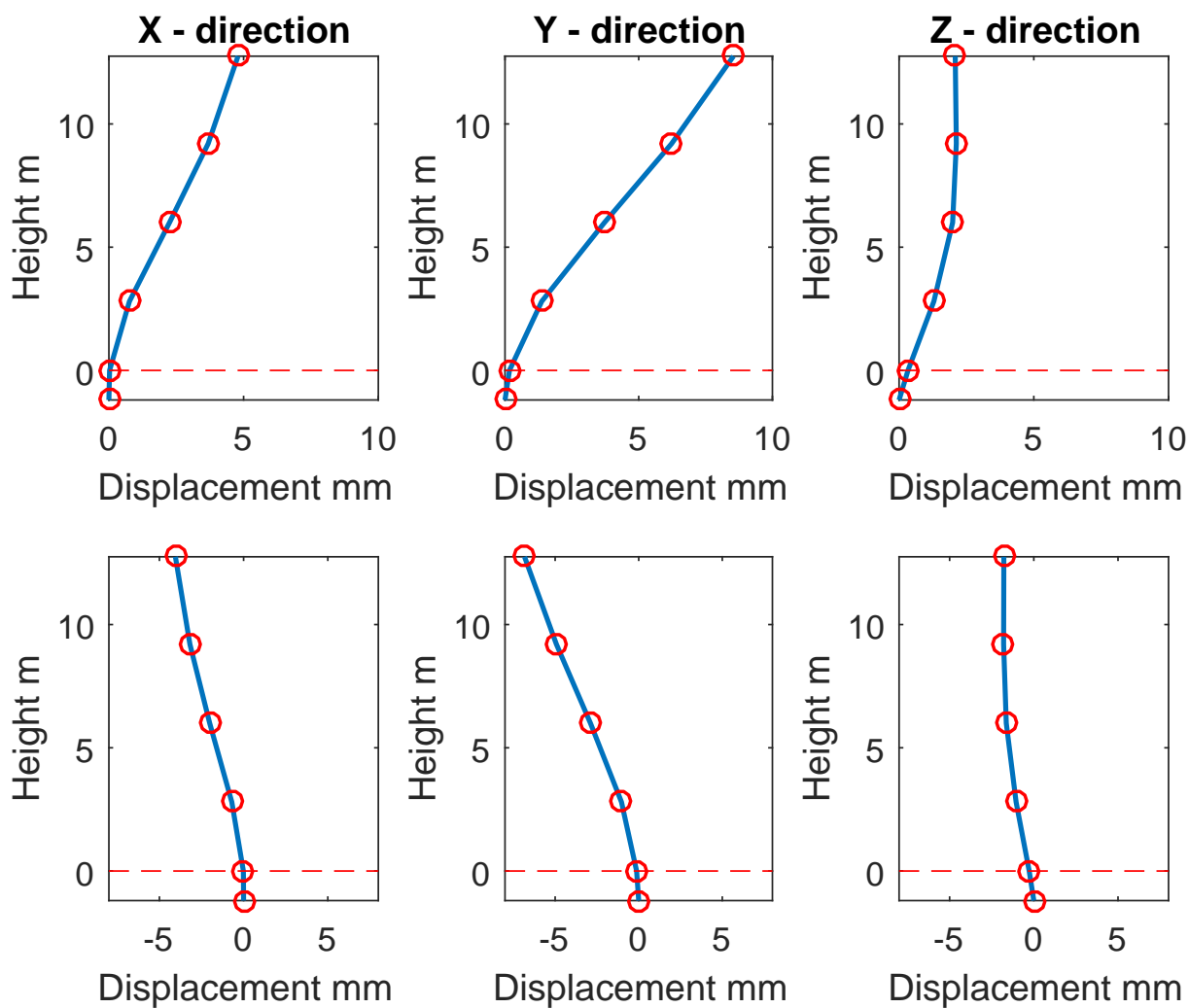


Figure 6.5: Displacement for Flagbjarnarholt earthquake action, the columns represent direction and lines represent max and min values with max values above.

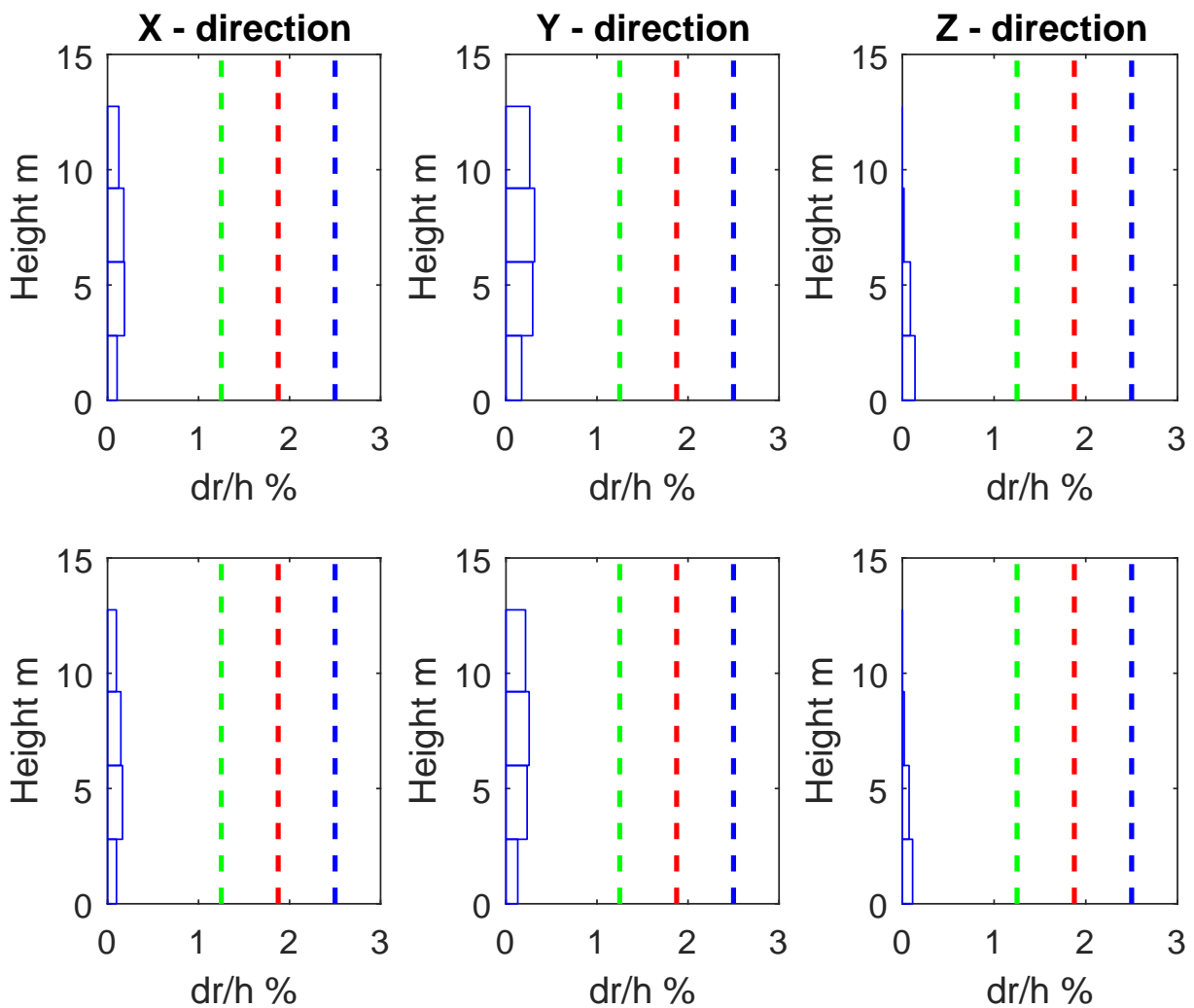


Figure 6.6: Storey drifts for Flagbjarnarholt earthquake action, the columns represent direction and lines represent max and min values with max values above.

6.3 Structural integrity

The design of the building consists of high ratio of concrete walls. These walls form a concrete core inside the building that is consistent through all floor levels except for a part of the cellar. The building is therefore relatively stiff as the natural frequency indicates. The following analysis will aim to estimate the forces induced in the hospital building.

The outer shell is most vulnerable for loads, this is because of the number of big doors and windows. Critical building components will be chosen for further inspection. The examined components will be introduced on following figures.

The following figures are prepared using the concrete design module in SAP2000. The figures show absolute maximum of the design force (N_{Des2}) in vertical direction accord-

ing to earthquake action RS 90. Figure 6.7 show how the load transfers to the columns between the windows. The columns are given name in order of A, B, C and D and number for each column.

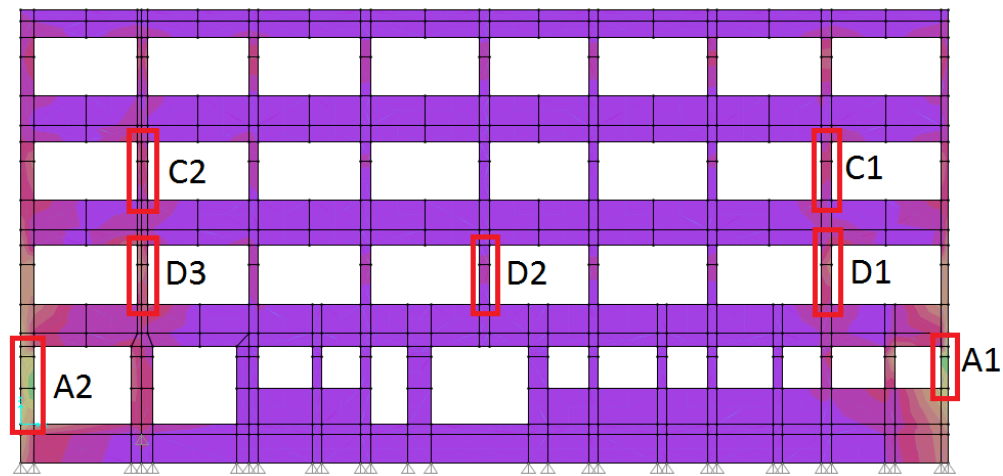


Figure 6.7: Wall facing S-W, critical cross sections used for further inspection

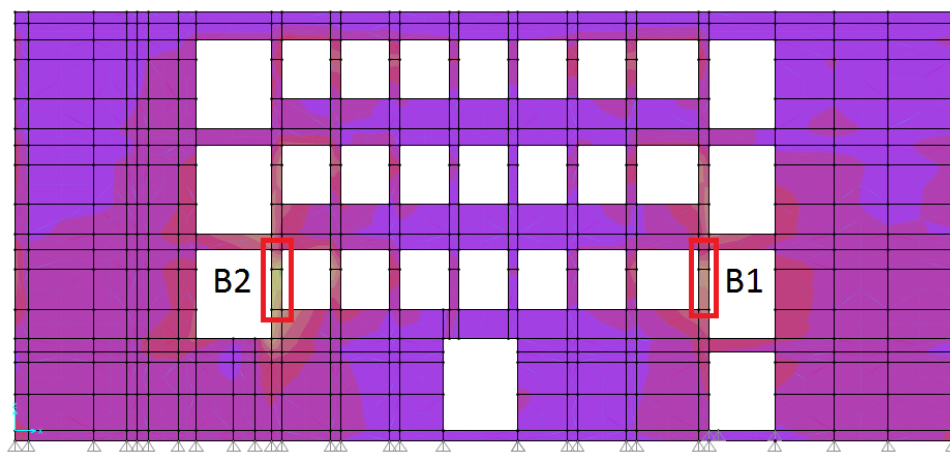


Figure 6.8: Wall facing N-E, critical cross sections used for further inspection

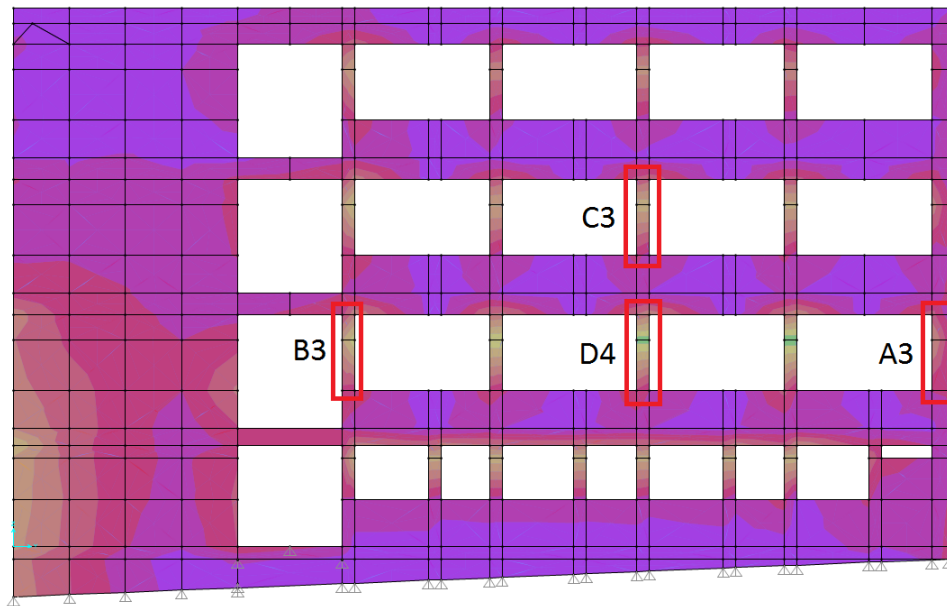


Figure 6.9: Wall facing S-E, critical cross sections used for further inspection

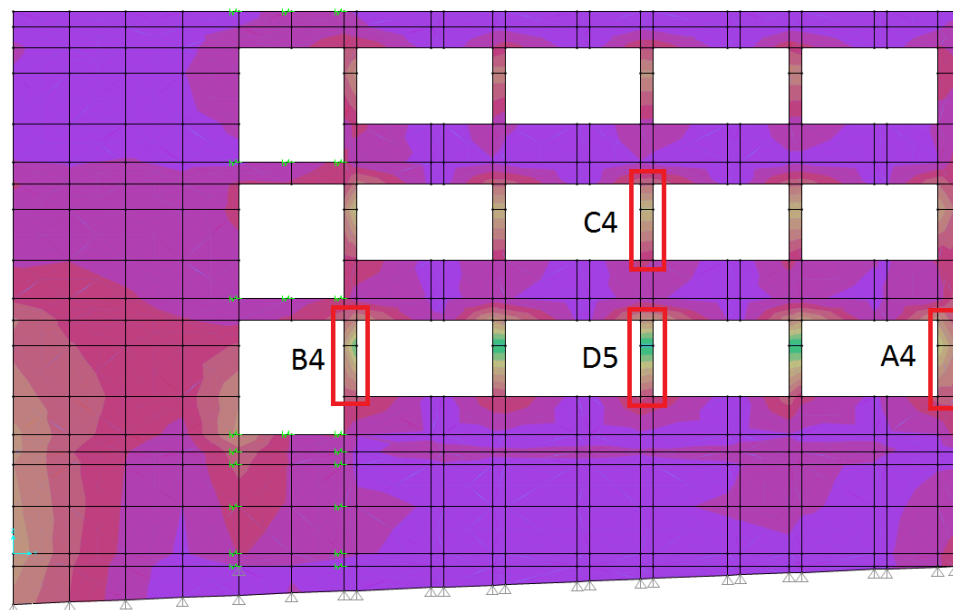


Figure 6.10: Wall facing N-W, critical cross sections used for further inspection

These figures show the force distribution for the RS 90° earthquake action as reference for chosen cross sections. The section cut tool in SAP2000 is used to obtain the forces in each column at given earthquake action. Figures 6.11 and 6.12 shows the reinforcement detailing of the columns. The figures show that column A and B are connected to adjacent walls and columns C and D are free-standing in-between windows.

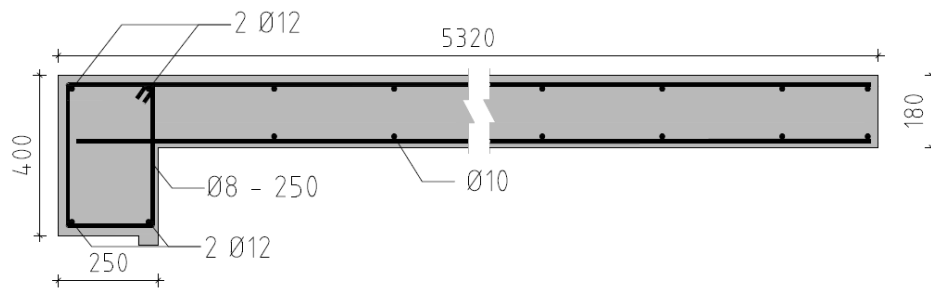


Figure 6.11: The reinforcement of column A

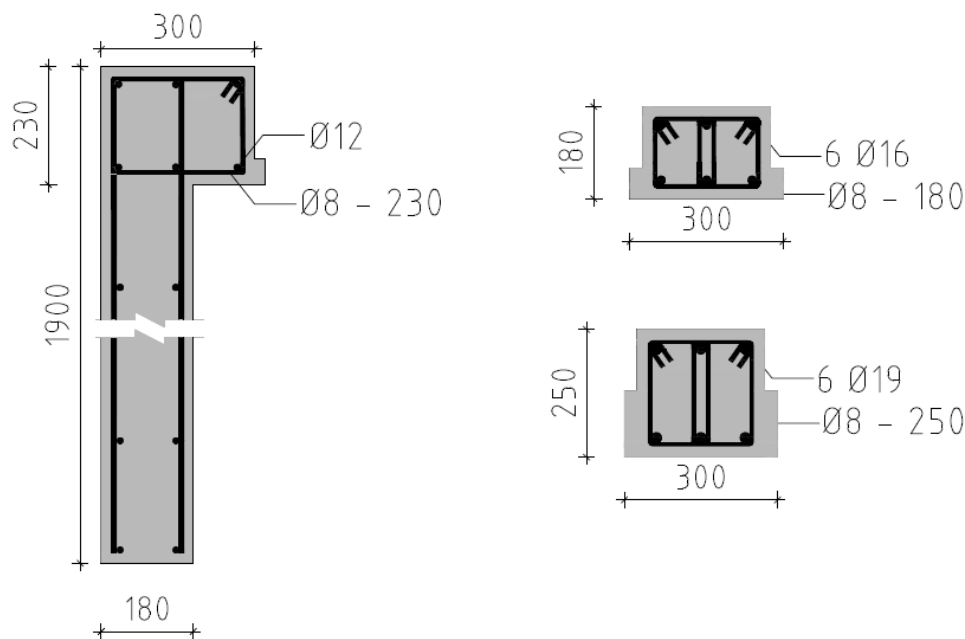


Figure 6.12: The reinforcement of column B, C and D, Column B to left and C to right above D.

The computed forces in the cross sections for each earthquake action are compared and the most critical cross sections are examined due to highest earthquake induced forces. Table 6.1 gives summary for cross sections A1, A4, B1 and B4 according to figure 6.10. Table 6.1 is based on tables in Appendix B showing section cut earthquake induced forces. These forces are represented as absolute values, the higher value of the min and max values in the tables in appendix B. Table 6.1 shows that the earthquake induced force is considerably highest for time histories from the retirement home and Sólheimar.

Table 6.1: Summary of earthquake induced forces, cross sections A1, B1, A4 and B4

Cross section	A1			B1			A4			B4		
Load case	P	M	V	P	M	V	P	M	V	P	M	V
	kN	kNm	kN	kN	kNm	kN	kN	kNm	kN	kN	kNm	kN
RS 0	398	46	51	391	60	52	471	6	2	496	4	3
RS 90	210	24	30	95	15	12	284	4	0	265	3	0
RS 45	315	37	41	283	43	38	386	5	1	394	3	2
Flagbjarnarholt	518	44	69	407	46	54	449	5	2	406	3	2
Kaldarholt	532	62	69	601	86	81	515	6	3	524	5	4
Sólheimar	361	96	49	861	128	113	916	10	4	453	4	4
Þjórsártún	556	52	70	451	79	60	667	7	3	600	3	4
Selfoss city hall	290	33	35	212	27	30	254	2	2	295	2	2
Retirement house	674	69	86	843	124	111	1201	12	4	784	7	6
EERC	101	5	12	164	19	20	156	1	0	173	2	2
Borgarhraun	298	43	37	252	38	31	283	3	2	422	3	2
Ljósafoos	49	9	6	44	11	6	78	2	1	97	1	0

The cross sections at hand are examined due to the forces that act on the structure at each time step. Table 6.1 gives the maximum values for the earthquake action envelope at the same time step. The axial force P is the compression force in the column without the compression due to dead load. The cyclic load due to earthquake gives the maximum force at given time step and therefore it can be interesting to examine the earthquake induced forces plotted against time. Following figures show the earthquake induced forces with the absolute maximum represented as a red dot and the maximum earthquake induced force according to the design response spectra RS 0° represented as a red dashed line. In appendix C figures for each section can be examined. Following are interesting examples for the earthquake actions retirement house and Sólheimar for column A1 and B1.

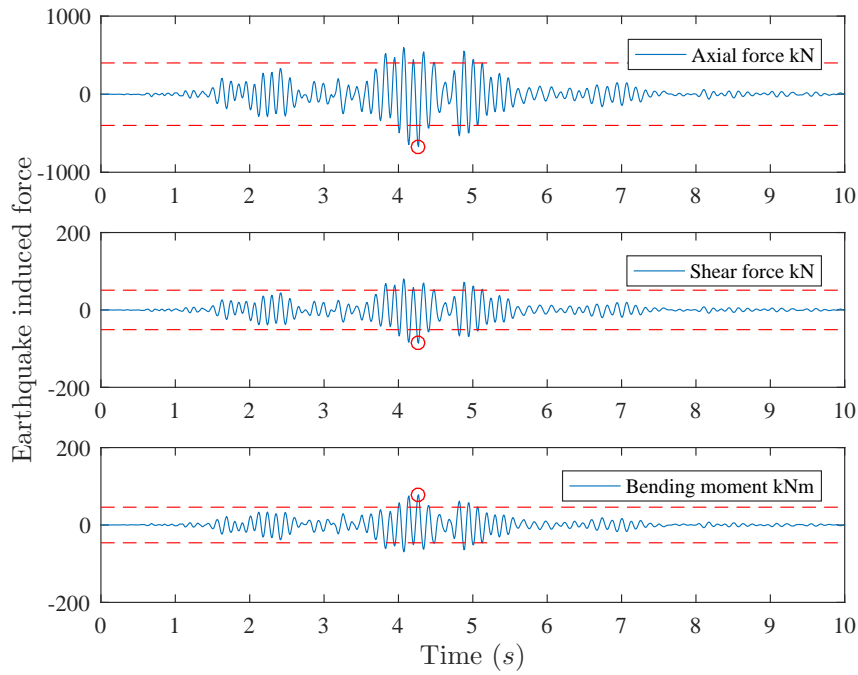


Figure 6.13: The earthquake induced forces against time for column A1 and Retirement home time history, the absolute max value is represented as a red dot, the maximum force according to the design response spectra is represented as a red dashed line.

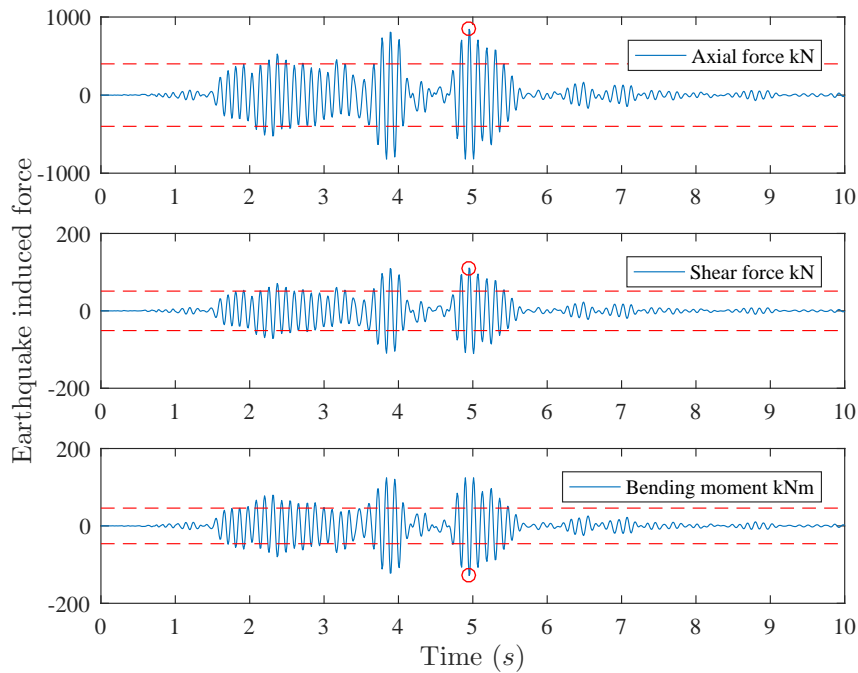


Figure 6.14: The earthquake induced forces against time for column B1 and Retirement home time history, the absolute max value is represented as a red dot, the maximum force according to the design response spectra is represented as a red dashed line.

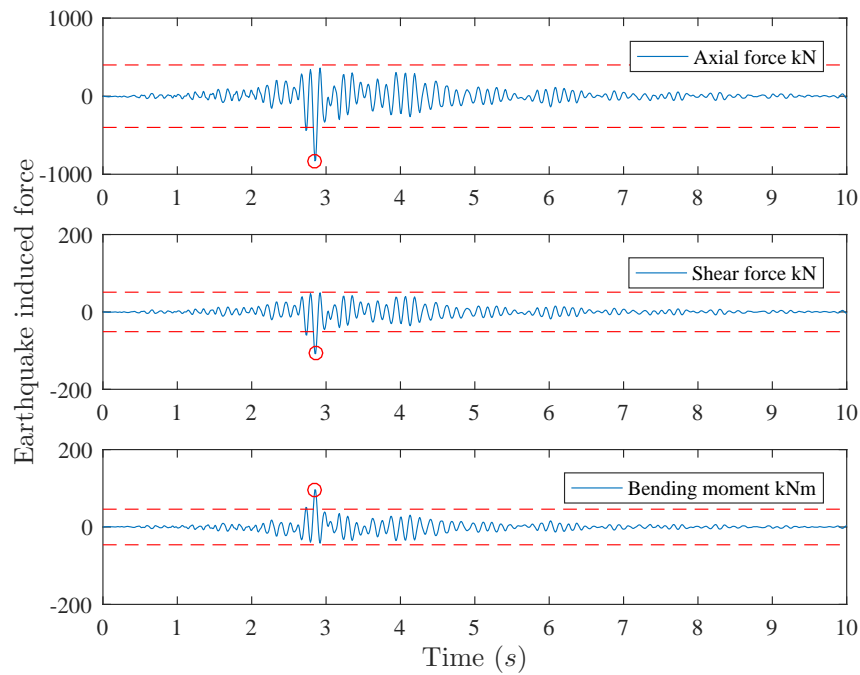


Figure 6.15: The earthquake induced forces against time for column A1 and Sólheimar time history, the absolute max value is represented as a red dot, the maximum force according to the design response spectra is represented as a red dashed line.

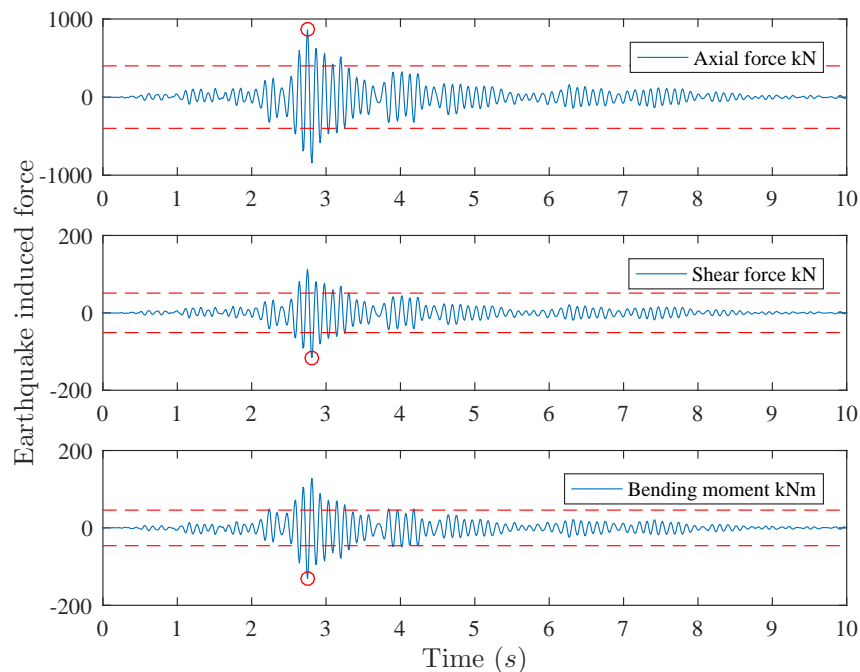


Figure 6.16: The earthquake induced forces against time for column B1 and Sólheimar time history, the absolute max value is represented as a red dot, the maximum force according to the design response spectra is represented as a red dashed line.

The time histories examined give higher earthquake induced forces than the design response spectra for short time intervals. This is particularly true for the Sólheimar

earthquake action as can be seen on figures 6.15 and 6.16. For this behaviour it is interesting to locate the natural period of the hospital for first three modes on the response spectra summary graph. Figure 6.17 shows how the fundamental periods of the house meet the acceleration peak of the response spectra. The figure is based on figure 4.26 and is now represented in log scale.

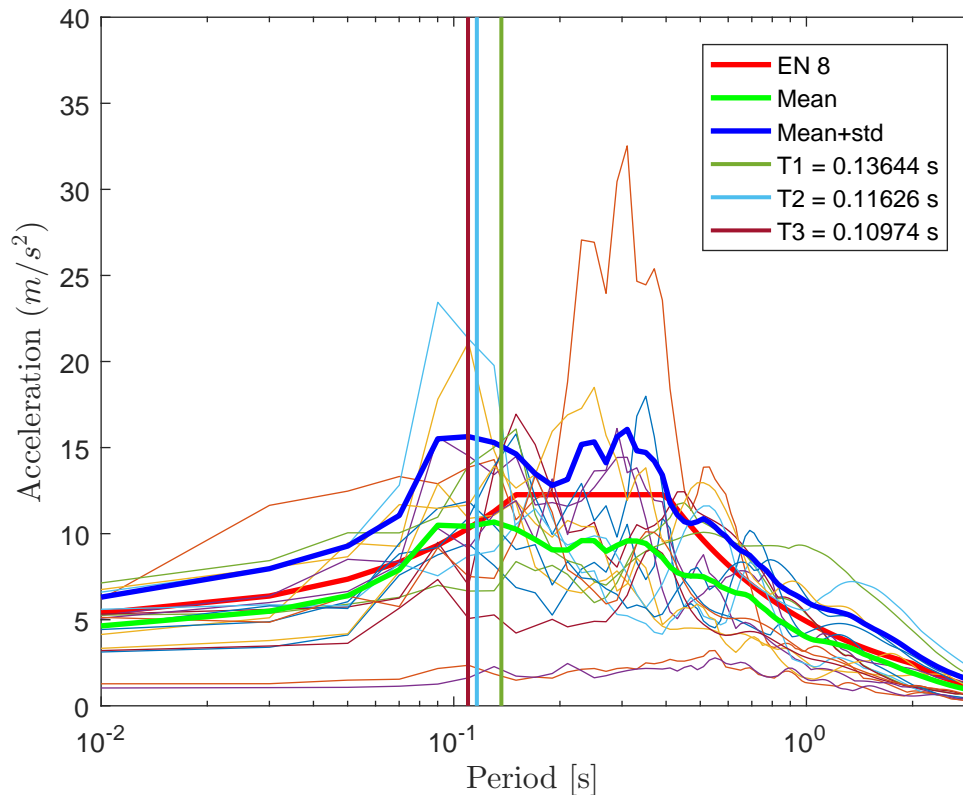


Figure 6.17: The natural periods for first three modes vs. the response spectra

Figure 6.17 shows how the building is responding to the horizontal components of the time histories recorded at south Iceland. The building responds at high acceleration and will induce high forces for this peak.

6.3.1 Axial force and bending moments

The structural integrity of the columns is verified using bending moment and axial force interaction diagram (M-N diagram). The diagram is a curve plot of points where each point has two ordinates. The ordinates are bending moment strength and corresponding axial force. The strength interaction diagram is built on calculations of various strength verifications and any combination of axial force and bending moment outside of the envelope will cause failure in the building component. The dead load is not accounted for in these calculations, and compared to the earthquake induced axial force the dead load is minimum. According to the calculations added compression

force will help the cross section. Figure 6.18 shows an example of the diagram. The yellow dot will cause failure in the cross section. [23].

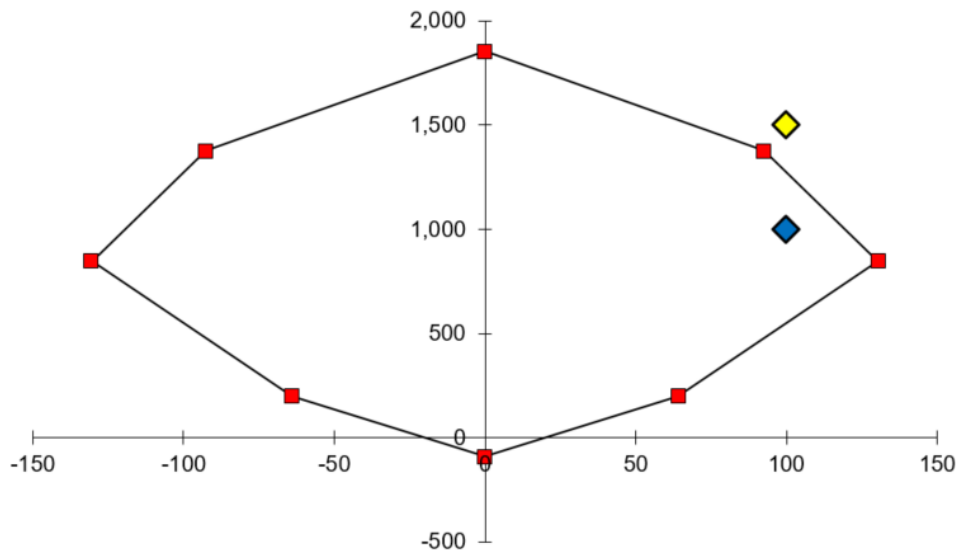


Figure 6.18: M - N diagram shows two combinations of axial force and bending moment. The yellow dot is outside of the envelope and will cause failure in the cross section. The x axis shows the axial force in kN and the y axis shows the bending moment in kNm.

The calculations for M - N interaction diagram are based on 5 (Brotform) strength criteria cases. The cases are following:

- The cross section is subjected to full compression.
- Compression failure, neutral axis located in tension reinforcement.
- Compression failure, tension plasticity in tension reinforcement.
- Compression failure, compression plasticity in compression reinforcement.
- The cross section is subjected to full tension.

The columns performance in earthquake are of vital importance for the structural integrity of a structure. Columns consists of areas that are critically affected by earthquake loads. To use the M-N diagram a simplification on the cross sections are made. The length of the cross section is relatively long versus the column cross section so it is treated as simple cross section. Because of this simplification the forces in those cross sections have to be re-evaluated and with the section cut the forces are estimated as before for earthquake action RS 0. Columns A and B can barely resist the loads according to the earthquake action. Figure 6.19 show the blue dot slightly outside of the diagram.

This estimation of the diagram has only 5 reference values and therefore the lines do not estimate the curve between points. Following figures –

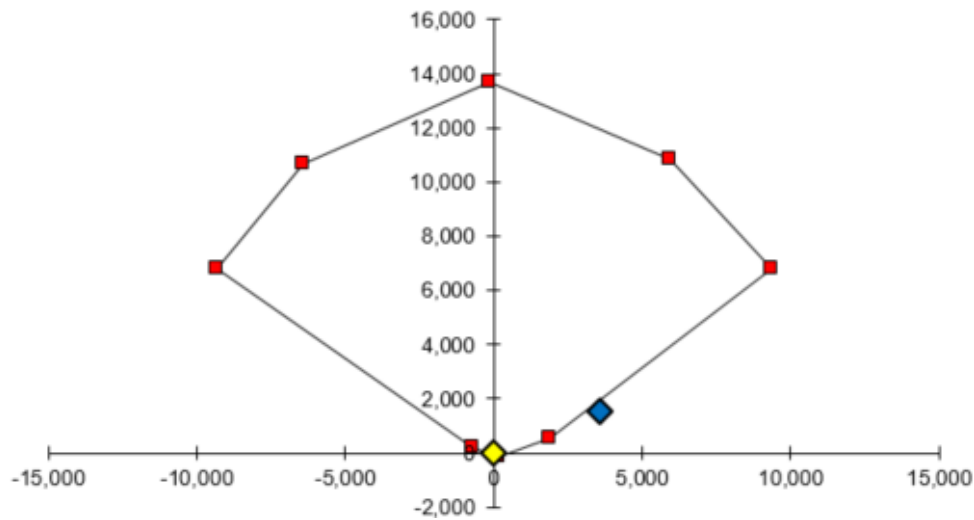


Figure 6.19: M - N diagram for column A, The x axis shows the axial force in kN and the y axis shows the bending moment in kNm.

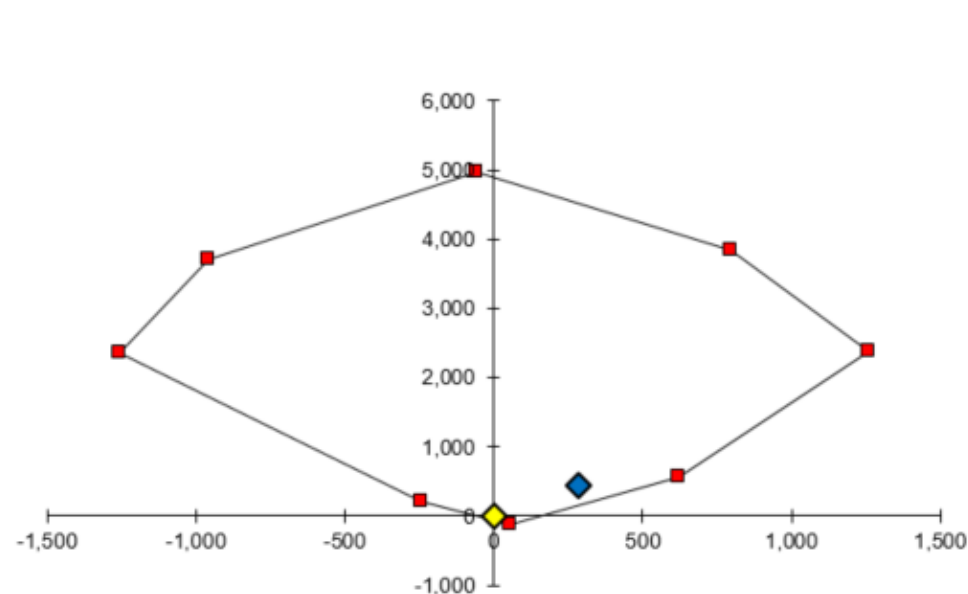


Figure 6.20: M - N diagram for column B, The x axis shows the axial force in kN and the y axis shows the bending moment in kNm.

The axial and bending moments subjected to columns C and D are not harmful to the cross sections. The cross sections do not transfer significant loads due to their relatively low stiffness.

Two critical beam sections will be examined in addition to the columns. The beams are showed on figure 6.21. Beam 1 to left is the beam beneath column D2 on figure

6.8. Beam 2 is the beam in the door openings. The forces for these beams are obtained using the section cut for earthquake action RS 0. Beam 1 is subjected to axial force of 62 kN and bending moment of 76 kNm. Beam 2 is subjected to axial force of 98 kN and bending moment of 37 kNm.

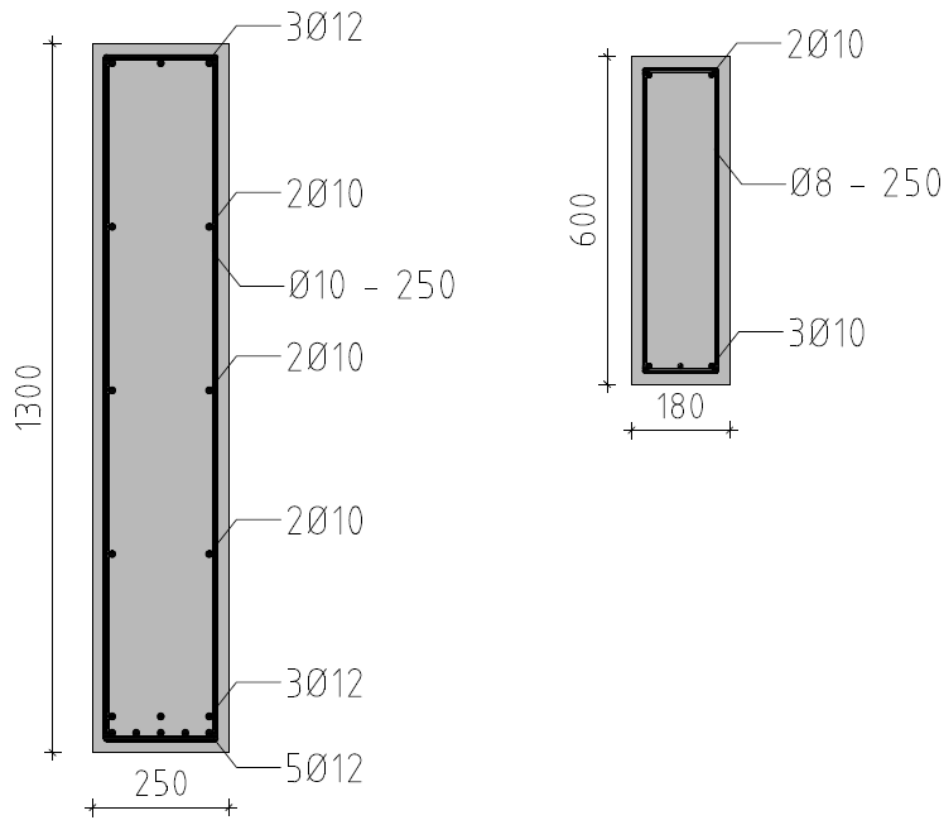


Figure 6.21: The beam cross sections to left beam 1 and to right beam 2

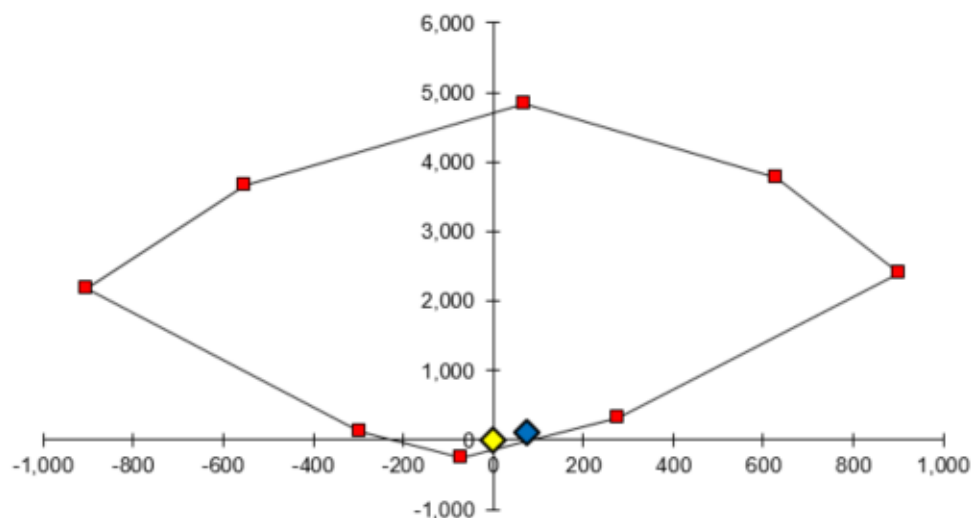


Figure 6.22: N-M diagram for beam 1, The x axis shows the axial force in kN and the y axis shows the bending moment in kNm.

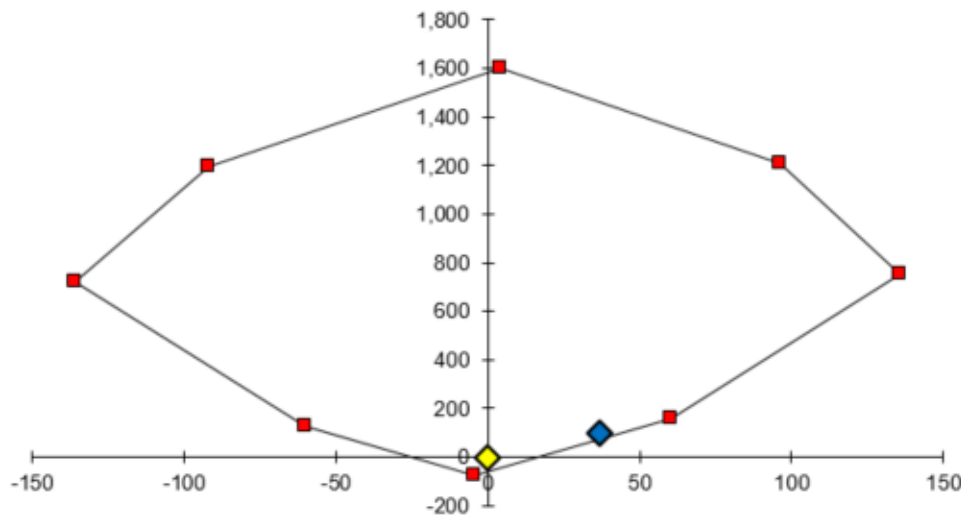


Figure 6.23: N-M diagram for beam 2, The x axis shows the axial force in kN and the y axis shows the bending moment in kNm.

6.3.2 Shear forces

Concrete building components must be capable of carrying shear forces caused by their self weight and externally imposed action such as earthquake excitation. Concrete sections may have enough shear capacity to resist small amount of shear forces. There is however in most cases a nominal or minimum amount of shear reinforcement provided in loaded components. There can be exceptions for lightly loaded components such as floor slabs, pad foundations and very minor beams such as short span, lightly loaded lintels over doors and windows [23].

The shear capacity of the building components was reviewed according to shear forces from the earthquake actions previously defined. The extreme cases were examined for column A and B and Beam 1 and 2. Calculations are in appendix E

Table 6.2: The shear capacity of cross sections

Cross section	Φ	S	V_{ED}^I	V_{ED}	$V_{RD,max}$	$V_{RD,c}$	$V_{rd,s}$
	mm	mm	kN	kN	kN	kN	kN
Column A	10	300	1594	1993	2300	218	1235
Column B	10	300	387	484	820	90	437
Beam 1	10	250	67	84	775	92	357
Beam 2	8	250	232	290	252	36	103

Table 6.2 show that the stirrups do not resist the forces due to the design response spectra as EN 1992-1 insists. The distance between the stirrups in columns and beams are

systematically equal to the height of the cross section. This will lead to cracks due to shear with 45° angle between the stirrups and they will not contribute as intended. According to EN 1992-1 the maximum allowable distance between stirrups is 75% of the distance to the tension reinforcement (d) and never more than 300mm [23] [16].

The most critical factor regarding strength capacity of a structure in case of earthquake are the stirrups. The design and detailing should always be in order of the regulations valid at the construction time. There have however been great improvement on reinforcing of building components since the construction of the hospital.

The presence of stirrups in concrete building components constitute the most crucial factors affecting the quality and the earthquake resistant strength of building. The following parameters are of major reliability for proper behaviour of concrete cross section. Hooks are necessary for the proper behaviour of stirrups and this is especially true during intense earthquakes. The hooks are the only anchoring mechanism when the concrete cracks. Stirrups must be bend in rolls with diameter at least equal to four times the diameter of the reinforcement and the distance between legs of a closed stirrup must be placed no more than 200 mm apart from each other. [24].

6.3.3 Walls

Reinforced concrete walls are an efficient system for buildings to sustain seismic actions and limit displacements. Recent analysis of buildings with large lightly reinforced walls have showed a lower damage level in comparison with buildings constructed with RC frames. These analyses have shown that the performance under seismic action is a function of the walls density. The wall density is defined as the floor and surface ratio. Buildings with walls density of 3 - 4 % in both directions have shown good performance subjected to earthquake excitation [25].

For the structural verification of the walls this observation will be used. The total cross section of walls shall be minimum 3,5 % of the floor area. There can be a difference between the values for x and y direction but the ratio should not be less than 1.5% in each direction. This only applies to walls that are continuous between foundations and top floor with vertical openings less then 50% of the wall area. These walls contribute significantly to the stiffness of buildings. The ratio of height to length shall not be more than 3. [26].

Tables 6.3 and 6.4 show the density ratio of the walls for both x and y direction. The total density of the house is 7 % of the total surface of 633 m². This is considerably higher ratio than the minimum value of 3.5%. The walls in the tables are numbered according to figure 6.24 and the walls that did not meet the criterias mentioned above are skipped.

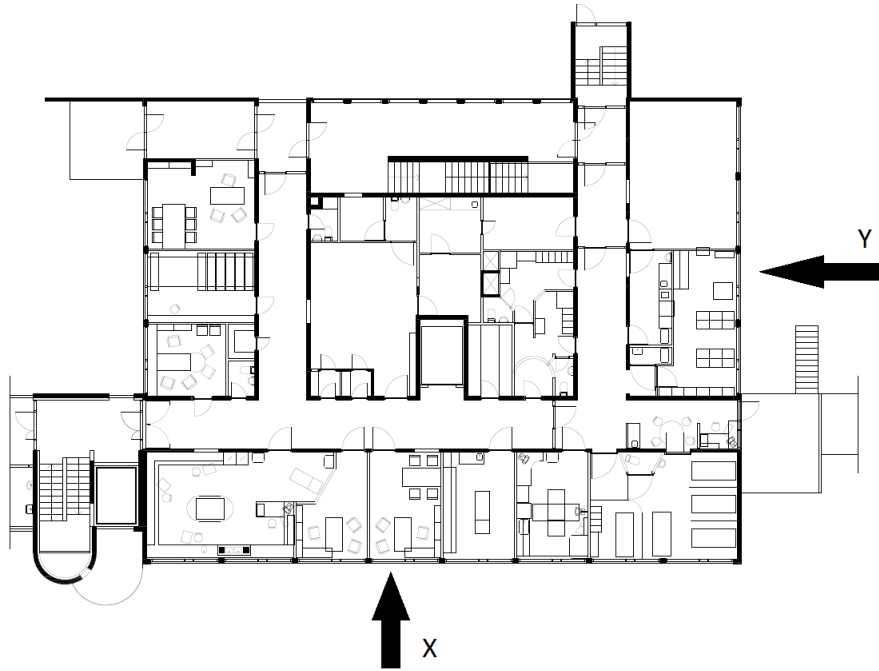


Figure 6.24: The counting order of walls, x is horizontal and y is vertical.

Table 6.3: The density ratio of walls, the floor and surface ratio for walls in x direction

Wall	Lenght	Width	Openings	Area
	m	m	%	m ²
Wall 1 x	28.5	0.2	0.45	5.7
Wall 2 x	28.5	0.18	0.24	5.1
Wall 3 x	28.5	0.18	0.28	5.1
Wall 8 x	13.3	0.18	0.04	2.4
Wall 11 x	28.5	0.2	0.27	5.7
Sum				24.1
Ratio				3.8%

Table 6.4: The density ratio of walls, the floor and surface ratio for walls in y direction

Wall	Lenght	Width	Openings	Area
	m	m	%	m ²
Wall 1 y	22.2	0.2	0.36	4.4
Wall 2 y	14.4	0.18	0.16	2.6
Wall 3 y	14.4	0.18	0.17	2.6
Wall 7 y	9.35	0.18	0.14	1.7
Wall 10y	14.4	0.18	0.16	2.6
Wall 11y	11.5	0.18	0.27	2.1
Wall 13y	22.2	0.2	0.30	4.4
Sum				20.4
Ratio				3.2%

7. Conclusion

The examined building is a 4 story height reinforced concrete building. Structural integrity of the building is of vital importance for civil protection and security of the local residents when a major earthquake occurs within the Tjörnes fracture zone. Since May 2015 a monitoring system has been used to record the acceleration response of the structure due to earthquake excitation. The system is part of the multidisciplinary strong motion array, ICEARRAY II.

The main focus of this study is to examine the structural characteristics, dynamic behaviour and structural integrity of the hospital. The structural characteristics are estimated through the observed strong ground motion and a FE model of the building. The instruments recorded 4 notable events and for the estimation of structural characteristics and the system identification event 3 was used. This event had magnitude of 3,7 Mw and an epicentral distance of 4,7 km.

Analysis of the low intensity data recorded in the building gives a fundamental natural frequency of 7,4 Hz for the first mode of vibration. The damping ratio at this low level of excitation was found to be of the order 2-3 % of critical. For higher intensity motion it can be expected that the damping will increase considerably whereas the natural frequency will decrease slightly. The calculated mode shapes underestimate the torsion at the location of the roof sensor. The dynamic modulus of elasticity was measured on site and was found to be 30.6 GPa. The response of the building however showed that the effective E-modulus is near 26 GPa, for low intensity motion recorded.

The system identification was carried out to estimate of the damping and the natural frequency. Section 5.2.1 shows the results of the response simulation. Comparative plots were published for the response computed and measured. The comparison between the computed and measured values is good for the 4th floor sensor. The roof sensor has good comparison for y component. The calculated mode shapes however underestimate the torsion at the location of the roof sensor in x direction as can be seen on figure 5.12. The sensors are located according to figures 3.5 and 3.6.

The structural integrity of the building was examined. The FE model was used to

obtain the earthquake induced forces according to a given earthquake excitation. The earthquake action was defined using selected recordings from the South Iceland Seismic Zone, as well as design response spectra from EN 1998-1 [5]. For the verification a few earthquake actions were defined. The design response spectra was defined for three directions and the time histories from south Iceland earthquakes 2000 and 2008 for x, y and z directions. The earthquake action giving the highest forces was used for further checks.

The earthquake actions that were found critical are the time histories measured at a retirement home in the town of Hveragerði and Sólheimar. The earthquake forces due to those earthquake actions were relatively high compared to forces obtained from other earthquake actions and the design response spectra according to EN 1998-1. Therefore earthquake forces were plotted in the columns to compare the load to the maximum forces due to the design response spectra. This observation revealed that the maximum force is the very peak for a very short time interval. This is especially true for the Sólheimar earthquake action shown at figures 6.15 and 6.14.

For a further inspection on those high forces the horizontal response spectra for each earthquake action was plotted on figure 6.17, logarithmic scale is used to make the figure more readable. The natural period for the first three modes of the building was compared to the response. This observation revealed that the short fundamental periods of the building induced high acceleration as the first three periods draw inertia forces from the peak of the response spectra.

A review of the capacity of building components was carried out using the design response spectra RS 0 as reference load. The building has many load carrying walls, in a structural system that provides a lot of redundancy. The building deformations are small or less than 1 cm. The storey drift is similarly well within the limits prescribed by EN 1998-1. The structural verification was performed for specific columns and beams. The verification was performed using the M-N interaction diagram and shear calculations according to EN 1992-1. The columns resist the interaction of axial force and bending moment. But the shear capacity of the stirrups in the cross sections can not resist the shear force. The importance of stirrups and elaborate detailing are crucial factors affecting the quality and earthquake resistant strength of buildings. The distance between the stirrups is systematically set equal to the width of the cross sections but not 75% of d as EN 1992-1 suggests. The walls are checked in accordance with analysis showing that buildings with large lightly reinforced walls have showed a lower damage level in comparison of buildings constructed with RC frames. The ratio between walls and floor surface was calculated and was found to be 7% for both directions. Experiments and numerical analysis have shown that ratio should not be less than 3 - 4 % if the building is expected to perform well under seismic action.

Bibliography

- [1] B. Halldorsson, S. Jónsson, A. Papageorgiou, R. Green, I. Kalogeras, H. Avery, S. Ólafsson, S. Remseth, C. Oliveira, O. Polat *et al.*, “Icearray ii: A new multi-disciplinary strong-motion array in north iceland,” in *15th World Conference on Earthquake Engineering (15WCEE)*, 2012.
- [2] The science of earthquakes. U.S. Geological survey. [electronic]. Af: <http://earthquake.usgs.gov/learn/eqscience.php> [download: 2016.02.08]
- [3] A. S. Elnashai og L. Di Sarno, *Fundamentals of earthquake engineering*. Wiley Chichester, UK, 2008.
- [4] P. Bisch, E. Carvalho, H. Degee, P. Fajfar, M. Fardis, P. Franchin, M. Kreslin, A. Pecker, P. Pinto, A. Plumier *et al.*, “Eurocode 8: seismic design of buildings worked examples,” *Luxembourg: Publications Office of the European Union*, 2012.
- [5] *Eurocode 8: Design of structures for earthquake resistance - Part 1: Genaral rules, Seismic actions and rules for buildings*, European committee for standardization EN 1998, Desember 2003.
- [6] V. Gioncu og F. Mazzolani, *Earthquake engineering for structural design*. CRC Press, 2010.
- [7] A. Elghazouli, *Seismic design of buildings to Eurocode 8*. CRC Press, 2009.
- [8] A. Björnsson, K. Sæmundsson, F. Sigmundsson, P. Halldórsson, R. Sigbjörnsson, J. Þ. Snæbjörnsson *et al.*, “Geothermal projects in iceland at krafla, bjarnarflag, gjástykki and theistareykir: assessment of geo-hazards affecting energy production and transmission systems emphasizing structural design criteria and mitigation of risk,” 2007.
- [9] B. Bessason og J. Ö. Bjarnason, “Seismic vulnerability of low-rise residential buildings based on damage data from three earthquakes (m w 6.5, 6.5 and 6.3),” *Engineering Structures*, vol. 111, pp. 64–79, 2016.
- [10] A. K. Chopra, *Dynamics of structures*. Prentice Hall New Jersey, 1995, vol. 3.

- [11] N. Satake, K.-i. Suda, T. Arakawa, A. Sasaki, og Y. Tamura, "Damping evaluation using full-scale data of buildings in japan," *Journal of structural engineering*, vol. 129, nr. 4, pp. 470–477, 2003.
- [12] T. K. Datta, *Seismic analysis of structures*. John Wiley & Sons, 2010.
- [13] J. P. Stewart, R. B. Seed, og G. L. Fenves, *Empirical evaluation of inertial soil-structure interaction effects*. Pacific Earthquake Engineering Research Center, 1998.
- [14] E. Safak, "Identification of linear structures using discrete-time filters," *Journal of Structural Engineering*, vol. 117, nr. 10, pp. 3064–3085, 1991.
- [15] T. Geirhardsson, "Design drawings husavik hospital," aTH vinnustofa.
- [16] *Eurocode 2: Design of concrete structures - Part 1 - 1: Genaral rules and rules for build-ings*, European committee for standardization EN 1992, April 2004.
- [17] Canterbury seismic instruments. [electronic]. Af: <http://csi.net.nz> [download: 2016.03.03]
- [18] *Operation and Installation Manual for The CUSP-3 series Acellerographs*, Canterbury Seismic Instruments.
- [19] R. Sigbjörnsson, S. Ólafsson, og J. T. Snæbjörnsson, "Macro seismic effects related to strong ground motion: a study of the south iceland earthquakes in june 2000," *Bulletin of Earthquake Engineering*, vol. 5, nr. 4, pp. 591–608, 2007.
- [20] B. Halldorsson og R. Sigbjörnsson, "The mw6. 3 ölfus earthquake at 15: 45 utc on 29 may 2008 in south iceland: Icearray strong-motion recordings," *Soil Dynamics and Earthquake Engineering*, vol. 29, nr. 6, pp. 1073–1083, 2009.
- [21] S. Kumar, "Live loads in office buildings: point-in-time load intensity," *Building and environment*, vol. 37, nr. 1, pp. 79–89, 2002.
- [22] A. J. Carr, "Dynamic analysis of structures," *Bulletin of the New Zealand Society for Earthquake Engineering*, vol. 27, nr. 2, pp. 129–146, 1994.
- [23] W. H. Mosley, R. Hulse, og J. H. Bungey, *Reinforced Concrete Design: to Eurocode 2*. Palgrave macmillan, 2012.
- [24] A. Konstantinidis, *Earthquake Resistant Buildings made of reinforced concrete*. Alta Grafico A.E, 2014, vol. A.
- [25] M. Pecce, F. Ceroni, F. A. Bibbo, og A. De Angelis, "Behaviour of rc buildings with large lightly reinforced walls along the perimeter," *Engineering Structures*, vol. 73, pp. 39–53, 2014.

- [26] V. Pentangelo, G. Magliulo, og E. Cosenza, "Analysis of buildings with large lightly reinforced walls," in *The 14th European conference on earthquake engineering, Ohrid, Macedonia*, 2010.

A. Earthquakes on southern Iceland

In this appendix the time history data will presented. For each time history there is a figure of the ground acceleration and Fourier spectra for x, y, and z components and horizontal and vertical response spectra.

A.1 Flagbjarnarholt

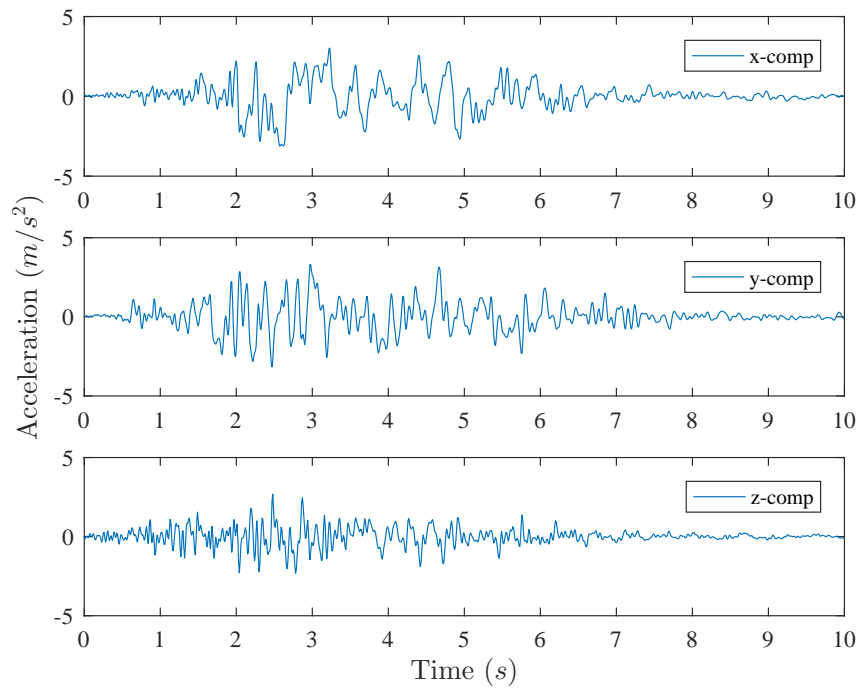


Figure A.1: Acceleration Flagbjarnarholt June 17. 2000.

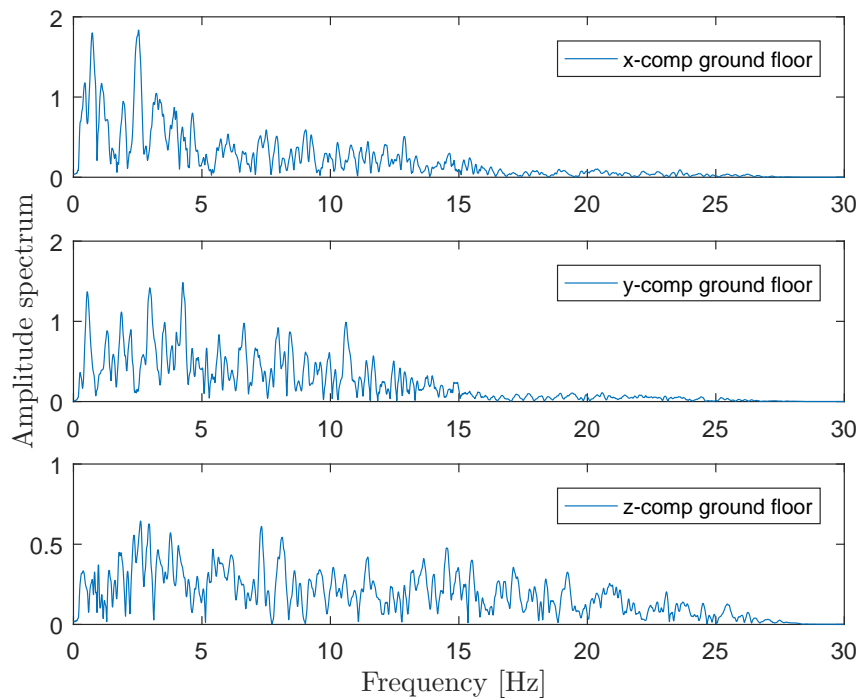


Figure A.2: Fourier spectra Flagbjarnarholt June 17. 2000.

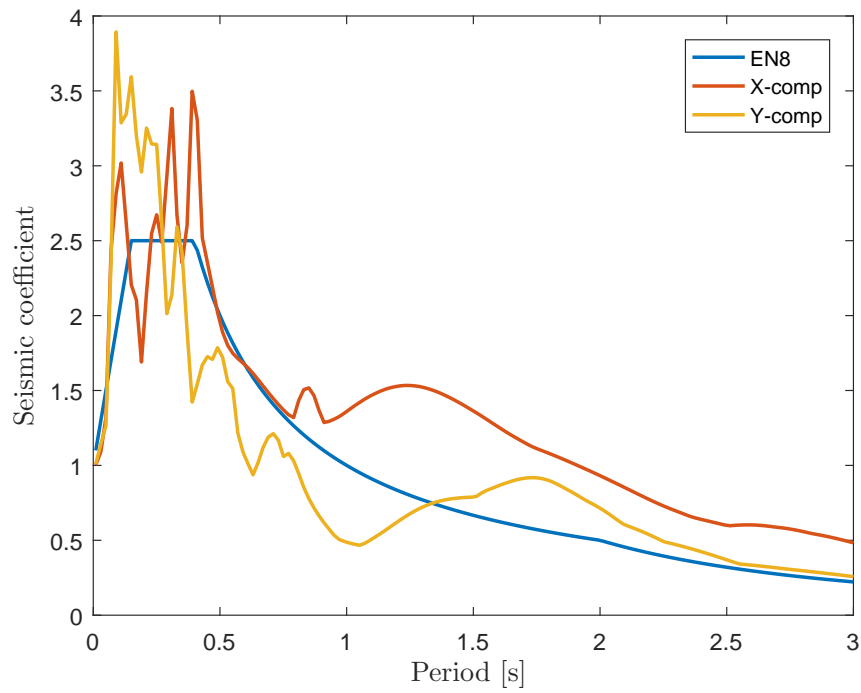


Figure A.3: Horizontal response spectra Flagbjarnarholt June 17. 2000.

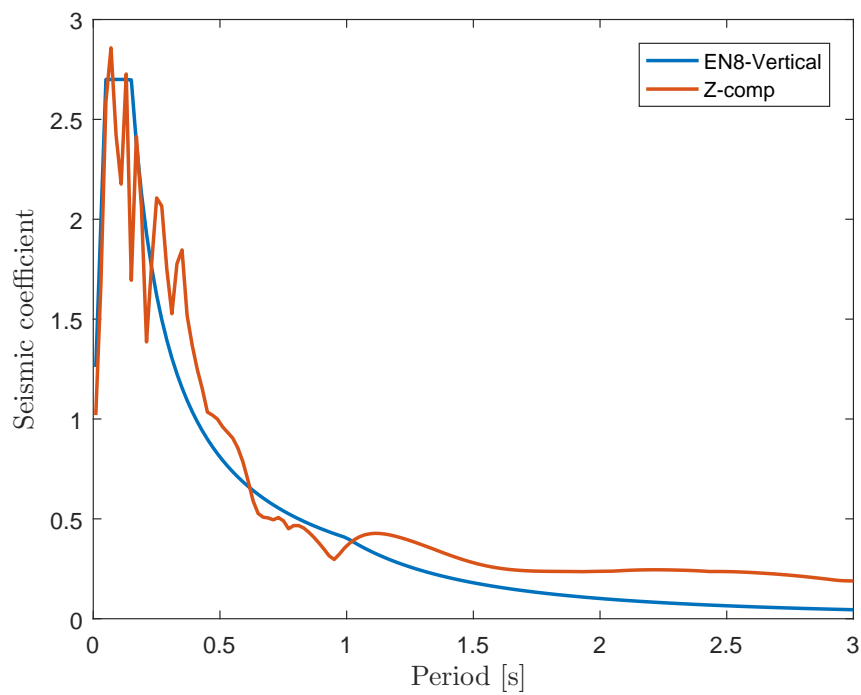


Figure A.4: Vertical response spectra Flagbjarnarholt June 17. 2000.

A.2 Kaldarholt

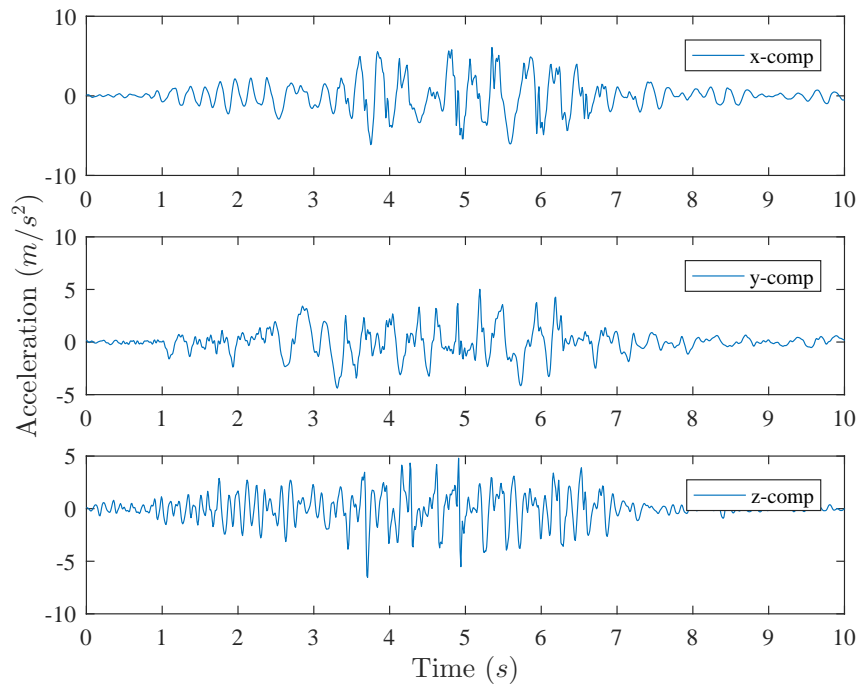


Figure A.5: Acceleration Kaldarholt June 17. 2000.

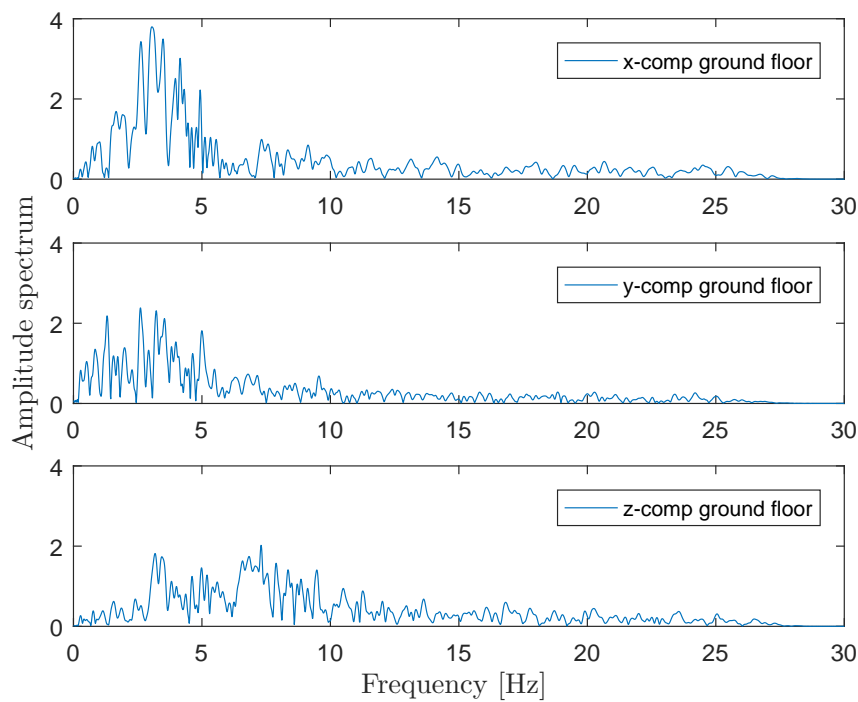


Figure A.6: Fourier spectra Kaldarholt June 17. 2000.

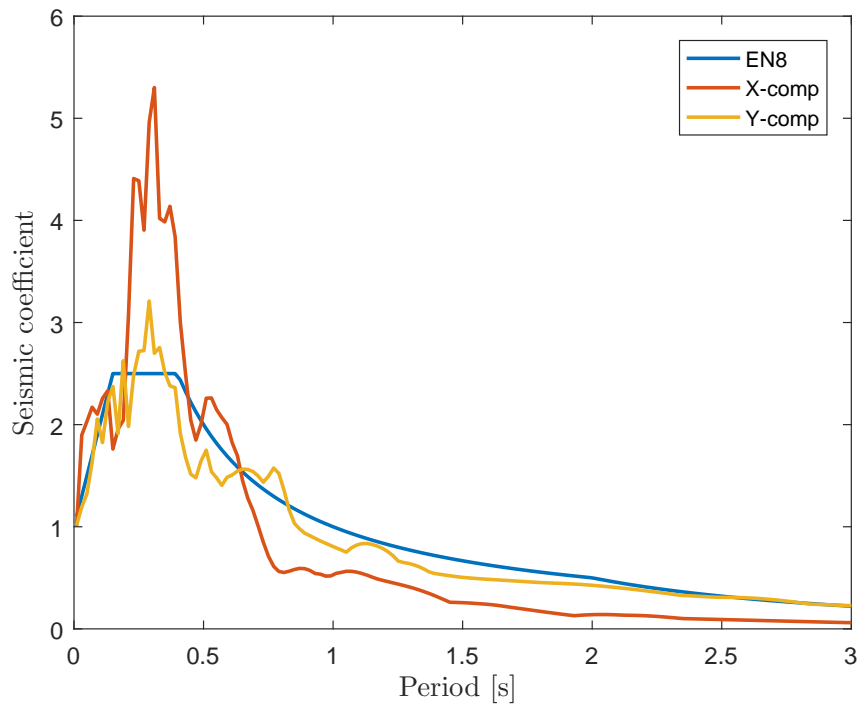


Figure A.7: Horizontal response spectra Kaldarholt June 17. 2000.

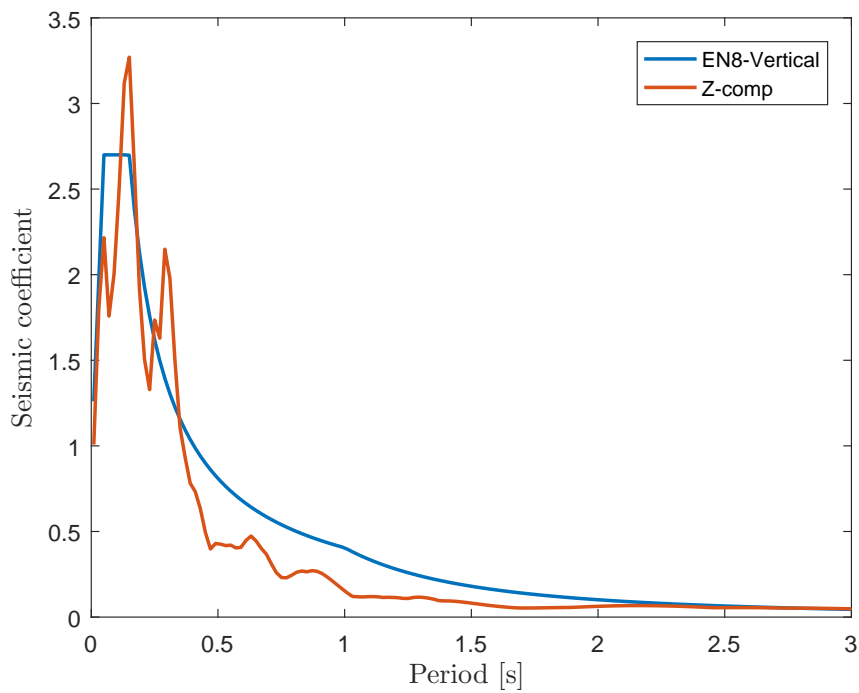


Figure A.8: Horizontal response spectra Kaldarholt June 17. 2000.

A.3 Selfoss EERC

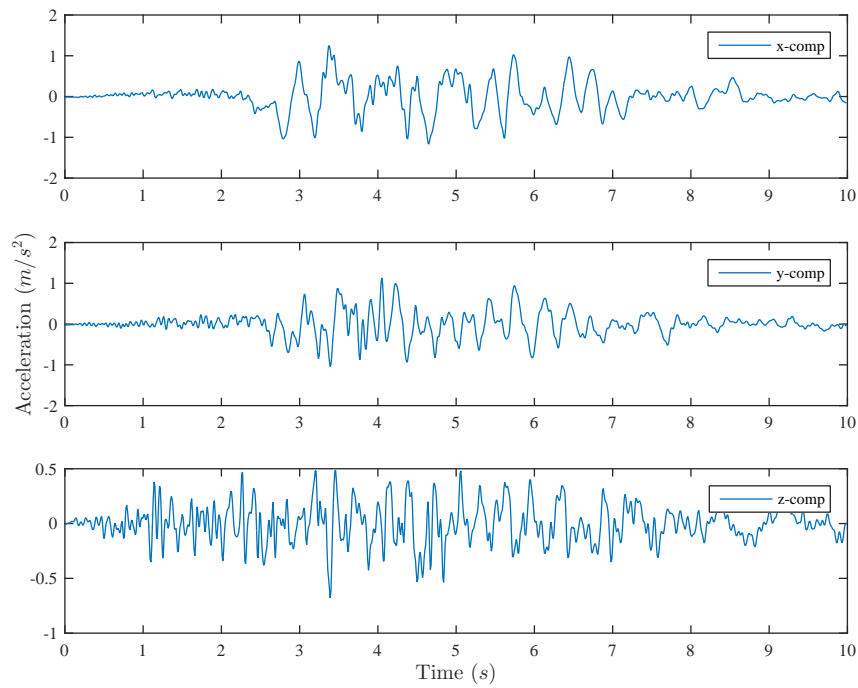


Figure A.9: Acceleration Selfoss EERC June 17. 2000.

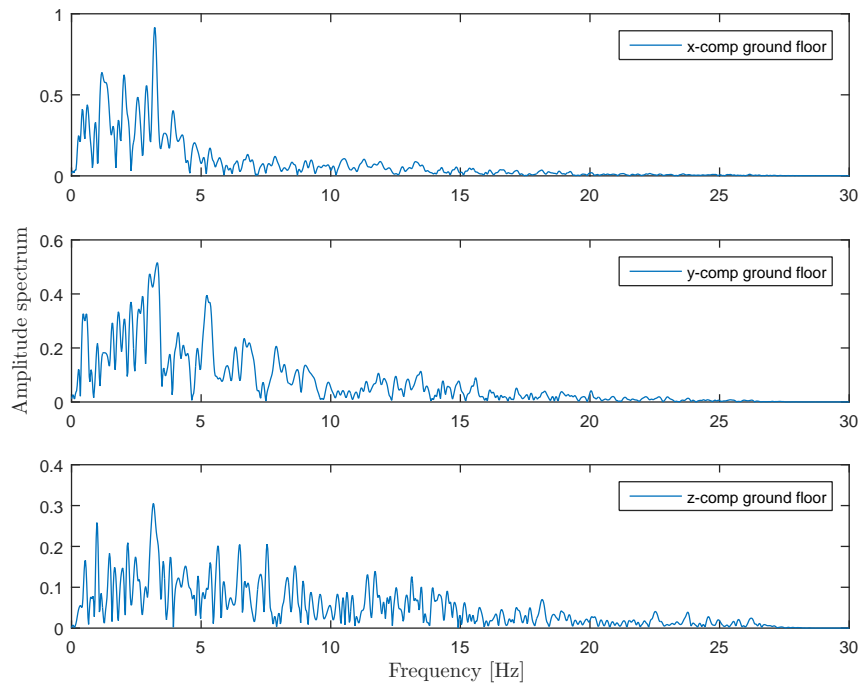


Figure A.10: Fourier spectra Selfoss EERC June 17. 2000.

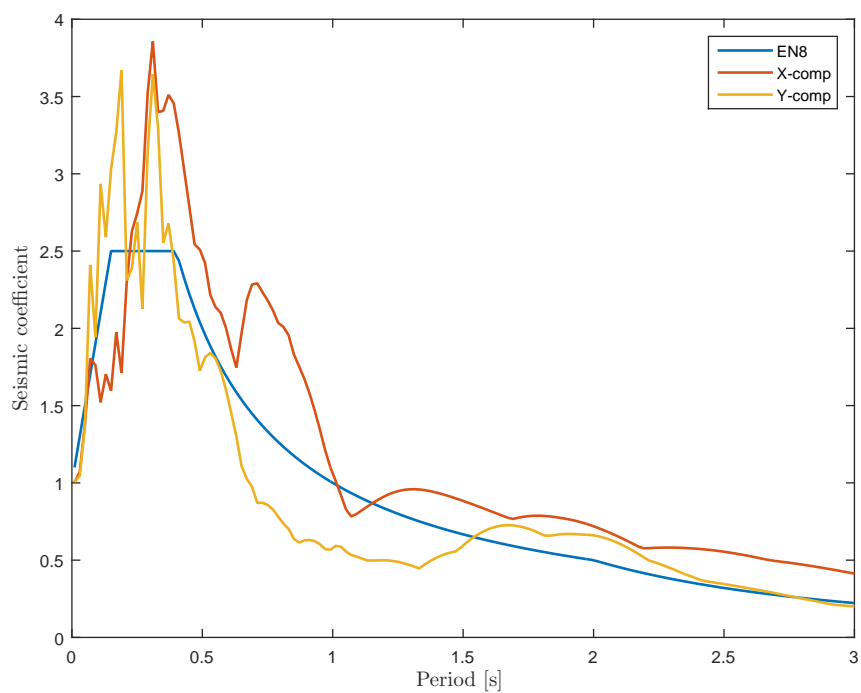


Figure A.11: Horizontal response spectra Selfoss EERC June 17. 2000.

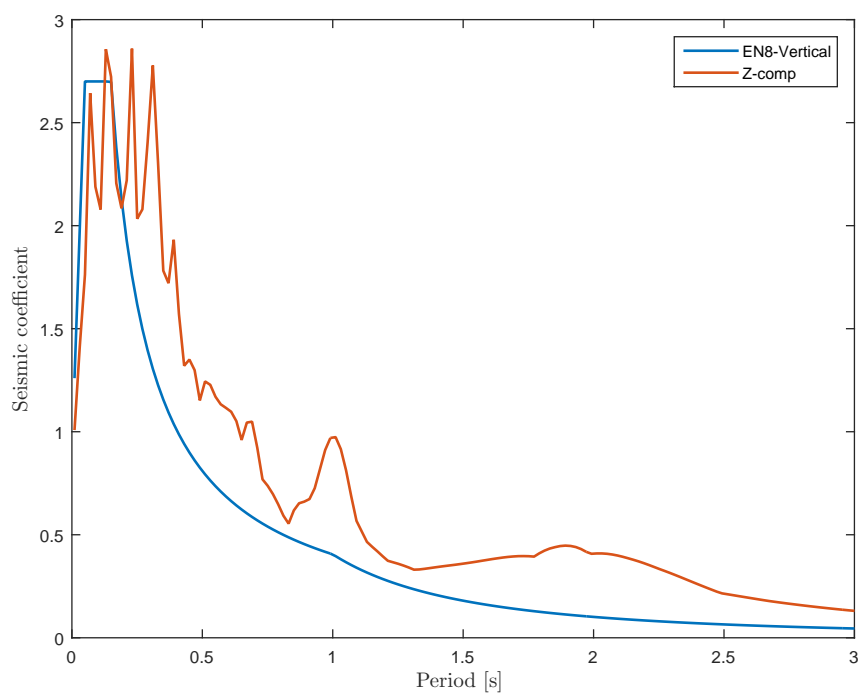


Figure A.12: Vertical response spectra Selfoss EERC June 17. 2000.

A.4 Sólheimar

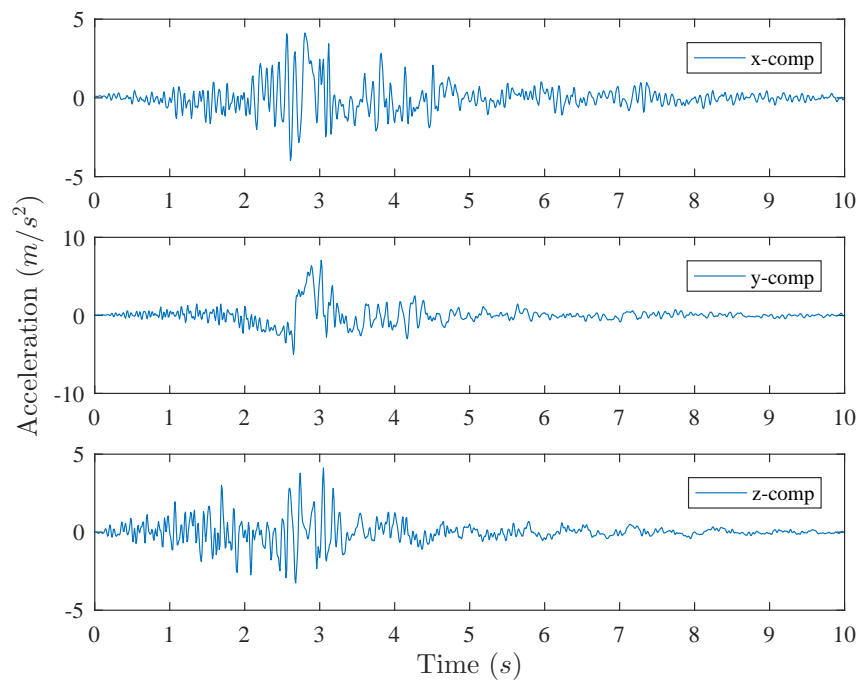


Figure A.13: Acceleration Sólheimar June 21. 2000.

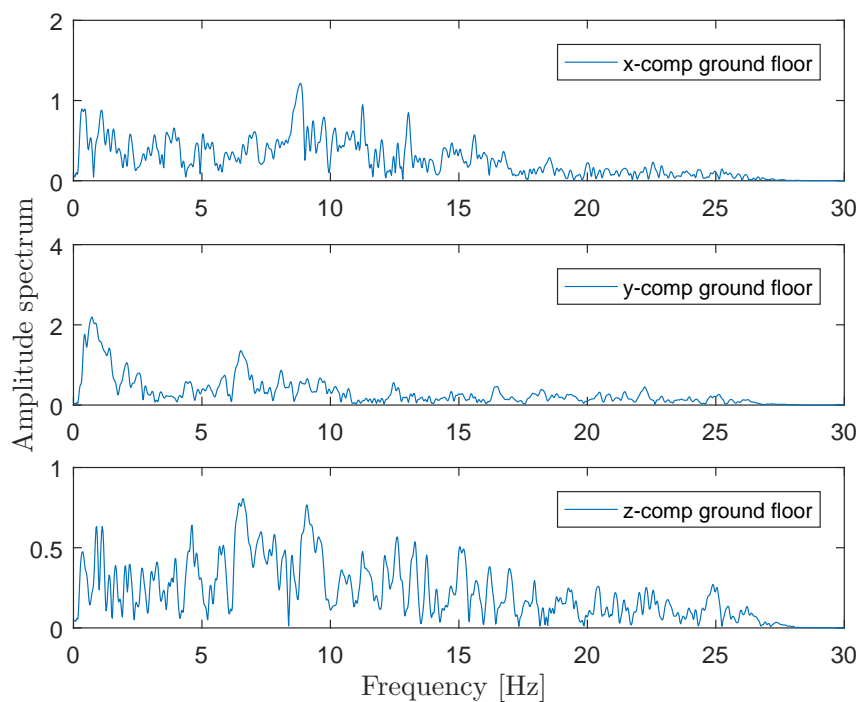


Figure A.14: Fourier spectra Sólheimar June 21. 2000.

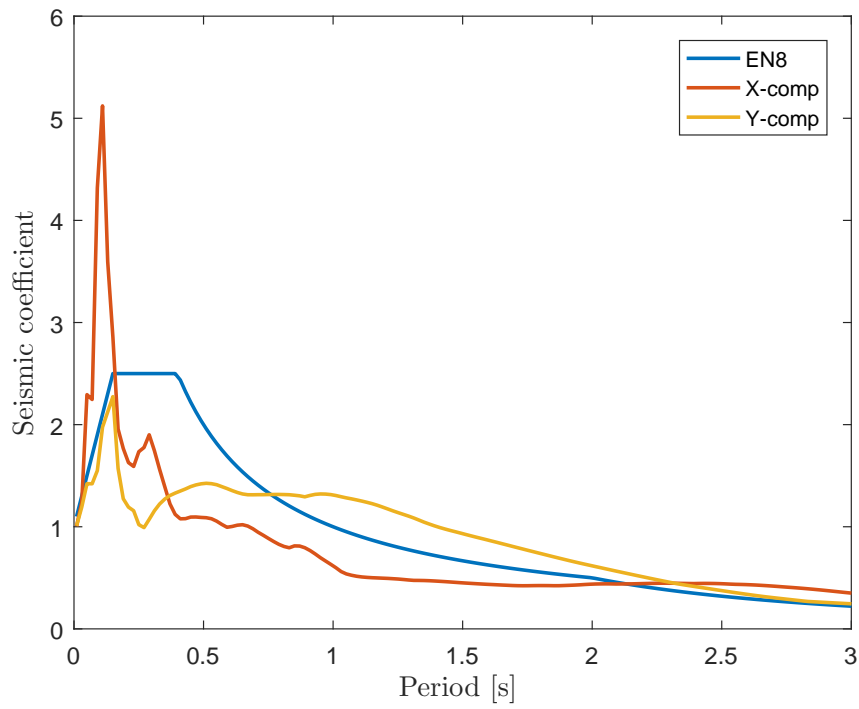


Figure A.15: Horizontal response spectra Sólheimar June 21. 2000.

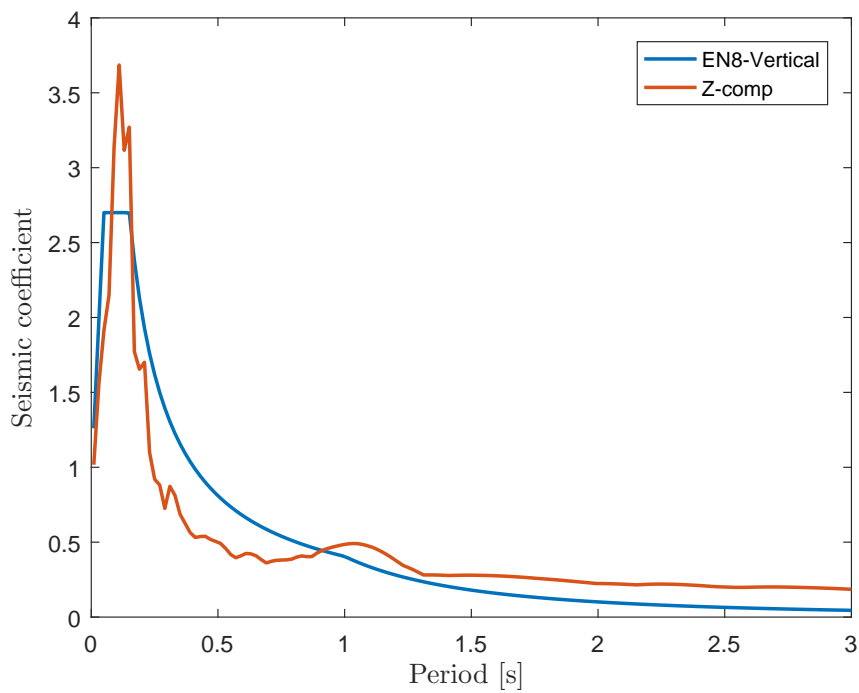


Figure A.16: Vertical response spectra Sólheimar June 21. 2000.

A.5 Þjórsártún

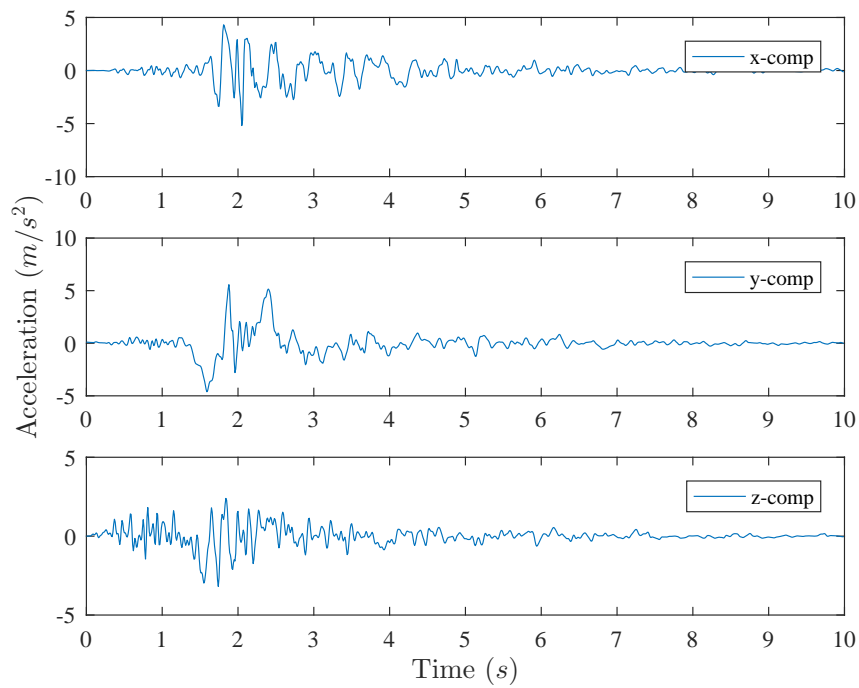


Figure A.17: Acceleration Þjórsártún June 21. 2000.

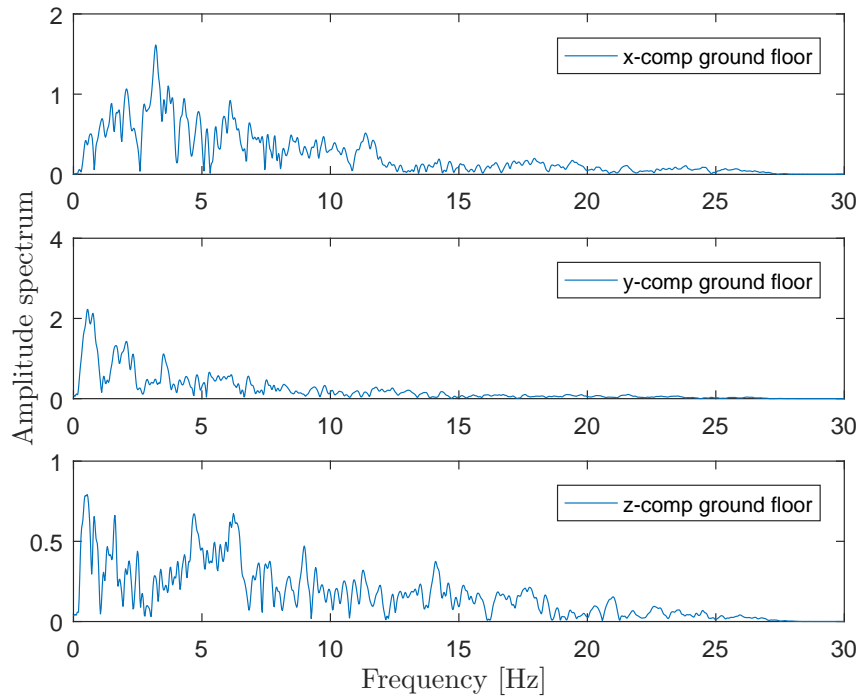


Figure A.18: Fourier spectra Þjórsártún June 21. 2000.

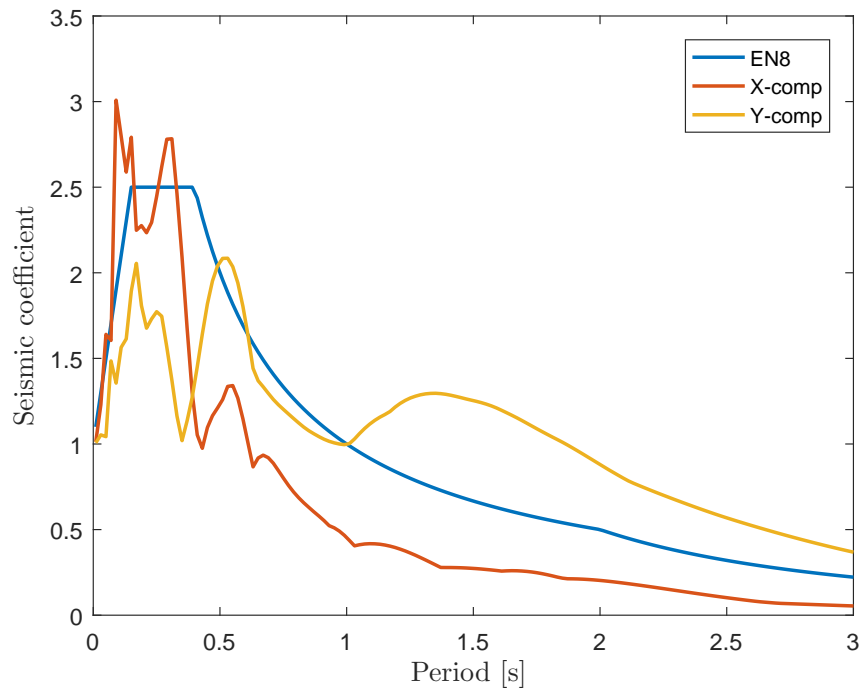


Figure A.19: Horizontal response spectra Þjórsártún June 21. 2000.

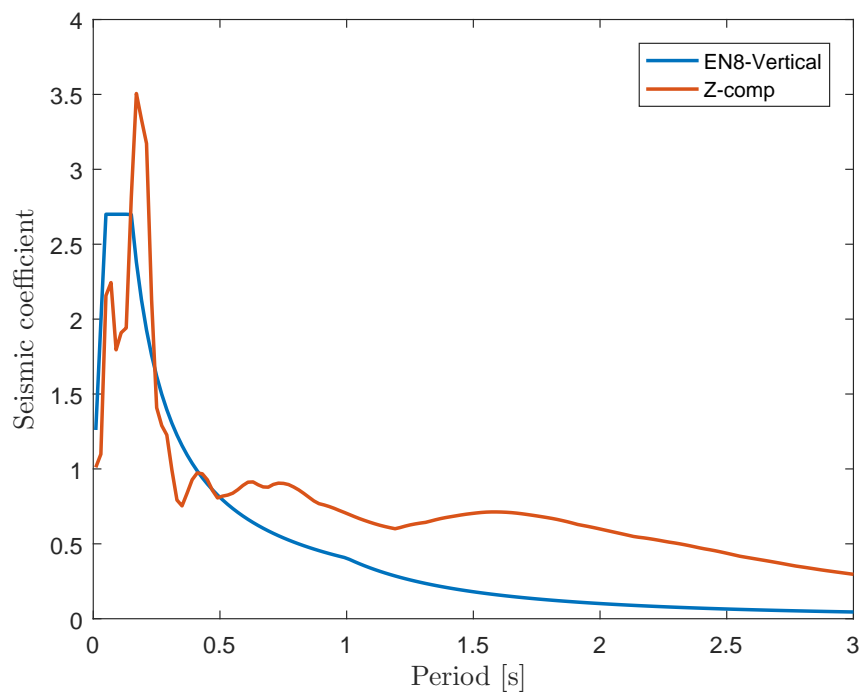


Figure A.20: Vertical response spectra Þjórsártún June 21. 2000.

A.6 Selfoss city hall

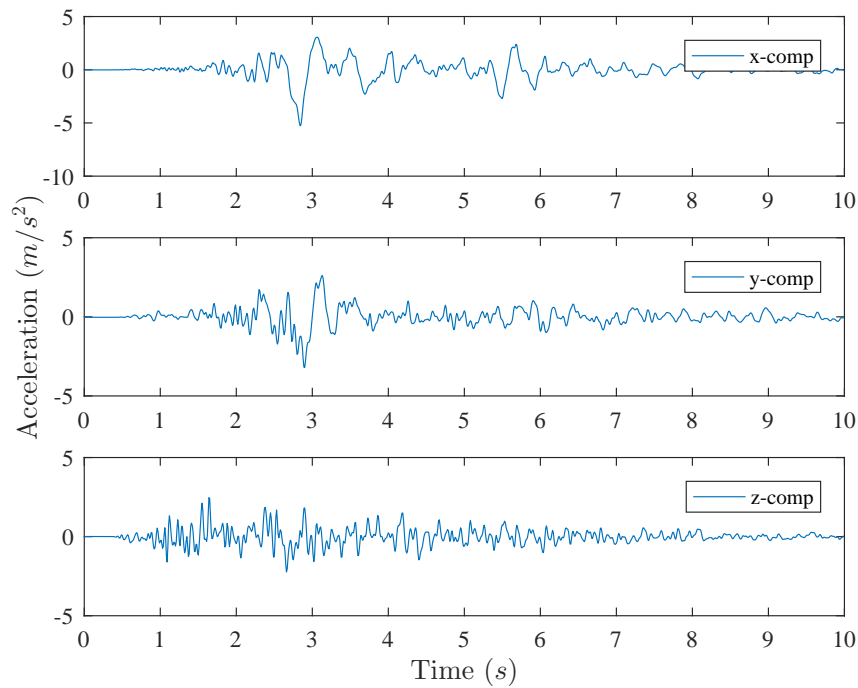


Figure A.21: Acceleration Selfoss city hall May 29. 2008.

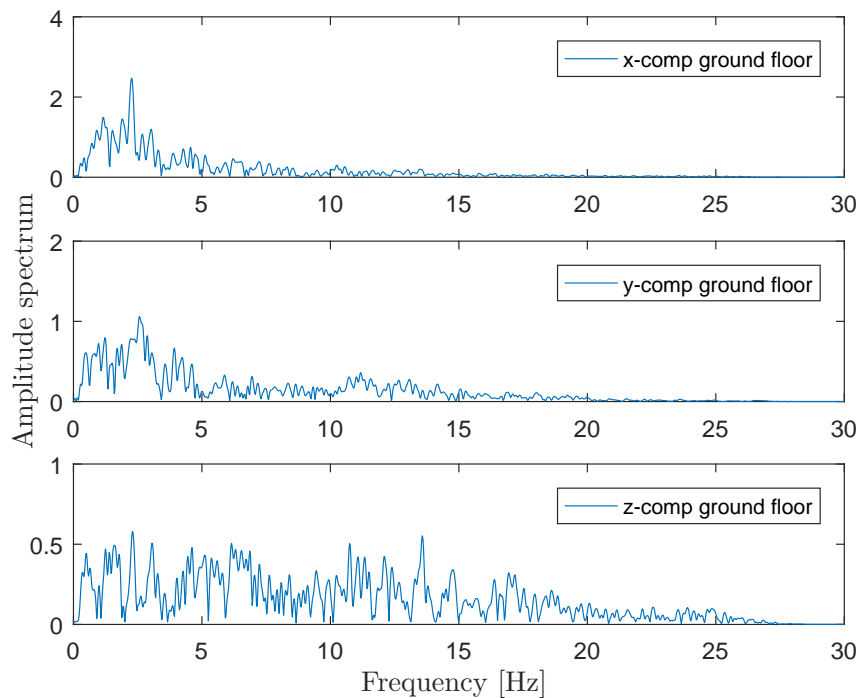


Figure A.22: Fourier spectra Selfoss city hall May 29. 2008.

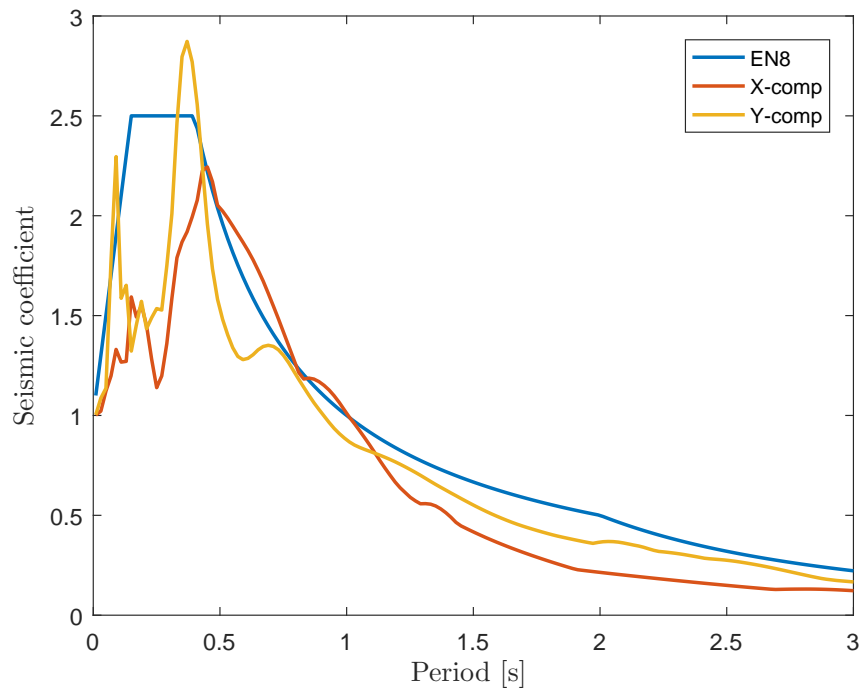


Figure A.23: Horizontal response spectra Selfoss city hall May 29. 2008.

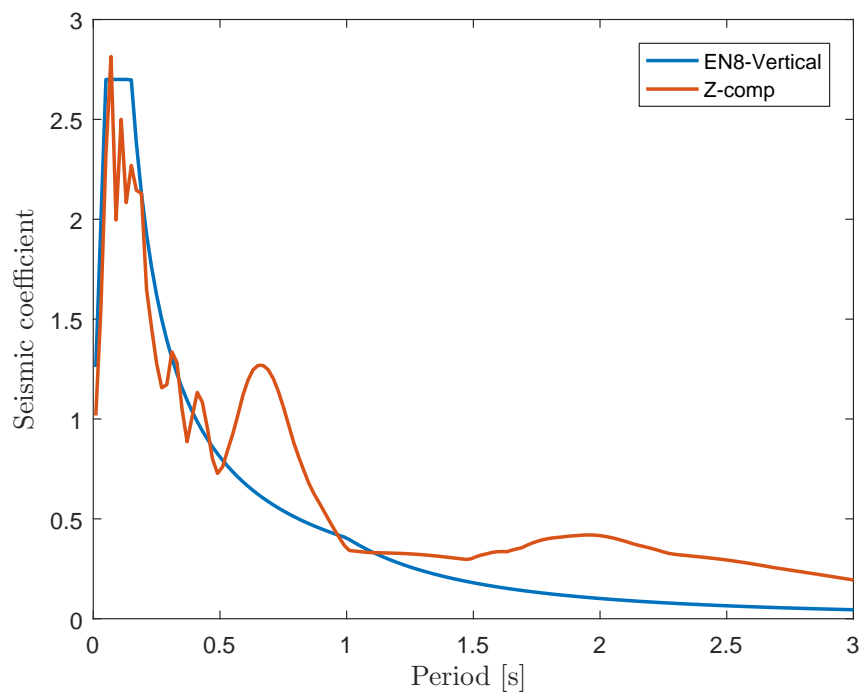


Figure A.24: Vertical response spectra Selfoss city hall May 29. 2008.

A.7 Hveragerði Retirement house

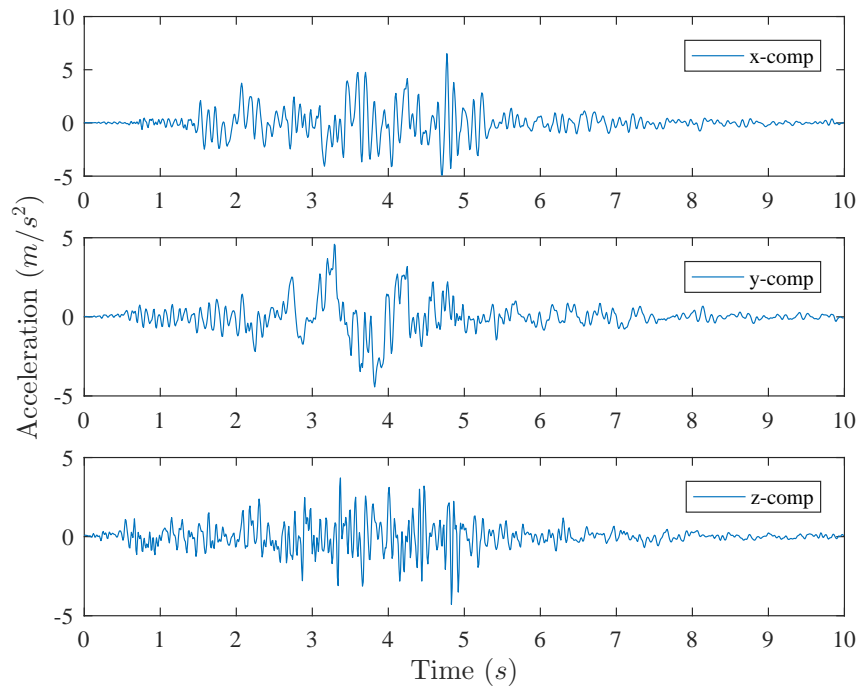


Figure A.25: Acceleration Hveragerði retirement house May 29. 2008.

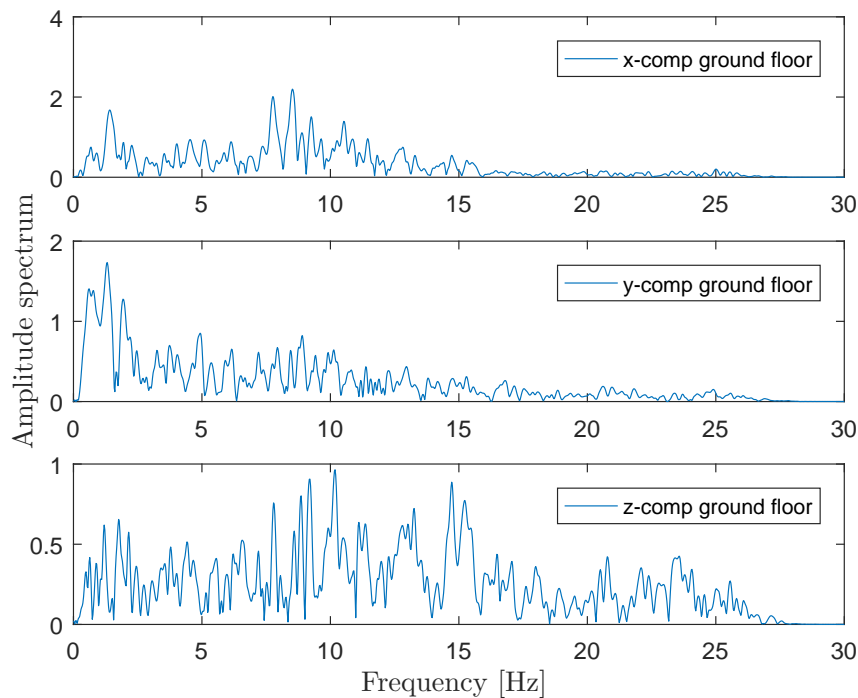


Figure A.26: Fourier spectra Hveragerði retirement house May 29. 2008.

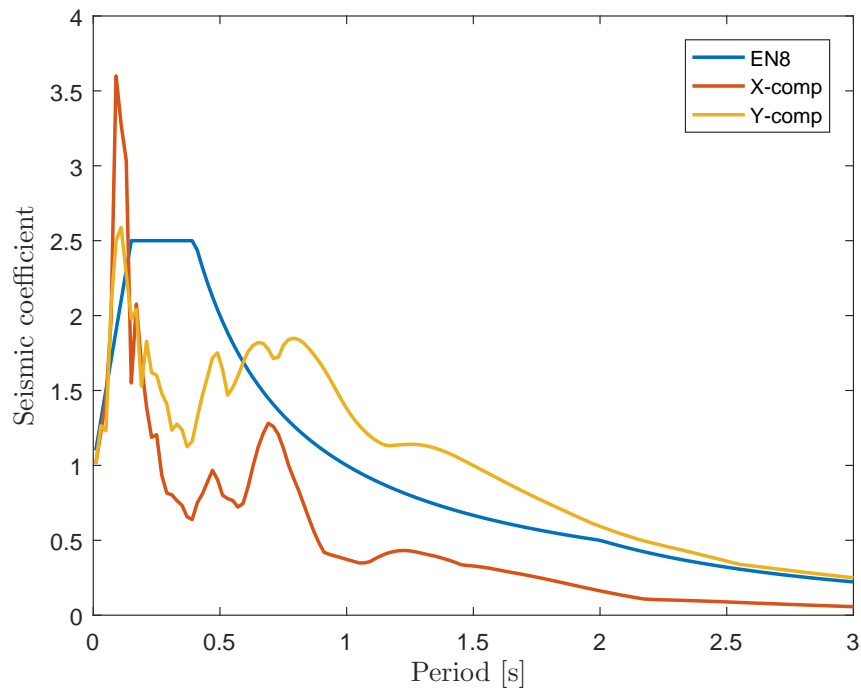


Figure A.27: Horizontal response spectra Hveragerði retirement house May 29. 2008.

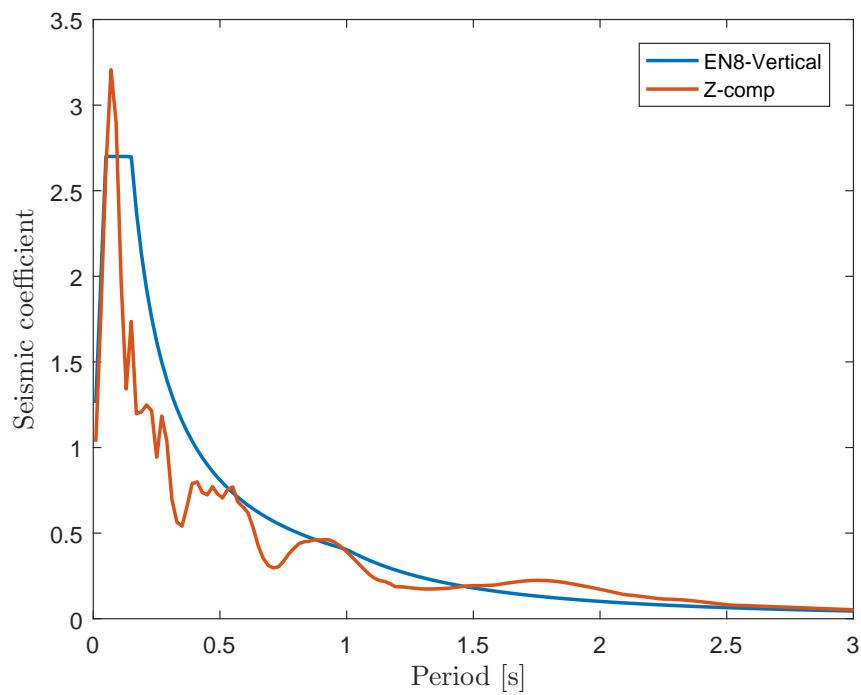


Figure A.28: Vertical response spectra Hveragerði retirement house May 29. 2008.

A.8 Ljósafoss-hydroelectric power station

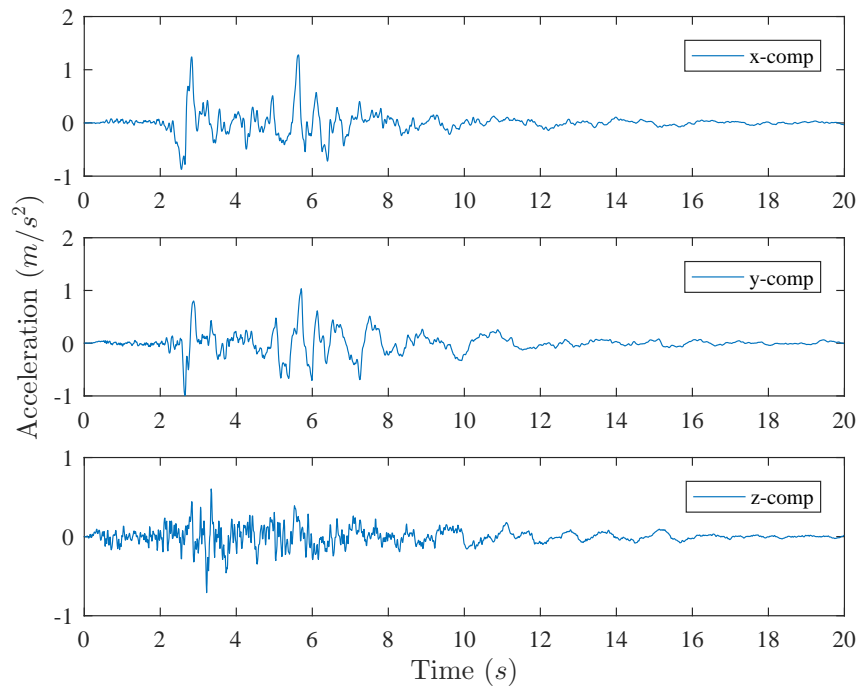


Figure A.29: Acceleration Ljósafoss hydro electric power station May 29. 2008.

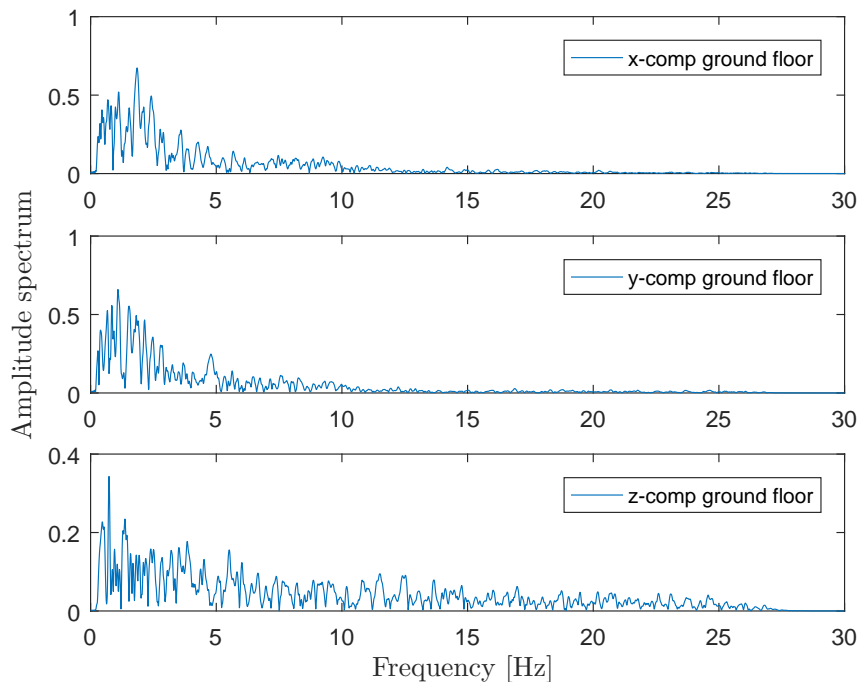


Figure A.30: Fourier spectra Ljósafoss hydro electric power station May 29. 2008.

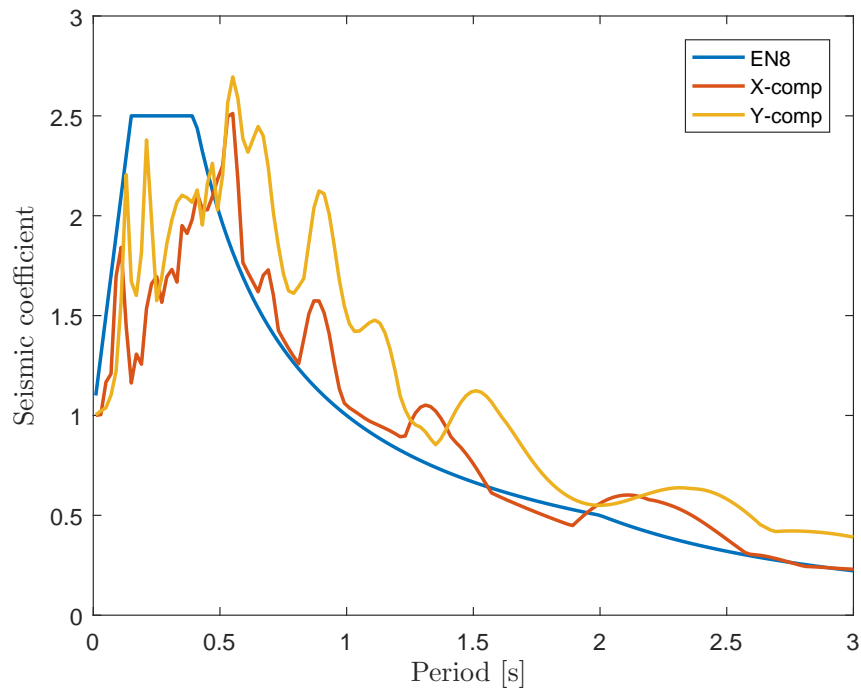


Figure A.31: Horizontal response spectra Ljósafoss hydro electric power station May 29. 2008.

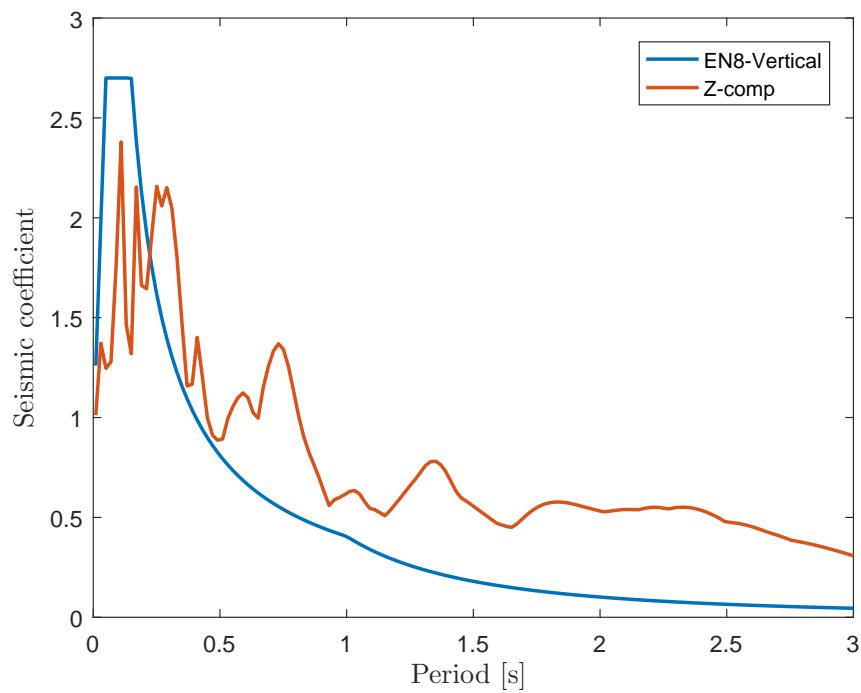


Figure A.32: Vertical response spectra Ljósafoss hydro electric power station May 29. 2008.

B. Time history response

In this appendix the calculated response of the time histories will be published. The figures show the calculated base share, displacements and storey drifts damage criteria. These figures are based on earthquake induced forces obtained in SAP2000 and showed in table for each earthquake action.

B.1 Flagbjarnarholt

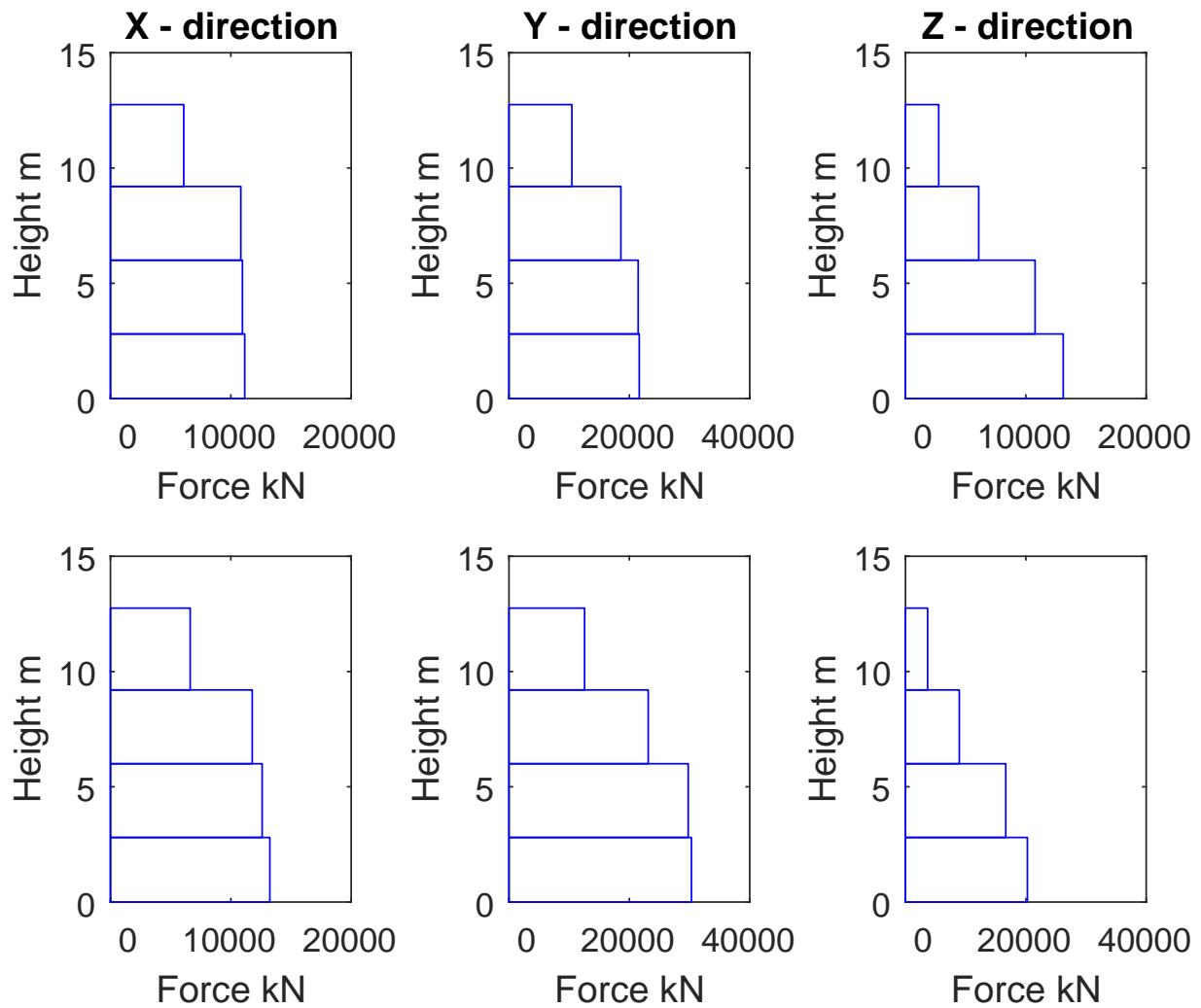


Figure B.1: Storey shear for Flagbjarnarholt earthquake action, the columns represent direction and lines represent max and min values with max values above.

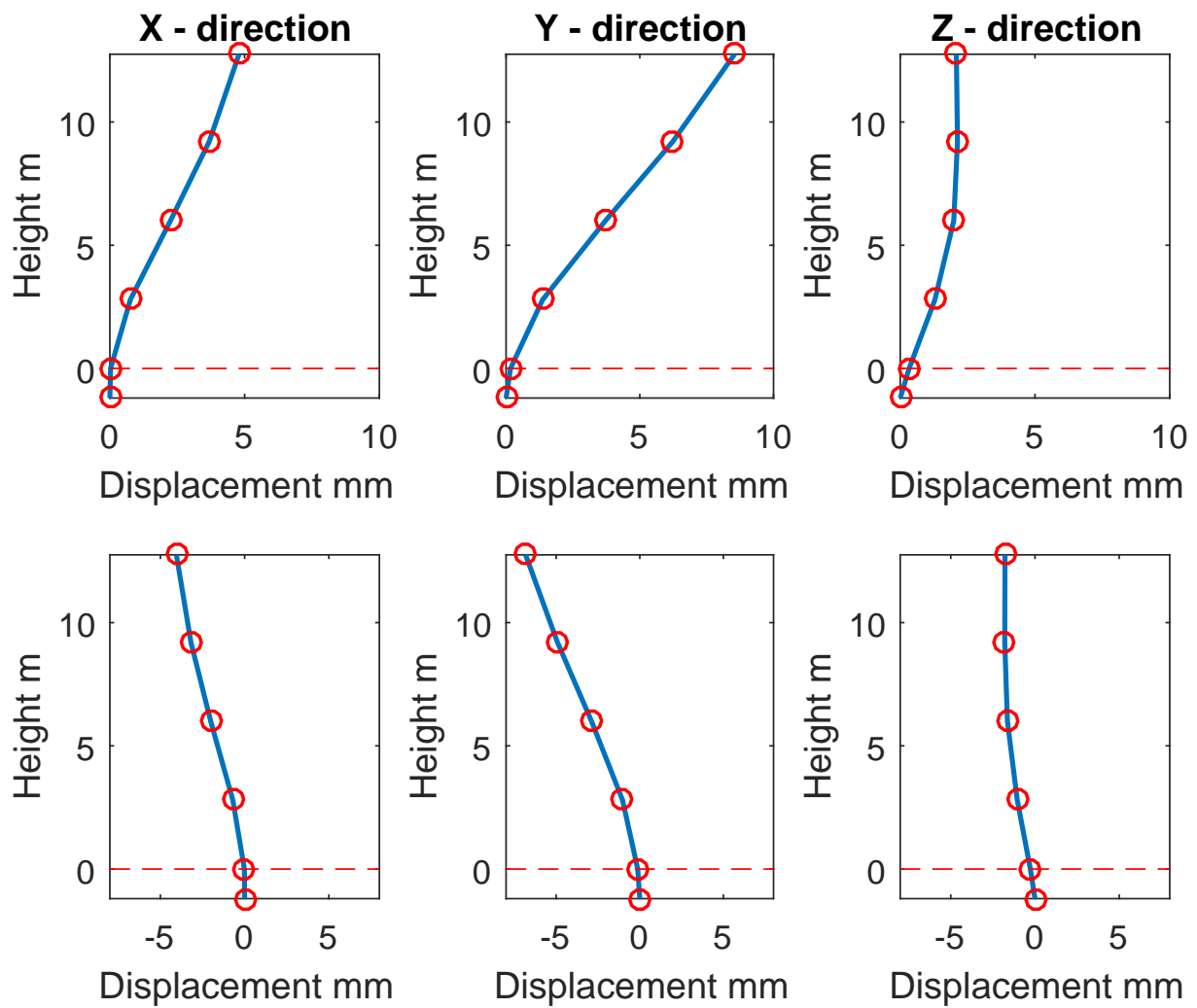


Figure B.2: Displacement for Flagbjarnarholt earthquake action, the columns represent direction and lines represent max and min values with max values above.

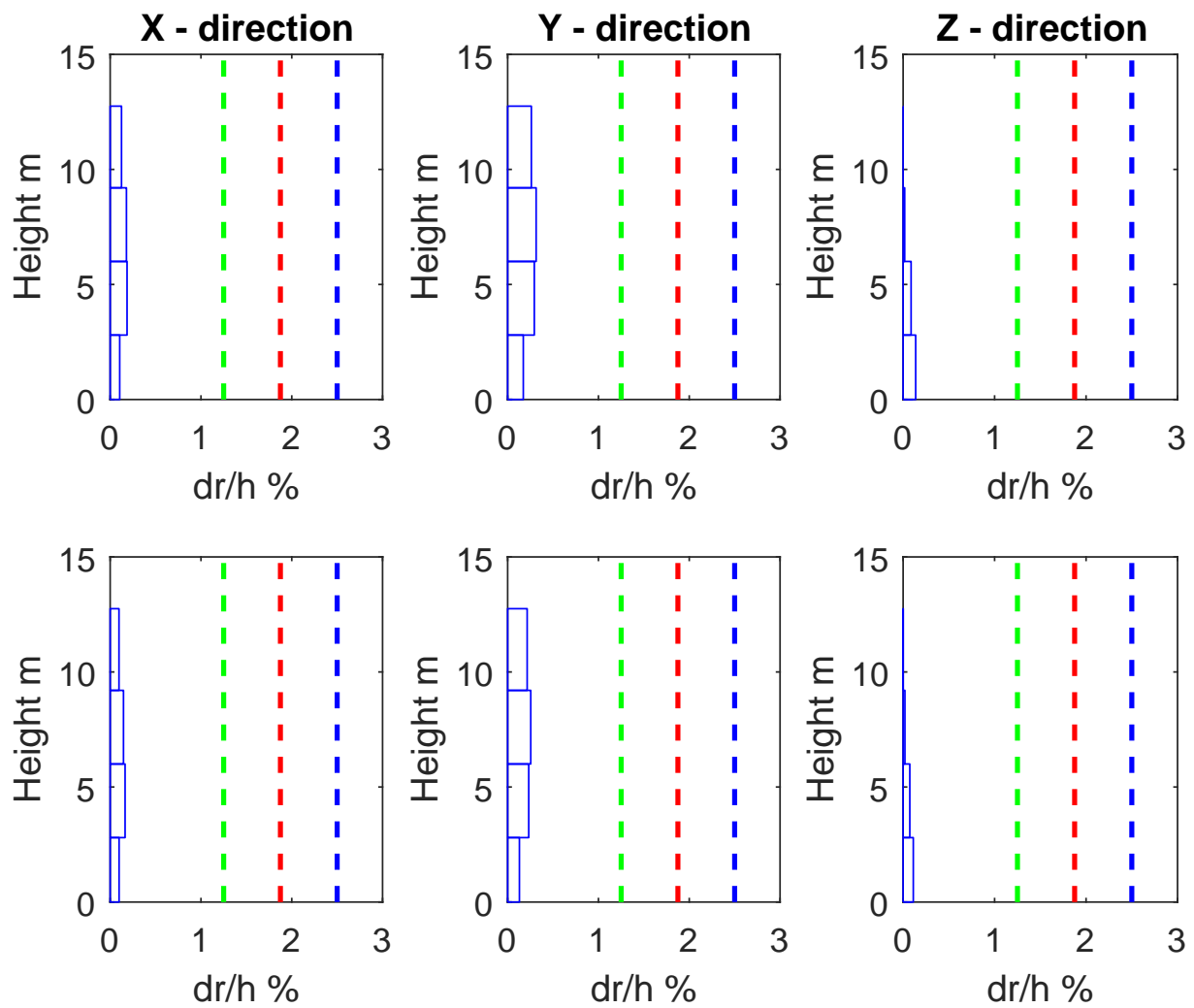


Figure B.3: Storey drifts for Flagbjarnarholt earthquake action, the columns represent direction and lines represent max and min values with max values above.

Table B.1: Section cut earthquake induced forces

TABLE: Section Cut Forces - Design									
SectionCut	OutputCase	CaseType	StepType	P	V2	V3	T	M2	M3
Text	Text	Text	Text	N	N	N	N-m	N-m	N-m
A1D	Flagbjarnarholt_TH	LinModHist	Max	517970	69377	6420	2746	-2493	43750
A1D	Flagbjarnarholt_TH	LinModHist	Min	-377156	-50671	-7356	-3919	1805	-60327
A2D	Flagbjarnarholt_TH	LinModHist	Max	270357	11837	4071	4729	-7141	57448
A2D	Flagbjarnarholt_TH	LinModHist	Min	-284193	-11397	-4368	-3750	6600	-60848
A3D	Flagbjarnarholt_TH	LinModHist	Max	627020	3511	31544	2922	-124547	2640
A3D	Flagbjarnarholt_TH	LinModHist	Min	-567669	-4399	-28508	-2149	112001	-3386
A4D	Flagbjarnarholt_TH	LinModHist	Max	448849	1987	18171	3446	-88829	4672
A4D	Flagbjarnarholt_TH	LinModHist	Min	-385921	-2409	-15093	-2763	76765	-5380
B1D	Flagbjarnarholt_TH	LinModHist	Max	407436	53566	25930	2188	-3649	45734
B1D	Flagbjarnarholt_TH	LinModHist	Min	-301179	-39609	-21451	-1552	4567	-62035
B2D	Flagbjarnarholt_TH	LinModHist	Max	218575	32701	13990	1949	-4165	33920
B2D	Flagbjarnarholt_TH	LinModHist	Min	-265746	-27767	-12903	-1585	3489	-41328
B3D	Flagbjarnarholt_TH	LinModHist	Max	428172	14728	34671	1643	-74436	5390
B3D	Flagbjarnarholt_TH	LinModHist	Min	-484934	-12853	-27760	-1499	65921	-6199
B4D	Flagbjarnarholt_TH	LinModHist	Max	405603	3017	18136	1214	-57027	3198
B4D	Flagbjarnarholt_TH	LinModHist	Min	-370185	-2108	-20123	-1098	62343	-3415
C1D	Flagbjarnarholt_TH	LinModHist	Max	2847	3884	7192	6	0	68
C1D	Flagbjarnarholt_TH	LinModHist	Min	-2336	-2987	-5742	-6	0	-54
C2D	Flagbjarnarholt_TH	LinModHist	Max	2780	3580	4591	39	0	39
C2D	Flagbjarnarholt_TH	LinModHist	Min	-2537	-2998	-4123	-34	0	-28
C3D	Flagbjarnarholt_TH	LinModHist	Max	4321	4746	9850	7	-89	0
C3D	Flagbjarnarholt_TH	LinModHist	Min	-4339	-3830	-7917	-7	101	0
C4D	Flagbjarnarholt_TH	LinModHist	Max	2028	3096	4010	4	-43	0
C4D	Flagbjarnarholt_TH	LinModHist	Min	-2132	-2433	-3752	-4	47	0
D1D	Flagbjarnarholt_TH	LinModHist	Max	1860	2563	4520	4	0	60
D1D	Flagbjarnarholt_TH	LinModHist	Min	-1271	-2378	-3781	-4	0	-47
D2D	Flagbjarnarholt_TH	LinModHist	Max	2090	2423	4937	3	0	40
D2D	Flagbjarnarholt_TH	LinModHist	Min	-1940	-2305	-3849	-3	0	-44
D3D	Flagbjarnarholt_TH	LinModHist	Max	1374	2484	3710	31	0	25
D3D	Flagbjarnarholt_TH	LinModHist	Min	-1408	-2332	-2992	-25	0	-24
D4D	Flagbjarnarholt_TH	LinModHist	Max	3114	4190	5836	4	-90	0
D4D	Flagbjarnarholt_TH	LinModHist	Min	-3531	-2657	-4328	-4	101	0
D5D	Flagbjarnarholt_TH	LinModHist	Max	1941	2960	2444	2	-51	0
D5D	Flagbjarnarholt_TH	LinModHist	Min	-2213	-1964	-1956	-2	50	0

B.2 Kaldarholt

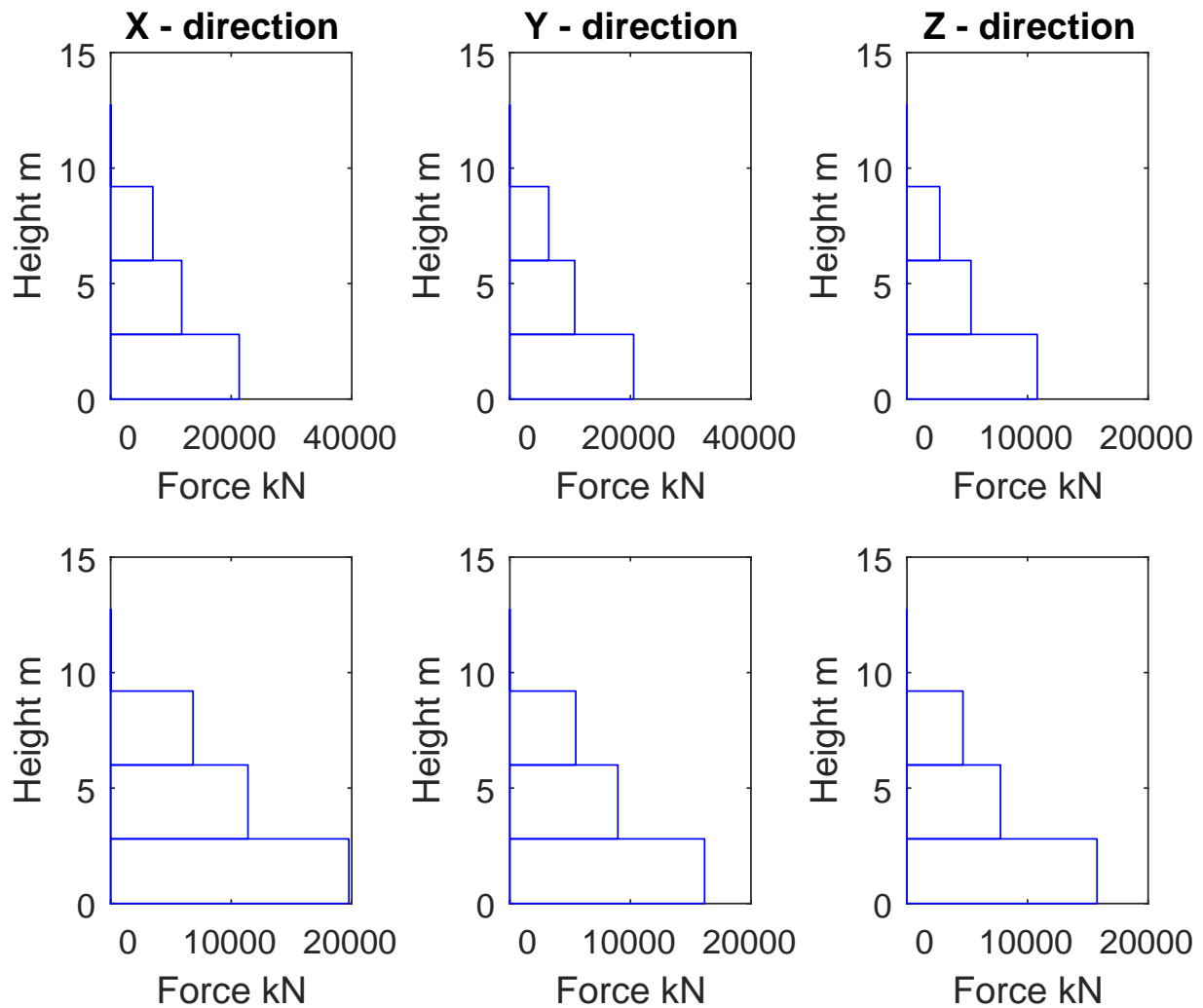


Figure B.4: Storey shear for Kaldarholt earthquake action, the columns represent direction and lines represent max and min values with max values above.

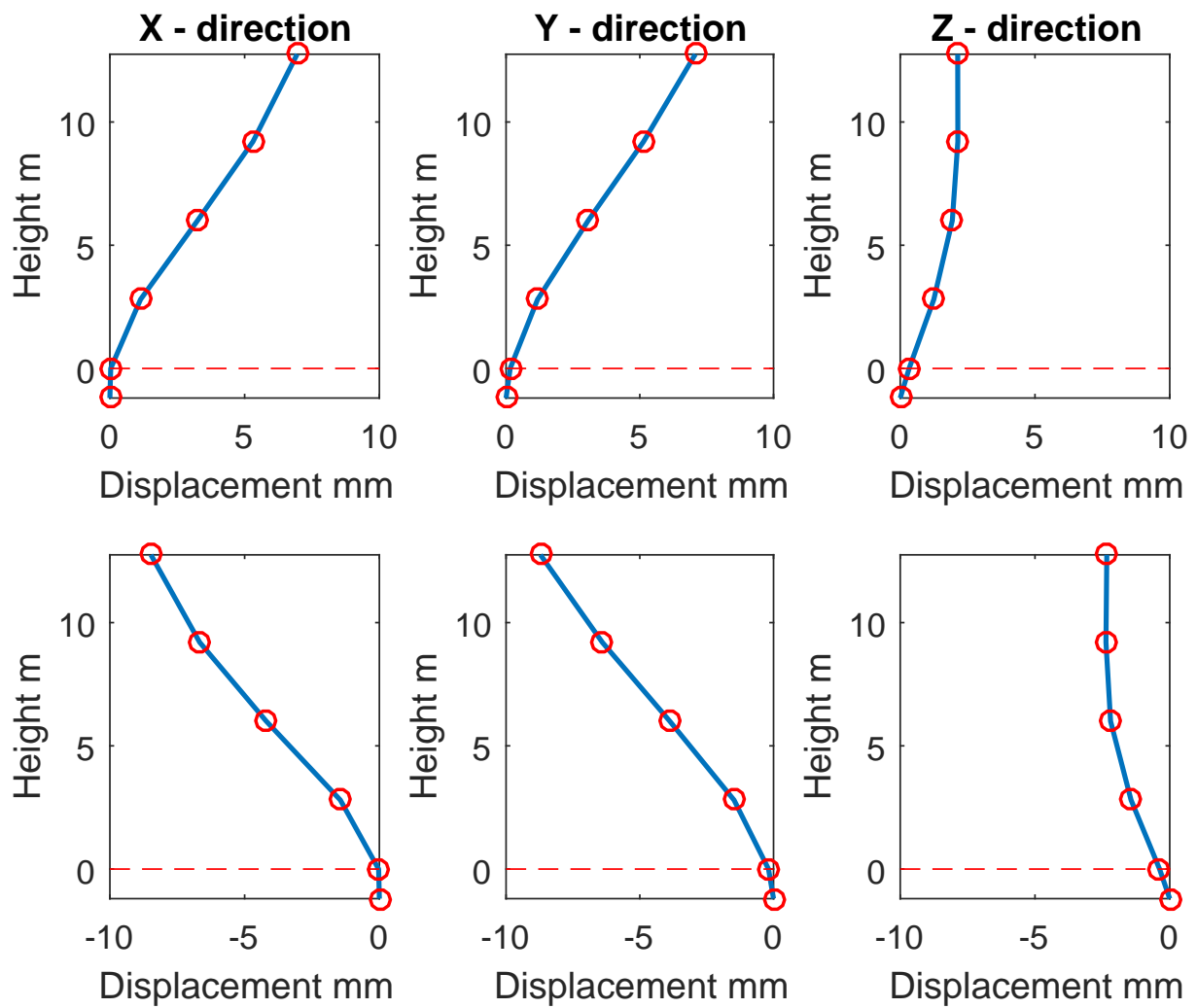


Figure B.5: Displacement for Kaldarholt earthquake action, the columns represent direction and lines represent max and min values with max values above.

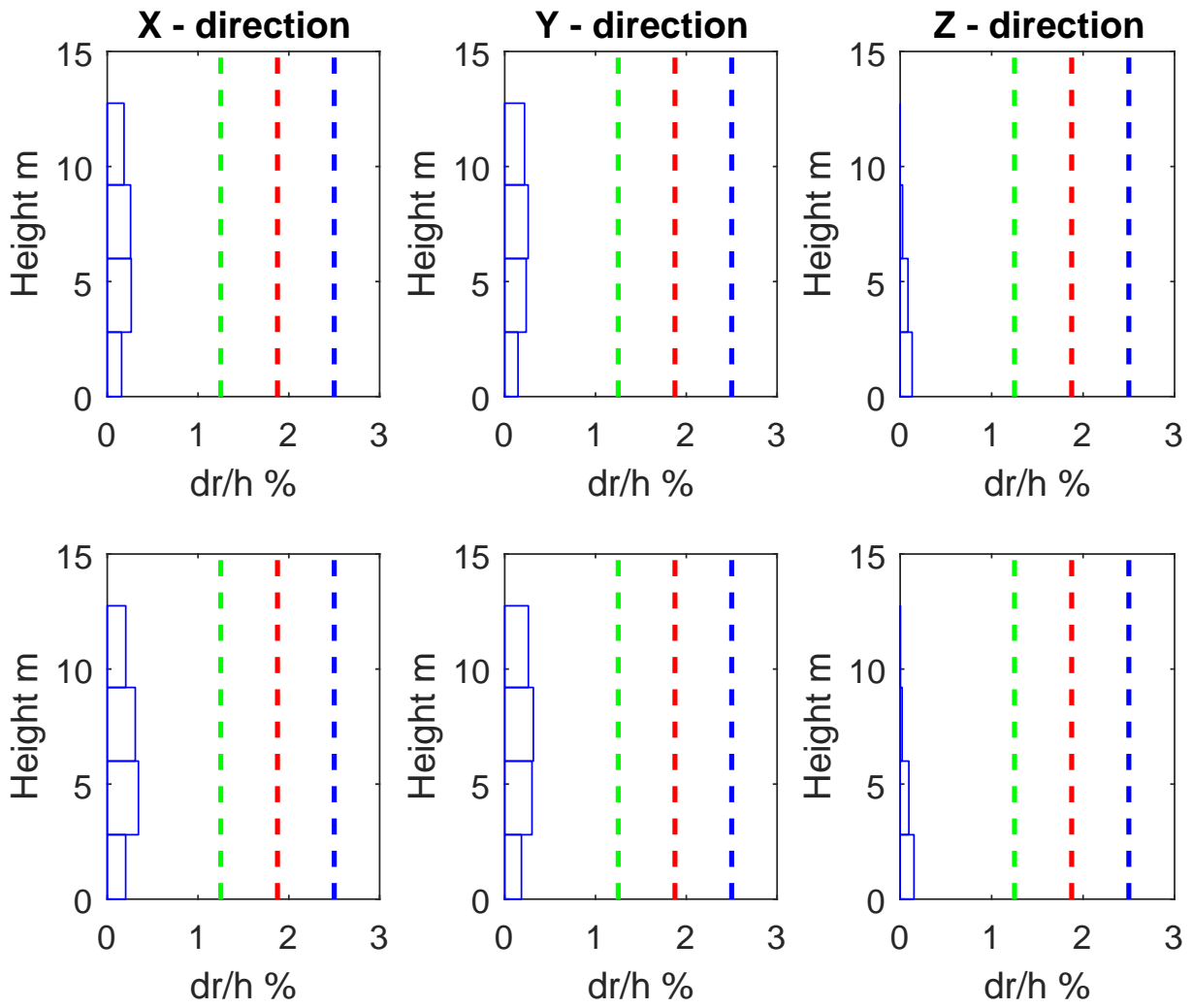


Figure B.6: Storey drifts for Kaldarholt earthquake action, the columns represent direction and lines represent max and min values with max values above.

Table B.2: Section cut earthquake induced forces

TABLE: Section Cut Forces - Design									
SectionCut	OutputCase	CaseType	StepType	P	V2	V3	T	M2	M3
Text	Text	Text	Text	N	N	N	N-m	N-m	N-m
A1D	Kaldarholt_TH	LinModHist	Max	532413	69284	10855	3873	-2304	61749
A1D	Kaldarholt_TH	LinModHist	Min	-531992	-70826	-8505	-3127	2759	-61849
A2D	Kaldarholt_TH	LinModHist	Max	430858	16927	4863	4258	-9202	93018
A2D	Kaldarholt_TH	LinModHist	Min	-360924	-12739	-4118	-3823	8568	-73148
A3D	Kaldarholt_TH	LinModHist	Max	765306	6734	36326	3929	-150932	4991
A3D	Kaldarholt_TH	LinModHist	Min	-742574	-5847	-36505	-4361	147029	-4990
A4D	Kaldarholt_TH	LinModHist	Max	490695	3544	23862	3952	-96763	5976
A4D	Kaldarholt_TH	LinModHist	Min	-514609	-3198	-18906	-4022	101857	-6062
B1D	Kaldarholt_TH	LinModHist	Max	570202	78599	18831	2054	-3657	91298
B1D	Kaldarholt_TH	LinModHist	Min	-600865	-80634	-21872	-2218	3123	-86440
B2D	Kaldarholt_TH	LinModHist	Max	313966	42756	16056	2127	-4018	48684
B2D	Kaldarholt_TH	LinModHist	Min	-310366	-42044	-13641	-2191	4164	-47682
B3D	Kaldarholt_TH	LinModHist	Max	608913	23370	28770	2376	-86118	7210
B3D	Kaldarholt_TH	LinModHist	Min	-561097	-27075	-35161	-2399	92770	-6144
B4D	Kaldarholt_TH	LinModHist	Max	523697	3693	31881	2246	-97718	5164
B4D	Kaldarholt_TH	LinModHist	Min	-636337	-4126	-24536	-1884	80729	-4504
C1D	Kaldarholt_TH	LinModHist	Max	6157	5355	6307	8	0	80
C1D	Kaldarholt_TH	LinModHist	Min	-3816	-6403	-7296	-8	0	-87
C2D	Kaldarholt_TH	LinModHist	Max	7475	5350	5142	43	0	81
C2D	Kaldarholt_TH	LinModHist	Min	-5052	-6597	-4080	-33	0	-98
C3D	Kaldarholt_TH	LinModHist	Max	7326	8181	9114	8	-122	0
C3D	Kaldarholt_TH	LinModHist	Min	-5303	-7229	-10057	-9	104	0
C4D	Kaldarholt_TH	LinModHist	Max	4421	5707	4488	5	-63	0
C4D	Kaldarholt_TH	LinModHist	Min	-2718	-4724	-3832	-5	57	0
D1D	Kaldarholt_TH	LinModHist	Max	3888	4333	4467	4	0	84
D1D	Kaldarholt_TH	LinModHist	Min	-2524	-4893	-5247	-5	0	-79
D2D	Kaldarholt_TH	LinModHist	Max	3941	4107	4809	4	0	80
D2D	Kaldarholt_TH	LinModHist	Min	-2571	-4954	-4074	-4	0	-68
D3D	Kaldarholt_TH	LinModHist	Max	3002	4460	5842	51	0	56
D3D	Kaldarholt_TH	LinModHist	Min	-2176	-5270	-3936	-34	0	-45
D4D	Kaldarholt_TH	LinModHist	Max	5660	8075	5786	5	-96	0
D4D	Kaldarholt_TH	LinModHist	Min	-4348	-6313	-6569	-5	93	0
D5D	Kaldarholt_TH	LinModHist	Max	3385	4810	3019	4	-72	0
D5D	Kaldarholt_TH	LinModHist	Min	-2763	-4244	-2861	-4	82	0

B.3 Sólheimar

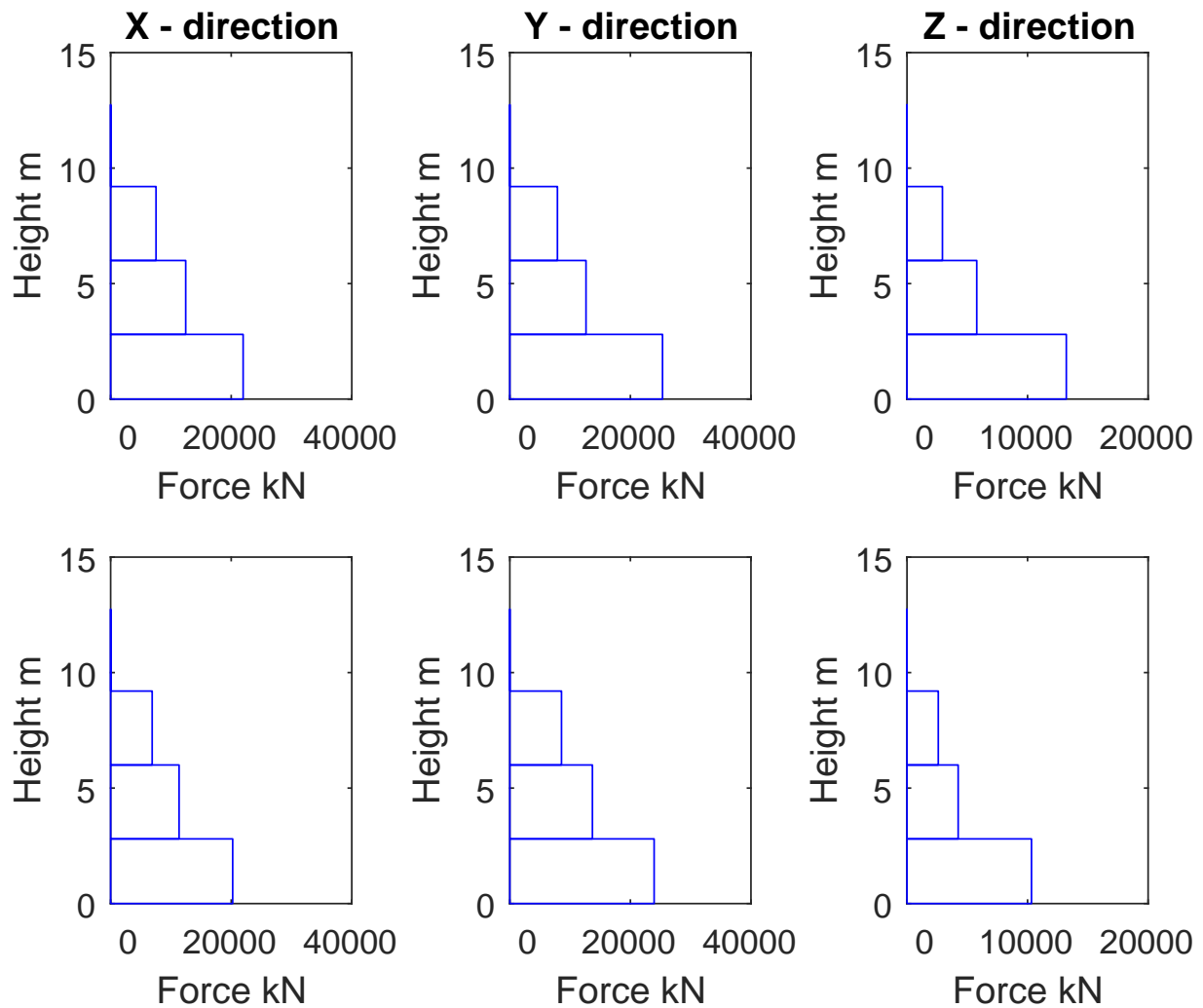


Figure B.7: Storey shear for Sólheimar earthquake action, the columns represent direction and lines represent max and min values with max values above.

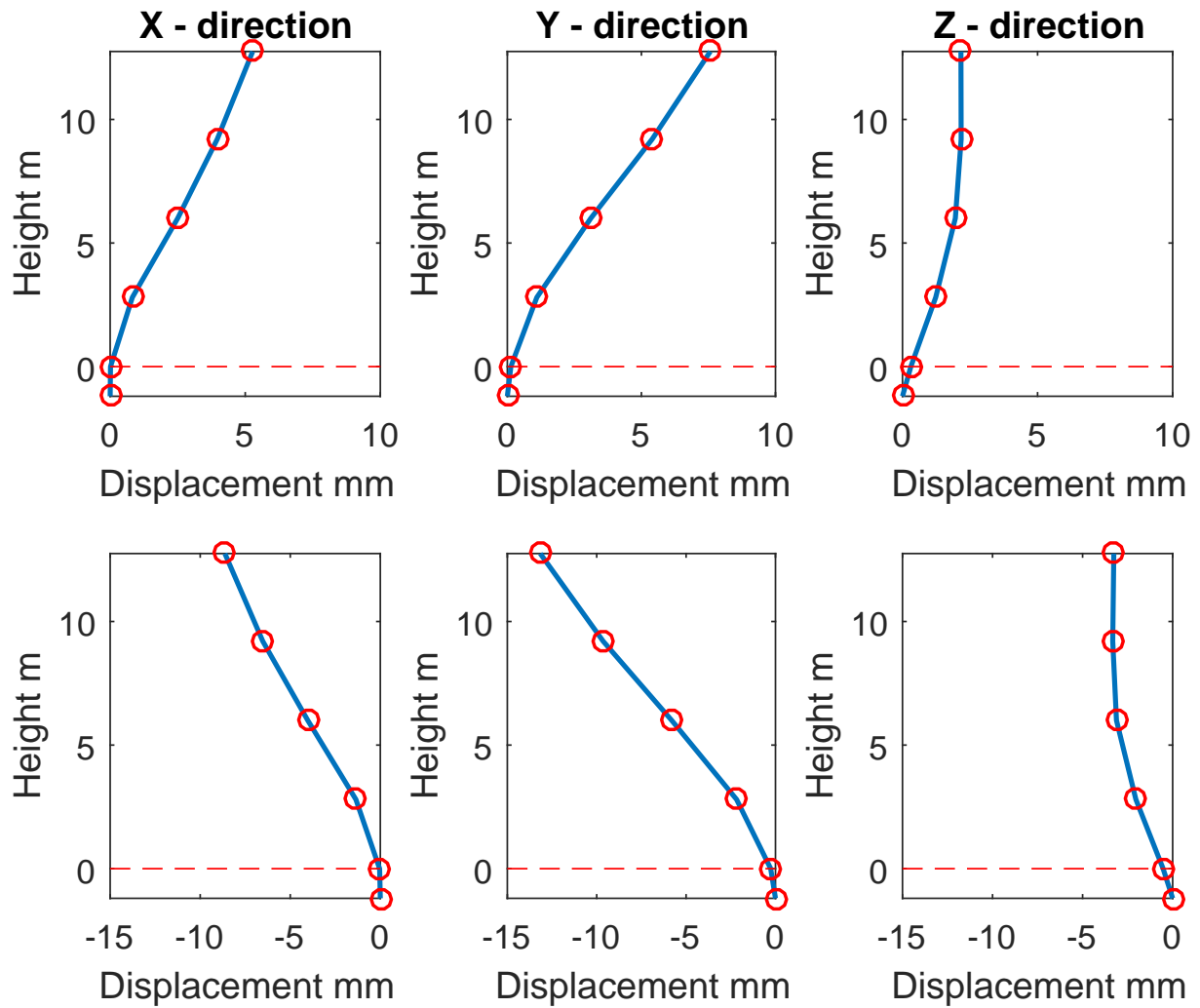


Figure B.8: Displacement for Sólheimar earthquake action, the columns represent direction and lines represent max and min values with max values above.

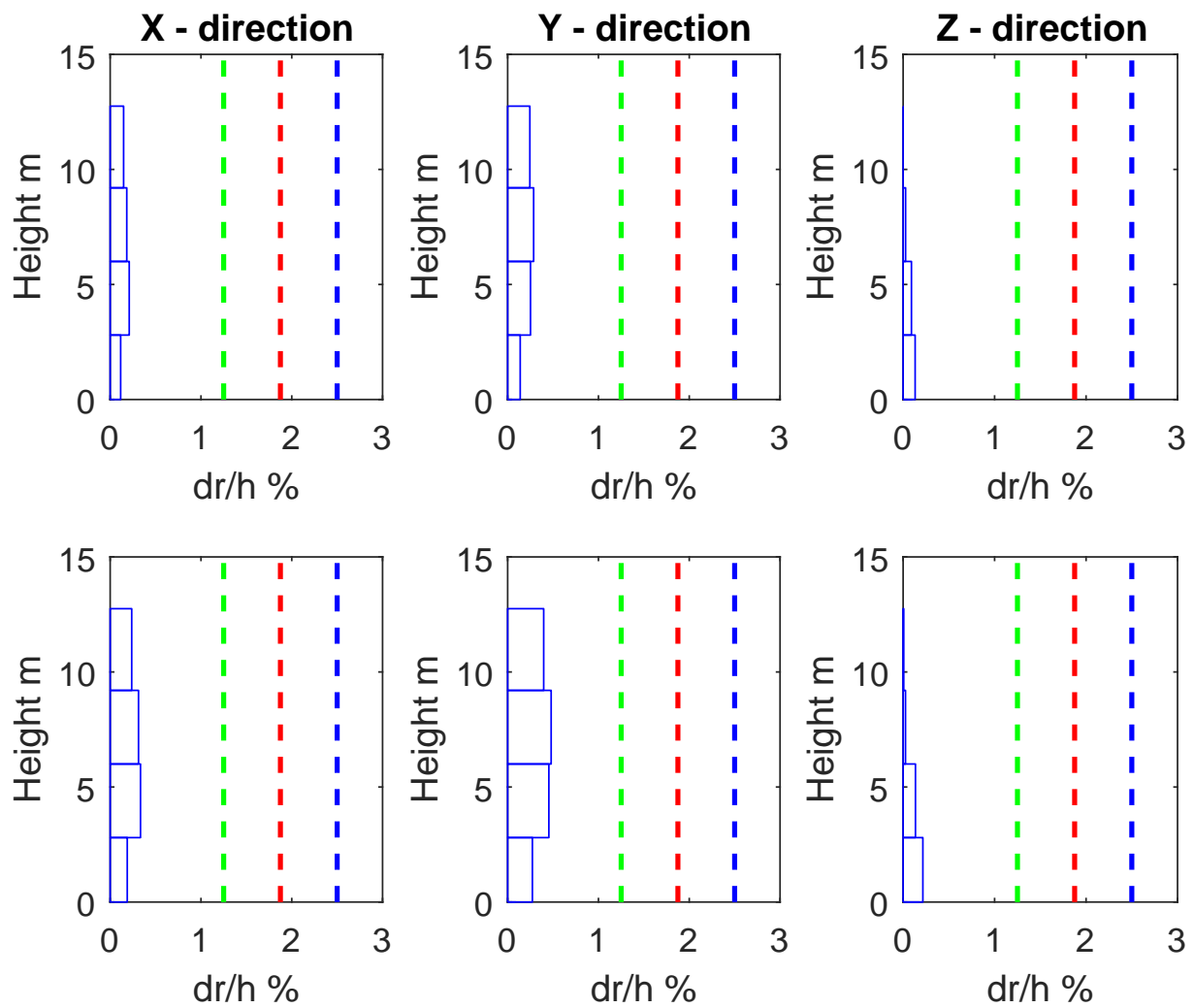


Figure B.9: Storey drifts for Sólheimar earthquake action, the columns represent direction and lines represent max and min values with max values above.

Table B.3: Section cut earthquake induced forces

TABLE: Section Cut Forces - Design									
SectionCut	OutputCase	CaseType	StepType	P	V2	V3	T	M2	M3
Text	Text	Text	Text	N	N	N	N-m	N-m	N-m
A1D	Solheimar_TH	LinModHist	Max	360986	49488	13601	5758	-1680	96387
A1D	Solheimar_TH	LinModHist	Min	-828187	-107844	-5986	-3276	4005	-41893
A2D	Solheimar_TH	LinModHist	Max	282526	18556	8652	7713	-10889	60019
A2D	Solheimar_TH	LinModHist	Min	-334864	-20500	-8243	-7944	13138	-69721
A3D	Solheimar_TH	LinModHist	Max	954290	9411	42593	6387	-188269	7719
A3D	Solheimar_TH	LinModHist	Min	-1075184	-8267	-56436	-6170	212626	-7452
A4D	Solheimar_TH	LinModHist	Max	806752	5033	33477	5654	-159829	11496
A4D	Solheimar_TH	LinModHist	Min	-916449	-3754	-35866	-6890	182196	-10104
B1D	Solheimar_TH	LinModHist	Max	860844	112734	22670	1995	-5353	127780
B1D	Solheimar_TH	LinModHist	Min	-842265	-115360	-30509	-3239	3651	-130673
B2D	Solheimar_TH	LinModHist	Max	561326	62808	21524	3262	-6926	86648
B2D	Solheimar_TH	LinModHist	Min	-457989	-74742	-22561	-3838	7507	-70123
B3D	Solheimar_TH	LinModHist	Max	814331	21238	27741	2815	-55340	10133
B3D	Solheimar_TH	LinModHist	Min	-363833	-25250	-55195	-2499	125191	-6314
B4D	Solheimar_TH	LinModHist	Max	452898	3584	24358	1522	-60301	4483
B4D	Solheimar_TH	LinModHist	Min	-391184	-3729	-28871	-1662	70082	-5019
C1D	Solheimar_TH	LinModHist	Max	2947	4383	6915	12	0	71
C1D	Solheimar_TH	LinModHist	Min	-4637	-6218	-10584	-11	0	-78
C2D	Solheimar_TH	LinModHist	Max	3069	4357	8727	70	0	69
C2D	Solheimar_TH	LinModHist	Min	-4529	-6150	-8363	-65	0	-53
C3D	Solheimar_TH	LinModHist	Max	5826	9227	10051	13	-133	0
C3D	Solheimar_TH	LinModHist	Min	-5783	-9287	-15289	-14	129	0
C4D	Solheimar_TH	LinModHist	Max	2360	6267	7758	8	-97	0
C4D	Solheimar_TH	LinModHist	Min	-2857	-6374	-8248	-9	78	0
D1D	Solheimar_TH	LinModHist	Max	2308	2979	4863	6	0	61
D1D	Solheimar_TH	LinModHist	Min	-3024	-4424	-7506	-6	0	-70
D2D	Solheimar_TH	LinModHist	Max	2810	2931	6071	6	0	57
D2D	Solheimar_TH	LinModHist	Min	-2912	-4209	-7929	-6	0	-56
D3D	Solheimar_TH	LinModHist	Max	2881	2953	8359	71	0	49
D3D	Solheimar_TH	LinModHist	Min	-2983	-4277	-6279	-53	0	-38
D4D	Solheimar_TH	LinModHist	Max	4219	6063	5018	7	-145	0
D4D	Solheimar_TH	LinModHist	Min	-4008	-6265	-10008	-7	138	0
D5D	Solheimar_TH	LinModHist	Max	2325	4206	4628	4	-123	0
D5D	Solheimar_TH	LinModHist	Min	-2376	-4461	-5192	-4	132	0

B.4 Tjorsartun

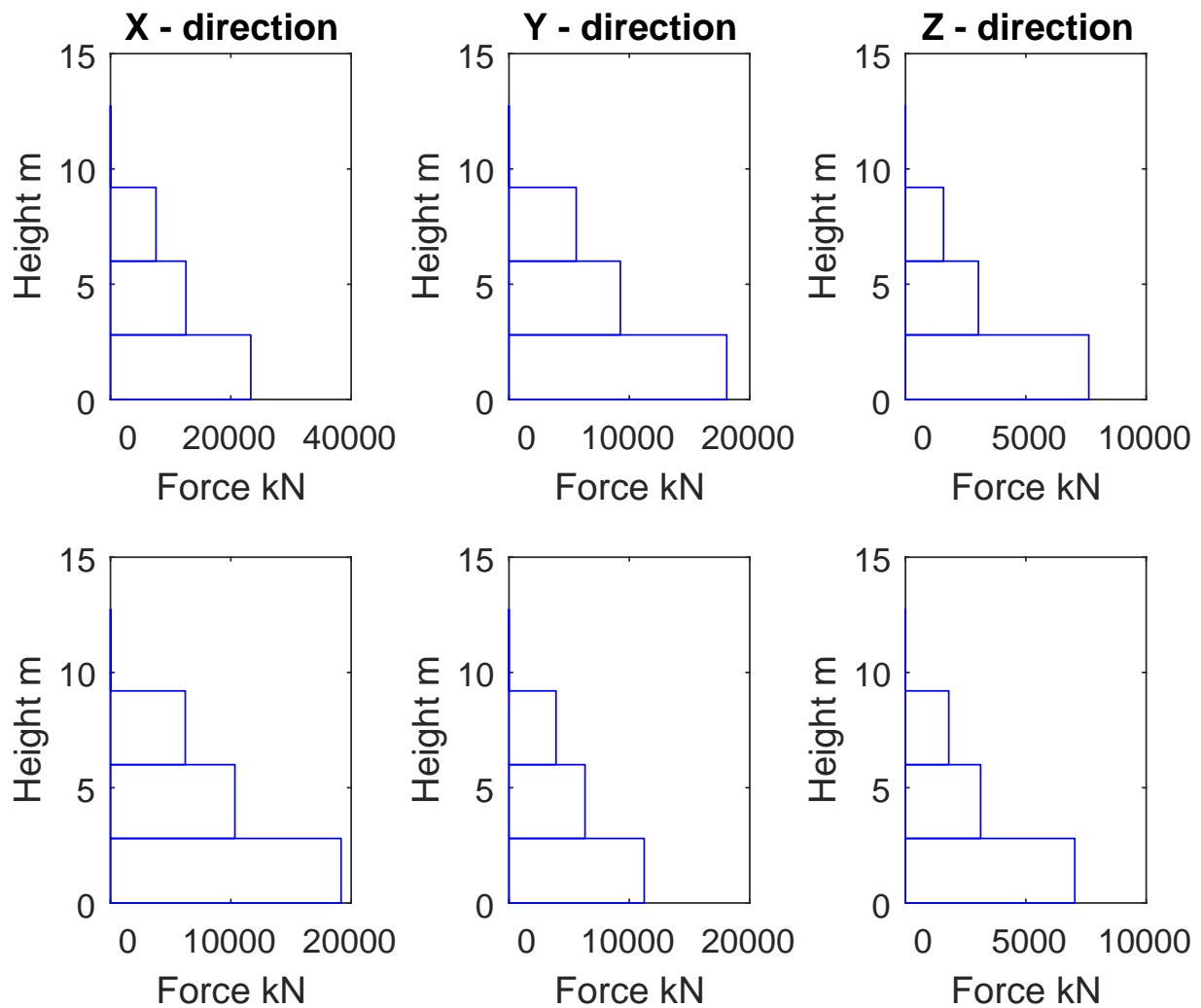


Figure B.10: Storey shear for Þjórsártún earthquake action, the columns represent direction and lines represent max and min values with max values above.

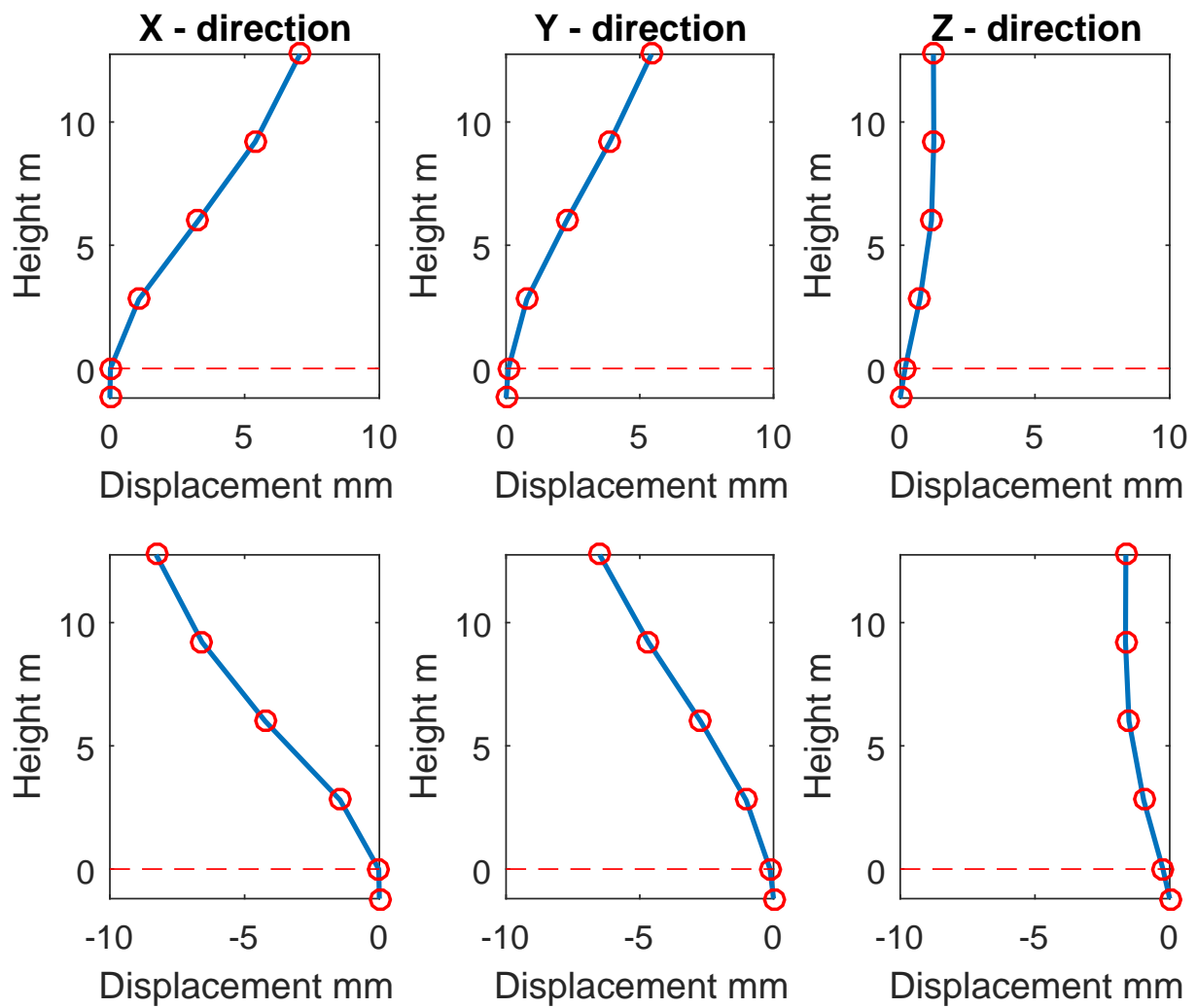


Figure B.11: Displacement for Þjórsártún earthquake action, the columns represent direction and lines represent max and min values with max values above.

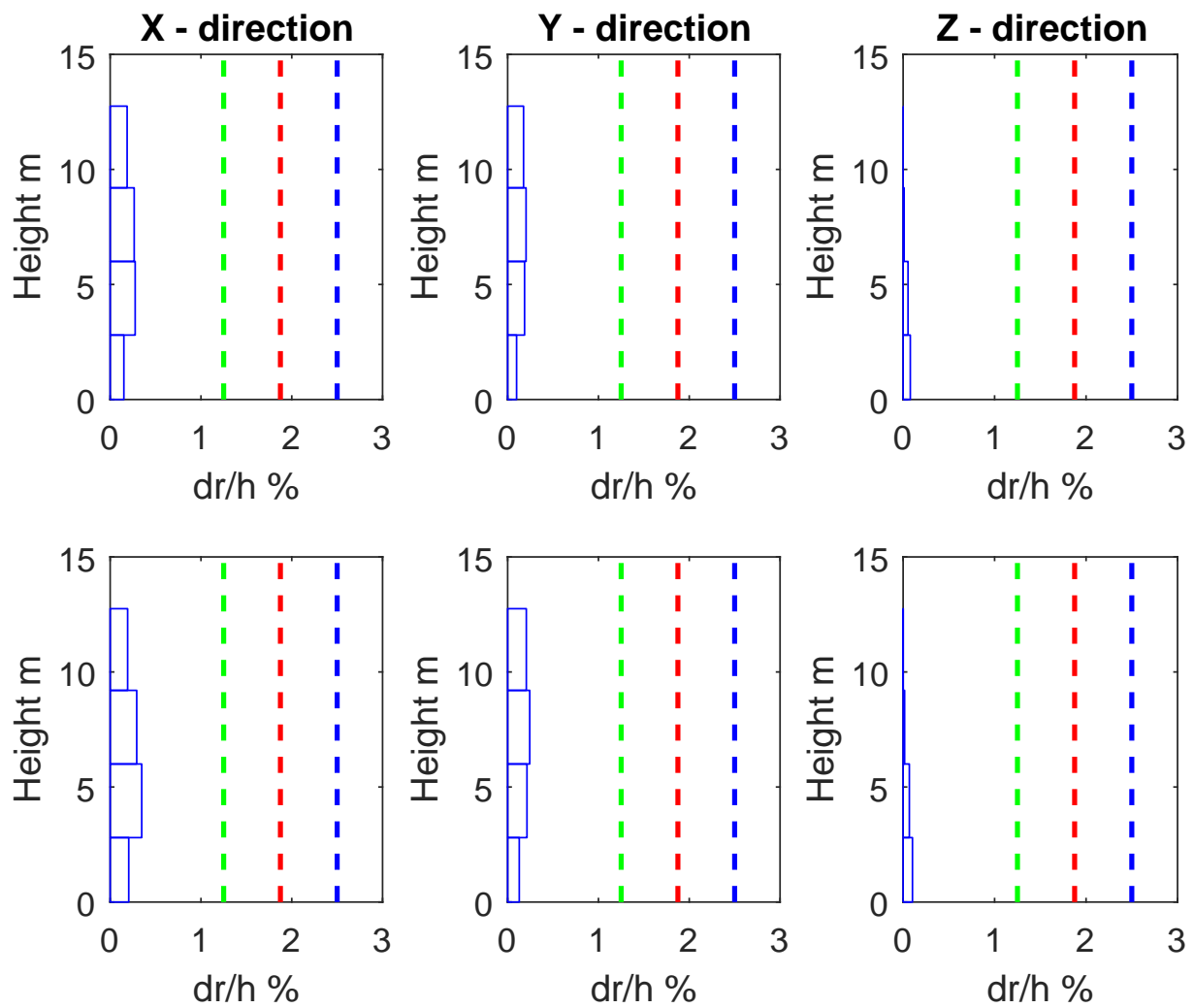


Figure B.12: Storey drifts for Bjórsártún earthquake action, the columns represent direction and lines represent max and min values with max values above.

Table B.4: Section cut earthquake induced forces

TABLE: Section Cut Forces - Design									
SectionCut	OutputCase	CaseType	StepType	P	V2	V3	T	M2	M3
Text	Text	Text	Text	N	N	N	N-m	N-m	N-m
A1D	Tjorsartun_TH	LinModHist	Max	448735	57903	8330	2618	-1623	64558
A1D	Tjorsartun_TH	LinModHist	Min	-556293	-70282	-6149	-2140	2001	-52184
A2D	Tjorsartun_TH	LinModHist	Max	295278	19379	5746	3608	-5506	63637
A2D	Tjorsartun_TH	LinModHist	Min	-422039	-10814	-6511	-6387	11837	-89297
A3D	Tjorsartun_TH	LinModHist	Max	447473	6861	22706	3613	-88374	5036
A3D	Tjorsartun_TH	LinModHist	Min	-606911	-5195	-29921	-3991	119848	-4171
A4D	Tjorsartun_TH	LinModHist	Max	558923	3441	18794	3804	-111153	8789
A4D	Tjorsartun_TH	LinModHist	Min	-667466	-2970	-26457	-4594	132273	-6779
B1D	Tjorsartun_TH	LinModHist	Max	451261	59613	15018	938	-3379	78726
B1D	Tjorsartun_TH	LinModHist	Min	-519667	-70630	-21065	-1583	2497	-68574
B2D	Tjorsartun_TH	LinModHist	Max	411822	40436	9414	2267	-4670	63668
B2D	Tjorsartun_TH	LinModHist	Min	-329028	-53535	-18511	-3009	5267	-51030
B3D	Tjorsartun_TH	LinModHist	Max	684855	23051	22976	1795	-76591	4911
B3D	Tjorsartun_TH	LinModHist	Min	-502158	-28134	-28156	-2241	104135	-3761
B4D	Tjorsartun_TH	LinModHist	Max	599931	4344	18959	2078	-66009	3110
B4D	Tjorsartun_TH	LinModHist	Min	-429932	-3962	-32300	-1716	92646	-5585
C1D	Tjorsartun_TH	LinModHist	Max	2539	5558	3521	8	0	88
C1D	Tjorsartun_TH	LinModHist	Min	-2435	-6967	-4850	-9	0	-68
C2D	Tjorsartun_TH	LinModHist	Max	1898	5483	3925	31	0	41
C2D	Tjorsartun_TH	LinModHist	Min	-2609	-7091	-6015	-47	0	-46
C3D	Tjorsartun_TH	LinModHist	Max	3204	8548	5610	9	-75	0
C3D	Tjorsartun_TH	LinModHist	Min	-3311	-9809	-7049	-9	67	0
C4D	Tjorsartun_TH	LinModHist	Max	1410	4982	3970	6	-59	0
C4D	Tjorsartun_TH	LinModHist	Min	-1525	-6105	-6022	-6	61	0
D1D	Tjorsartun_TH	LinModHist	Max	1463	4255	2908	5	0	82
D1D	Tjorsartun_TH	LinModHist	Min	-1717	-5610	-4146	-4	0	-77
D2D	Tjorsartun_TH	LinModHist	Max	2414	4260	2874	4	0	80
D2D	Tjorsartun_TH	LinModHist	Min	-1902	-5533	-4348	-4	0	-75
D3D	Tjorsartun_TH	LinModHist	Max	1511	4448	3550	31	0	37
D3D	Tjorsartun_TH	LinModHist	Min	-1352	-5739	-4043	-32	0	-32
D4D	Tjorsartun_TH	LinModHist	Max	2387	6918	3346	6	-68	0
D4D	Tjorsartun_TH	LinModHist	Min	-2619	-7774	-5032	-5	71	0
D5D	Tjorsartun_TH	LinModHist	Max	1464	4100	1895	4	-68	0
D5D	Tjorsartun_TH	LinModHist	Min	-1842	-4858	-3609	-3	72	0

B.5 Selfoss city hall

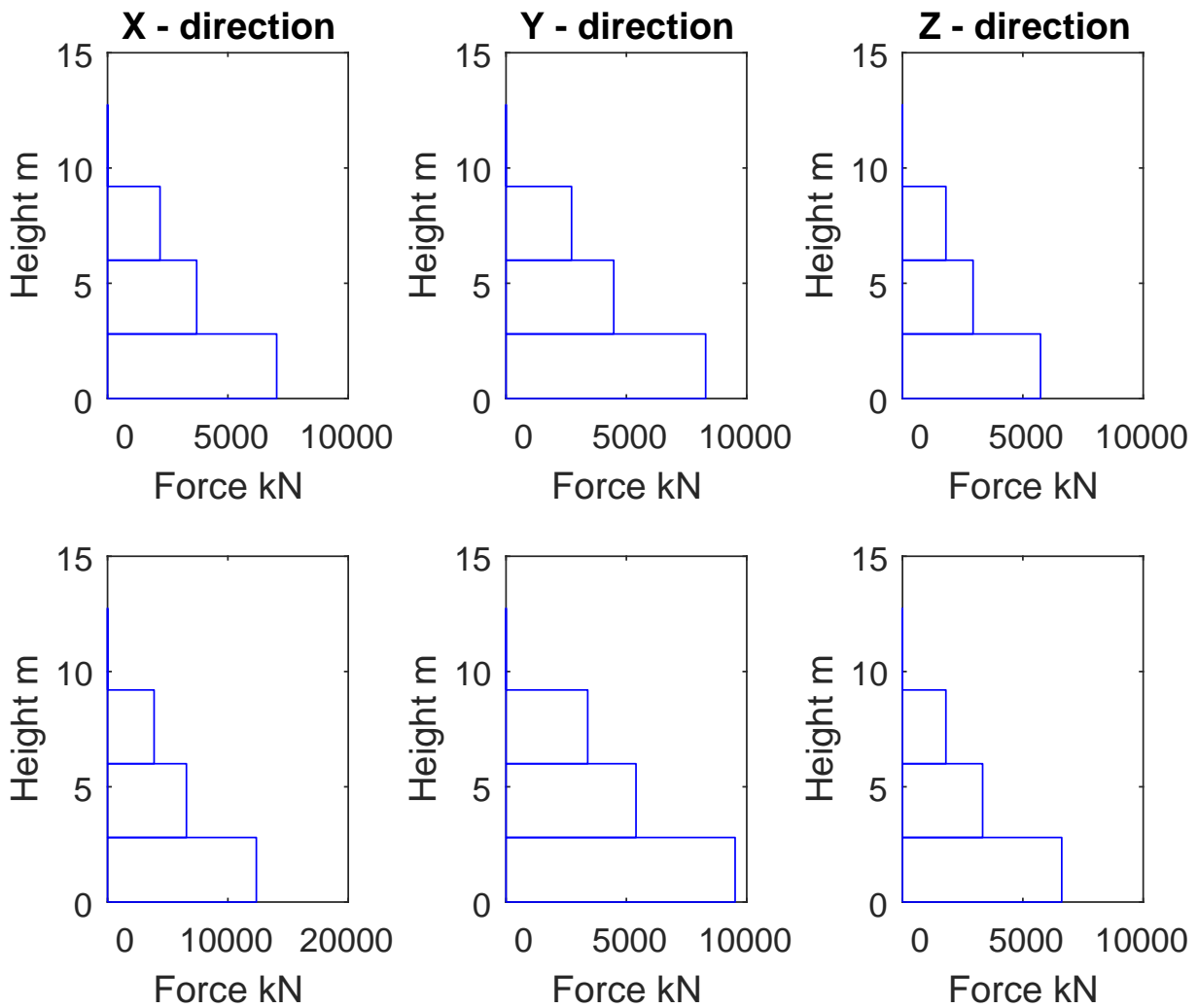


Figure B.13: Storey shear for Selfoss city hall earthquake action, the columns represent direction and lines represent max and min values with max values above.

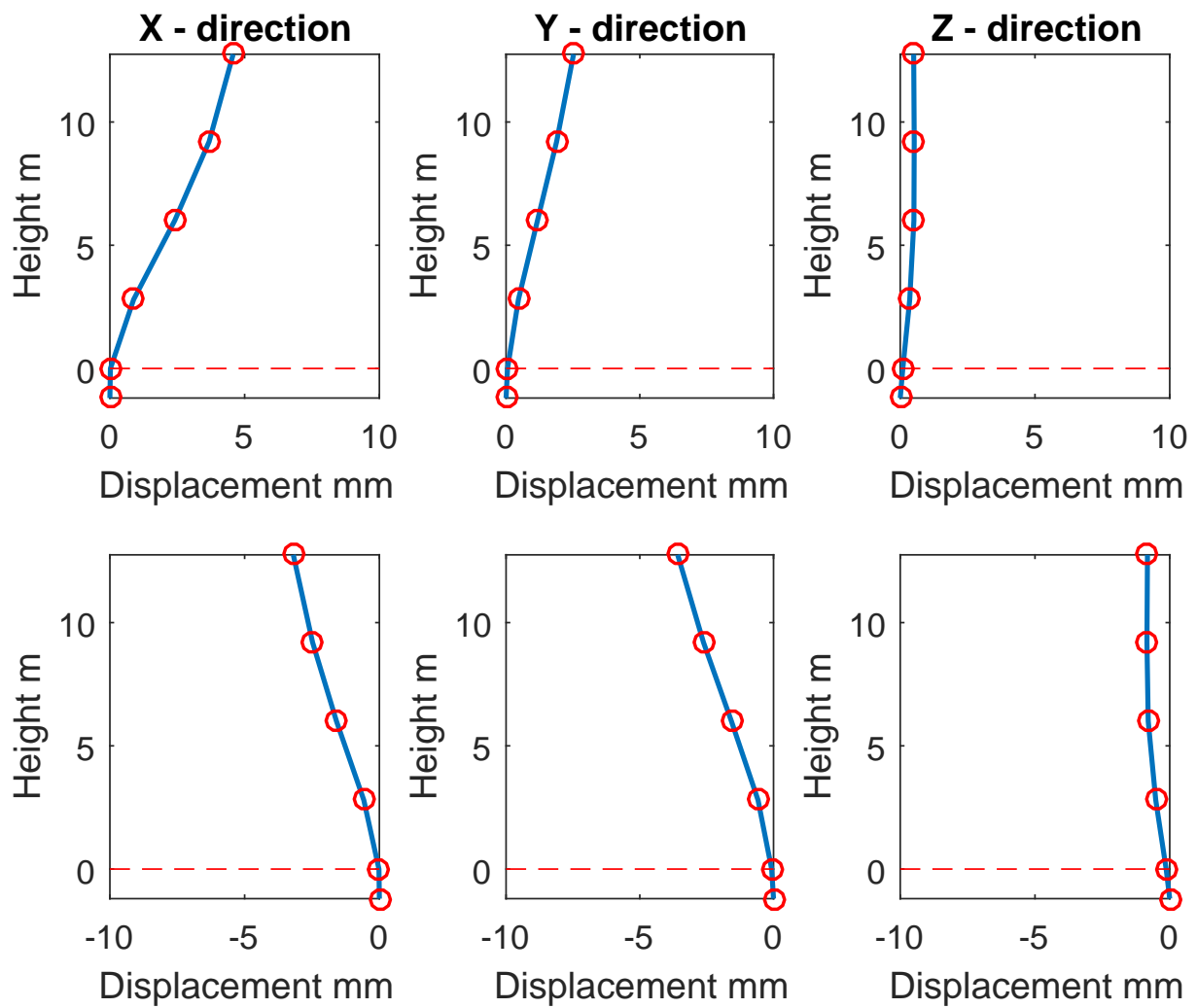


Figure B.14: Displacement for Selfoss city hall earthquake action, the columns represent direction and lines represent max and min values with max values above.

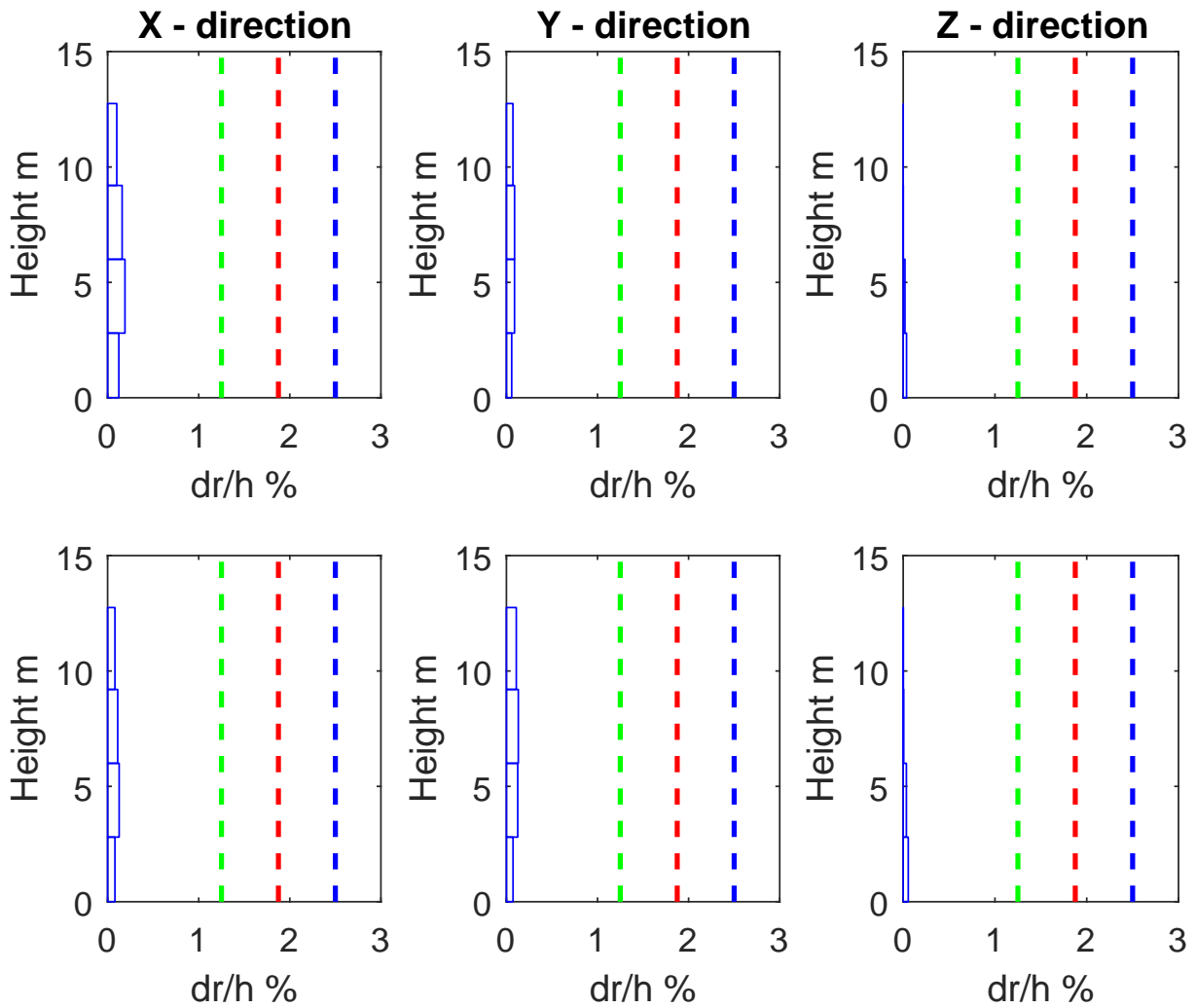


Figure B.15: Storey drifts for Selfoss city hall earthquake action, the columns represent direction and lines represent max and min values with max values above.

Table B.5: Section cut earthquake induced forces

TABLE: Section Cut Forces - Design									
SectionCut	OutputCase	CaseType	StepType	P	V2	V3	T	M2	M3
Text	Text	Text	Text	N	N	N	N-m	N-m	N-m
A1D	Cityhall_TH	LinModHist	Max	289691	35315	4007	1616	-1038	32803
A1D	Cityhall_TH	LinModHist	Min	-281914	-36697	-3269	-1167	1227	-33741
A2D	Cityhall_TH	LinModHist	Max	168360	8767	3390	2575	-3250	35837
A2D	Cityhall_TH	LinModHist	Min	-208019	-5991	-1880	-1841	4404	-44021
A3D	Cityhall_TH	LinModHist	Max	153143	3058	8181	1613	-30571	1570
A3D	Cityhall_TH	LinModHist	Min	-161790	-4384	-9089	-1454	31619	-1964
A4D	Cityhall_TH	LinModHist	Max	254479	1650	10094	1726	-50530	2394
A4D	Cityhall_TH	LinModHist	Min	-162797	-2400	-6556	-1398	32550	-3176
B1D	Cityhall_TH	LinModHist	Max	211558	29560	9979	726	-1917	27411
B1D	Cityhall_TH	LinModHist	Min	-180083	-24081	-11399	-731	1673	-32152
B2D	Cityhall_TH	LinModHist	Max	123769	23861	7894	1368	-2528	19100
B2D	Cityhall_TH	LinModHist	Min	-169880	-16864	-8219	-974	1491	-26146
B3D	Cityhall_TH	LinModHist	Max	303432	15489	13195	1233	-51137	2554
B3D	Cityhall_TH	LinModHist	Min	-338400	-9284	-15335	-701	46464	-1661
B4D	Cityhall_TH	LinModHist	Max	294754	1842	11186	800	-39052	2079
B4D	Cityhall_TH	LinModHist	Min	-253364	-1683	-13324	-1036	45412	-2527
C1D	Cityhall_TH	LinModHist	Max	2037	3403	2317	2	0	24
C1D	Cityhall_TH	LinModHist	Min	-1798	-2402	-2774	-2	0	-35
C2D	Cityhall_TH	LinModHist	Max	2480	3261	2604	21	0	16
C2D	Cityhall_TH	LinModHist	Min	-1869	-2301	-2621	-22	0	-26
C3D	Cityhall_TH	LinModHist	Max	2750	4484	2650	2	-33	0
C3D	Cityhall_TH	LinModHist	Min	-2958	-2864	-3513	-2	25	0
C4D	Cityhall_TH	LinModHist	Max	1261	2433	2436	2	-28	0
C4D	Cityhall_TH	LinModHist	Min	-1401	-1587	-2327	-2	29	0
D1D	Cityhall_TH	LinModHist	Max	1262	2859	1912	2	0	22
D1D	Cityhall_TH	LinModHist	Min	-1276	-1729	-1823	-2	0	-26
D2D	Cityhall_TH	LinModHist	Max	2044	2753	2003	1	0	25
D2D	Cityhall_TH	LinModHist	Min	-1897	-1806	-2016	-1	0	-22
D3D	Cityhall_TH	LinModHist	Max	1223	2724	1890	17	0	14
D3D	Cityhall_TH	LinModHist	Min	-1228	-1915	-1530	-13	0	-22
D4D	Cityhall_TH	LinModHist	Max	2022	3757	2255	2	-28	0
D4D	Cityhall_TH	LinModHist	Min	-2495	-2586	-2227	-1	23	0
D5D	Cityhall_TH	LinModHist	Max	1405	2237	1419	1	-36	0
D5D	Cityhall_TH	LinModHist	Min	-1609	-1567	-1135	-1	30	0

B.6 Retirement home

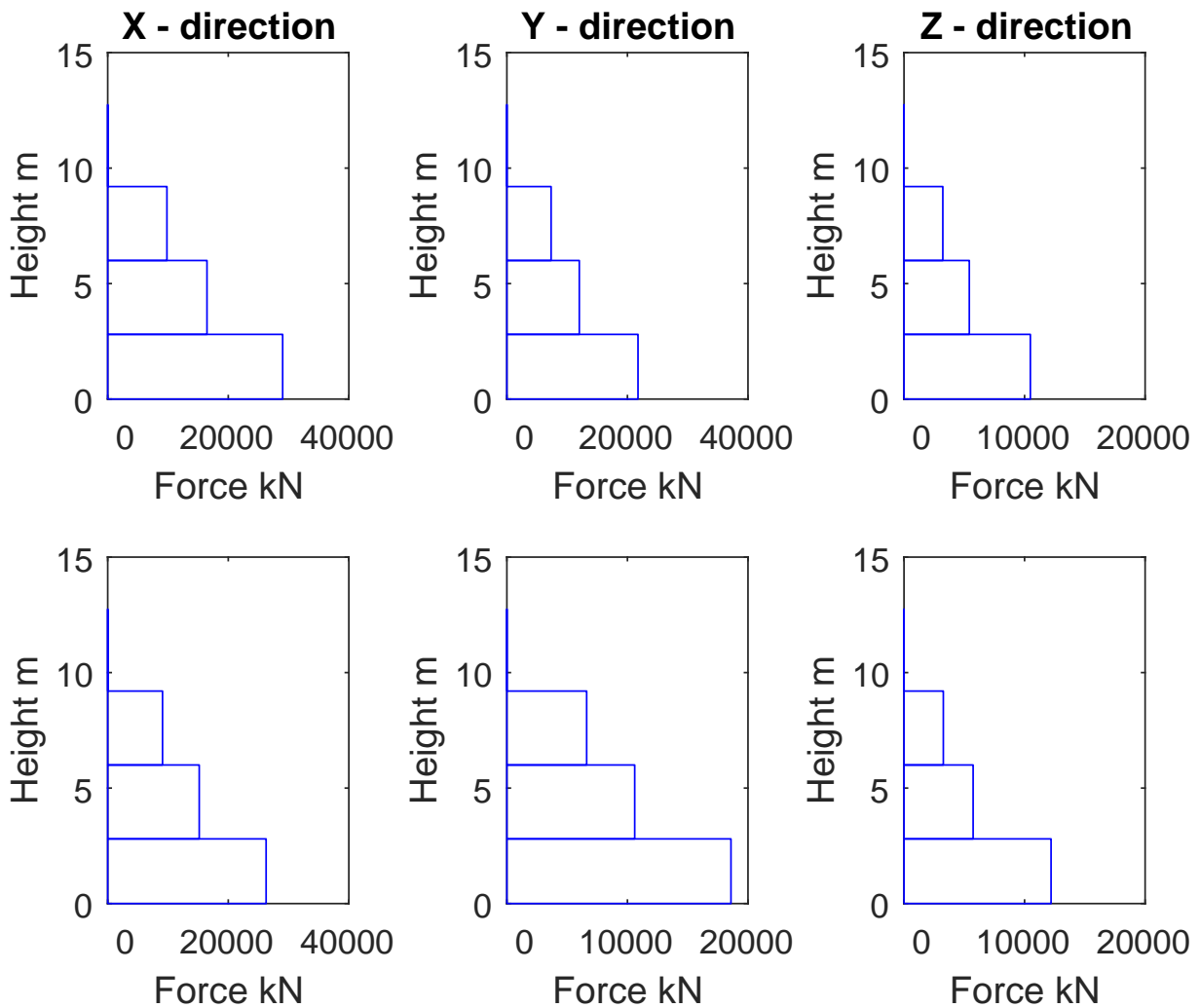


Figure B.16: Storey shear for Retirement home earthquake action, the columns represent direction and lines represent max and min values with max values above.

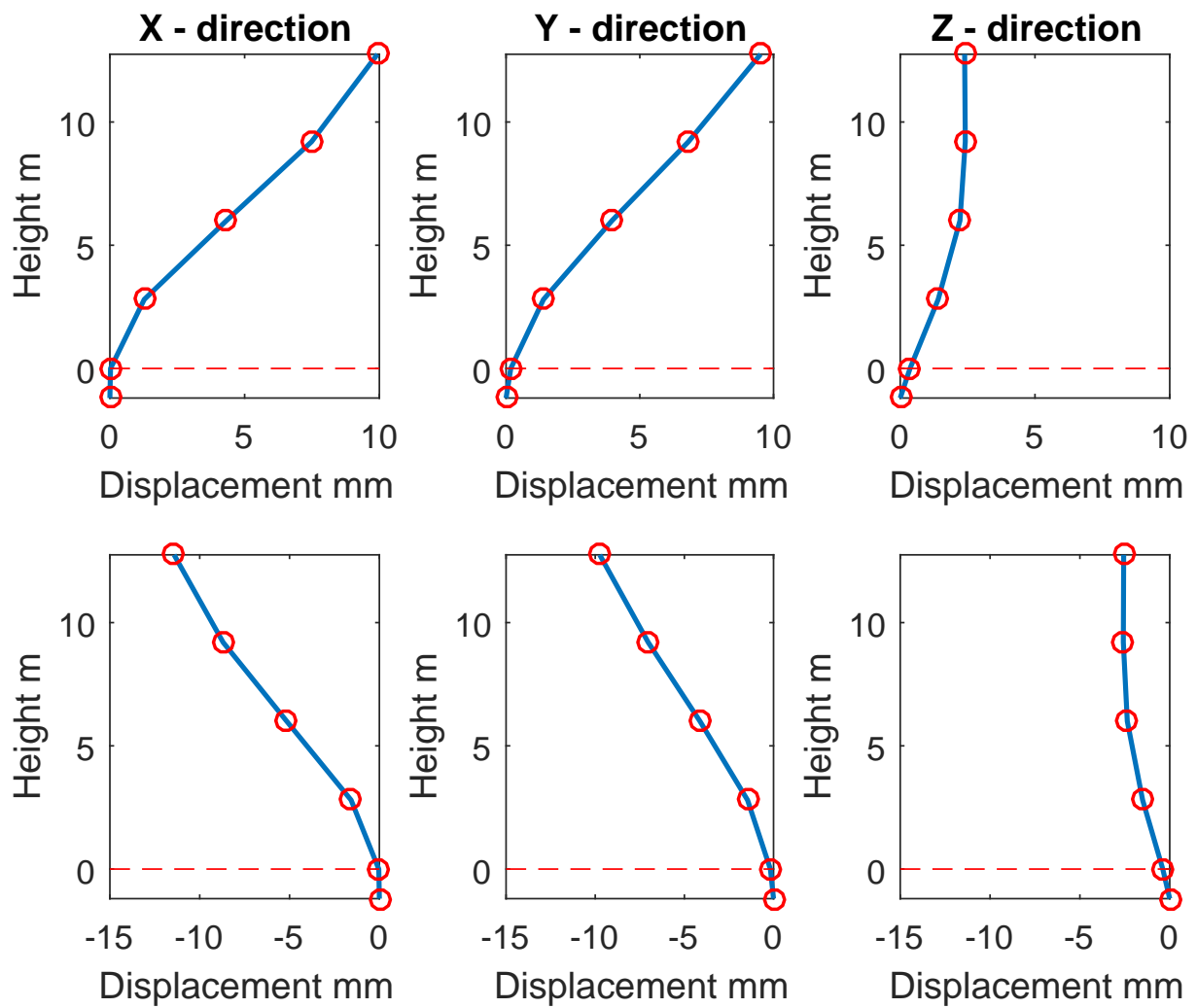


Figure B.17: Displacement for Retirement home earthquake action, the columns represent direction and lines represent max and min values with max values above.

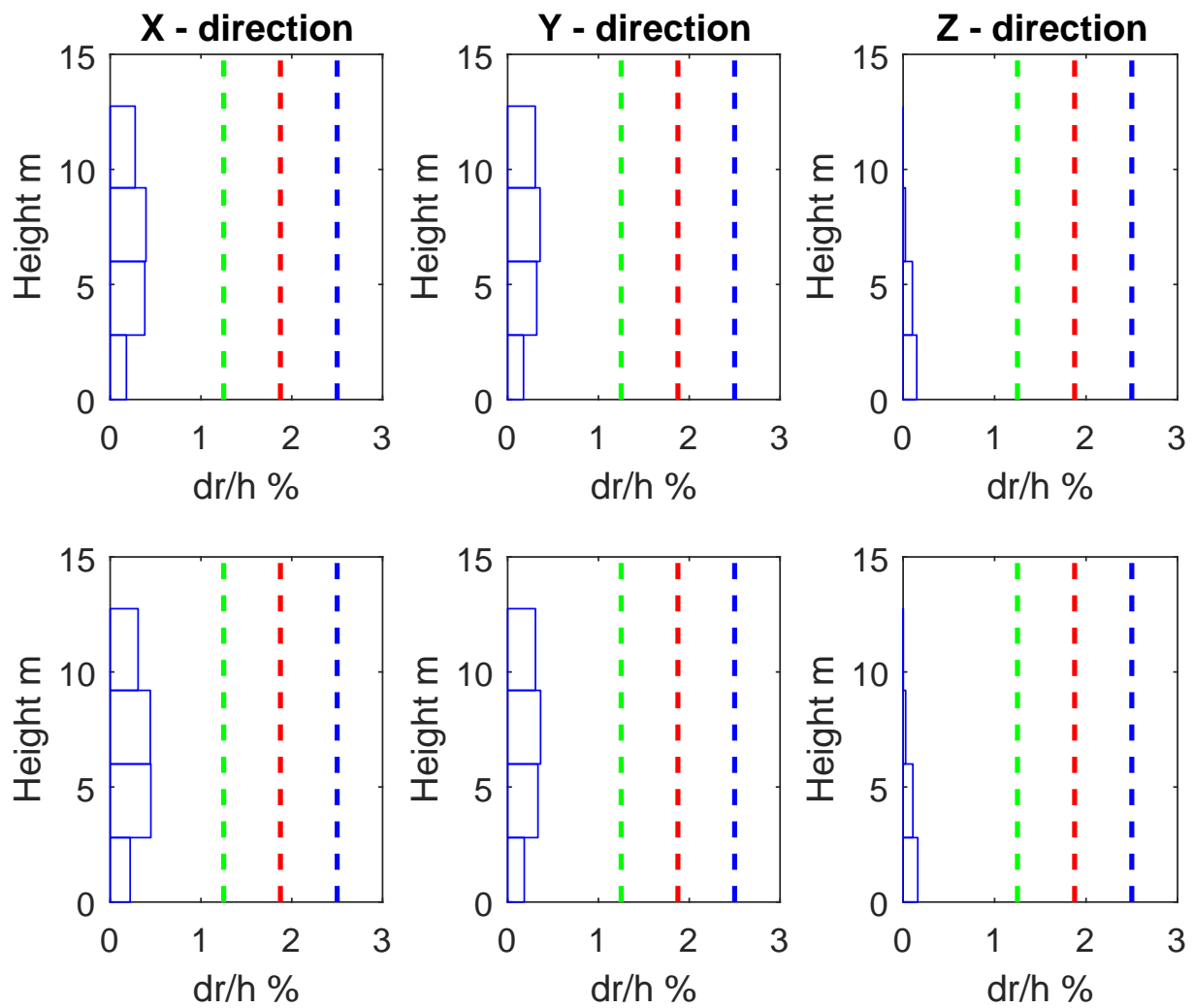


Figure B.18: Storey drifts for Retirement home earthquake action, the columns represent direction and lines represent max and min values with max values above.

Table B.6: Section cut earthquake induced forces

TABLE: Section Cut Forces - Design									
SectionCut	OutputCase	CaseType	StepType	P	V2	V3	T	M2	M3
Text	Text	Text	Text	N	N	N	N-m	N-m	N-m
A1D	Retirement_TH	LinModHist	Max	597778	80378	8845	3921	-2558	78141
A1D	Retirement_TH	LinModHist	Min	-673801	-86053	-8364	-3872	2749	-69419
A2D	Retirement_TH	LinModHist	Max	473658	18095	8601	8783	-14369	99677
A2D	Retirement_TH	LinModHist	Min	-444665	-22123	-9347	-6097	9952	-92593
A3D	Retirement_TH	LinModHist	Max	1065164	8053	49048	6539	-210069	7669
A3D	Retirement_TH	LinModHist	Min	-1071475	-8489	-51521	-6275	210861	-7888
A4D	Retirement_TH	LinModHist	Max	1201330	4319	44618	8300	-238529	11921
A4D	Retirement_TH	LinModHist	Min	-974731	-4891	-33198	-6928	193281	-14673
B1D	Retirement_TH	LinModHist	Max	843179	110862	23523	2402	-5145	124334
B1D	Retirement_TH	LinModHist	Min	-820149	-110483	-29534	-2188	4141	-128203
B2D	Retirement_TH	LinModHist	Max	573148	81203	25110	4627	-9912	88633
B2D	Retirement_TH	LinModHist	Min	-664756	-73675	-18709	-4016	7738	-103228
B3D	Retirement_TH	LinModHist	Max	804278	32290	37297	2787	-98686	7891
B3D	Retirement_TH	LinModHist	Min	-643948	-36422	-41266	-2851	122572	-7312
B4D	Retirement_TH	LinModHist	Max	697921	6277	40379	2992	-120862	7170
B4D	Retirement_TH	LinModHist	Min	-783723	-6303	-33583	-2491	107561	-6010
C1D	Retirement_TH	LinModHist	Max	4767	7324	7267	14	0	135
C1D	Retirement_TH	LinModHist	Min	-5258	-8461	-7729	-13	0	-108
C2D	Retirement_TH	LinModHist	Max	4983	7315	8783	68	0	87
C2D	Retirement_TH	LinModHist	Min	-5110	-8987	-7116	-55	0	-81
C3D	Retirement_TH	LinModHist	Max	7078	9465	10641	16	-130	0
C3D	Retirement_TH	LinModHist	Min	-8586	-9619	-11521	-17	134	0
C4D	Retirement_TH	LinModHist	Max	3567	7702	9100	11	-101	0
C4D	Retirement_TH	LinModHist	Min	-3884	-6366	-7362	-11	106	0
D1D	Retirement_TH	LinModHist	Max	2549	4501	4553	8	0	99
D1D	Retirement_TH	LinModHist	Min	-2877	-5290	-4770	-9	0	-104
D2D	Retirement_TH	LinModHist	Max	4143	4041	4465	7	0	98
D2D	Retirement_TH	LinModHist	Min	-3682	-5430	-4510	-7	0	-108
D3D	Retirement_TH	LinModHist	Max	3196	4113	5304	43	0	67
D3D	Retirement_TH	LinModHist	Min	-3719	-5725	-5129	-43	0	-72
D4D	Retirement_TH	LinModHist	Max	5865	5377	6605	9	-133	0
D4D	Retirement_TH	LinModHist	Min	-5873	-6876	-6482	-9	120	0
D5D	Retirement_TH	LinModHist	Max	3661	5282	4866	5	-124	0
D5D	Retirement_TH	LinModHist	Min	-3703	-4273	-3226	-5	135	0

B.7 Earthquake engineering research centre

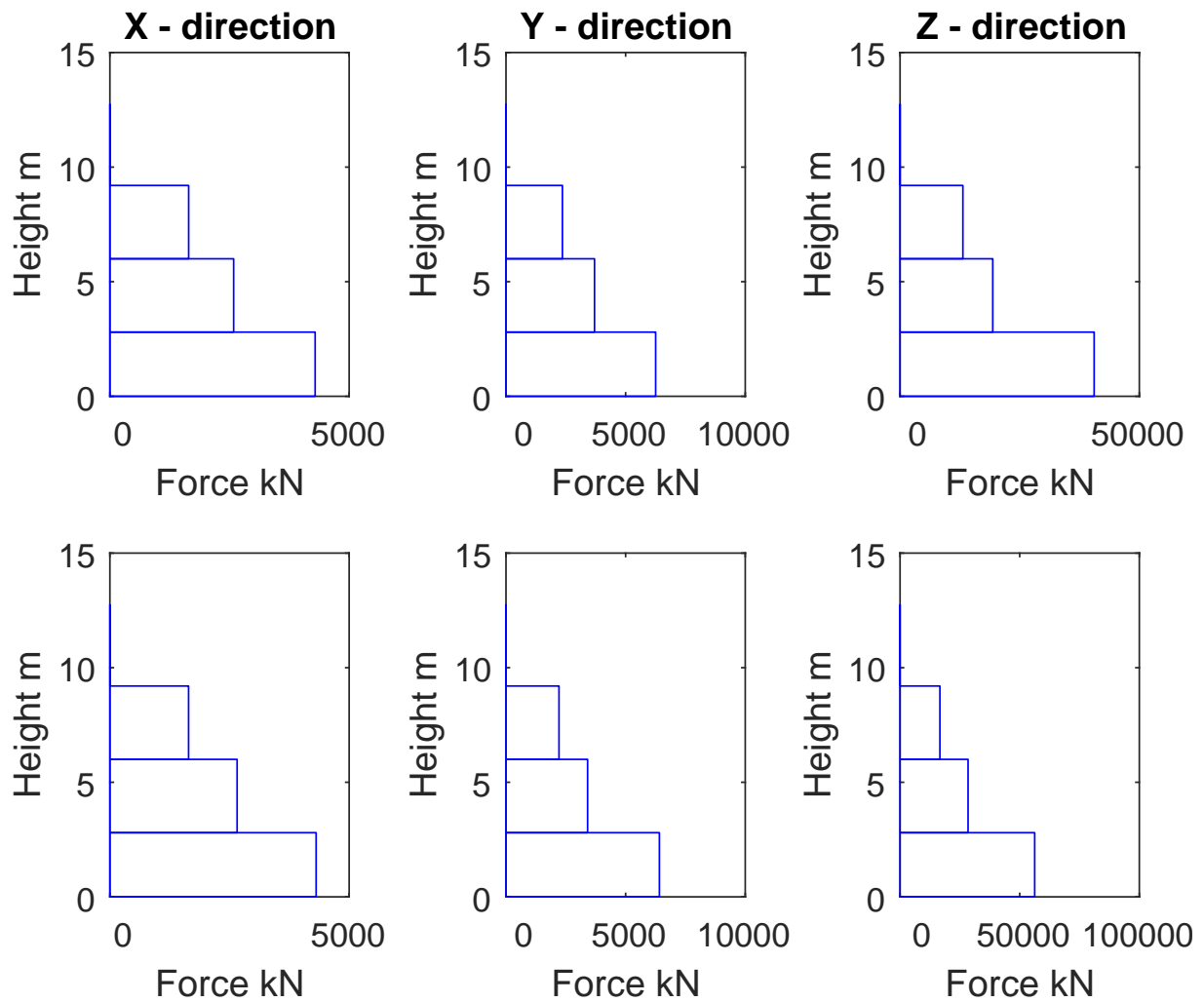


Figure B.19: Storey shear for EERC earthquake action, the columns represent direction and lines represent max and min values with max values above.

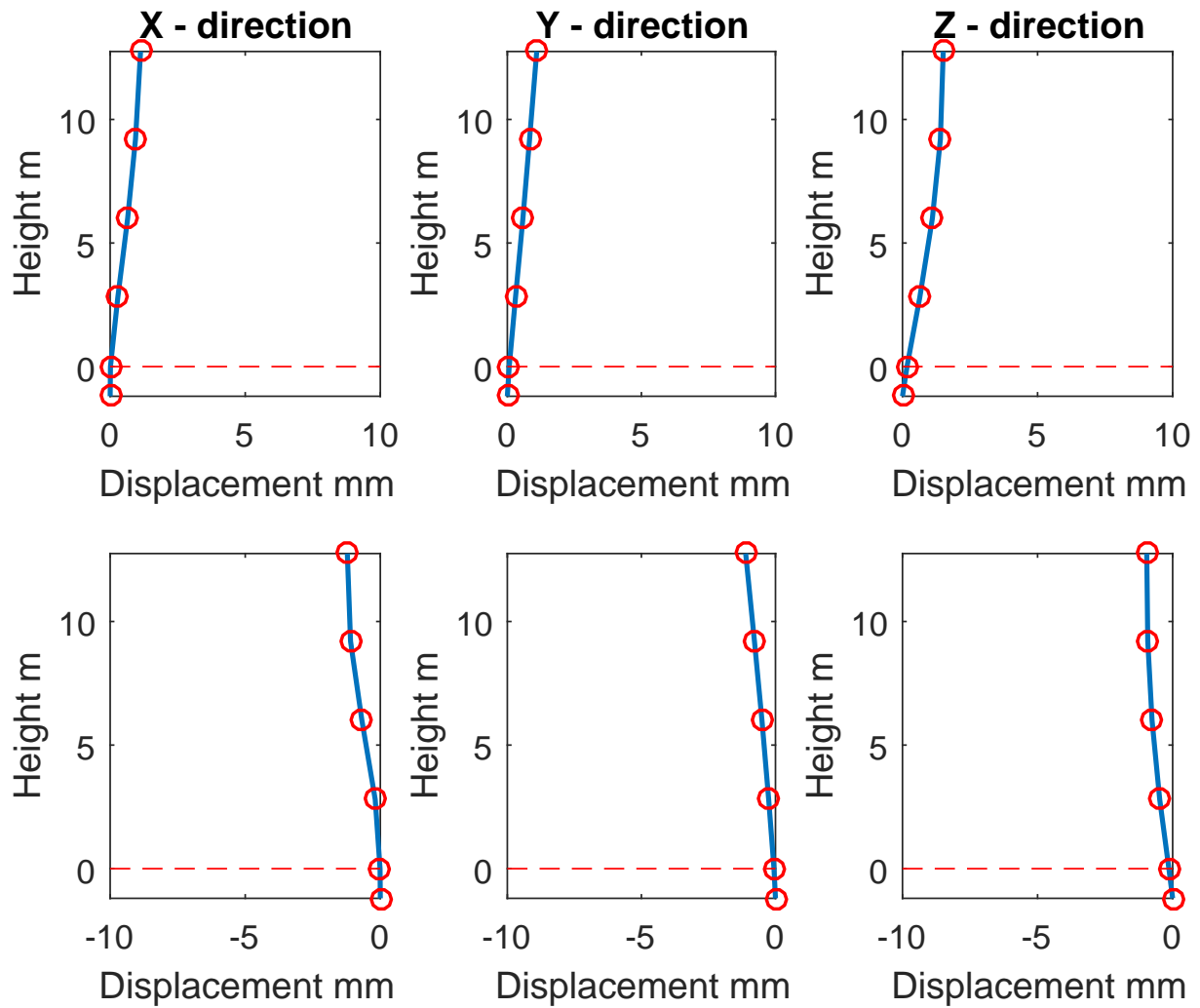


Figure B.20: Displacement for EERC earthquake action, the columns represent direction and lines represent max and min values with max values above.

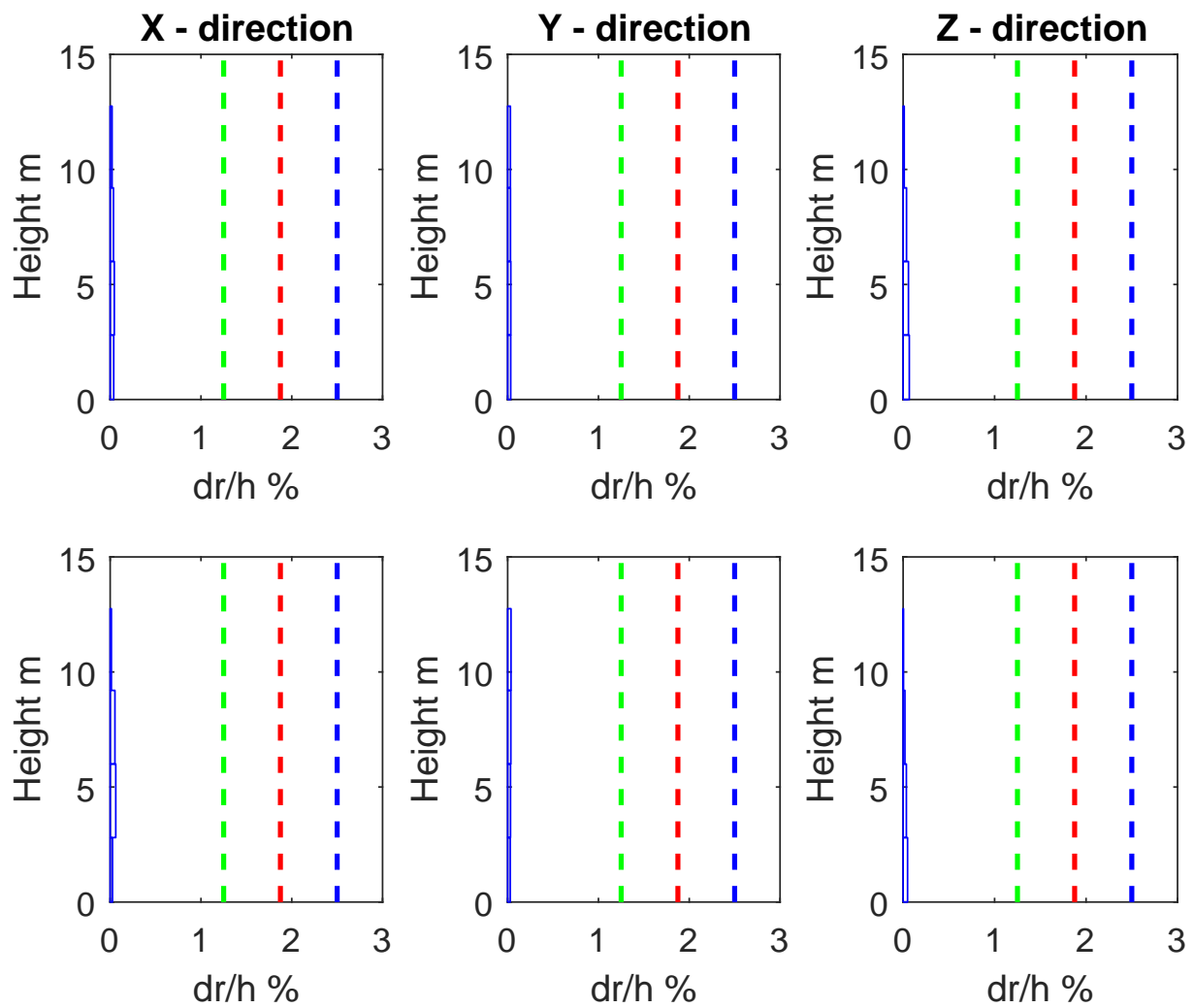


Figure B.21: Storey drifts for EERC earthquake action, the columns represent direction and lines represent max and min values with max values above.

Table B.7: Section cut earthquake induced forces

TABLE: Section Cut Forces - Design									
SectionCut	OutputCase	CaseType	StepType	P	V2	V3	T	M2	M3
Text	Text	Text	Text	N	N	N	N-m	N-m	N-m
A1D	EERC_TH	LinModHist	Max	101281	12496	11314	701	-959	5196
A1D	EERC_TH	LinModHist	Min	-40692	-5999	-11015	-750	722	-11921
A2D	EERC_TH	LinModHist	Max	33190	13464	5948	2050	-2906	6303
A2D	EERC_TH	LinModHist	Min	-70575	-13127	-6758	-2719	2315	-16024
A3D	EERC_TH	LinModHist	Max	134304	2285	4639	2357	-29148	803
A3D	EERC_TH	LinModHist	Min	-169470	-2532	-5632	-2325	34686	-1281
A4D	EERC_TH	LinModHist	Max	156418	453	5177	1875	-31394	1357
A4D	EERC_TH	LinModHist	Min	-102455	-1717	-5857	-1239	21493	-2003
B1D	EERC_TH	LinModHist	Max	164096	20053	7006	404	-754	18542
B1D	EERC_TH	LinModHist	Min	-118032	-3978	-4987	-615	1192	-24781
B2D	EERC_TH	LinModHist	Max	74265	16450	6909	1979	-2487	10770
B2D	EERC_TH	LinModHist	Min	-153492	-13277	-4243	-792	895	-23661
B3D	EERC_TH	LinModHist	Max	114470	7321	4144	698	-20439	3378
B3D	EERC_TH	LinModHist	Min	-136960	-9831	-3356	-623	19603	-2854
B4D	EERC_TH	LinModHist	Max	164363	2768	7583	647	-26768	2156
B4D	EERC_TH	LinModHist	Min	-172823	-2204	-3781	-1202	25975	-1768
C1D	EERC_TH	LinModHist	Max	17728	1465	2797	6	0	114
C1D	EERC_TH	LinModHist	Min	-12705	-1624	-3850	-5	0	-83
C2D	EERC_TH	LinModHist	Max	18816	1634	2985	25	0	88
C2D	EERC_TH	LinModHist	Min	-11151	-1444	-3280	-30	0	-160
C3D	EERC_TH	LinModHist	Max	15463	4992	1643	3	-34	0
C3D	EERC_TH	LinModHist	Min	-27153	-5807	-1572	-3	24	0
C4D	EERC_TH	LinModHist	Max	9799	4206	2315	1	-31	0
C4D	EERC_TH	LinModHist	Min	-11448	-4302	-1377	-2	31	0
D1D	EERC_TH	LinModHist	Max	11610	988	1671	6	0	47
D1D	EERC_TH	LinModHist	Min	-10966	-1058	-2553	-6	0	-41
D2D	EERC_TH	LinModHist	Max	15824	1651	5075	2	0	15
D2D	EERC_TH	LinModHist	Min	-13364	-889	-3446	-2	0	-49
D3D	EERC_TH	LinModHist	Max	10294	2072	4036	37	0	77
D3D	EERC_TH	LinModHist	Min	-9921	-1158	-6178	-55	0	-122
D4D	EERC_TH	LinModHist	Max	13819	3785	1669	4	-18	0
D4D	EERC_TH	LinModHist	Min	-20043	-4231	-1701	-4	37	0
D5D	EERC_TH	LinModHist	Max	8265	5288	1536	2	-15	0
D5D	EERC_TH	LinModHist	Min	-10362	-5213	-766	-3	48	0

B.8 Borgarhraun

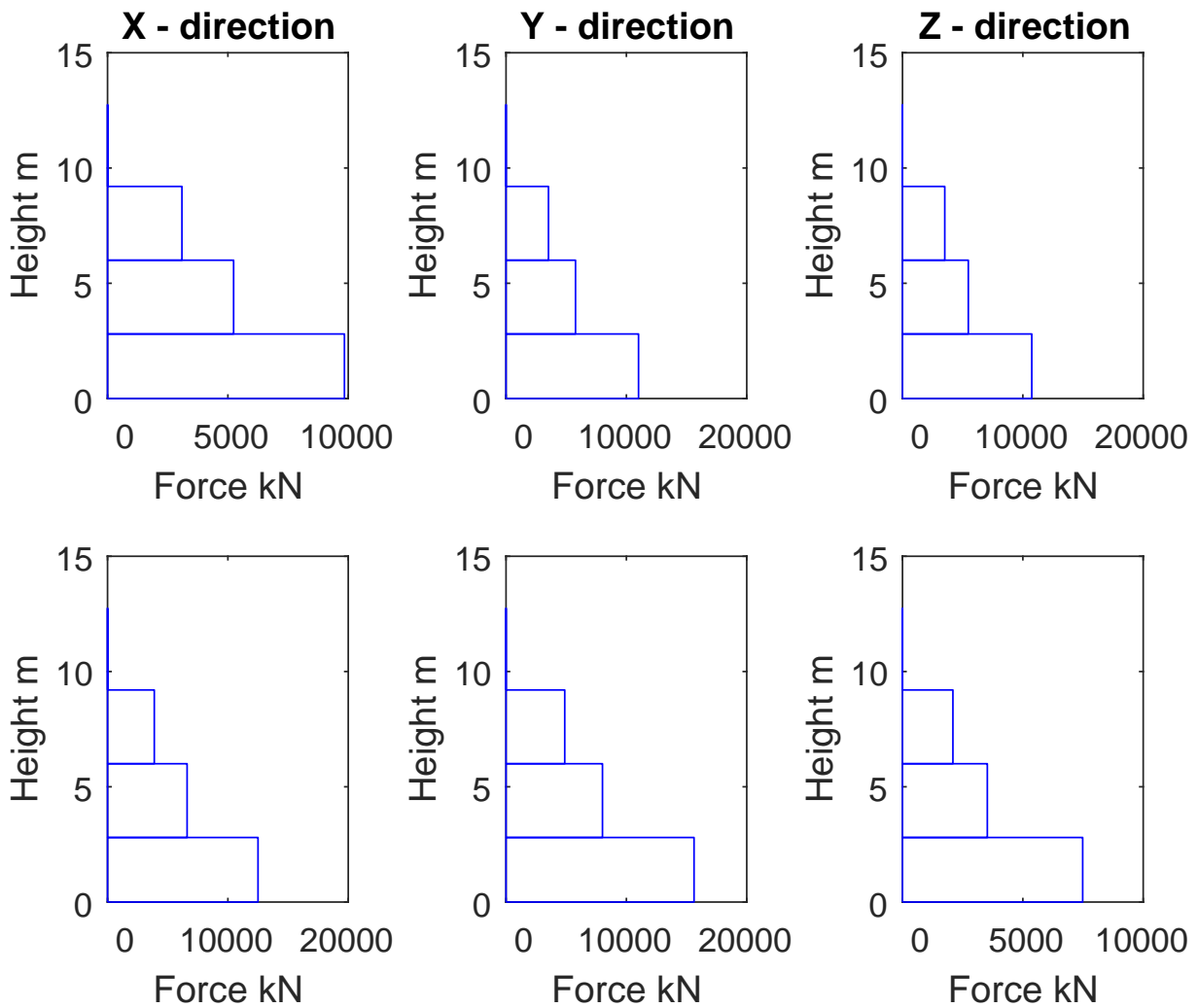


Figure B.22: Storey shear for Borgarhraun earthquake action, the columns represent direction and lines represent max and min values with max values above.

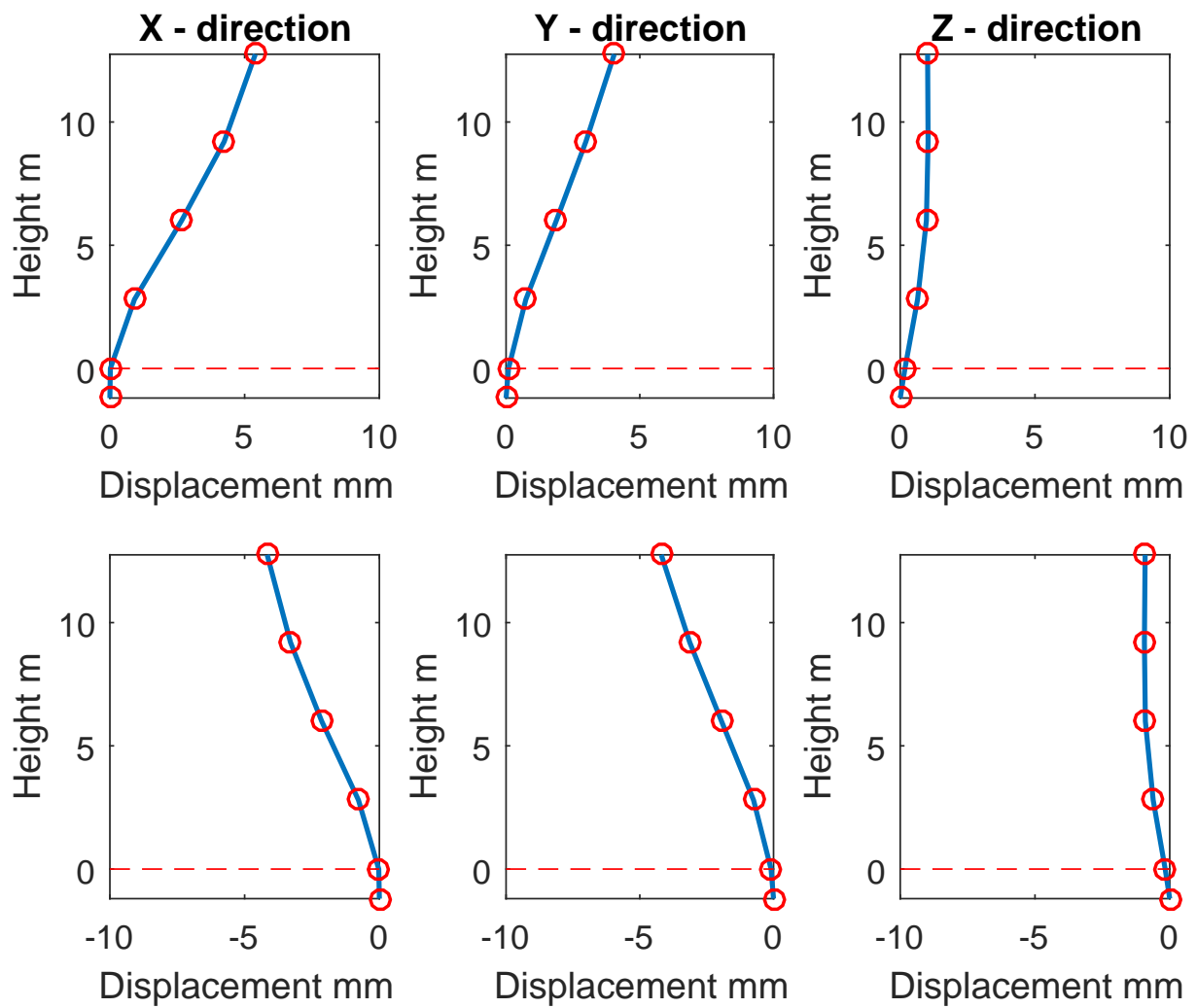


Figure B.23: Displacement for Borgarhraun earthquake action, the columns represent direction and lines represent max and min values with max values above.

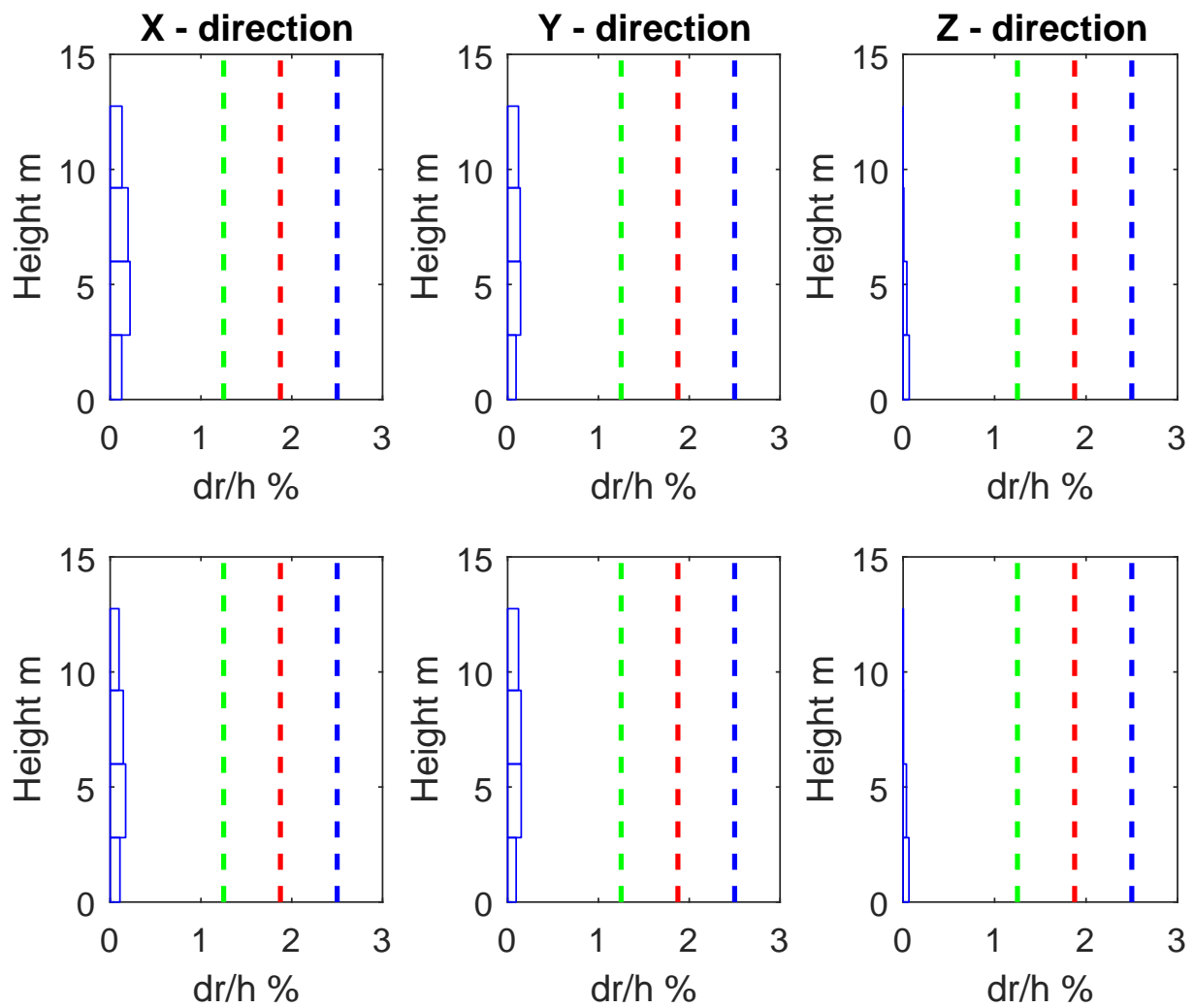


Figure B.24: Storey drifts for Borgarhraun earthquake action, the columns represent direction and lines represent max and min values with max values above.

Table B.8: Section cut earthquake induced forces

TABLE: Section Cut Forces - Design									
SectionCut	OutputCase	CaseType	StepType	P	V2	V3	T	M2	M3
Text	Text	Text	Text	N	N	N	N-m	N-m	N-m
A1D	Borgarhraun_TH	LinModHist	Max	297609	36971	5981	1862	-1559	43104
A1D	Borgarhraun_TH	LinModHist	Min	-370657	-46468	-7285	-1769	1671	-34515
A2D	Borgarhraun_TH	LinModHist	Max	219707	9842	2567	4510	-8028	46012
A2D	Borgarhraun_TH	LinModHist	Min	-290476	-11169	-3232	-2963	5788	-62250
A3D	Borgarhraun_TH	LinModHist	Max	271506	3655	15291	1868	-54322	2171
A3D	Borgarhraun_TH	LinModHist	Min	-342289	-3879	-18362	-1927	67972	-1861
A4D	Borgarhraun_TH	LinModHist	Max	282919	2221	13411	1969	-56285	3135
A4D	Borgarhraun_TH	LinModHist	Min	-233856	-2132	-10460	-1803	46765	-3845
B1D	Borgarhraun_TH	LinModHist	Max	224394	30927	14903	1257	-2445	38221
B1D	Borgarhraun_TH	LinModHist	Min	-251616	-33321	-15089	-1170	2302	-34146
B2D	Borgarhraun_TH	LinModHist	Max	155377	18883	12341	1268	-2611	23937
B2D	Borgarhraun_TH	LinModHist	Min	-150475	-21115	-8053	-1332	2276	-23535
B3D	Borgarhraun_TH	LinModHist	Max	399792	17039	18862	1453	-49899	2992
B3D	Borgarhraun_TH	LinModHist	Min	-324823	-12938	-19828	-1269	61102	-3128
B4D	Borgarhraun_TH	LinModHist	Max	422320	1795	17705	929	-48867	2936
B4D	Borgarhraun_TH	LinModHist	Min	-317414	-1419	-19580	-1261	65028	-3388
C1D	Borgarhraun_TH	LinModHist	Max	2009	3857	3615	3	0	29
C1D	Borgarhraun_TH	LinModHist	Min	-3563	-3005	-3172	-3	0	-34
C2D	Borgarhraun_TH	LinModHist	Max	2483	4039	3818	32	0	28
C2D	Borgarhraun_TH	LinModHist	Min	-3092	-3085	-2714	-22	0	-29
C3D	Borgarhraun_TH	LinModHist	Max	3253	4263	4600	3	-29	0
C3D	Borgarhraun_TH	LinModHist	Min	-4848	-3234	-4609	-3	41	0
C4D	Borgarhraun_TH	LinModHist	Max	1563	2466	3235	2	-28	0
C4D	Borgarhraun_TH	LinModHist	Min	-2670	-2233	-2282	-2	28	0
D1D	Borgarhraun_TH	LinModHist	Max	1724	2767	3727	2	0	42
D1D	Borgarhraun_TH	LinModHist	Min	-2886	-2509	-2624	-2	0	-29
D2D	Borgarhraun_TH	LinModHist	Max	2167	2801	3781	2	0	36
D2D	Borgarhraun_TH	LinModHist	Min	-3389	-2531	-2691	-2	0	-33
D3D	Borgarhraun_TH	LinModHist	Max	1704	2974	3305	28	0	23
D3D	Borgarhraun_TH	LinModHist	Min	-2471	-2619	-2739	-23	0	-24
D4D	Borgarhraun_TH	LinModHist	Max	2848	3617	4136	2	-28	0
D4D	Borgarhraun_TH	LinModHist	Min	-3774	-2777	-3599	-2	35	0
D5D	Borgarhraun_TH	LinModHist	Max	1854	2145	2667	2	-40	0
D5D	Borgarhraun_TH	LinModHist	Min	-2325	-2094	-1808	-2	38	0

B.9 Ljosafoss power station

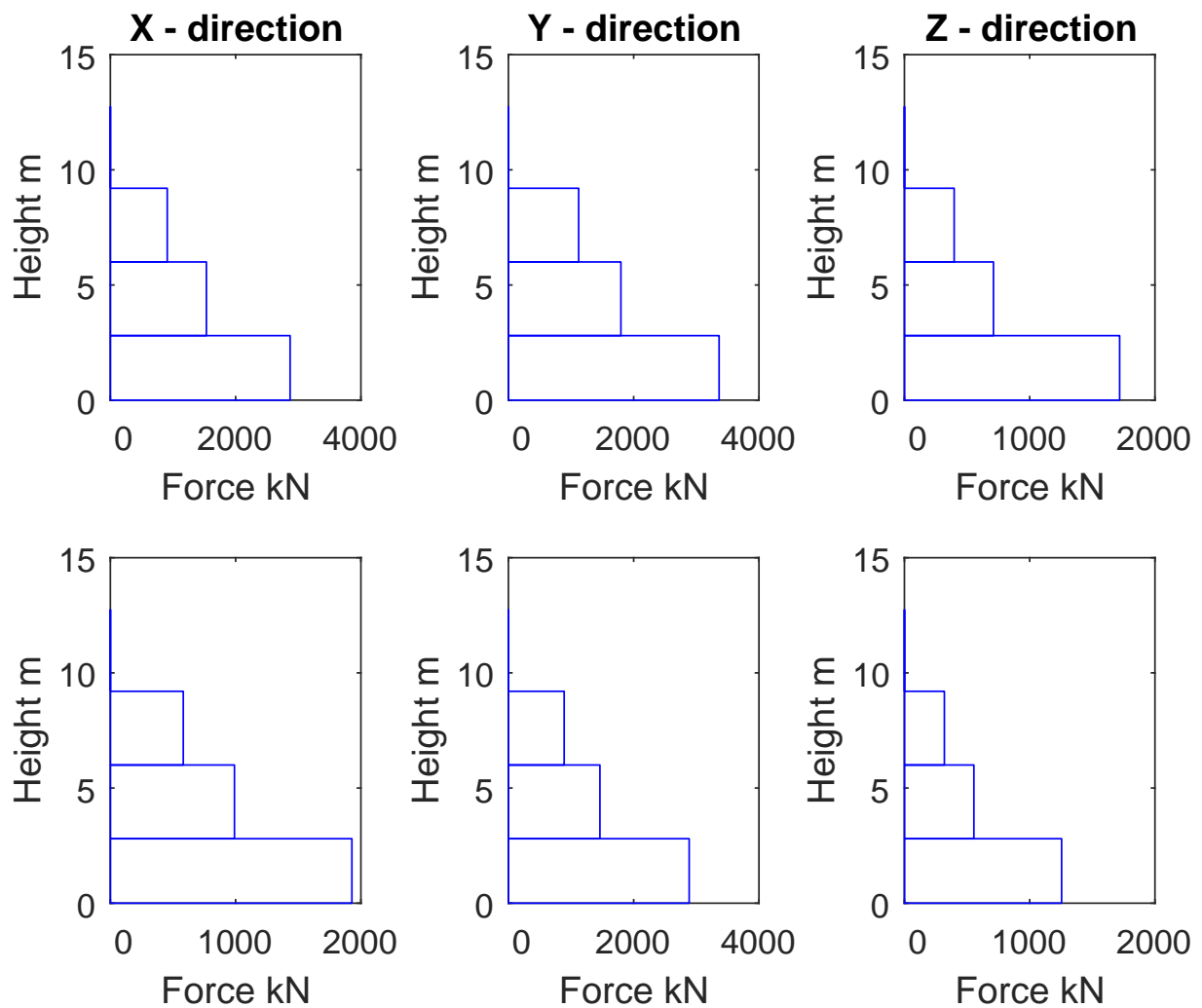


Figure B.25: Storey shear for Ljósafoss power station earthquake action, the columns represent direction and lines represent max and min values with max values above.

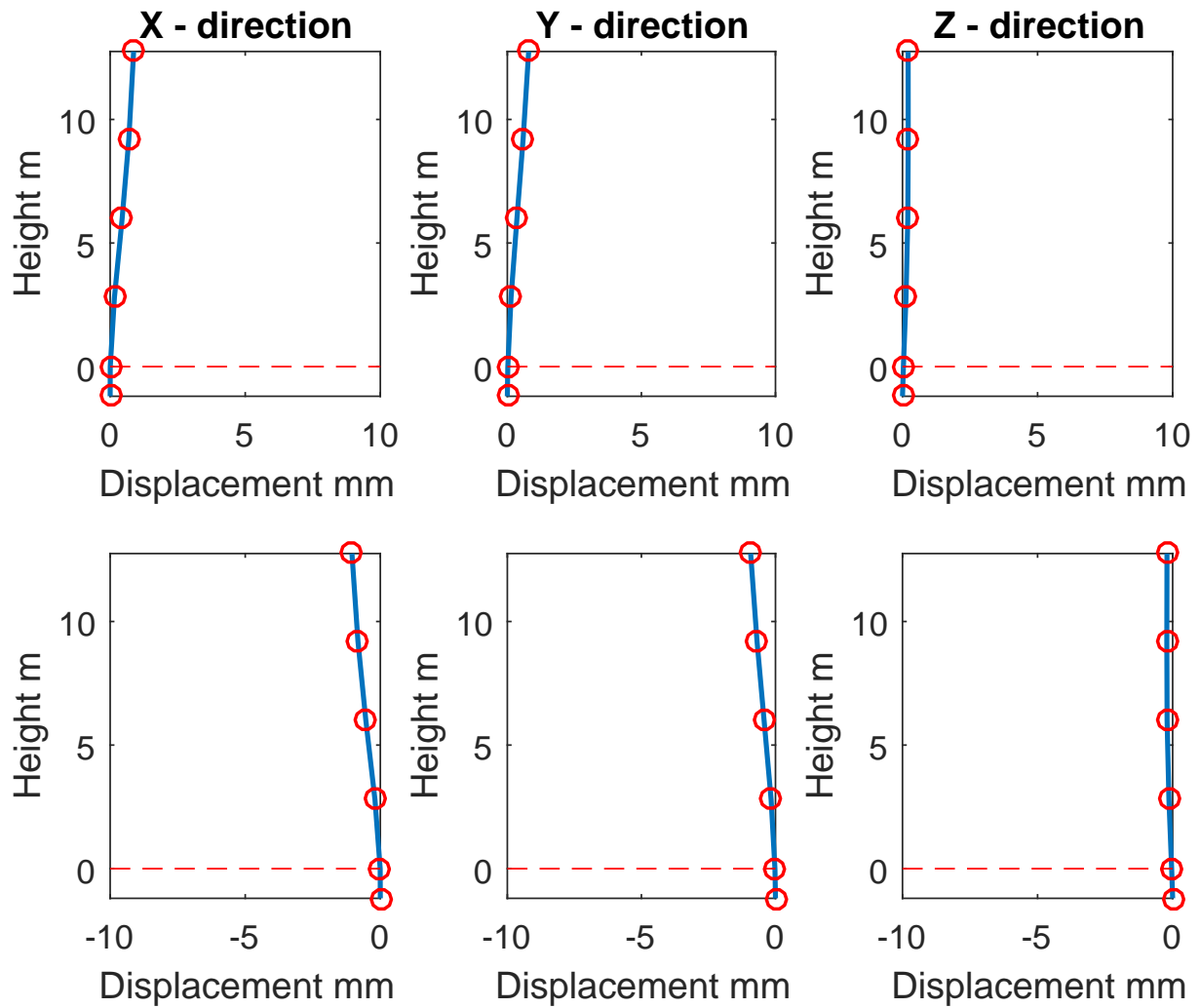


Figure B.26: Displacement for Ljósafoss power station earthquake action, the columns represent direction and lines represent max and min values with max values above.

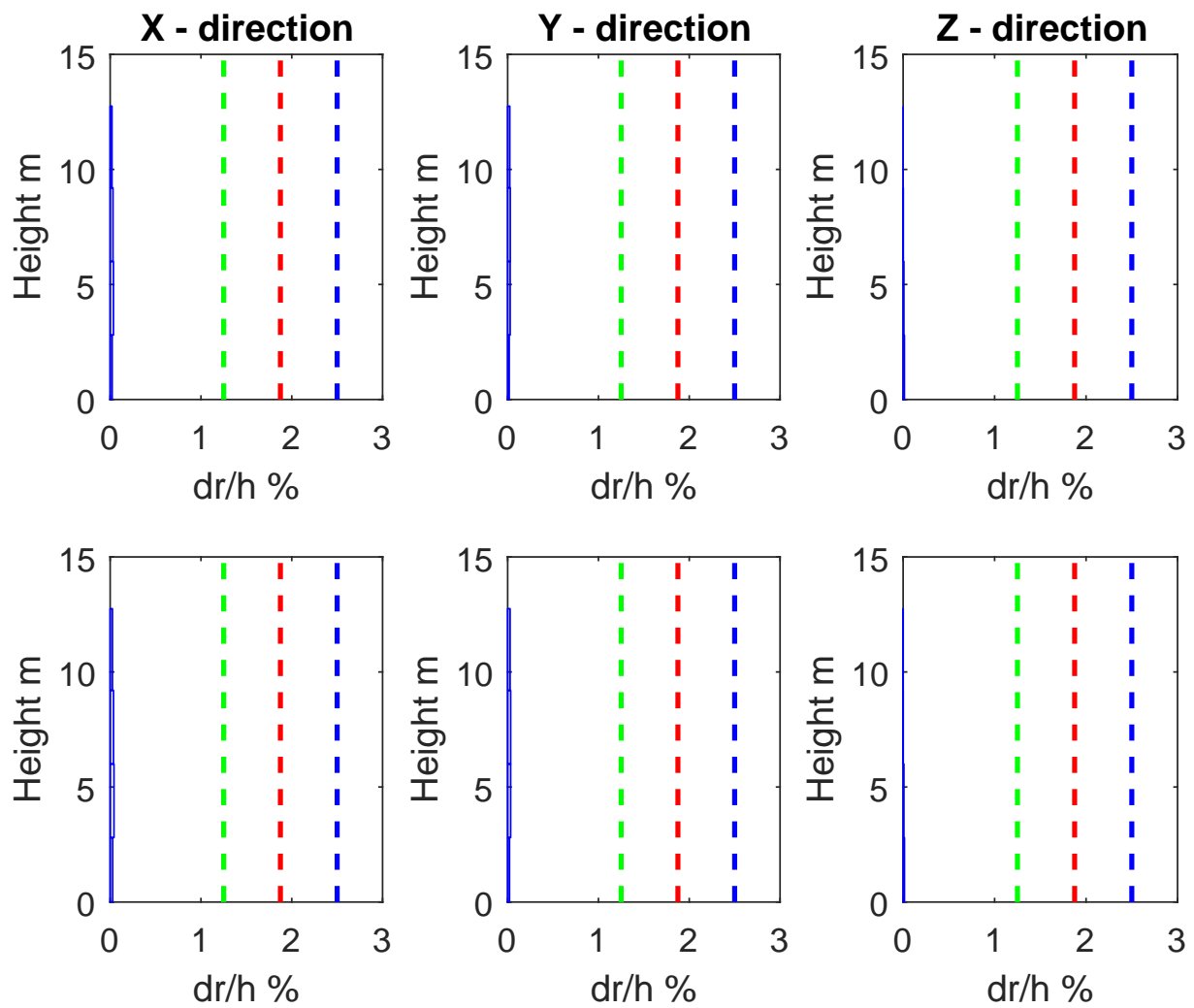


Figure B.27: Storey drifts for Ljósafoss power station earthquake action, the columns represent direction and lines represent max and min values with max values above.

Table B.9: Section cut earthquake induced forces

TABLE: Section Cut Forces - Design									
SectionCut	OutputCase	CaseType	StepType	P	V2	V3	T	M2	M3
Text	Text	Text	Text	N	N	N	N-m	N-m	N-m
A1D	Ljosafoss_TH	LinModHist	Max	48603	6373	1273	402	-256	9205
A1D	Ljosafoss_TH	LinModHist	Min	-79179	-9867	-1169	-351	348	-5647
A2D	Ljosafoss_TH	LinModHist	Max	66734	2207	747	894	-1534	14294
A2D	Ljosafoss_TH	LinModHist	Min	-50524	-2932	-1203	-1207	1496	-10694
A3D	Ljosafoss_TH	LinModHist	Max	59697	1278	3361	323	-11779	747
A3D	Ljosafoss_TH	LinModHist	Min	-65623	-704	-3373	-573	12988	-423
A4D	Ljosafoss_TH	LinModHist	Max	77622	824	3249	490	-15406	1516
A4D	Ljosafoss_TH	LinModHist	Min	-125451	-435	-4857	-941	24949	-984
B1D	Ljosafoss_TH	LinModHist	Max	44360	6113	2660	206	-568	10807
B1D	Ljosafoss_TH	LinModHist	Min	-71251	-10347	-3742	-233	416	-6735
B2D	Ljosafoss_TH	LinModHist	Max	77245	4685	2709	311	-654	12030
B2D	Ljosafoss_TH	LinModHist	Min	-39680	-9617	-3092	-638	1190	-6186
B3D	Ljosafoss_TH	LinModHist	Max	87152	2642	3380	252	-8107	664
B3D	Ljosafoss_TH	LinModHist	Min	-52931	-3494	-4289	-316	13293	-642
B4D	Ljosafoss_TH	LinModHist	Max	71412	339	4836	281	-14974	832
B4D	Ljosafoss_TH	LinModHist	Min	-97279	-434	-3971	-209	11015	-683
C1D	Ljosafoss_TH	LinModHist	Max	405	630	676	1	0	7
C1D	Ljosafoss_TH	LinModHist	Min	-439	-776	-700	-1	0	-8
C2D	Ljosafoss_TH	LinModHist	Max	414	630	849	7	0	7
C2D	Ljosafoss_TH	LinModHist	Min	-543	-792	-1128	-9	0	-7
C3D	Ljosafoss_TH	LinModHist	Max	512	654	925	1	-7	0
C3D	Ljosafoss_TH	LinModHist	Min	-511	-1149	-957	-1	6	0
C4D	Ljosafoss_TH	LinModHist	Max	334	432	779	1	-10	0
C4D	Ljosafoss_TH	LinModHist	Min	-282	-770	-1049	-1	9	0
D1D	Ljosafoss_TH	LinModHist	Max	304	512	539	1	0	5
D1D	Ljosafoss_TH	LinModHist	Min	-282	-643	-551	0	0	-6
D2D	Ljosafoss_TH	LinModHist	Max	321	506	619	0	0	5
D2D	Ljosafoss_TH	LinModHist	Min	-303	-650	-589	0	0	-6
D3D	Ljosafoss_TH	LinModHist	Max	336	512	722	6	0	6
D3D	Ljosafoss_TH	LinModHist	Min	-329	-658	-673	-6	0	-6
D4D	Ljosafoss_TH	LinModHist	Max	465	577	659	1	-7	0
D4D	Ljosafoss_TH	LinModHist	Min	-491	-955	-738	-1	8	0
D5D	Ljosafoss_TH	LinModHist	Max	339	382	547	0	-11	0
D5D	Ljosafoss_TH	LinModHist	Min	-357	-654	-647	0	10	0

C. Earthquake induced forces

In this appendix the earthquake induced forces for each time step where plotted against time and compared to the response spectra earthquake action RS 0° for the critical time histories. The critical time histories are The retirement house in Hveragerði and Sólheimar. Details for those time histories can be found in Appendix A.

C.1 Retirement house

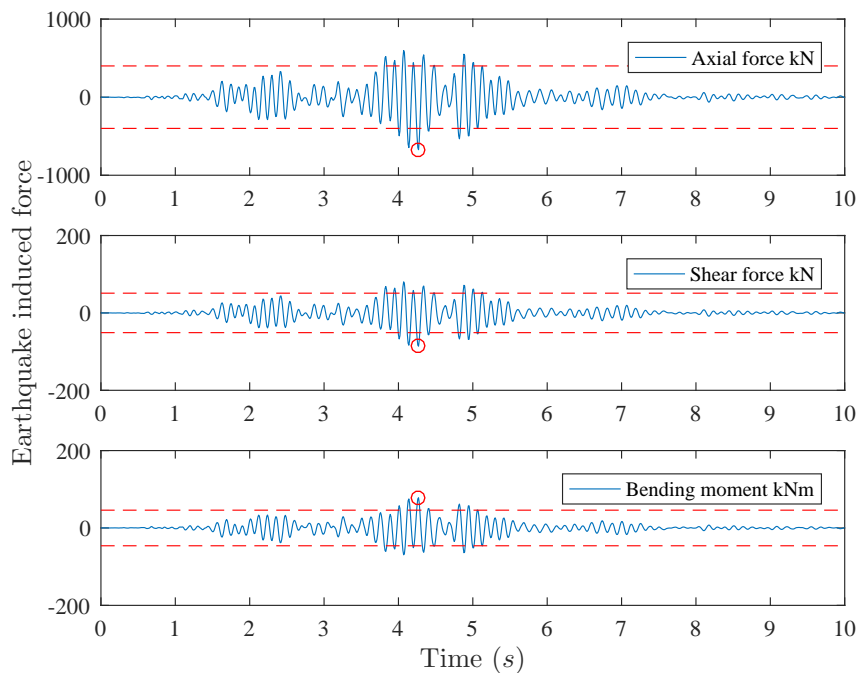


Figure C.1: The earthquake induced forces against time for column A1 and Retirement home time history, the absolute max value is represented as red dot, the maximum force according to the design response spectra is represented as red dashed line.

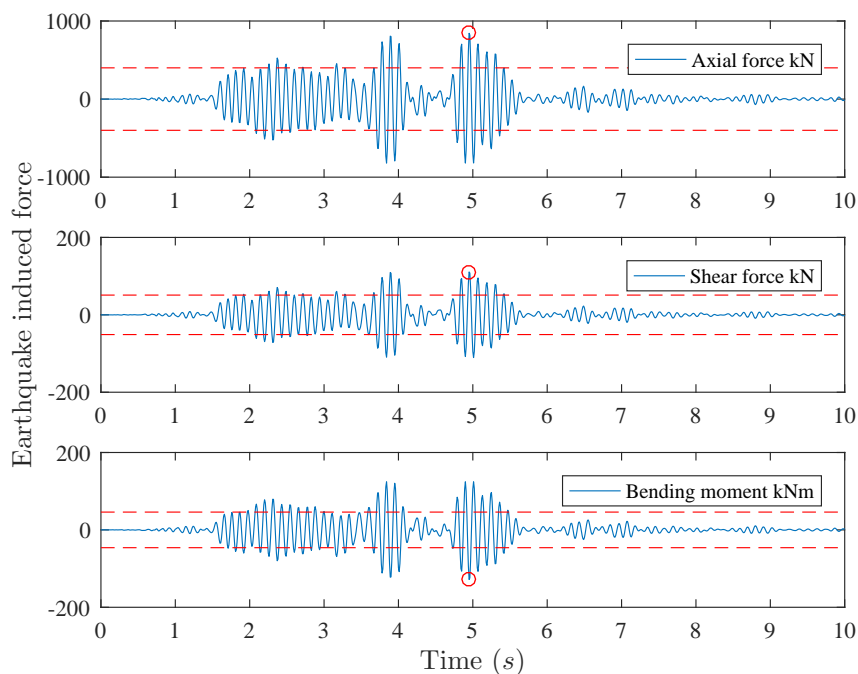


Figure C.2: The earthquake induced forces against time for column B1, the absolute max value is represented as red dot, the maximum force according to the design response spectra is represented as red dashed line.

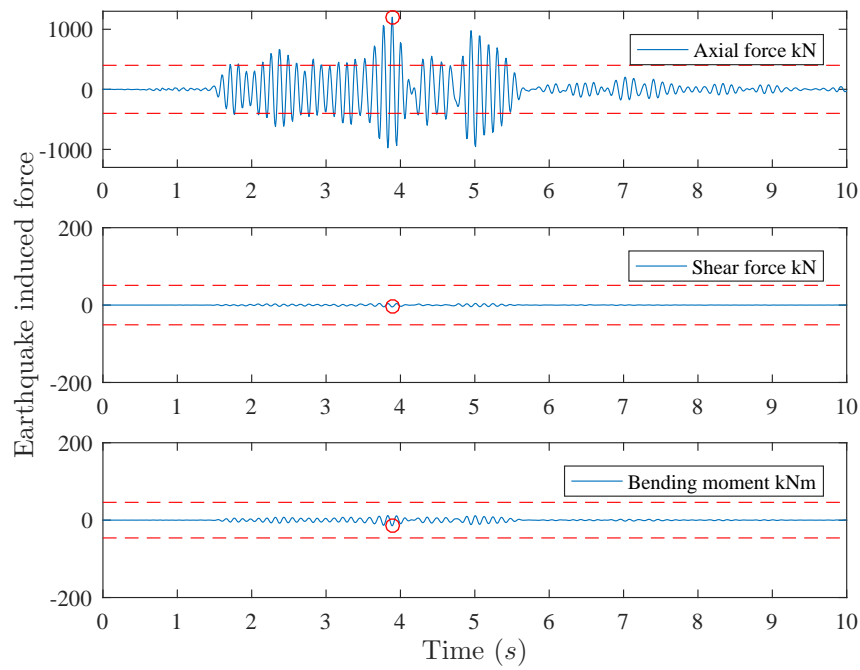


Figure C.3: The earthquake induced forces against time for column A4, the absolute max value is represented as red dot, the maximum force according to the design response spectra is represented as red dashed line.

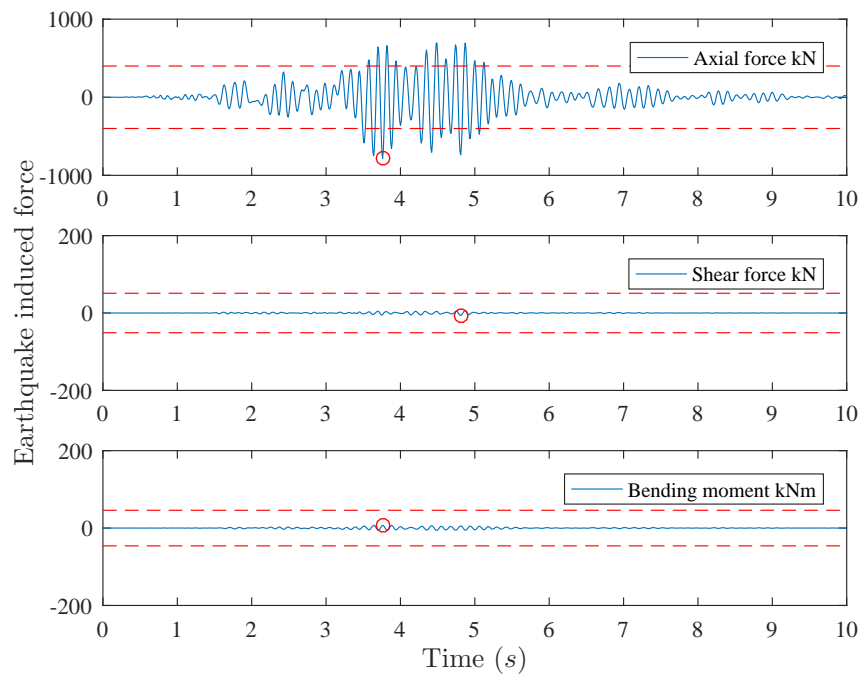


Figure C.4: The earthquake induced forces against time for column B4, the absolute max value is represented as red dot, the maximum force according to the design response spectra is represented as red dashed line.

C.2 Sólheimar

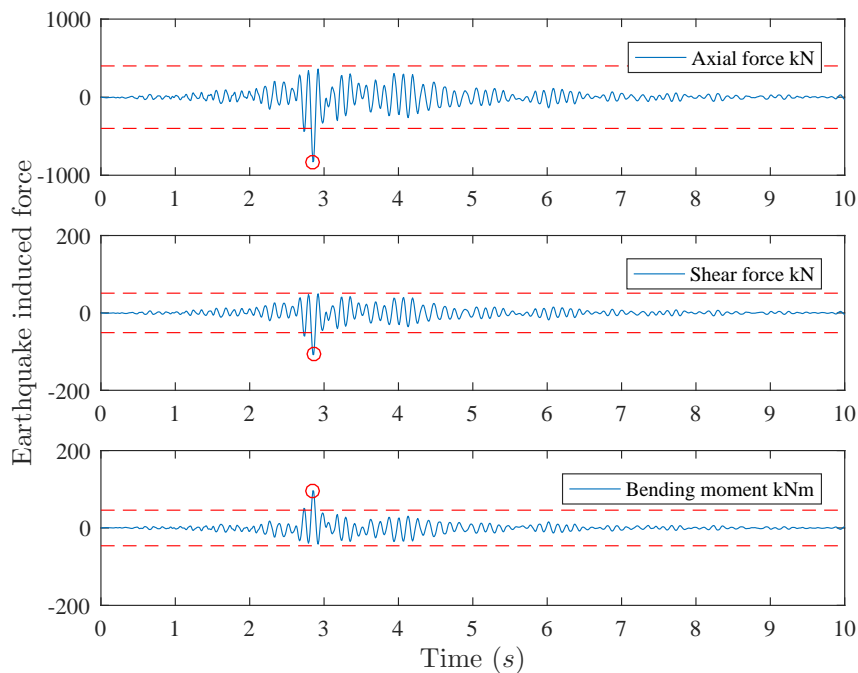


Figure C.5: The earthquake induced forces against time for column A1 and Retirement home time history, the absolute max value is represented as red dot, the maximum force according to the design response spectra is represented as red dashed line.

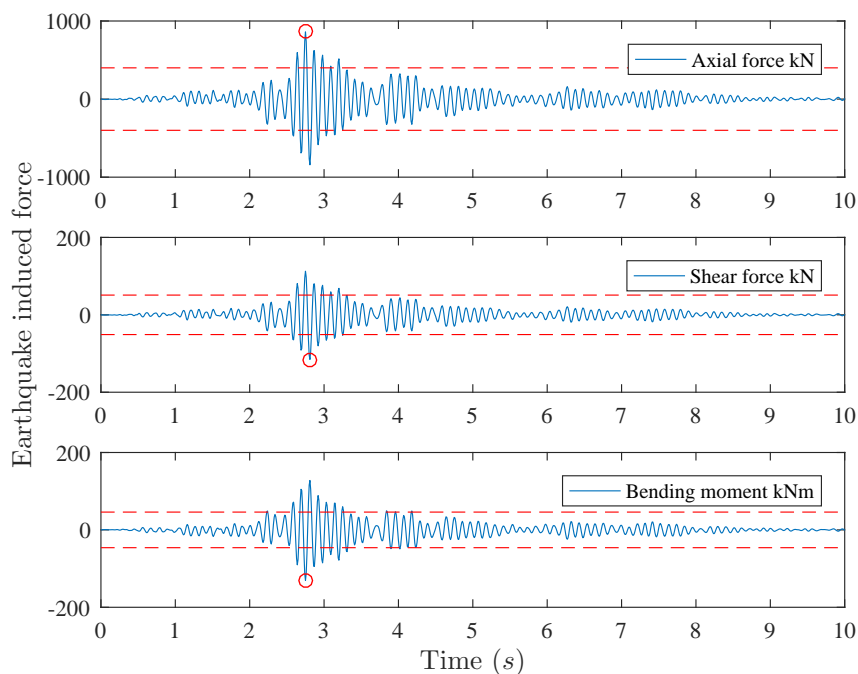


Figure C.6: The earthquake induced forces against time for column B1, the absolute max value is represented as red dot, the maximum force according to the design response spectra is represented as red dashed line.

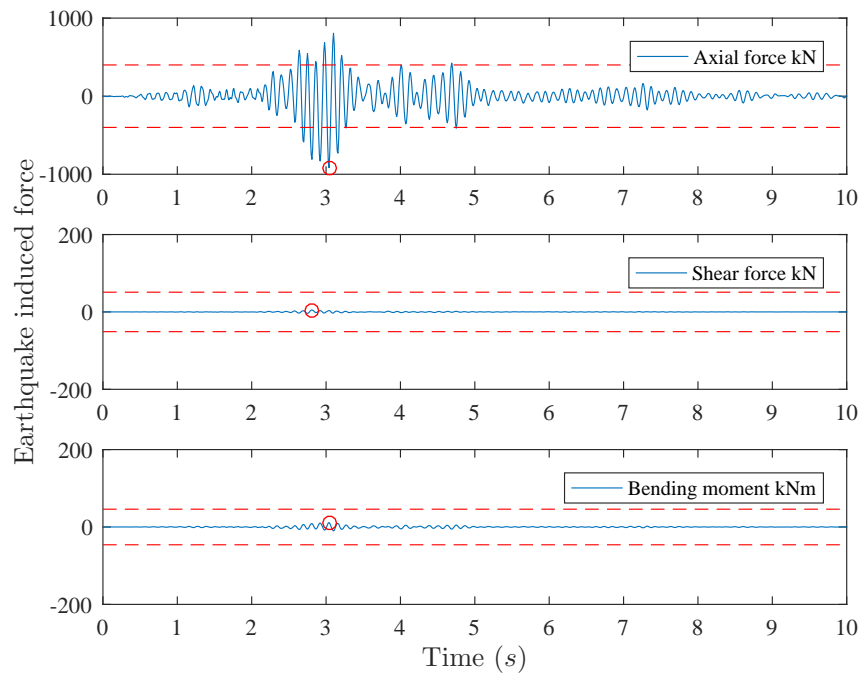


Figure C.7: The earthquake induced forces against time for column A4, the absolute max value is represented as red dot, the maximum force according to the design response spectra is represented as red dashed line.

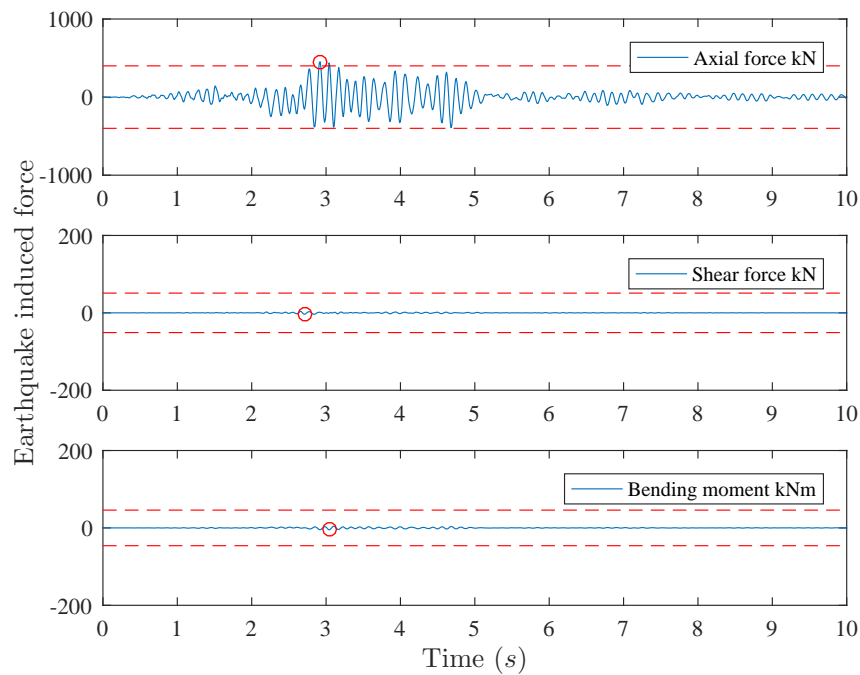


Figure C.8: The earthquake induced forces against time for column B4, the absolute max value is represented as red dot, the maximum force according to the design response spectra is represented as red dashed line.

D. Design of building components

In this appendix the design of the building components are carried out according to earthquake action RS 0. This is the design response spectra according to EN 1998-1 with behaviour factor of 1.5. The calculations are based on sections on following figures according to the section cut forces obtained in SAP2000. Section A is subjected to 4076 kNm bending moment and 1357 kN axial force. Section B is subjected to 284 kNm bending moment and 433 kN axial force. As can be seen in the the following excel sheets the columns barely resist the load. Though the blue dot is slightly outside the line it is ok because in the reality the line is curved. The cross sections does not meet the AS min criteria.

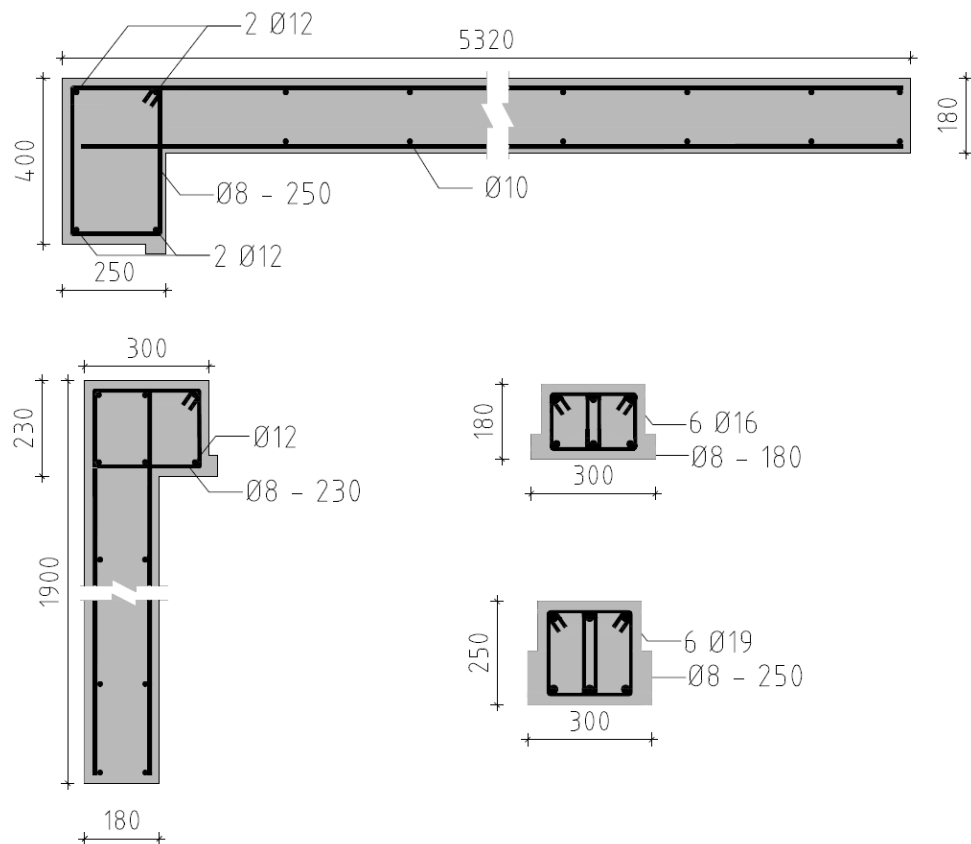


Figure D.1: The reinforcement of columns

M-N Interaction diagram

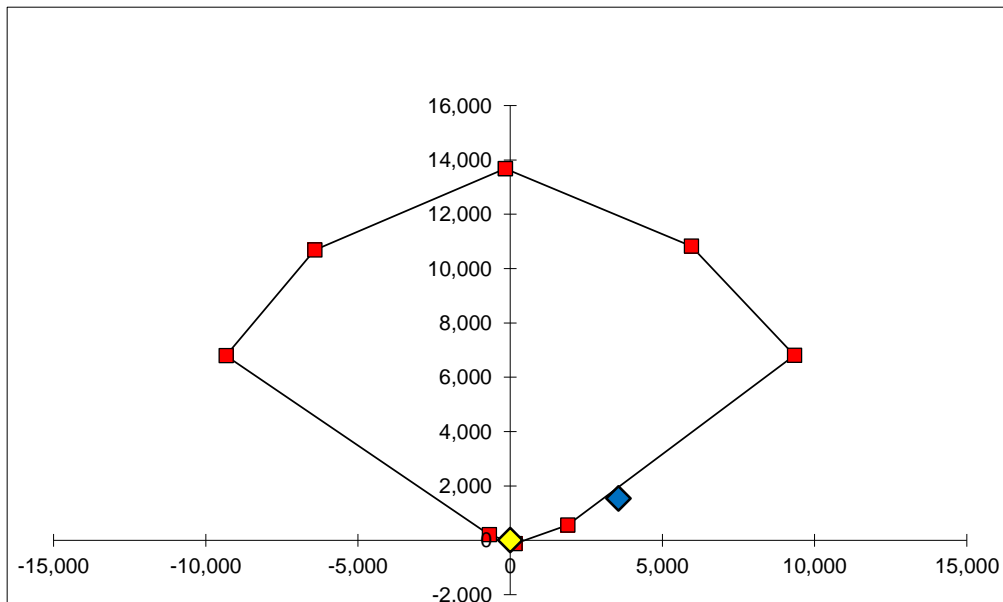
Column A

h	5320 mm	fck	25 N/mm ²	alfa	0.85
b	180 mm	fyk	230 N/mm ²	yc	1.5
d	5290 mm	As'	452 mm ²	ys	1.15
d'	130 mm	As	157 mm ²	Eult	3.5 ‰
				Es	2 ‰
				E _{steel}	2.00E+05 N/mm ²

Max As _{total} =	38304 mm ²	OK, AS < AS Max
Min As _{total} =	1915.2 mm ²	769 mm ² Not ok, Not enough reinforcement

nr.	X(0)	F _C	F _{s'}	F _s	Z _c	Z _e	Z _n	Mult	Nult
	mm	N	N	N	mm	mm	mm	kNm	kN
1		13,557,373	31,400	90,400	0	2530	2630	-158.31	13,679.17
2	5290	10,791,600	31,400	0	544.0	2530	2630	5,950.07	10,823.00
3	3366	6,867,382	31,400	-90,400	1313.5	2530	2630	9,337.19	6,808.38
4	303	618,800	31,400	-90,400	2538.7	2530	2630	1,888.12	559.80
5		0	-31,400	-90,400		2530	2630	158.31	-121.80
4'	-70	142,800	-31,400	90,400	-2632.0	2530	2630	-693.04	201.80
3'	-3303	6,737,564	-31,400	90,400	-1338.9	2530	2630	-9,338.18	6,796.56
2'	-5190	10,587,600	0	90,400	-584.0	2530	2630	-6,420.91	10,678.00
1		13,557,373	31,400	90,400	0	2530	2630	-158.31	13,679.17

	Blue value		Yellow value
Med	3550 KNm	Med	0 KNm
Ned	1538 KN	Ned	0 KN



M-N Interaction diagram

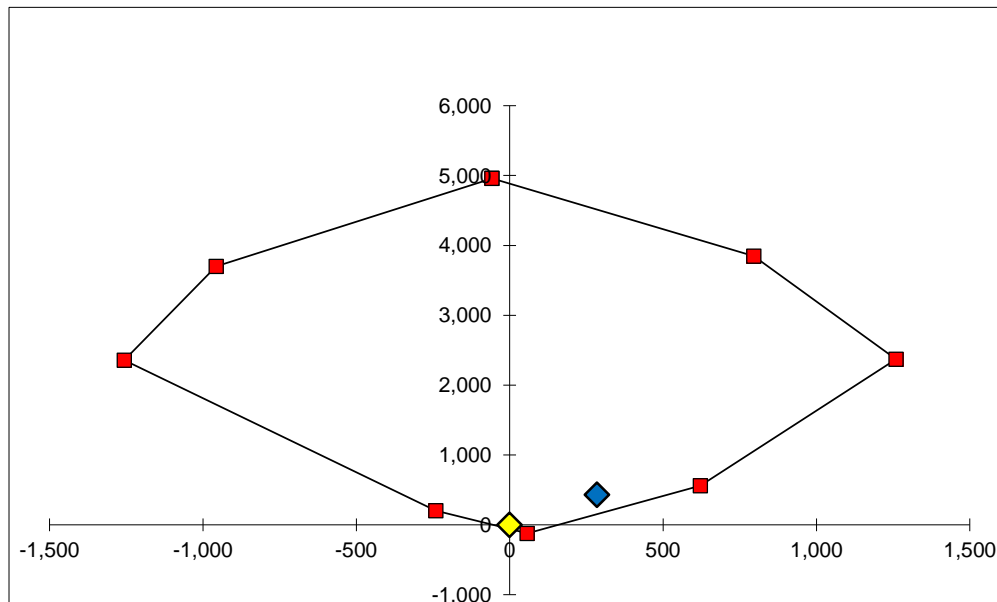
Column B

h	1900 mm	fck	25 N/mm ²	alfa	0.85
b	180 mm	fyk	230 N/mm ²	yc	1.5
d	1870 mm	As'	452 mm ²	ys	1.15
d'	130 mm	As	157 mm ²	Eult	3.5 ‰
				Es	2 ‰
				E _{steel}	2.00E+05 N/mm ²

Max As_{total}= 13680 mm² OK, AS < AS Max
 Min As_{total}= 684 mm² 217 mm² Not ok, Not enough reinforcement

nr.	X(0)	F _C	Fs'	Fs	Zc	Ze	Zn	Mult	Nult
	mm	N	N	N	mm	mm	mm	kNm	kN
1		4,836,373	31,400	90,400	0	820	920	-57.42	4,958.17
2	1870.0	3,814,800	31,400	0	202.0	820	920	796.34	3,846.20
3	1190.0	2,427,600	31,400	-90,400	474.0	820	920	1,259.60	2,368.60
4	303.3	618,800	31,400	-90,400	828.7	820	920	621.69	559.80
5		0	-31,400	-90,400		820	920	57.42	-121.80
4'	-70.0	142,800	-31,400	90,400	-922.0	820	920	-240.58	201.80
3'	-1126.4	2,297,782	-31,400	90,400	-499.5	820	920	-1,256.55	2,356.78
2'	-1770.0	3,610,800	0	90,400	-242.0	820	920	-956.98	3,701.20
1		4,836,373	31,400	90,400	0	820	920	-57.42	4,958.17

	Blue value		Yellow value
Med	284 KNm	Med	0 KNm
Ned	433 KN	Ned	0 KN



M-N Interaction diagram

Beam 1

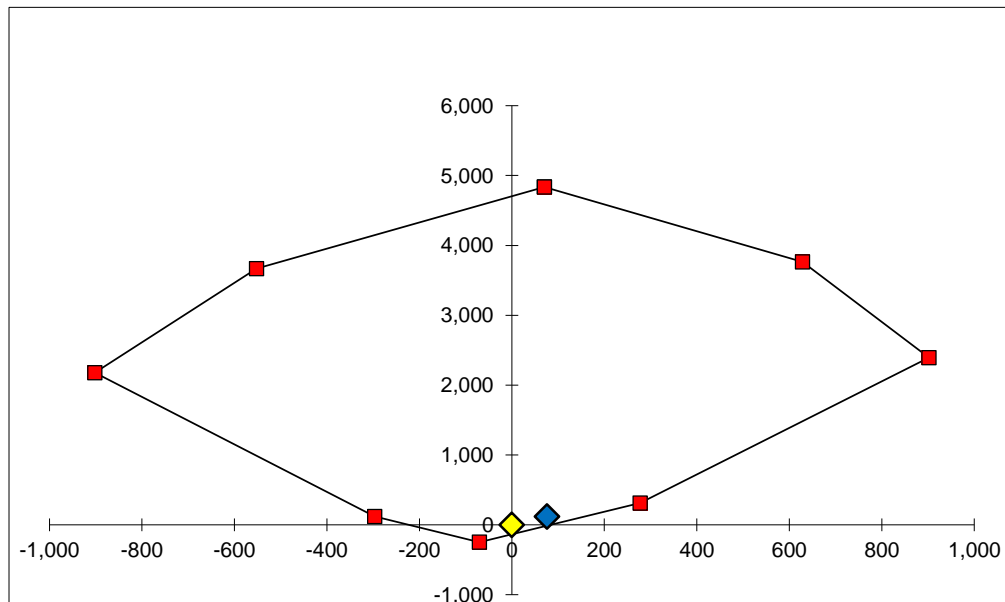
h	1300 mm	fck	25 N/mm ²	alfa	0.85
b	250 mm	fyk	230 N/mm ²	yc	1.5
d	1265 mm	As'	339 mm ²	ys	1.15
d'	30 mm	As	905 mm ²	Eult	3.5 ‰
				Es	2 ‰
				E _{steel}	2.00E+05 N/mm ²

Max As_{total}= 13000 mm² OK, AS < AS Max

Min As_{total}= 650 mm² 59 mm² OK, AS > AS Min

nr.	X(0)	F _C	F _{s'}	F _s	Z _c	Z _e	Z _n	Mult	Nult
	mm	N	N	N	mm	mm	mm	kNm	kN
1		4,586,543	181,000	67,800	0	620	615	70.52	4,835.34
2	1265	3,584,167	181,000	0	144.0	620	615	628.34	3,765.17
3	805	2,280,833	181,000	-67,800	328.0	620	615	902.03	2,394.03
4	70	198,333	181,000	-67,800	622.0	620	615	277.28	311.53
5		0	-181,000	-67,800		620	615	-70.52	-248.80
4'	-82	231,389	-181,000	67,800	-617.3	620	615	-296.76	118.19
3'	-808	2,289,848	-181,000	67,800	-326.7	620	615	-902.07	2,176.65
2'	-1270	3,598,333	0	67,800	-142.0	620	615	-552.66	3,666.13
1		4,586,543	181,000	67,800	0	620	615	70.52	4,835.34

	Blue value		Yellow value
Med	76 KNm	Med	0 KNm
Ned	117 KN	Ned	0 KN



M-N Interaction diagram

Beam 2

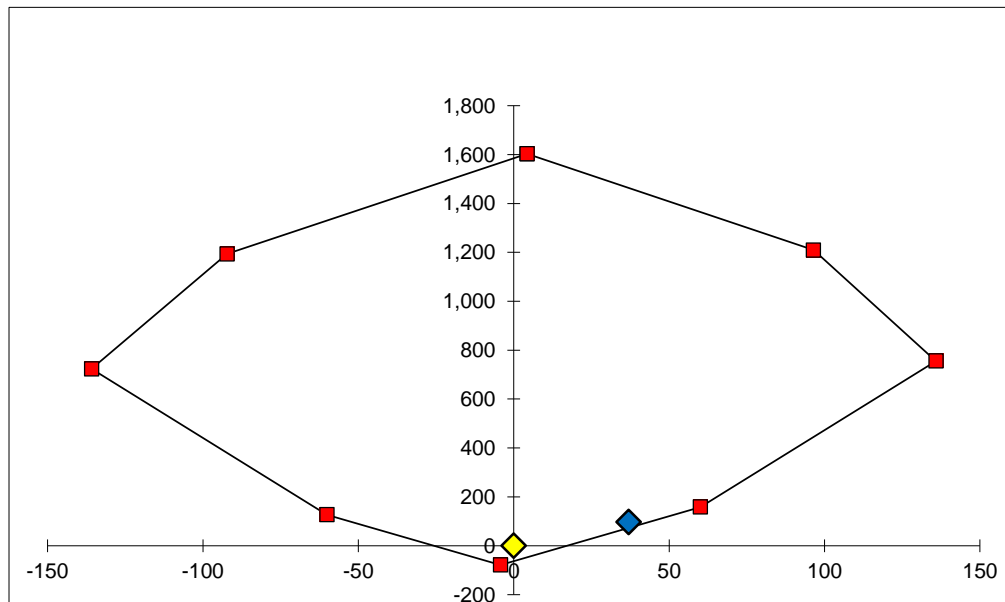
h	600 mm	fck	25 N/mm ²	alfa	0.85
b	180 mm	fyk	230 N/mm ²	yc	1.5
d	570 mm	As'	157 mm ²	ys	1.15
d'	30 mm	As	236 mm ²	Eult	3.5 ‰
				Es	2 ‰
				E _{steel}	2.00E+05 N/mm ²

Max As_{total}= 4320 mm² OK, AS < AS Max

Min As_{total}= 216 mm² 49 mm² OK, AS > AS Min

nr.	X(0)	F _C	Fs'	Fs	Zc	Ze	Zn	Mult	Nult
	mm	N	N	N	mm	mm	mm	kNm	kN
1		1,524,433	47,200	31,400	0	270	270	4.27	1,603.03
2	570	1,162,800	47,200	0	72.0	270	270	96.47	1,210.00
3	363	739,964	47,200	-31,400	154.9	270	270	135.85	755.76
4	70	142,800	47,200	-31,400	272.0	270	270	60.06	158.60
5		0	-47,200	-31,400		270	270	-4.27	-78.60
4'	-70	142,800	-47,200	31,400	-272.0	270	270	-60.06	127.00
3'	-363	739,964	-47,200	31,400	-154.9	270	270	-135.85	724.16
2'	-570	1,162,800	0	31,400	-72.0	270	270	-92.20	1,194.20
1		1,524,433	47,200	31,400	0	270	270	4.27	1,603.03

	Blue value		Yellow value
Med	37 KNm	Med	0 KNm
Ned	98 KN	Ned	0 KN



E. Shear calculations

In this appendix calculations of shear capacity are checked according to EN-1992-1 and Reinforced concrete design to Eurocode 2.

Shear strength of building component - Column A

$$\begin{aligned}
 b &:= 180 \quad (mm) & h &:= 5320 \quad (mm) & c &:= 20 \quad (mm) \\
 k_{tie} &:= 10 \quad (mm) & A_s &:= \pi \cdot \left(\frac{k_{tie}}{2} \right)^2 = 79 & V_{ed}' &:= 1594 \cdot 10^3 \\
 q &:= 1.5 & & & V_{ed} &:= V_{ed}' \cdot \left(\frac{q+1}{2} \right) = 1.993 \cdot 10^6 \\
 d &:= h - c - \frac{k_{tie}}{2} = 5.295 \cdot 10^3 \quad (mm)
 \end{aligned}$$

Material properties of concrete and steel

$$\begin{aligned}
 f_{ck} &:= 25 \quad (MPa) & \gamma_c &:= 1.5 & f_{yk} &:= 230 \quad (MPa) & \gamma_s &:= 1.15 \\
 & & & & & & \alpha_{cc} &:= 0.85
 \end{aligned}$$

$$Crd.c := \frac{0.18}{\gamma_c} = 0.12 \quad k_1 := 0.15$$

$$k := 1 + \sqrt{\frac{200}{d}} = 1.194 \quad k \leq 2.0 = 1 \quad \sigma_{cp} := 0$$

$$V_{min} := 0.035 \cdot k^{\frac{3}{2}} \cdot f_{ck}^{\frac{1}{2}} = 0.228$$

$$\rho := \frac{A_s}{b \cdot d} = 8.24 \cdot 10^{-5} \quad \rho \leq 0.02 = 1$$

The shear capacity of concrete is the higher value of those two

$$V_{rd.c_{bb}} := \max \left(\left[\left(Crd.c \cdot k \cdot (100 \cdot \rho \cdot f_{ck})^{\frac{1}{3}} + k_1 \cdot \sigma_{cp} \right) \cdot b \cdot d \right], \left[(V_{min} + k_1 \cdot \sigma_{cp}) \cdot b \cdot d \right] \right) = 218 \cdot 10^3 \quad (N)$$

The shear capacity ratio is

$$\frac{V_{ed}}{V_{rd.c_{bb}}} = 9.15 \quad \text{Shear reinforcement required}$$

The minimum allowable shear reinforcement - Column A

$s := 300$ space between stirrups

$$A_{sw.min} := \frac{0.08 \cdot s \cdot b \cdot \sqrt{f_{ck}}}{f_{yk}} = 93.913 \quad (mm^2)$$

$$z := 0.9 \cdot d = 4.766 \cdot 10^3 \quad v_1 := 0.6 \cdot \left(1 - \frac{f_{ck}}{250}\right) = 0.54 \quad f_{cd} := 0.6 \cdot \frac{f_{ck}}{\gamma_c} = 10$$

$$V_{Rd.max} := b \cdot z \cdot v_1 \cdot f_{cd} \cdot \frac{1}{1 + 1} = 2.3 \cdot 10^6 \quad (N) \quad V_{Rd.max} > V_{ed} = 1 \quad OK$$

$$\theta := 0.5 \cdot \arcsin\left(\frac{V_{rd.c_{bb}}}{V_{Rd.max}}\right) = 2.697 \text{ deg} \quad \text{This degree has to be between } 22 - 45^\circ$$

$$\theta_{val} := 22 \text{ deg} \quad \text{The minimum value is used}$$

Shear resistant of stirrup

$$A_{sw} := \pi \cdot \left(\frac{k_{tie}}{2}\right)^2 \cdot 2 = 157.1$$

$$V_{rd.s} := \frac{A_{sw}}{s} \cdot z \cdot \frac{f_{yk}}{\gamma_s} \cdot \cot(\theta_{val}) = 1.235 \cdot 10^6 \quad (N)$$

$$V_{rd.s} \geq V_{ed} = 0 \quad \frac{V_{ed}}{V_{rd.s}} = 1.613$$

Shear capacity is not OK

Shear strength of building component - Column B

$$\begin{aligned}
 b &:= 180 \quad (mm) & h &:= 1900 \quad (mm) & c &:= 20 (mm) \\
 k_{tie} &:= 10 \quad (mm) & A_s &:= \pi \cdot \left(\frac{k_{tie}}{2} \right)^2 = 79 & V_{ed}' &:= 387 \cdot 10^3 \\
 q &:= 1.5 & & & V_{ed} &:= V_{ed}' \cdot \left(\frac{q+1}{2} \right) = 484 \cdot 10^3 \\
 d &:= h - c - \frac{k_{tie}}{2} = 1.875 \cdot 10^3 \quad (mm)
 \end{aligned}$$

Material properties of concrete and steel

$$\begin{aligned}
 f_{ck} &:= 25 \quad (MPa) & \gamma_c &:= 1.5 & f_{yk} &:= 230 \quad (MPa) & \gamma_s &:= 1.15 \\
 & & & & & & \alpha_{cc} &:= 0.85
 \end{aligned}$$

$$Crd.c := \frac{0.18}{\gamma_c} = 0.12 \quad k_1 := 0.15$$

$$k := 1 + \sqrt{\frac{200}{d}} = 1.327 \quad k \leq 2.0 = 1 \quad \sigma_{cp} := 0$$

$$V_{min} := 0.035 \cdot k^{\frac{3}{2}} \cdot f_{ck}^{\frac{1}{2}} = 0.267$$

$$\rho := \frac{A_s}{b \cdot d} = 2.327 \cdot 10^{-4} \quad \rho \leq 0.02 = 1$$

The shear capacity of concrete is the higher value of those two

$$V_{rd.c_{bb}} := \max \left(\left[\left(Crd.c \cdot k \cdot (100 \cdot \rho \cdot f_{ck})^{\frac{1}{3}} + k_1 \cdot \sigma_{cp} \right) \cdot b \cdot d \right], \left[(V_{min} + k_1 \cdot \sigma_{cp}) \cdot b \cdot d \right] \right) = 90.2 \cdot 10^3 \quad (N)$$

The shear capacity ratio is not ok

$$\frac{V_{ed}}{V_{rd.c_{bb}}} = 5.36 \quad \text{Shear reinforcement required}$$

The minimum allowable shear reinforcement - Column B

$s := 300$ space between stirrups

$$A_{sw.min} := \frac{0.08 \cdot s \cdot b \cdot \sqrt{f_{ck}}}{f_{yk}} = 93.913 \quad (mm^2)$$

$$z := 0.9 \cdot d = 1.688 \cdot 10^3 \quad v_1 := 0.6 \cdot \left(1 - \frac{f_{ck}}{250}\right) = 0.54 \quad f_{cd} := 0.6 \cdot \frac{f_{ck}}{\gamma_c} = 10$$

$$V_{Rd.max} := b \cdot z \cdot v_1 \cdot f_{cd} \cdot \frac{1}{1 + 1} = 820.1 \cdot 10^3 \quad (N) \quad V_{Rd.max} > V_{ed} = 1 \quad OK$$

$$\theta := 0.5 \cdot \arcsin\left(\frac{V_{rd.c_{bb}}}{V_{Rd.max}}\right) = 3.159 \text{ deg} \quad \text{This degree has to be between } 22 - 45^\circ$$

$$\theta_{val} := 22 \text{ deg} \quad \text{The minimum value is used}$$

Shear resistant of stirrup

$$A_{sw} := \pi \cdot \left(\frac{k_{tie}}{2}\right)^2 \cdot 2 = 157.1$$

$$V_{rd.s} := \frac{A_{sw}}{s} \cdot z \cdot \frac{f_{yk}}{\gamma_s} \cdot \cot(\theta_{val}) = 437 \cdot 10^3 \quad (N)$$

$$V_{rd.s} \geq V_{ed} = 0 \quad \frac{V_{ed}}{V_{rd.s}} = 1.106$$

Shear capacity is not OK

Shear strength of building component - Beam 1

$$\begin{aligned}
 b &:= 250 \quad (mm) & h &:= 1300 \quad (mm) & c &:= 20 \quad (mm) \\
 k_{tie} &:= 10 \quad (mm) & A_s &:= \pi \cdot \left(\frac{k_{tie}}{2} \right)^2 = 79 & V_{ed}' &:= 67 \cdot 10^3 \\
 q &:= 1.5 & & & V_{ed} &:= V_{ed}' \cdot \left(\frac{q+1}{2} \right) = 84 \cdot 10^3 \\
 d &:= h - c - \frac{k_{tie}}{2} = 1.275 \cdot 10^3 \quad (mm)
 \end{aligned}$$

Material properties of concrete and steel

$$\begin{aligned}
 f_{ck} &:= 25 \quad (MPa) & \gamma_c &:= 1.5 & f_{yk} &:= 230 \quad (MPa) & \gamma_s &:= 1.15 \\
 & & & & & & \alpha_{cc} &:= 0.85
 \end{aligned}$$

$$C_{rd,c} := \frac{0.18}{\gamma_c} = 0.12 \quad k_1 := 0.15$$

$$k := 1 + \sqrt{\frac{200}{d}} = 1.396 \quad k \leq 2.0 = 1 \quad \sigma_{cp} := 0$$

$$V_{min} := 0.035 \cdot k^{\frac{3}{2}} \cdot f_{ck}^{\frac{1}{2}} = 0.289$$

$$\rho := \frac{A_s}{b \cdot d} = 2.464 \cdot 10^{-4} \quad \rho \leq 0.02 = 1$$

The shear capacity of concrete is the higher value of those two

$$V_{rd,c_{bb}} := \max \left(\left[\left(C_{rd,c} \cdot k \cdot \left(100 \cdot \rho \cdot f_{ck} \right)^{\frac{1}{3}} + k_1 \cdot \sigma_{cp} \right) \cdot b \cdot d \right], \left[V_{min} + k_1 \cdot \sigma_{cp} \right) \cdot b \cdot d \right] \right) = 92 \cdot 10^3 \quad (N)$$

The shear capacity ratio is OK

$$\frac{V_{ed}}{V_{rd,c_{bb}}} = 0.91 \quad \text{Shear reinforcement not required}$$

The minimum allowable shear reinforcement - Beam 1

$s := 250$ space between stirrups

$$A_{sw.min} := \frac{0.08 \cdot s \cdot b \cdot \sqrt{f_{ck}}}{f_{yk}} = 108.696 \quad (mm^2)$$

$$z := 0.9 \cdot d = 1.148 \cdot 10^3 \quad v_1 := 0.6 \cdot \left(1 - \frac{f_{ck}}{250}\right) = 0.54 \quad f_{cd} := 0.6 \cdot \frac{f_{ck}}{\gamma_c} = 10$$

$$V_{Rd.max} := b \cdot z \cdot v_1 \cdot f_{cd} \cdot \frac{1}{1 + 1} = 774.6 \cdot 10^3 \quad (N) \quad V_{Rd.max} > V_{ed} = 1 \quad OK$$

$$\theta := 0.5 \cdot \arcsin\left(\frac{V_{rd.c_{bb}}}{V_{Rd.max}}\right) = 3.411 \text{ deg} \quad \text{This degree has to be between } 22 - 45^\circ$$

$$\theta_{val} := 22 \text{ deg} \quad \text{The minimum value is used}$$

Shear resistant of stirrup

$$A_{sw} := \pi \cdot \left(\frac{k_{tie}}{2}\right)^2 \cdot 2 = 157.1$$

$$V_{rd.s} := \frac{A_{sw}}{s} \cdot z \cdot \frac{f_{yk}}{\gamma_s} \cdot \cot(\theta_{val}) = 357 \cdot 10^3 \quad (N)$$

$$V_{rd.s} \geq V_{ed} = 1 \quad \frac{V_{ed}}{V_{rd.s}} = 0.235$$

Shear capacity is OK

Shear strength of building component - Beam 2

$$\begin{aligned}
 b &:= 180 \quad (mm) & h &:= 600 \quad (mm) & c &:= 20 \quad (mm) \\
 k_{tie} &:= 8 \quad (mm) & A_s &:= \pi \cdot \left(\frac{k_{tie}}{2} \right)^2 = 50 & V_{ed}' &:= 232 \cdot 10^3 \\
 q &:= 1.5 & & & V_{ed} &:= V_{ed}' \cdot \left(\frac{q+1}{2} \right) = 290 \cdot 10^3 \\
 d &:= h - c - \frac{k_{tie}}{2} = 576 \quad (mm)
 \end{aligned}$$

Material properties of concrete and steel

$$\begin{aligned}
 f_{ck} &:= 25 \quad (MPa) & \gamma_c &:= 1.5 & f_{yk} &:= 230 \quad (MPa) & \gamma_s &:= 1.15 \\
 & & & & & & \alpha_{cc} &:= 0.85
 \end{aligned}$$

$$Crd.c := \frac{0.18}{\gamma_c} = 0.12 \quad k_1 := 0.15$$

$$k := 1 + \sqrt{\frac{200}{d}} = 1.589 \quad k \leq 2.0 = 1 \quad \sigma_{cp} := 0$$

$$V_{min} := 0.035 \cdot k^{\frac{3}{2}} \cdot f_{ck}^{\frac{1}{2}} = 0.351$$

$$\rho := \frac{A_s}{b \cdot d} = 4.848 \cdot 10^{-4} \quad \rho \leq 0.02 = 1$$

The shear capacity of concrete is the higher value of those two

$$V_{rd.c_{bb}} := \max \left(\left[\left(Crd.c \cdot k \cdot (100 \cdot \rho \cdot f_{ck})^{\frac{1}{3}} + k_1 \cdot \sigma_{cp} \right) \cdot b \cdot d \right], \left[(V_{min} + k_1 \cdot \sigma_{cp}) \cdot b \cdot d \right] \right) = 36 \cdot 10^3 \quad (N)$$

The shear capacity ratio is not ok

$$\frac{V_{ed}}{V_{rd.c_{bb}}} = 7.98 \quad \text{Shear reinforcement required}$$

The minimum allowable shear reinforcement - Beam 2

$s := 250$ space between stirrups

$$A_{sw.min} := \frac{0.08 \cdot s \cdot b \cdot \sqrt{f_{ck}}}{f_{yk}} = 78.261 \quad (mm^2)$$

$$z := 0.9 \cdot d = 518.4 \quad v_1 := 0.6 \cdot \left(1 - \frac{f_{ck}}{250}\right) = 0.54 \quad f_{cd} := 0.6 \cdot \frac{f_{ck}}{\gamma_c} = 10$$

$$V_{Rd.max} := b \cdot z \cdot v_1 \cdot f_{cd} \cdot \frac{1}{1 + 1} = 252 \cdot 10^3 \quad (N)$$

$V_{Rd.max} > V_{ed} = 0$ Not ok, necessary to enlarge the cross section

$$\theta := 0.5 \cdot \arcsin\left(\frac{V_{rd.c_{bb}}}{V_{Rd.max}}\right) = 4.148 \text{ deg} \quad \text{This degree has to be between } 22 - 45^\circ$$

$\theta_{val} := 22 \text{ deg}$ The minimum value is used

Shear resistant of stirrup

$$A_{sw} := \pi \cdot \left(\frac{k_{tie}}{2}\right)^2 \cdot 2 = 100.5$$

$$V_{rd.s} := \frac{A_{sw}}{s} \cdot z \cdot \frac{f_{yk}}{\gamma_s} \cdot \cot(\theta_{val}) = 103 \cdot 10^3 \quad (N)$$

$$V_{rd.s} \geq V_{ed} = 0 \quad \frac{V_{ed}}{V_{rd.s}} = 2.81$$

Shear capacity is not OK